Regulation of Voltage-gated Potassium (Kv) and Two-Pore Domain Potassium (K2P) Channels implicated in Pulmonary Hypertension

Mun Ching Lee

A thesis submitted in partial fulfilment of the requirements of the University of Kent and the University of Greenwich for the Degree of Doctor of Philosophy

Declaration

I certify that this work has not been accepted in substance for any degree, and is not concurrently being submitted for any degree other than that of Doctor of Philosophy being studied at the Universities of Kent and Greenwich. I also declare that this work is the result of my own investigations except where otherwise identified by references and that I have not plagiarised the work of others.

Signed: Mun Ching Lee 

Date : 16 July 2018

Acknowledgement

Thank you to my supervisor, Professor Alistair Mathie, for believing in me, for helping me to make this 'leap' into the world of electrophysiology. Your dedication throughout the project, questions and ideas, are all important building blocks of this thesis. I would always be grateful for the chance to be part of your research group.

I also owe a debt of gratitude to Dr Emma Veale, who had so patiently helped me in the lab. Whenever I needed something in the lab, all I had to do was ask. A lot of students who have graduated reminisced about the days that they had Emma coming to their aid, I believe I will be no exception.

And to the person who taught me how to do patch clamp, Yvonne- thank you so much for tolerating me sitting next to you for the first few weeks of my PhD and for patiently guiding me until I got my first 'patch'. Those who taught others how to do patch clamp would agree that our job is like a priest sometimes, to tell others to 'keep going' especially when we don't see the electrode under the microscope. I also admire how you always managed to fix any hiccups with the rig.

And thank you Mustafa, for sharing your knowledge so generously, for helping me to navigate around the pClampfit software- The initial stages of data analysis would not have been possible have you not shown me how to do it.

To my other lab colleagues, Kevin and Robin, thank you for being there, your presence in the lab meetings have led to the exchange of many interesting ideas for the lab group. I would also like to thank the staff of Medway School of Pharmacy for their help, which is essential for the smooth running of the PhD.

The execution of one chapter in this thesis would not have been possible without the unwavering support of a dear friend, Zahra Ali. Thank you for teaching me how to do Immunohistochemistry and I cannot tell you how glad I am that our paths crossed albeit for a very short period. I am grateful that you find time to teach me even though you have a heavy workload.

And I will never forget the person who lends me a helping hand, starting from the very first day of PhD itself- Jen. Thank you for showing me generosity by providing me shelter for the first week of being in Medway. I hope you will meet people as generous as you in whatever you do. And thank you to Keith, who worked tirelessly with me on the Bio Art Project- it was an invaluable experience winning the Postgraduate Experience Award with you! To the other PhD colleagues whom I had the pleasure of knowing- Carmen, Stefania, Evelina, Soumya, Stratos, Voula, Rafal, Isabel, Stuart, Filip, Kayleigh, Tracey, Diana, Lynsey, and Danielle- thank you for the conversation and guidance. And thank you to the members of Dr Claire Peppiatt-Wildman's team, especially Kirsti, Louise, and Rebecca for having me at Charles River Margate, for making me feel like 'in the office' away from office.

And these three years have been made interesting thanks to the opportunity to be involved in the iGEM team. Thank you to Dr Wei Feng Xue for having me in the team and to the iGEM teams of 2014, 2015, and 2016- I really enjoyed spending time

as an advisor in all your projects, and to see so many of you who were once team members and now turned into advisors has made me happy and proud.

And there are friends whose support is instrumental in different aspects of my life- Pei Ying for always checking up on me- I have been so blessed to have a true, loyal friend who goes through ups and downs with me; Zi Ying, who I always look up to for words of wisdom; Jessica, who is my role model; Claudia for being a savior in many difficult situations; Nina for being such a fun and supportive friend; Elizabeth and John for providing me a place where I can seek solace whenever I am sad, Nimisha for always calling me to guide me on my thesis- I am so lucky that I do not even need to ask, and you would volunteer to guide me!

While most will thank their parents for their love and support, the number one thing I cherished most from them is the freedom that they have given me to pursue anything I want. Your willingness to give me space is actually the best support I could have ever asked for. To my brothers, it was a joy being a sister to both of you and I have learnt so much from you.

And to my grandma, who has a big influence in my life. It was rather unfortunate that you left without saying goodbye, while I was on the first year of my PhD, and just ten days before I was homebound. To have grown up with you was one of the best things that happened to me and thank you for watching out for me from above. Thankfully I have my aunt, Tse Levy, who reprises your role and cheered me on this PhD journey.

And to the person who so selflessly attended to me, tolerated my complains whenever there is a rough patch in this PhD or in life, I owe you a big thank you. Radek, you are also an inexhaustible source of inspiration to me, constantly reminding me to believe in myself and you see the potential in my ideas and convinced me that they are worth pursuing.

Table of Contents

List of Tables

List of Equations

List of Figures

Abbreviations

4-AP	4-aminopyridine
AGS	Gastric adenocarcinomas cell line
ali1 or Alivin1	Alive, activity-dependent leucine-rich repeat and Ig superfamily survival-related protein
AMIGO	Amphoterin-induced gene and open reading frame
ANOVA	Analysis of variance
ATP	Adenosine triphosphate
BKCa	Large-conductance calcium-activated potassium channel
Ca^{2+}	Calcium
CaM	Calmodulin
cDNA	Complementary deoxyribonucleic acid
CNS	Central nervous system
Ch-T	Chloramine T
cAMP	Cyclic adenosine monophosphate
DAG	Diacylglycerol
DEGA	Differentially expressed in human gastric adenocarcinomas
DNA	Deoxyribonucleic acid
DTT	Dithiothreitol
DTNB	5,5'-dithiobis-(2-nitrobenzoic acid)
ET-1	Endothelin
GFP	Green fluorescent protein
GSH	Glutathione
H_2O_2	Hydrogen peroxide
hypoxic pulmonary vasoconstriction	hypoxic pulmonary vasoconstriction
IP3	Inositol phosphate-3
K^+	Potassium
K2P	Two-pore domain potassium channels
KO	Knock out

LRR	Leucine-rich repeats
mm	Millimetre
mPAP	Mean pulmonary arterial pressure
mRNA	Messenger ribonucleic acid
mV	millivolt
NADPH	Nicotinamide adenine dinucleotide phosphate
NgR	Nogo receptor
NO	Nitric oxide
Nox	NADPH oxidase
O_2	Oxygen
PAH	Pulmonary arterial hypertension
PAEC	Pulmonary artery endothelial cells
PASMC	Pulmonary artery smooth muscle cells
PBS	Phosphate-buffered saline
pH	Log hydrogen ion concentration
PH	Pulmonary hypertension
PIP2	Phosphatidylinositol 4,5 bisphosphate
PKA	Protein kinase A
PKC	Protein kinase C
PLC	Protein lipase C
PPI	Prepulse inhibition
RAGE	Receptor of advanced glycation end products
RMP	Resting membrane potential
RMCA	Rat middle cerebral arteries
RT-PCR	Reverse transcription polymerase chain reaction
Stromatoxin	ScTx-1
TASK-1	TWIK-related acid-sensitive potassium channel-1
TEA	Tetraethylammonium
TM	Transmembrane
TGF-beta	Transforming growth factor-beta
TWIK	Two-pore weakly inward rectifying potassium channel
WT	Wild type

Abstract

Background

Kv2.1 and TASK-1 channels are two main contributors of K^+ currents in pulmonary artery smooth muscle cells (PASMC). Dysregulation of these channels has been implicated in the pathogenesis of pulmonary hypertension (PH). This thesis aims to delve deeper into the implications of the regulation of Kv2.1 by Kv9.3 in PH. Another subject of interest would be whether NADPH oxidase type 4 (Nox4), one of the major reactive oxygen species (ROS) producers in the PASMC, modulates Kv2.1, Kv9.3, and TASK-1 channels. The effects of several redox agents are also investigated as potential modulators of Kv2.1, Kv9.3, and TASK-1. In addition, this thesis also examined the effect of a Kv2–channel blocker, stromatoxin, on Kv2.1 and Kv9.3. Finally, since amphoterin-induced gene and open reading frame (AMIGO) proteins have recently been shown as novel Kv2.1-interacting partners, their effects on Kv2.1 and/or Kv9.3 are also explored in this study.

Experimental approach

Whole-cell patch clamp electrophysiology was used to measure currents of the ion channels expressed in modified tsA-201 cells, in the absence and presence of Nox4 AMIGO and other regulatory molecules. Immunohistochemistry was deployed to visualize the distribution of Kv2.1 and Kv9.3 proteins in the rat lungs and hearts.

Key results and Conclusions

This study supports the findings that Kv9.3 regulates Kv2.1 by increasing the current amplitude, shifting the activation threshold to a more negative voltage range, and prolonging the slow component of time constant of deactivation. These effects could be beneficial in PH as this would mean cells could be brought back to its resting membrane potential faster and the transduction of the next action potential can be delayed. Kv2.1 and Kv9.3 have also been detected at the endothelium and PASMC in rat lungs and hearts, further substantiating the claim that these channels are potential players in regulating PH. AMIGO1 and AMIGO2 proteins are confirmed as regulators of Kv2.1 and Kv9.3 proteins. Nox4 does not regulate Kv2.1, Kv9.3, and TASK-1 channels expressed in tsA-201 cells. While hydrogen peroxide (H_2O_2) does not have any effect on Kv2.1 and Kv9.3, it abolished the current reduction effect of

AMIGO2 on Kv2.1/Kv9.3. Other redox agents used in this study such as dithiothreitol (DTT), 5,5'-dithiobis-(2-nitrobenzoic acid) (DTNB), and chloramine T (Ch-T) are not modulators of these channels expressed in tsA-201 cells. The lack of effect from Nox4 and these redox agents could suggest that the redox regulation of different Nox subunit/Kv channels combination varies for different cell types due to the different regulatory proteins present in different heterologous expression systems. As with the case of H_2O_2 and AMIGO2, it is likely that the regulatory proteins, which could facilitate the hypoxia-sensing properties of Nox4 and the effects of the redox agents on the ion channels, are missing in our heterologous expression system, compared with other host cells.

Chapter 1: Introduction

1.1 Pulmonary Hypertension

1.1.1 Classification of PH

Pulmonary hypertension (PH) is a complex cardiopulmonary disorder that can be caused by several factors. The characteristics of this disorder include progressive sustained increase in mean pulmonary arterial pressure (mPAP), leading to right-sided heart failure and death. PH can occur due to precapillary (arterial) or postcapillary (venous) pathomechanisms (Guignabert et al, 2015). In 2013, the World Health Organization classified PH into five groups, which are pulmonary arterial hypertension, pulmonary hypertension due to left heart disease, pulmonary hypertension due to lung diseases and hypoxia, chronic thromboembolic pulmonary hypertension, and pulmonary hypertension with unclear and multifactorial mechanisms (Goldberg et al., 2017). The first group, pulmonary arterial hypertension (PAH) is further divided into idiopathic, hereditary, drug- and toxin-induced, and associated forms namely connective tissue diseases, human immunodeficiency virus (HIV) infection, portal hypertension, congenital heart diseases, and schistosomiasis (Goldberg et al, 2017). European Society of Cardiology guidelines defined pulmonary arterial hypertension as having an mPAP of ≥ 25 mm Hg at rest, with a normal pulmonary artery wedge pressure ≤ 15 mm Hg, and pulmonary vascular resistance > 3 Woods unit. Unlike Group 2 PH, pulmonary arterial hypertension is precapillary PH because obstruction to flow happens at the precapillary level (Goldberg et al., 2017).

1.1.2 Pathogenic mechanisms of Pulmonary Hypertension

There are two main pathogenic mechanisms of PH, which are hypoxic pulmonary vasoconstriction and pulmonary vascular remodelling (Kuhr et al., 2012).

1.1.2.1 Hypoxic pulmonary vasoconstriction

Although hypoxic pulmonary vasoconstriction is implicated in PH, it is actually an important physiological response where resistance pulmonary blood vessels constrict to divert blood from poorly ventilated regions of the lung to regions with a higher O_2 tension to improve gas exchange during hypoxia (low oxygen availability) (Archer et al., 1998). However, long-term hypoxia causing sustained hypoxic pulmonary vasoconstriction could lead to PH especially in chronic obstructive pulmonary diseases (e.g. chronic bronchitis, emphysema) and in people living at high altitudes (Kuhr et al., 2012; Morrell et al., 2009; Ward and McMurtry, 2009). This study concerns the properties of K^+ channels which have a role in setting the resting membrane potentials (RMP) in the PASMC, which in turn regulate the Ca^{2+} signalling pathways to control the pulmonary vascular tone (Ko et al., 2010; Kuhr et al., 2012).

1.1.2.2 Pulmonary vascular remodelling

Pulmonary vascular remodelling is a process where structural changes occurring in the pulmonary arteries leads to hypertrophy and/or luminal obstruction (Huang et al., 2010; Kuhr et al., 2012). Pulmonary vascular remodelling leads to the onset of PH because the increment in the thickness and tissue mass of the pulmonary arterial walls causes an increase in pulmonary vascular resistance due to narrowing or obstruction of vessel lumen. The increase in tissue mass occurs because of uncontrolled cell proliferation.

Multiple factors contribute to the disruption of this vascular apoptosis-proliferation homeostasis process such as alteration of ROS stalk between cells within the vascular wall, compromised functions of inflammatory cells, inhibition of apoptosis pathways and excessive activation of signalling pathways promoting cell proliferation, survival, and migration, and imbalance of systemic hormones, local growth factors, cytokines, transcription factors, and germline mutations (Guignabert et al., 2015). Several cell types within the vascular wall such as PASMC, pulmonary artery endothelial cells (PAEC), myofibroblasts, and pericytes, can alter structurally and functionally during vascular remodelling (Guignabert et al., 2015; Kuhr et al., 2012). Meanwhile,

deposition of inflammatory cells, platelet, and, progenitor cells causes thrombotic lesions which increases the pulmonary vascular resistance and obstructs blood flow in small arteries and arterioles (Kuhr et al., 2012).

The pulmonary vascular remodeling process happens in five stages, beginning with the innermost tunica intima layer and ending at the outermost tunica adventitia layer (Figure 1.1). Intimal thickening occurs due to endothelial cells von Willebrand factor, a blood glycoprotein responsible for blood coagulation and fibrinolysis, which eventually lead to accumulation of collagen and proliferation of myofibroblasts.

Medial thickening is characterized by medial hypertrophy and neomuscularization. Medial hypertrophy refers to the thickening and growth of PASMC. Neomuscularization is associated with the differentiation of fibroblasts and pericytes within non-muscular arteries such as distal alveolar duct and wall pulmonary arteries into smooth muscle cells that subsequently proliferate (Rabinovitch, 2008, Kuhr et al., 2012).

The loss of small precapillary arteries, probably due to vessel occlusion, could also be attributed to endothelial cell alteration and/or pericytes differentiation. In the fourth stage of the remodeling process, it is thought that gradual thickening of the wall of more proximal intra-acinar and pre-acinar muscular arteries coupled with obliteration that happened during neointimal formation may be responsible for increased proliferation and migration of cells that are likely to be SMC. These cells are hypothesized to be a specialized subpopulation of SMC or may have originated as stem cells or fibrocytes or may even have originated as endothelial cells. Cell culture studies have shown that endothelial cells release factors such as FGF_2 which stimulate SMC proliferation. In idiopathic PAH patients, there is a noticeable Tie2 receptor upregulation and activation in endothelial cells which is associated with increased serotonin release. This further leads to serotonin-mediated SMC proliferation.

Later stage of the disease is characterized by the development of plexiform lesion. It is hypothesized that clonal expansion of apoptosis-resistant endothelial cells or circulating endothelial progenitor cells that concentrate at sites of endothelial denudation or injury could give rise to the formation of aberrant channels in otherwise obliterated lumen vessels and in the adventitia. Interestingly, it has been found that

PAEC of idiopathic PAH patients synthesize lower amounts of nitric oxide, NO. NO, an important vasodilator and inhibitor of SMC proliferation, is mostly produced from eNOS in PAEC. L-arginine is a substrate of NO synthase to produce NO and L-citrulline, but L-arginine can also be broken down by arginase thereby reducing the bioavailability of NO. This agrees with the finding that PAEC of idiopathic PAH patients express a high level of arginase. PAEC from these patients have also been found to proliferate in response to growth factors (such as platelet-derived growth factor) and have a high glycolysis rate (Rabinovitch, 2008). The increased proliferation is concomitant with malformation of endothelial tubes in culture, which is in line with the apoptosis of precapillary vessels and failure to replenish these vessels. Changes to the adventitia layer in the remodelled vessels can be quantified by increased amount of transforming growth factor β (TGF-β) and accumulation of extracellular matrix components such as collagen, elastin, fibronectin, tenascin-C, and glycosaminoglycans, in addition to fibroblast proliferation (Kuhr et al., 2012). Immunohistochemical studies also demonstrated increased expression of immune cells such as macrophages, T cells, fractalkine, and metastasin 1 (also known as S100A4) (Rabinovitch, 2008). The increased amount of TGF-β is an interesting hallmark of PAH as several researchers have recently found that mutation in BMPR2, which encodes a type 2 receptor member (bone morphogenetic protein receptor 2 [BMPR2]) of the TGF-β superfamily of cell-signalling molecules account for 70% of hereditary PAH and 10-40% of idiopathic PAH cases (Ma and Chung, 2017; Navas Tejedor et al., 2017).

The breakdown of extracellular matrix, accumulation of collagen, and increased endothelial and smooth muscle cell proliferation also lead to enhanced wall stiffness (Kuhr et al., 2012). This is another factor that further leads to increased pulmonary vascular resistance, which results in increased workload on the right ventricle. Thus, right heart failure occurs at a higher frequency in PAH patients (Huang et al., 2010; Kuhr et al., 2012). As with hypoxic pulmonary vasoconstriction, Ca^{2+} elevation in PASMC plays a major role in vascular remodelling as it stimulates the PASMC proliferation process (Kuhr et al., 2012).

In addition, extracellular matrix breakdown also generates fragments that can directly

regulate proliferation, migration, and protease activation to further cause local pulmonary vascular remodelling. Activation of several proteases such as elastase, matrix metalloproteinase (MMP), chymase, tryptase, as well as urokinase-type plasminogen activator plasmin system or the tissue- type plasminogen activator plasmin system have been shown to promote pulmonary vascular remodelling (Guignabert et al., 2015). Extracellular matrix disintegration also causes growth factors and other molecules which are previously embedded to be activated. Remodelling of the extracellular matrix also leads to exposure of functionally important cryptic sites in collagen, elastin, laminins or bronectin, which predisposes the vasculature to pulmonary vascular remodelling (Guignabert et al., 2015; Huang et al., 2010; Kuhr et al., 2012).

One of the examples of how DNA damage can render apoptotic-resistant phenotype in PASMC is the upregulation of hypoxia-inducible factor 1α leading to downregulation of miR-223, and upregulation of poly (ADP-ribose) polymerase 1 (PARP-1). Meloche et al., 2015 provided evidence that miR-223 is downregulated in human PAH lungs, distal PAs, and isolated PASMCs. They have also shown that restoration of miR-223 expression in monocrotaline-induced PAH ameliorated PAH by having positive impacts on vascular remodelling, pulmonary resistance, right ventricle hypertrophy, and survival (Meloche et al., 2015).

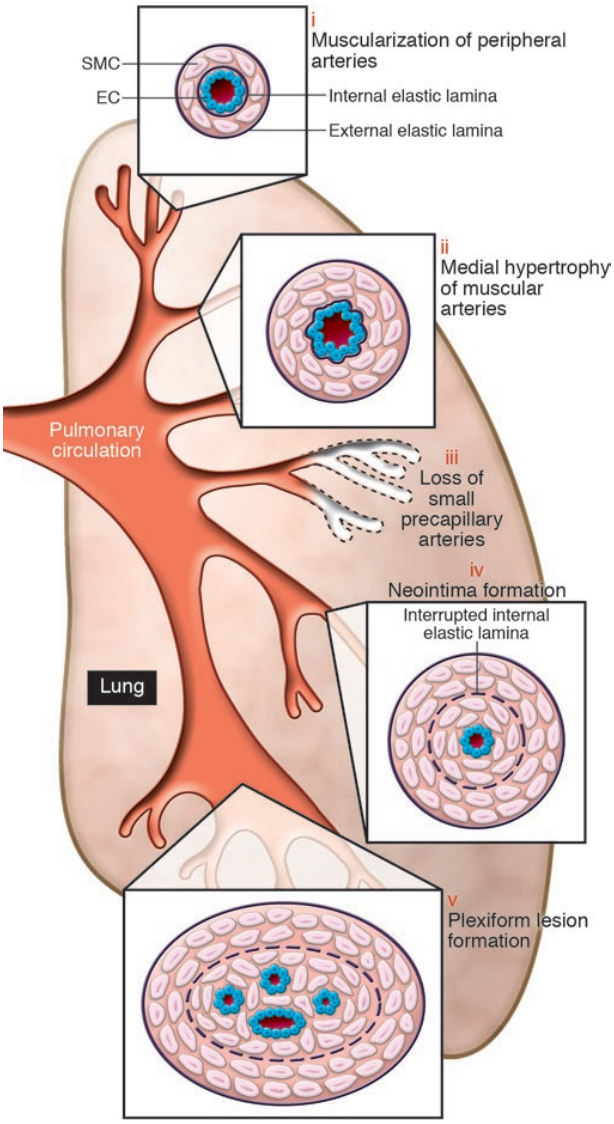

Figure 1.1: Schematic illustration of the stages in pulmonary vascular remodeling. The stages are i) neomuscularization of peripheral arteries, ii) medial thickening of large muscular pulmonary arteries, iii) loss of precapillary arteries, iv) neointimal formation in vessels of 100-500μm, v) development of plexiform lesions. Adapted from Rabinovitch, 2008.

1.1.3 Relationship between ROS and PH

ROS are major contributors of hypoxic pulmonary vasoconstriction as they can mediate both the hypoxic pulmonary vasoconstriction and pulmonary vascular

remodelling processes. Increased ROS production, especially superoxide and hydrogen peroxide (H_2O_2), coupled with decreased nitric oxide bioavailability or other antioxidants causes vasoconstriction in PASMC, indicating a pathophysiological role in hypoxic pulmonary vasoconstriction. ROS mediate their effect via the interaction with protein kinases, guanylyl cyclase (Ko et al., 2010) and most importantly for this project, K^+ channels (Perez-Vizcaino et al., 2010).

A secondary event that could occur due to endothelial dysfunction is the reduction in nitric oxide (a vasodilator) bioavailability. This is because ROS (specifically superoxide) bind with NO to form peroxynitrite ($ONOO^-$) which can nitrate tyrosine residues on proteins as well as cause lipid peroxidation and single strand breaks in DNA (Figure 1.2) (Modun et al., 2014). ROS can increase the intracellular calcium concentration directly or; indirectly by inhibiting K^+ channels (Harrison et al., 2007; Touyz, 2004).

Several research groups have documented the effects of different redox agents such as H2O2, dithiothreitol (DTT), 5,5-dithio-bis-(2-nitrobenzoic acid) (DTNB), and chloramine T (Ch-T) on the pulmonary vasculature (Duprat et al., 1997; Park et al., 1997a; S. W. Park et al., 2015). However, the results remain contradictory or inconclusive. For example, H2O2 has been found to act as either a vasodilator, vasoconstrictor or both (S. W. Park et al., 2015). Furthermore, the redox agents hypothesized to be implicated in PH mediate their effects by reducing K+ current. (see 'Relationship between K+ channels and PH). Due to the gap in the current literature, the effects of these redox agents on Kv2.1, Kv9.3, and TASK-1 are explored in Chapter 3, Chapter 5, and Chapter 6.

1.1.3.1 NADPH oxidases are a source of ROS

Although there are multiple enzymes which are possible candidate for the ROS synthesis in PASMC, Mittal et al., 2007 and Touyz, 2004 argued that the primary source of vascular ROS is nicotinamide adenine dinucleotide phosphate (reduced form) NADPH oxidase complex. NADPH oxidase complex is a heteromeric enzyme, where its catalytic subunit is called Nox, catalyzes superoxide production whereby

NAD(P)H donates an unpaired electron to oxygen (Figure 1.2) (Touyz, 2004). Vascular Nox has at least 4 subunits which are sometimes known as accessory proteins: cell membrane–associated p22phox and gp91phox (or gp91phox [Nox2] homologues, Nox1 and Nox4), and cytosolic subunits, p47phox and p67phox (Brandes et al., 2010; Harrison et al., 2007; Touyz, 2004).

Under normal conditions, Nox is synthesized in a small quantity to function as signalling molecules to regulate endothelial function and vascular contraction-relaxation. Interestingly, the function of Nox can be modulated by physical factors (stretch, pulsatile strain, and shear stress) and humoral factors (cytokines, growth factors, and vasoactive agents) (Harrison et al., 2007). Deviation from normal Nox function in the events of increased ROS bioavailability would cause events which are characteristics of hypoxic pulmonary vasoconstriction such as increased vessel contractility, endothelial dysfunction; and pulmonary vascular remodelling such as lipid peroxidation, inflammation, monocyte invasion, and, accumulation of extracellular matrix proteins (Harrison et al., 2007).

RT-PCR data has confirmed the mRNA expression of Nox1 to Nox5 (except Nox3) in the cardiovascular system, with Nox4 having the highest expression compared to the rest (Brandes et al., 2010). The mode of activation of Nox depends on its interaction with p22phox (a transmembrane scaffolding protein) (Brandes et al., 2010). Of these Nox proteins, Nox2 and Nox4 are postulated to be involved in hypoxia-induced endothelial dysfunction and PH (Brandes et al., 2010). Both of these proteins have been shown to modulate the function of K^+ channels during hypoxia and vascular remodelling process (Brandes et al., 2010; Buttigieg et al., 2012; Harrison et al., 2007; Mittal et al., 2012; Touyz, 2004).

Mittal et al., 2012 demonstrated that Nox4 is upregulated in hypoxia-induced pulmonary hypertension in both rats and mice and helps PASMC proliferation via the phosphorylation of retinoblastoma protein. Immunocytochemistry experiments performed by Lee et al., 2006 showed that Nox4 is co-localized with TASK-1 and functionally inhibits the channel current.

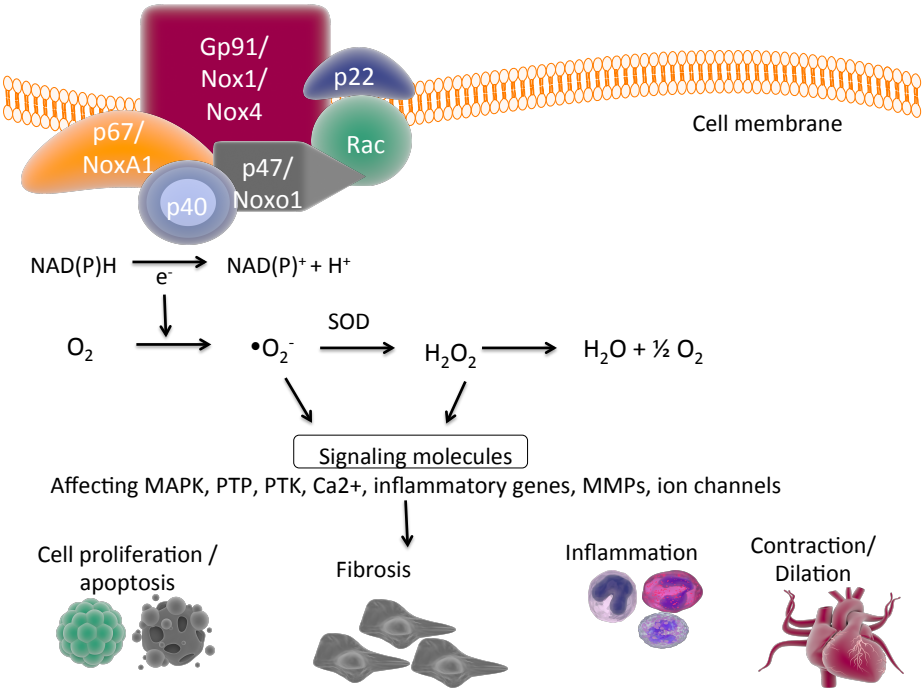

$$^{\bullet}O\text{–}^{\bullet}O + e^{-} \longleftrightarrow {}^{\bullet}O\text{–}O^{-}$$

$$^{\bullet}O\text{–}O^{-} + e^{-} \longleftrightarrow {}^{-}O\text{–}O^{-}$$

$$^{-}O\text{–}O^{\bullet} + N^{\bullet}\text{=}\mathbf{O} \longleftrightarrow {}^{-}O\text{–}O\text{–}N = \mathbf{O}$$

$$^{-}O\text{–}O\text{–}N\text{=}\mathbf{O} \longrightarrow O(\mathbf{O})N\mathbf{O}^{-}$$

$$2\ {}^{-}O\text{–}O\text{–}N\text{=}\mathbf{O} + 2GSH$$

$$\longrightarrow 2\ {}^{-}O\text{–}N\text{=}\mathbf{O} + GSSG + H_2O_2$$

$$^{-}O\text{–}\mathbf{O}\text{–}N\text{=}\mathbf{O} + TyrH \longrightarrow \mathbf{O}\text{–}\ (\mathbf{O}\text{=})\ N\text{–}Tyr + HO^{-}$$

Figure 1.2: Molecular scheme of NADPH oxidase complex (its catalytic subunit is called Nox) and generation of ROS leading to pulmonary arterial smooth muscle cells (PASMC) contraction and vascular remodelling. Abbreviations- NADP(H): nicotinamide adenosine dinucleotide phosphate (reduced form), H^{+}: hydrogen ion, O_2: oxygen, $\bullet O^{2-}$: superoxide anion, SOD: superoxide dismutase, H_2O_2: hydrogen peroxide, H_2O: water, MAPK: mitogen-activated protein kinase, PTP: protein tyrosine phosphatase, PTK: tyrosine kinase, MMP: matrix metalloproteinase. O_2 molecule received an electron, forming the ROS superoxide anion. The superoxide anion has a strong tendency to receive another electron to form a more stable peroxide dianion, which can be protonated to form hydrogen peroxide (H_2O_2), another ROS. When superoxide anion meets NO, a reactive nitrogen species, peroxynitrite ($ONOO^{-}$) is formed. Peroxynitrite is extremely reactive because the two O atoms of the peroxide group of peroxynitrite are incompletely reduced and the N atom of peroxynitrite is incompletely oxidized. Nitrate ($O(O)NO^{-}$) is formed when intramolecular transfer of two electrons from the N atom to the peroxide group occurs. Two missing electrons are provided by other biomolecules such as reduced glutathione, GSH, and tyrosine, TyrH. Reproduced from Touyz, 2004 and Modun et al., 2014.

1.1.4 Involvement of K^+ channels in hypoxic pulmonary vasoconstriction and pulmonary vascular remodelling

When PASMCs are depolarized to above -35mV, either activation of Ca^{2+} channels to initiate an action potential (AP) or activation of K^+ channels for hyperpolarization can occur (Gurney et al., 2010). PASMC exhibit a large K^+ current outflow, suggesting that this strong repolarizing effect is essential in preventing the smaller Ca^{2+} current from inducing another AP (Gurney et al., 2010; Ko et al., 2010; Morrell et al., 2009). Therefore, K^+ channels are fundamental in limiting excitability to maintain the low vascular tone, an intrinsic property of the pulmonary arteries (Gurney et al., 2010; Kuhr et al., 2012).

Failure of K^+ channels to activate will cause PASMC to remain depolarized, which lead to an elevation in the cytoplasmic Ca^{2+} concentration ($[Ca^{2+}]$cyt) (Kuhr et al., 2012). Interaction of Ca^{2+} with calmodulin (CaM) activates myosin light chain kinase which then phosphorylates the regulatory light chain of myosin (Kuhr et al., 2012). Subsequently, the myosin ATPase is activated, which then hydrolyses ATP and thus provides energy for the cross-bridging cycles between myosin and actin filaments (Kuhr et al., 2012). These mechanisms underlie cellular contraction, which in the context of PASMC, is termed pulmonary vasoconstriction (Ko et al., 2010; Kuhr et al., 2012) (Figure 1.3).

Through regulation of the resting membrane potential, Ca^{2+} influx through L-type voltage-dependent Ca^{2+} channels (VDCC) and hence the cytosolic Ca^{2+} concentration are controlled (Kuhr et al., 2012). This has implications in the homeostasis between cell proliferation and apoptosis by allowing proliferation of the PASMC population while simultaneously inhibiting apoptosis and cytoplasmic caspase activity (Figure 1.3) (Kuhr et al., 2012). A rise in $[Ca^{2+}]$cyt in PASMC stimulates cell proliferation and migration, leading to pulmonary vascular remodelling (Kuhr et al., 2012). The mechanisms involved in the regulation of $[Ca^{2+}]$cyt directly control vascular wall thickness; a major determinant of pulmonary vascular resistance (Kuhr et al., 2012) . Because pulmonary vascular resistance is inversely proportional to the fourth power of the radius (r) of the pulmonary arterial lumen (pulmonary vascular remodelling $=8L\eta/\pi r^4$), a very small change in r would thus cause a large change in pulmonary vascular resistance (Kuhr et al., 2012). As a consequence, pulmonary vasoconstriction

will also increase by reducing the arterial radius. Pulmonary arterial pressure (PAP), a diagnostic criterion for PAH, is a product of pulmonary vascular remodelling and cardiac output (Kuhr et al., 2012). Pulmonary vasoconstriction and vascular medial hypertrophy caused by excessive PASMC proliferation and migration contribute considerably to the elevated pulmonary vascular remodelling in patients with pulmonary hypertension (Kuhr et al., 2012).

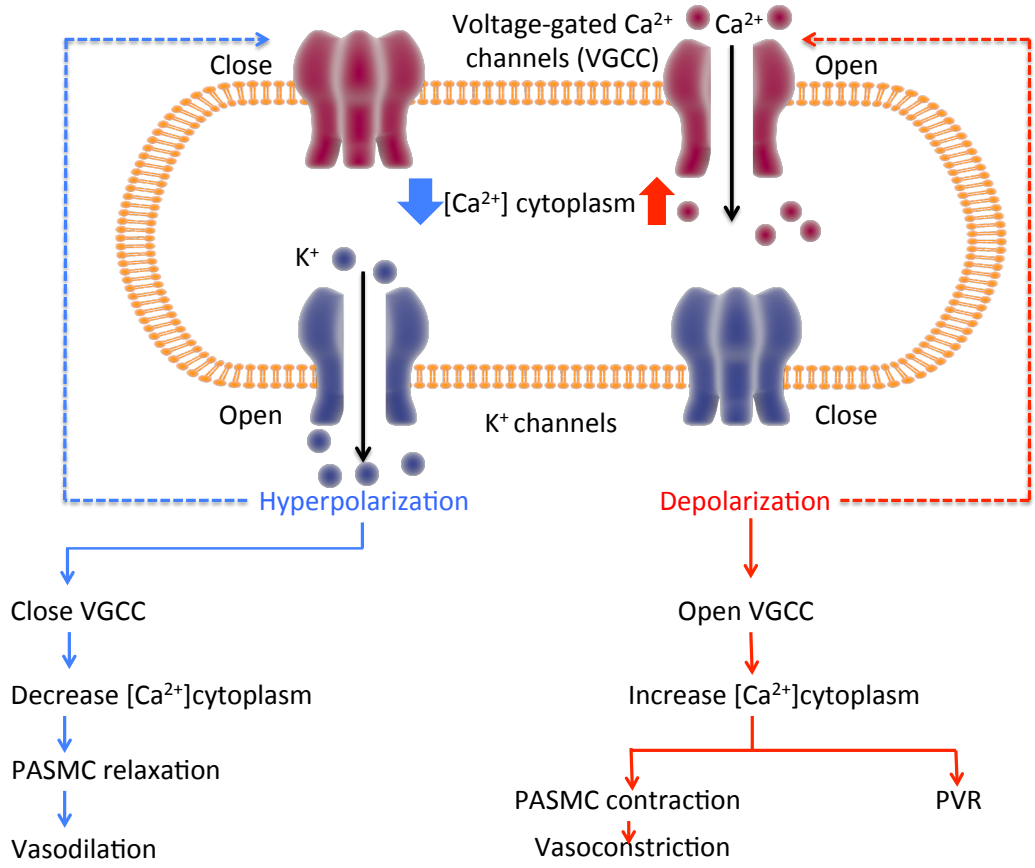

Figure 1.3: Schematic representation of the relationship between K^+ and Ca^{2+} channels in regulating pulmonary vasoconstriction and vascular remodelling. Closure of K^+ channels or opening of Ca^{2+} channels lead to rise in cytoplasmic Ca^{2+} concentration and pulmonary vasoconstriction (Left); Rise in cytoplasmic Ca^{2+} concentration causes cell cycle progression and vascular remodeling (Right). Reproduced from (Kuhr et al., 2012).

1.2 Potassium (K^+) channels

In general, there are four families of K^+ channels, namely calcium-activated K^+ channels, voltage- gated K^+ channels (Kv), inwardly-rectifying K^+ channels and two-pore domain K^+ channels (K2P) (Figure 1.4) (Levitan and Kaczmarek, 2002). K^+ channels are usually composed of pore-forming α-subunits and regulatory β-subunits (Levitan and Kaczmarek, 2002). K^+ channels are very diverse due to three reasons: the large number of genes (80 genes) encoding the α-subunit; the heteromeric assembly of different α subunits, β-subunits; and the intracellular interaction of different signalling proteins with the channel for modulation purposes (Bonnet and Archer, 2007; Levitan, 2002).

Electrophysiology has been used to characterize several K^+ channels in the pulmonary vasculature and those that are implicated in hypoxic pulmonary vasoconstriction include voltage-gated K^+ channels (Kv), inwardly-rectifying K^+ channels and two-pore domain K^+ channels (K2P), Ca^{2+} -activated channel (KCa), M-type K^+ channels, the ATP-sensitive K^+ channel (KATP) (Olschewski et al., 2014). However, several arguments support the notion that the main mediators are Kv channels, particularly Kv1.5 and Kv2.1 (see Kv9.3 channels and modulation of Kv2.1 below) because initiation of hypoxic pulmonary vasoconstriction occurs mostly due to hypoxic inhibition of Kv channels in PASMC (Archer et al., 1998, 2004; Bonnet and Archer, 2007). However, TASK channels are potentially interesting candidates due to their activation at a very negative membrane potential and therefore is postulated to play a role in setting the RMP (Morrell et al., 2009). Therefore, this study will specifically probe into the regulation of Kv2.1 and TASK channels.

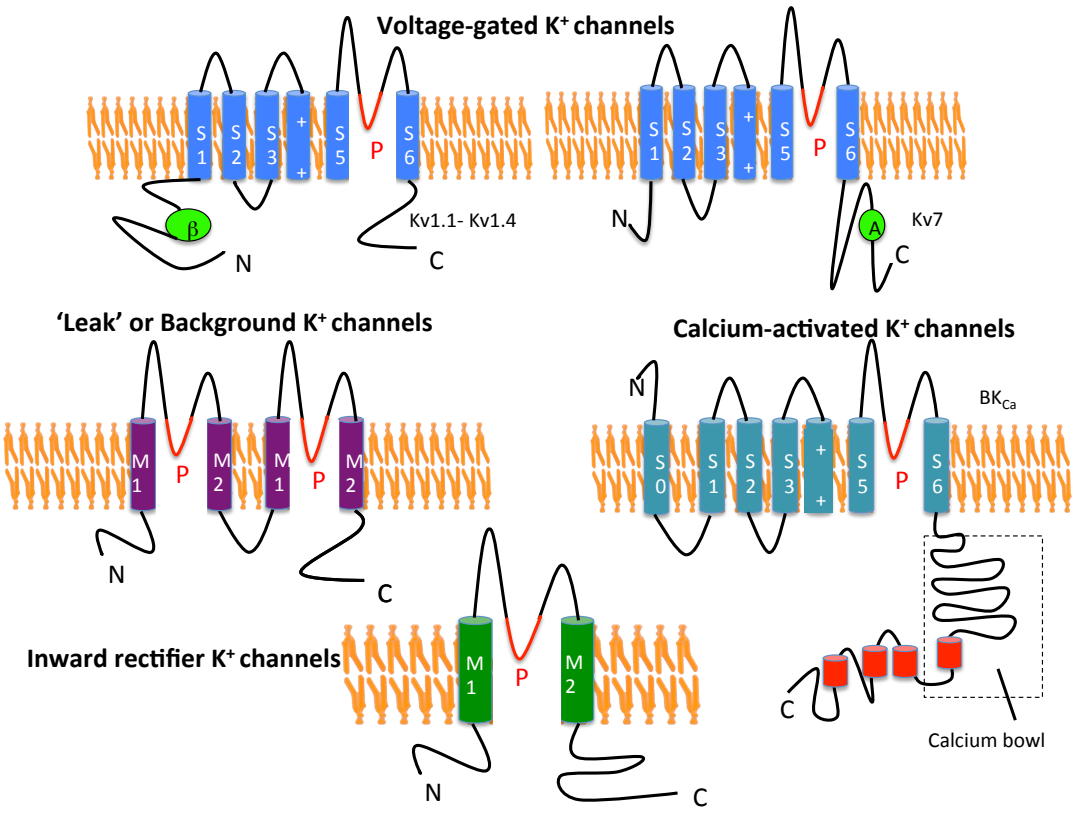

Figure 1.4: Families of K^+ channels. Clockwise: Voltage-gated K^+ channels, Calcium-activated K^+ channels, Inward rectifier K^+ channels, and 'Leak' or Background K^+ channels.

1.2 Voltage-gated and two-pore domain K^+ channels

1.2.1 Voltage-gated K^+ (Kv) channels

Like most of the K^+ channels, Kv channels are composed of a tetramer of α subunits (Levitan and Kaczmarek, 2002). Each α-subunit has six transmembrane domains (TMD) and a single pore-forming domain. The α-subunit is made up of a voltage sensor in the fourth TMD region which is rich in positively charged amino acids and a domain which is essential for the linkage between the four α-subunits and between α- and β-subunits (Levitan, 2002). The β-subunits modulate inactivation kinetics or drug sensitivity of the channel (Bonnet and Archer, 2007; Levitan, 2002).

Kv channels have been postulated to be implicated in hypoxic pulmonary vasoconstriction with evidence coming from pharmacological profiling, molecular

biology, and functional characterizations. Pharmacological profile of adult PASMC indicated that a Kv current that can be inhibited by 4-aminopyridine (4-AP) but not charybdotoxin is mostly responsible in establishing the membrane potential during hypoxic stimulation (Archer et al, 2004). By further analyzing the pharmacological profile of the Kv populations that have been studied in expression systems such as the *Xenopus* oocyte, the candidates were narrowed down to Kv1.5 and Kv2.1. The pharmacological profile of Kv2.1 has an exact match, where it is susceptible to 4-AP and tetraethylammonium (TEA), but insensitive to charybdotoxin (Archer et al., 2004, 1998; Bonnet and Archer, 2007).

With molecular biology approaches, it has been found that small pulmonary arteries in rat have high Kv channel expression (Archer et al., 1998, 2004). Meanwhile, functional characterization of Kv channels have shown that downregulation of Kv channels have been implicated in both hypoxic pulmonary vasoconstriction and pulmonary vascular remodelling (Guignabert et al., 2015; Olschewski et al., 2006). Inhibition of Kv channels causes reduction in the whole cell K^+ current, which leads to the opening of L-type voltage-gated Ca^{2+} channels and Ca^{2+} influx. This further causes PASMC contraction and eventually hypoxic pulmonary vasoconstriction. With regards to pulmonary vascular remodelling, it has been shown that therapies targeting the upregulation of Kv channels such as DCA (dichloroacetate), Kv1.5 gene therapy, and dehydroepiandrosterone could have beneficial effects in experimental PAH patients (Olschewski et al., 2014).

With respect to the α-subunits, most studies examining the molecular subtypes of Kv channels in PASMCs report the expression of Kv1.1, Kv1.2, Kv1.5, Kv2.1, and Kv9.3 (Archer et al., 1998, 2004; Yuan et al., 1998c; Osipenko et al., 2000; Coppock et al., 2001; Davies and Kozlowski, 2001; Platoshyn et al., 2001). Expression levels of Kv1.3, Kv1.4, and Kv1.6 are relatively controversial in PASMCs. Archer et al. 1998 proposed the presence of Kv1.1, Kv1.2, Kv1.3, Kv1.5, Kv1.6, and Kv2.1, but they failed to detect Kv1.4. At about the same time, Yuan et al., 1998 demonstrated the expression of Kv1.1, Kv1.2, Kv1.4, Kv1.5, Kv1.6, Kv2.1, and Kv9.3, but not Kv1.3. A few years later, expression of the Kv3.1 subtype was reported by other groups (Osipenko et al., 2000: Coppock et al., 2001; Archer et al., 2004). Although other subtypes (Kv1.7, Kv4.1, and Kv9.2) have also been identified (Davies and Lozlowski,

2001), Kv1.1, Kv1.2, Kv1.5, Kv2.1, Kv9.3, and additionally Kv3.1 subtypes are expressed in PASMCs, and one (or a co-assembly) of these types may act as oxygen sensors.

Combinations of α-subunits with β-subunits increase the diversity of Kv channel function in PASMC (Morales et al., 1996). Different combinations can result in difference in terms of inactivation and deactivation kinetics, and voltage sensitivity (Morales et al., 1996). Among the four types of β -subunits (Kv β 1–4) that have been identified so far, Kv β 1, Kv β2, and Kv β3 subunits are expressed in PASMCs (Standen and Quayle, 1998). Although the exact function of β–subunits is not known, it has been postulated that these subunits play a crucial role as a redox sensor and in hypoxic adaptation (Pérez-García and López-López, 2000).

Functionally, Cogolludo et al., 2006 established the link between the inhibition of Kv channels with the activation of thromboxane (TP) receptors in rat and porcine pulmonary arteries. TP receptors, coupled with G-protein, Gq, act via protein kinase C to inhibit the activation of Kv channels, causing membrane depolarization and activation of L-type Ca^{2+} channels to bring about hypoxic pulmonary vasoconstriction and pulmonary vascular remodelling **(**Cogolludo et al., 2006**).** In addition, Belohlávková et al., 2001 have also reported that dopamine receptor agonist pergolide and certain serotonin (5-HT) reuptake inhibitors could inhibit Kv channels, leading to membrane depolarization and eventually PH.

1.2.1.1 Kv2.1 channels

Kv2.1 channels are thought to be essential in modulating neuronal excitability due to their expression in virtually every nerve cell (Chiara et al., 1999). For example, Kv2.1 is the major contributor to the delayed rectifier K^+ current in neuronal cells such as the hippocampal neurons (Chiara et al., 1999) and cardiac cells (Patel et al., 1997). Therefore, Kv2.1 is involved in the repolarization of action potential in these cells. Although there is a vast amount of evidence emphasizing the role of Kv2.1 as an oxygen-sensitive channel responsible in PH, little is known about the specific oxygen-sensing component of the channel (Patel et al., 1999, 1997; Patel and Honoré, 2001). This oxygen-sensing property might be conferred by a built-in component within Kv2.1 or as a result of interaction with a binding protein such as Kv9.3 or Nox4, or even amphotericin-induced gene and open reading frame (AMIGO) proteins (which are the subjects of these studies) or other interacting partners, which are still unknown.

1.2.1.2 Kv9.3 channels and modulation of Kv2.1

Kv9.3 channels are electrically-silent channels. Interestingly, Kv2.1 can form a heteromer with Kv9.3 and its function is modulated as a result of this interaction (Patel et al, 1997). Therefore, Kv2.1, and very possibly Kv2.1/Kv9.3, are major contributors to the delayed rectifier K^+ current. Both channels are activated by intracellular ATP and are reversibly inhibited by hypoxia and the extents of these modulations are different for Kv2.1 and Kv2.1/Kv9.3 (Patel et al., 1999, 1997; Patel and Honoré, 2001). This has led to the speculation that their activities are tightly connected to the glycolytic pathway/ metabolic status of the PASMC. There are four separate findings which supported their connection with the metabolic state of the cells. Rounds and McMurty, 1981 discovered that inhibitors of oxidative phosphorylation and glycolysis cause transient pressor responses as well as hypoxic vasoconstriction in the perfused rat lung. Two separate findings; the first one concerning 2-deoxyglucose and carbonyl cyanide p-trifluoromethoxyphenylhydrazone (FCCP), and the second one concerning rotenone

and antimycin A (inhibitors of activated oxygen species biosynthesis from the electron transport chain and ATP synthesis); showed that these compounds inhibit Kv channels, raise cytoplasmic Ca^{2+} concentration and lead to PASMC contraction (Patel et al., 1997). Lastly, Evans et al (1994) showed that rise in intracellular ATP levels elevated the delayed rectifier K^+ current amplitude in rabbit PASMC (Evans et al., 1994).

Kv2.1 homomers have a fast open-state inactivation and a slow closed-state inactivation (Kerschensteiner, 2003). However, co-expression with Kv9.3 results in slow open-state inactivation and a fast and complete closed-state inactivation (Kerschensteiner, 2003). Although Kv9.3 is electrically silent, co-expression of Kv9.3 with Kv2.1 causes Kv2.1 to preferentially exhibit closed-state inactivation (Kerschensteiner, 2003). Activation of Kv2.1 might be crucial in preventing action potential firing in neurons. Pharmacologically, their co-expression resulted in the reduction in sensitivity to the K channel blockers, 4-AP and TEA (Kerschensteiner, 2003).

1.2.2 Two-pore domain K^+ (K2P) channels

Two-pore domain K^+ (K2P) channels were discovered relatively recently compared to the other families of K^+ channels (Goldstein et al., 2001). There are three features which make these channels unique, which are, their structure, their constitutive activation, and the regulation of their activity by various chemical and physical stimuli (Enyedi and Czirjak, 2010; Goldstein et al., 2001). There are six subfamilies, divided according to their structure and function in mammals (Enyedi and Czirjak, 2010). They are namely the TWIK (two-pore domain weakly inward rectifying K^+ channel); TASK (TWIK-related acid-sensitive K^+); TREK (TWIK-related K^+); TALK (TWIK-related alkaline activated K^+); THIK (tandem pore domain halothane-inhibited K^+); and TRESK (TWIK-related spinal cord K^+) subfamilies (Enyedi and Czirjak, 2010; Lotshaw, 2007).

1.2.2.1 Structure of K2P channels and constitutive activation

The feature which differentiates K2P family from the others is their unique structure of four transmembrane domains assembled into two pore-forming regions, hence earning them their name (Enyedi and Czirjak, 2010; Goldstein et al., 2001; Lotshaw, 2007; Mathie et al., 2010b). Secondly, they are constantly open at physiological resting membrane potential to allow K^+ ions to pass through the channels. This second feature earns them the name 'leak K^+ channels' (Goldstein et al., 2001). These 'leak currents' are subjected to little rectification (Goldstein et al., 2001). The molecular basis of this leak conductance had been elusive, but mounting evidence suggest that this conductance is fundamental to function of nerves and muscles, such as to set the resting membrane potential and input resistance in excitable cells, particularly in PASMC (Enyedi and Czirjak, 2010; Lotshaw, 2007).

1.2.2.2 Discovery of K2P channels

The discovery of K2P channels started in 1995, when TOK1 was found in the sequence database for the yeast *Saccharomyces cerevisiae*. TOK1 possess eight

predicted transmembrane segments and is the first example of a non-voltage-gated outward rectifier (Ketchum et al., 1995; Reid et al., 1996).

In 1996, *KCNK0* was cloned from the neuromuscular tissues of the adult fruit fly *Drosophila melanogaster* (Goldstein et al., 2001). *KCNK0* was able to restore the function of K^+ transport in mutant yeast cells (Goldstein et al., 2001). In contrast to TOK1, KCNK0 only has four transmembrane segments and is the first example of a canonical K^+- selective leak conductance channel. KCNK1, the first mammalian gene for a 2P/4TM subunit was also discovered but it was later found to be a non-functional channel (Goldstein et al., 2001).

1.2.2.3 Leak current

Since the early days of electrophysiology, the 'leak' current has remained a mystery (Enyedi and Czirjak, 2010; Goldstein et al., 2001). Electrophysiologists noticed that the membrane potential rises from a resting potential in order to generate an action potential and once the cell is depolarized again, the membrane potential resets itself to the resting potential again (Goldstein et al., 2001). Even at the resting potential, the ions still crosses the membrane, and ionic and electrical gradients are established (Goldstein et al., 2001). The word 'leak' is used to describe fixed background currents when the membrane is at rest and to currents that increases instantaneously with the voltage steps (Goldstein et al., 2001). These 'leak currents' can be attributable to movement of non-selective ions across membrane (in the case where the membrane is damaged) or to movement of specific ions (Goldstein et al., 2001).

When a K^+ channel is activated, K^+ ions are permitted to flow out of the cell down the K^+ concentration gradient (Goldstein et al., 2001). However, there are negative counter ions which remain inside the cells (Goldstein et al., 2001). This causes the net outflow of K^+ to only go on until the chemical energy favouring this outflow is balanced by the electrostatic energy favouring the inflow of K^+ ions (Goldstein et al., 2001). At equilibrium, the chemical and electrostatic forces cancel out each other, resulting in zero net movement of K^+ ions (Goldstein et al., 2001). Nernst potential is the membrane voltage at which a particular ion at a given ionic gradient reaches

equilibrium (Goldstein et al., 2001). For example, a hypothetical membrane that only permits the passage of K^+ ions will have a Nernst potential that is equivalent to the equilibrium reversal potential for K^+ ions, E_K, and is described by equation 1:

$$E_K = \frac{RT}{zF} \ln \frac{K_{ext}}{K_{in}}$$

Equation 1: Calculation of Nernst potential; R is the gas constant, T is temperature in degrees Kelvin, z is the charge of the ion, F is Faraday's constant, K_{ext} and K_{in} the concentrations of K^+ the external and internal compartments. Equation adapted from Goldstein et al, 2001.

For physiological K^+ concentrations at physiological temperature (37°C), RT/zF is ~27mV and E is ~–97mV (predicted to be -85mV, if taking K^+ concentration as 5mM outside and 140mM inside) (Goldstein et al., 2001). However, resting membrane potential for mammalian cells is slightly positive, ranging from –60 to –90 mV because K^+ ions are not the only ions that move at rest (Goldstein et al., 2001). Leak Na^+ and Cl^- ions move across the membrane to reach their Nernst potentials of +67 and –93 mV, respectively (Goldstein et al., 2001). The PASMC on the other hand, have even more positive range of resting potentials, ranging from -65 to -50mV (Platoshyn et al, 2004).

So, why is this leak current important? Leak current is essential in setting the resting membrane potential. Excitability of the cells is governed by whether an action potential can be fired. Only when the membrane voltage is shifted past a threshold level that an action potential is generated and this happens when the voltage-gated channels open (Goldstein et al., 2001). These channels eventually become inactive. The key thing to note is that, firing of the next action potential can only happen when these channels have recovered from inactivation by returning to the resting membrane potential, which is maintained by leak channels (Enyedi and Czirjak, 2010; Goldstein et al., 2001; Lotshaw, 2007).

1.2.2.4 Gating of K2P channels

As mentioned, another interesting feature about K2P channels is their gating mechanism (activation or inhibition) can be regulated by various chemical and physical stimuli, ranging from arachidonic acid, pH, inhaled anaesthetics and membrane stretch (Enyedi and Czirjak, 2010; Mathie et al., 2010a). Both crystallographic data and homology modelling have elucidated that all K^+ channels share a highly-conserved structure for ion selectivity and gating mechanisms (Mathie et al., 2010a). Similar to other K^+ channels, K2P channels are thought to have two primary conserved gating mechanisms: an activation gate at the intracellular entrance to the channel involving key, identified, hinge glycine residues and an inactivation (or C-type) gate at the selectivity filter close to the extracellular side of the channel (Mathie et al., 2010a).

Several activators and inhibitors interact differently with either the activation or inactivation gates of K2P channels. For example, the inhibition of *Drosophila* KCNK0 and mammalian TASK channels occurs when zinc and hydrogen ions, respectively, bind to their inactivation gate (Mathie et al., 2010a). Meanwhile, voltage dependence of TASK3 is regulated through its activation gate (Brickley et al., 2007; Mathie et al., 2010a). It remains equivocal whether other regulatory gating pathways exist, or other regulatory compounds that may interact with either the activation or inactivation gate to modulate the channels (Mathie et al., 2010a).

Family	Family members	Activators	Inhibitors
TWIK	TWIK1 (K2P 1.1)		Acid pHi
	TWIK2 (K2P 6.1)		PKC
	KCNK7 (K2P 7.1)		
TREK	TREK1 (K2P 2.1)	Acid pHi	
	TREK2 (K2P 10.1)	Acid pHo (TREK1)	
	TRAAK (K2P 4.1)	Arachidonic acid, depolarizing voltage, Gαi, heat, lysophospholipids, Nitric oxide (TREK-1), polyunsaturated fatty acids, stretch	
TASK	TASK1 (K2P 3.1)	Alkaline pHo (TASK1)	Acid pHo
	TASK3 (K2P 9.1)	Depolarizing voltage (TASK3)	Gαq
	TASK5 (K2P 15.1)		Zinc (TASK3)
TALK	TASK2 (K2P 5.1)	Alkaline pHo	
	TALK1 (K2P 16.1)		
	TASK4 (K2P17.1)		
THIK	THIK1 (K2P13.1)	Arachidonic acid	
	THIK2 (K2P 12.1)		
TRESK	TRESK (K2P 18.1)	Calcium, Gαq	Arachidonic acid

Table 1: Physiological activators and inhibitors of K2P channels. Adapted from Mathie et al (2010)

Initially, there are thought to be two primary conserved gating mechanisms of K^+ channels: an activation gate at the intracellular entrance to the channel and a distant slow inactivation gate at the selectivity filter close to the extracellular side of the channel, called the C-type inactivation (Yellen, 2002). However, a third mechanism, called the N-type inactivation also exists and this mechanism is restricted to certain Kv channels (Mathie et al., 2010a). The N-type inactivation occurs due to binding of an auto-inhibitory peptide that is part of the N terminus of the channel protein, which inhibits current flow leading to fast inactivating A-type currents (Mathie et al., 2010a; Yellen, 2002). The C-type inactivation occurs when the amino acids at the narrow selectivity filter pinch shut causing pore closure. This happens at a slower rate than N-type inactivation (Choi et al., 1991; Hoshi et al., 1991). In KcsA channels, the extent of C-type inactivation is determined by the hydrogen bonds between amino acid residues in the selectivity filter and its adjacent pore helix (Mathie et al., 2010a). The precise residues might vary in different K^+ channels, but this mechanism is generally accepted as a cognate C-type gating in other K^+ channels (Mathie et al., 2010a).

In the second mechanism, channel opens or closes depending on movement of amino acids at the intracellular entrance to the pore region (Mathie et al., 2010a). For Kv channels, the stimulus for this to occur is depolarization and the movement of the S4 transmembrane segment (Mathie et al., 2010a).

Jiang et al., 2002 have resolved the crystal structures of the closed-state bacterial channels KcsA and opened-state MthK (a calcium-gated, inwardly-rectifying, K^+ channel) in its open state and have discovered the hinge glycine residues were situated in the inner helices and that these residues bend to give way for ions passing when the channel is open. In most K^+ channels, K2P included, these residues are conserved (Jiang et al., 2002). Meanwhile, hydrogen ions inhibit TASK1 and TASK3 currents, mainly through binding to residues situated next to the GFG selectivity filter (Y. Kim et al., 2000; Lopes et al., 2005; Rajan et al., 2000). Moreover, residues in the outer pore mouth of TASK1 channels confer ion selectivity and protonation of H98 brings about ‘C-type’ gating response which causes conformational change in the selectivity filter of TASK1 (Yuill et al., 2007).

It has been suggested that K2P channels are preferentially in the open state after noticing that the mutant KCNK0, which is devoid of most of its C-terminus, still has

an activation gate and this gate possess a high single channel open probability (P_O) of 0.8 (Ben-Abu et al., 2009). The team also inferred that the reason for such high P_O is attributable to the presence of glycine residues in K2P channels (Ben-Abu et al., 2009). The role that these glycine residues play in promoting channel opening is further supported by the finding that mutation of these residues with hydrophobic residues in both KCNK0 and indeed in TASK3 caused a reduction in P_O (Ashmole et al., 2009). The situation is a little more complicated with full-length mammalian K2Ps as their resting P_O is not nearly so high (Ashmole et al. 2009).

Different amino acids at the activation gate govern different processes to influence the P0 of the channel. For example, Ashmole et al. 2009 suggested that natural alanine residue interacts with L128 in M2 region to stabilize the closed state of the channel whereas in hERG channels an equivalent alanine residue (A653) near the glycine hinge has also been shown to interacts strongly to residues in adjacent subunits to promote channel closure (Ashmole et al., 2009). In contrast, mutation of A237 to threonine stabilizes the channel open state by altering side-chain interactions between residues, possibly with N133 in M2 region (Mathie et al., 2010a).

Moreover, a region of six amino acids in TASK1 and TASK3 (VLRFLT in the case of the latter) is imperative for anaesthetic activation, methanandamide inhibition and GPCR mediated inhibition (Mathie et al., 2010a). These residues are located at the interface between the final transmembrane domain (M4) and the cytoplasmic C terminus. This region has been suggested to transduce the signal to the gate ensuing the binding of the regulatory molecule instead of being part of the gate of the binding site(s) themselves (Andres-Enguix et al., 2007; Talley and Bayliss, 2002; Veale et al., 2007). Another interesting thing to note is that this region is situated near A237 in M4, which implies that regulatory molecule affecting this region might interact with the activation gate too (Ashmole et al., 2009; Yuill et al., 2007). The closest finding to explain this hypothesis is that several researchers have noticed that TASK channels are mildly-sensitive to membrane potential and in the A237 TASK3 mutant, P_O increased dramatically at a less positive voltage compared to WT (Ashmole et al., 2009; Yuill et al., 2007).

1.2.2.5 Two-pore domain K^+ (K2P) channels implicated in the development of PH

The first clue, which pinpointed the involvement of these channels in PH, has come from the finding that TREK1 and TASK1 proteins are present in heart, and therefore could underlie the cardiac action potential (Gurney et al., 2003). This is further supported by RT-PCR, which detected several K2P channels such as TASK-1, TASK-2, THIK-1, TREK-2, and TWIK-2 are expressed in the PA, with TWIK-2 being upregulated in hypoxia and contributed to endothelial-dependent hyperpolarization (Nielsen et al., 2013). The speculation that these channels are implicated in PH may not be surprising given the fact that they are activated constitutively, even at resting conditions (Gurney et al., 2003, Lotshaw, 2007). This feature satisfies the criteria of a channel that is hypoxia-sensitive, which are: 1) The channels impeded by hypoxia will depolarize membrane only if the channel is open, 2) The channels must allow K^+ passage under resting membrane potential (Lotshaw, 2007; Nielsen et al., 2013). Functional characterization of these channels, particularly using anandamide or bupivacaine (putative TASK-1 blockers) has been shown to cause modest rise in the PA tone (Gardener et al., 2004; Nielsen et al., 2013). Recent findings have shown that several mutations of TASK-1 channels are connected with PH onset (Ma et al., 2013 and Navas Tejedor et al., 2017). Additionally, there is evidence suggesting that phosphorylation pathway, which leads to hypoxia-induced PH, are mediated through the inhibition of TASK-1 channels (Nagaraj et al., 2013; Tang et al., 2009).

1.2.2.6 TASK-1 channels

The current generated by TASK channels is pH-sensitive being inhibited by acidification due to protonation of H98, hence the name TWIK-related acid-sensitive K channel (Kim et al., 1999; Lopes et al., 2005; Lotshaw, 2007). TASK-1 was discovered first, and the TASK subfamily later expanded to include, TASK-3 (KCNK9, K2P9) and TASK-5 (KCNK15, K2P15) (Enyedi and Czirjak, 2010). TASK-1 and TASK-3 are structurally closest compared to other members, and they also behave in similar manner where endothelial cell acidification and regulation by

certain factors affect both channels in the same direction (Enyedi and Czirjak, 2010). Interestingly, TASK-2 and TASK-4 actually do not belong to the TASK family but rather to TALK family, due to low amino acid sequence resemblance to TASK1 and are more sensitive to inhibition in the alkaline pH range (Enyedi and Czirjak, 2010).

Involvement of TASK-1 channels in cardiac action potential

The first K2P channel to be cloned from a mouse cardiac cDNA library was termed cTBAK-1, and was found to be distributed primarily in the heart (Kim et al., 1999). Duprat et al., 1997 have described the TASK-1 channel and Kim et al, 1999 have found that the cTBAK-1 is similar to the aforementioned TASK-1. This spurred other researchers to speculate the link between expression of TASK-1 in heart/PASMC and heart function. However, the evidence suggesting the relative abundance of TASK-1 in the heart differs, with some investigators citing it as moderate (Duprat et al., 1999) while others finding high expression TASK-1 mRNA and protein in the heart (Kim et al., 1999; Leonoudakis et al., 1998; Putzke et al., 2007). Since TASK-3 expression has been found to be negligible (Y. Kim et al., 2000; Putzke et al., 2007), and the silent TASK-5 expression was moderate (Ashmole et al., 2001), TASK-1 is speculated to be the primary channels governing cardiac action potential (Enyedi and Czirjak, 2010). Interestingly, TASK-1 mRNA expression in rat heart increases as the rat developed from embryonic to adult stage (Liu and Saint, 2004). TASK-1 protein expression has been confirmed by Western blot and found to be localized in rat atrial and ventricular tissue (Jones et al., 2002; Li et al., 2006). Immunofluorescence with TASK-1 antibody showed that it was expressed in the intercalated disks and T-tubule network in the ventricular cardiomyocytes (Jones et al., 2002; Li et al., 2006). Studies using another TASK-1 antibody found the channel was localized throughout the myocardium during early development, but are exclusive to the electrical conduction system of the ventricles in adult mice and chicken (Graham et al., 2006). These contradicting results showed that robust immunodetection of sparsely-expressed channels is challenging compared with highly-expressed cytoplasmic proteins (Enyedi and Czirjak, 2010).

The detection of TASK-1 expression in the heart could indicate that TASK-1 is a prime candidate that underlies the cardiac background current in guinea pig ventricular myocytes, which would mean it could also control action potential duration (Backx and Marban, 1993; Jones et al., 2002). Indeed, an outward K^+ current in mouse cardiomyocytes that was perturbed by the inflammatory phospholipid, carbamyl-platelet activating factor (c-PAF), a non-metabolized analog of platelet activating factor, and showing characteristics of TASK-1 current, has been described (Barbuti et al., 2002). According to Barbuti et al, 2002, the c-PAF-inhibited current was inhibited by anandamide, methanandamide, acidosis, and Zn^{2+}. Furthermore, TASK-1 expressed in CHO cells was shown to be inhibited by c-PAF (Barbuti et al., 2002). This effect is mediated through the PAF receptors linked to the protein kinase C (PKC) pathway (Barbuti et al., 2002). The researchers hypothesized that TASK-1 has a role in PAF-induced arrhythmias, which is observed when PAF is released by polymorphonuclear leucocytes following ischemia (Barbuti et al., 2002). Other findings have supported this hypothesis where the presence of a TASK-1-like current in rat ventricular myocytes that lead to net outward current during the plateau phase of the cardiac action potential was demonstrated (Putzke et al., 2007). The same authors have also found that a novel TASK-1 inactivator increases the action potential (at 50 and 90% of total duration) (Putzke et al., 2007). However, caution has to be considered, given that the action potentials were recorded using a high, non-physiological stimulation rate (4Hz) which itself gives rise to increased action potential duration (Putzke et al., 2007).

There are also several pieces of contradicting evidence suggesting TASK-1 is either not the primary channel underlying cardiac background current nor the only channel involved. This is illustrated by the finding that pharmacological profiles of the background K^+ current in rabbit were not identical to those of TASK-1 (Gurney et al., 2003). It is well-known that cardiac action potential duration can be increased by α_{1A}–adrenergic receptors stimulation due to inhibition of a sustained outward current (Ravens et al., 1989). Secondly, outward current inhibited by the stimulation with the α_{1A}–agonist, phenylephrine was time-independent and this inhibitory effect was aborted by extracellular acidosis (Choisy et al., 2004). While acid-sensitivity is a feature of TASK-1 channel, the study concluded that acidosis had negligible effect on the phenylephrine-sensitive outward current when phenylephrine is absent, and this

current is not inhibited by TASK inhibitors such as anandamide, Zn^{2+} or ruthenium red (Choisy et al., 2004). Additionally, the estimated single channel conductance of this channel was too large (at least 78pS) compared to that of a characteristic TASK-1 channel (14pS) (Choisy et al., 2004; Kim et al., 1999). Conversely, TASK-1 could have high conductance as it was found that an outward current inhibited by another selective α_1–adrenergic receptors agonist, methoxamine, was almost obliterated at pH6 (Putzke et al., 2007). The effect of methoxamine can be counteracted by α_{1A}–adrenergic receptor blocker, 5-methyl-urapidil, thereby confirming the involvement of α_1–adrenergic receptors (Putzke et al, 2007). Interestingly, TASK-1 expressed in Chinese hamster ovary cells can also be reduced by methoxamine, strengthening the argument that the current could very well be TASK1 (Putzke et al, 2007). It was reported that α_1–adrenergic receptors couple to Gq to mediate the activation of phospholipase C, resulting in hydrolysis of phosphatidylinositol-4,5-biphosphate (PIP_2), and this finding is parallel to other studies showing that PIP_2 is a modulator of TASK channels (Lopes et al., 2005). Angiotensin II receptor which is responsible for the development of arrhythmia in the context of ischemia perfusion is also activated via the Gq-coupled receptors pathway (Charpentier, 2007).

Results described above have not allowed for a conclusion to be drawn. Several authors reported a current in the heart which is phenylephrine-sensitive and resembling the current carried by a voltage-gated K^+ channel, Slick (Bhattacharjee et al., 2003; Choisy et al., 2004). This, coupled with the fact that other K2P channels have been shown to be present in different compartments of the heart, allows for the speculation that it is likely that several other channels such as TREK1 and TWIK2 make up the cardiac background current (Liu and Saint, 2004).

TASK channels support a background current in pulmonary artery smooth muscle cells

After establishing the presence and possible involvement of TASK-1 in the heart, several researchers sought to perform molecular and functional studies of TASK-1 in the PASMC to strengthen the link of TASK-1 with PH (Gurney et al., 2010; Nielsen

et al., 2013; Tang et al., 2009). Aforementioned, the pulmonary circulation behaves differently from the systemic circulation, in the sense that the former constricts in response to hypoxia to divert blood flow to better oxygenated areas of the lung, thereby optimizing the blood perfusion and air ventilation (Gurney et al., 2010; Moudgil et al., 2006). This constriction occurs due to cell depolarization, which is brought about by inhibition of K^+ channels, opening of VGCC which causes Ca^{2+} influx (Gurney et al., 2010; Moudgil et al., 2006). The opposite occurs in the systemic circulation where hypoxia causes vasodilation. While the role of Kv channels such as Kv1.5 and Kv2.1 are well known, there is a rising consensus that K2P channels underlie a background current which could also have an important role (Gurney et al., 2010; Gurney and Joshi, 2006).

The electrophysiological data obtained from rabbit PASMC confirmed the presence of a non-inactivating K^+ current (which persisted even after inactivation of delayed rectifier) that was insensitive to glibenclamide and TEA (Evans et al., 1996). This suggests that the current is responsible for background conductance and is an important regulator of the resting potential and that these features match the description of TASK-1 (Evans et al., 1996). Since this current was insensitive to classical inhibitors of Ca^{2+} -activated K^+ channels (TEA, charybdotoxin, iberiotoxin, apamin), K_{IR} channels ($BaCl_2$) and the Na^+/K^+ ATPase (ouabain, digitoxin), as well as non-specific K^+ -channel inhibitors like quinine (0.100 M) and clofilium (1 mM; inhibits Kv1.5, TASK-2, KCNQ1), these channels can be ruled out (Enyedi and Czirjak, 2010). There are conflicting results with 4-AP, with studies showing that the extent of inhibition with this non-selective K^+ channel inhibitor to be variable (Enyedi and Czirjak, 2010).

Voltage ramp recordings in symmetrical K^+ conditions have been useful in revealing the presence of both voltage-dependent and voltage-independent properties in the current, with 4-AP shown to consistently block the former (Gurney and Joshi, 2006; Olschewski et al., 2006). This Kv current was found to be inhibited reversibly by acute hypoxia in both human and rabbit (Gurney and Joshi, 2006). This would mean the channels carrying this current can act as an oxygen sensor and hence control the membrane potential (Olschewski et al. 2006).

In other studies performed by Gurney et al, 2003, the current in question can be

modulated by hydrogen ions in the physiological range, with 50% activation at pH7.3. This observation was consistent with the properties of current in cells transfected with TASK-1 (Duprat et al. 1997; Patel et al. 1999). The resting potential of the PASMC was depolarized by 20mV at pH6.5 but hyperpolarized by mV at pH8.5 (Gurney et al, 2003). This observation further substantiates that TASK-1 underlies a background current capable of regulating the resting potential.

Other evidence supporting the notion that TASK-1 is the underlying current include pharmacological data which revealed that halothane activated, while Zn^{2+} and anandamide inhibited the current (Leonoudakis et al., 1998). Although it has been proposed that inhibition by Zn^{2+} will more likely influence TASK-3, others have confirmed that TASK-3 has a negligible presence in pulmonary arteries and therefore, TASK-3 can be ruled out (Clarke et al., 2004; Gardener et al., 2004). However, caution must be taken before jumping to the conclusion that TASK-1 is the only contributing factor. This is because there are several pieces of contradictory evidences, which showed that halothane could also sometimes inhibit the said K^+ current and anandamide at a concentration, sufficient to inhibit 90% of the TASK-1 current in heterologous expression systems could in reality only affect 25% of the said K^+ current (Maingret, 2001), where it means that there are other components which are affected.

However, this current has been found to be abolished while also leading to membrane depolarization if small interfering RNA silencing TASK-1 is applied to cells (Olschewski et al., 2006). This fosters the other findings that suggest TASK-1 is indeed the channel responsible for background conductance in PASMC and its perturbation by hypoxia is the reason for membrane depolarization (Olschewski et al., 2006). Moreover, this is in line with the role of TASK-1 as an oxygen sensor in carotid body and cerebellar granule neurons (Gurney et al, 2003).

Second compelling evidence to argue that TASK-1 is a contributor of K^+ current is through the use of microelectrode studies on intact vessels from rat (Gardener et al., 2004; Gönczi et al., 2006) rather than using isolated or cultured PASMC. The response of membrane potential due to pH changes and anandamide remained unaltered compared to isolated PASMC. Bupivacaine, a non-specific TASK channel inhibitor, still causes depolarization albeit less potently than anandamide. The

function of these inhibitors is not affected regardless of presence of classical K^+ channels inhibitors and in endothelium-free vessels (Gardener et al., 2004).

In contrast, prostacyclin is a physiological and therapeutic dilator of pulmonary arteries (Humbert et al., 2004). A prostacyclin analog, treprostinil, which is a prescribed treatment in PH is also believed to target TASK-1 as it was found to enhance PASMC current at clinically-relevant concentrations (Humbert et al., 2004). It is mediated via a mechanism involving cAMP-dependent phosphorylation (Olschewski et al., 2006). Presence of iberiotoxin does not alter the action of treprostinil on PASMC current, therefore, allowing BKCa channels to be ruled out (Olschewski et al., 2006). Interestingly, this response is abolished when small interfering RNA directed against TASK-1 was applied (Olschewski et al., 2006). In short, these data suggest that prostanoids may target a current that is carried by, or at least partially carried by TASK-1 channels.

1.2.2.7 Mutations of TASK-1 and connection with PH

Ma and colleagues (2013) have used in silico bioinformatics tools to predict deleterious mutation and have found a novel missense variant present at c.608 G→A (G203D). Furthermore, homologic modeling of hTASK-1 confirmed that G203 is present at the highly conserved second pore region of the protein, which is critical for the channel gating function (Ma et al., 2013). Another two mutations (G97R and V221L) were identified using whole-exome sequencing of probands from patients with familial pulmonary arterial hypertension (Ma et al., 2013). In addition, three novel mutations with heterozygous amino acid substitutions: T8K, E182K, and Y192C, were found during analysis of patients with sporadic pulmonary arterial hypertension (Ma et al., 2013). Alignment of the TASK-1 channel with other K2P channels reveals that most of the mutations found from their studies occurred at conserved residues that were likely to be critical for function and biophysical properties of the channel (refer topologic map in Figure 1.5) (Ma et al., 2013).

The mutation T8K occurs at the N-terminal, which is integral for TASK-1 surface expression as it is required to interact with 14-3-3 proteins in order to be transported

out of the endoplasmic reticulum (Ma et al., 2013). G97R, G203D, Y192C and E182K mutations, which are located in the pore region/ selectivity filter, are hypothesized to cause potassium selectivity defects while V221L in the TMD could affect dimerization (Figure 1.5) (Ma et al., 2013).

Electrophysiology studies confirmed that there is a reduction in K^+ channel current in these six mutant channels (T8K, G97R, E182K, Y192C, G203D, V221L), confirming that they are loss of function mutations. Because TASK-1 channel is not voltage-dependent and are open at negative potentials, these mutations probably cause depolarization of the resting membrane potential, which could lead to pulmonary artery vasoconstriction. The molecular mechanisms for loss of function probably vary according to the location of the mutation in the channel (Ma et al., 2013).

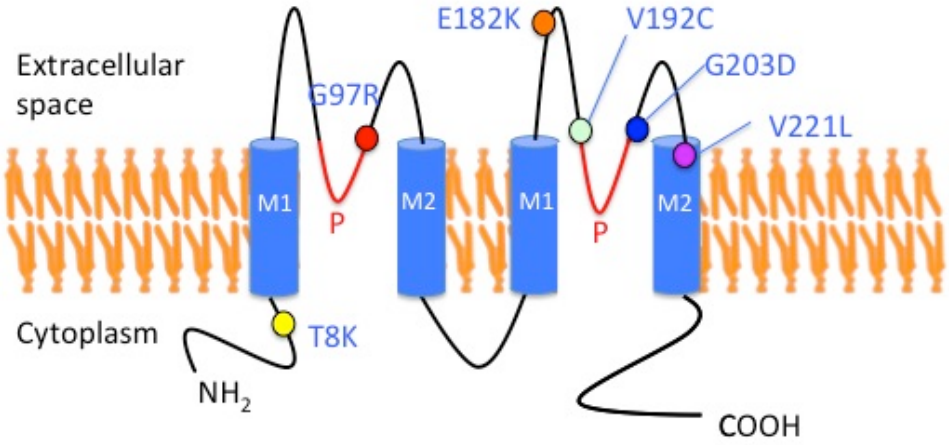

Figure 1.5: Topologic map of the TASK-1 regions where the mutated residues are situated. Sequence alignment of the TASK-1 channel with other K2P channels has revealed that these residues are highly conserved. Adapted from (Ma et al., 2013).

Besides mutations of conserved residues encoding TASK-1, Antigny and colleagues, 2016 provided evidence that reduction in TASK-1 (or KCNK3 gene) expression could lead to compromised function of TASK-1 channel in human PAH and monocrotaline-induced PH in rats. Inhibition of TASK-1 current causes membrane depolarization, which further brought about neomuscularization and other early haemodynamic events in rats that are exposed to monocrotaline (Antigny et al, 2016). Long term pharmacological activation of TASK-1 using the phospholipase A2 inhibitor, ONO-RS-082, significantly reduced PH induced by monocrotaline, as long as the activator

is given within two weeks of monocrotaline exposure (Antigny et al, 2016). This is because TASK-1 expression would be completely abolished in rats that are exposed longer than two weeks (Antigny et al., 2016).

Recently, Navas Tejedor et al, 2017 have identified two other TASK-1 mutations, G106R and L214R carried by three patients from two families. These mutations have never been identified in control populations and these patients have been confirmed not to carry any mutation in the other three genes, BMPR2, TBX4, and EIF2KA4, which are well-known for the diagnosis of PAH. Patient 1 was a Caucasian woman, carrying a missense mutation (c.766 T>G; p.L214R), who developed an aggressive form of PH at the young age of 35 (Navas Tejedor et al., 2017). Meanwhile, patient 2 was diagnosed even earlier, at the age of 2 months, with a severe form of PH and had lung transplantation at age 5 (Navas Tejedor et al., 2017). Patient 2 was a carrier of a TASK1 missense variant (c.316G>C; p.Gly106Arg) (Navas Tejedor et al., 2017). Patient 3 is patient 2's mother, a woman who was diagnosed at age 19 with PAH at advanced clinical stage (Navas Tejedor et al., 2017).

Given the fact that Patient 2 and Patient 3 belong to a high-rate consanguineous, Gypsi-Romani family, it is not surprising that SNP-based homozygosity mapping revealed that chromosome 2 which encompasses TASK-1 suffered a loss of heterozygosity (Navas Tejedor et al., 2017). The G106R mutation affects a highly-conserved amino acid through evolution and can be found in *C. elegans* and other 15 species (Navas Tejedor et al., 2017). The pathogenic consequences of this mutation have also been predicted via *in silico* analysis (Navas Tejedor et al., 2017). The mutation involved a replacement of an amino acid with aliphatic hydrophobic side chain to another with a basic side chain, with moderate to severe alterations in the physicochemical properties [Grantham distance: 125 (0 – 215)] (Navas Tejedor et al., 2017). G106 is situated in between an 'in-membrane' (aa 78-101) and 'transmembrane' (aa 108-128) regions (Navas Tejedor et al., 2017). Patient 3 was a heterozygous carrier for this G106R variant (Navas Tejedor et al., 2017). The father of Patient 2 was revealed to be an asymptomatic carrier of G106R variant, and this coupled with the fact that both father and mother carry the mutation, explained why Patient 2 is present with a homozygous TASK-1 mutation (Navas Tejedor et al., 2017). This phenomenon leads to a double-dose allele defect, has been shown to give

rise to a more severe phenotype (incomplete dominance, also known as partial- or semi-dominance) (Navas Tejedor et al., 2017).

1.2.2.8 Phosphorylation pathway which causes hypoxia-induced PH acts via TASK-1 inhibition

Meanwhile, the pathway through which endothelin-1, ET-1 inhibits TASK-1 channels has been established by Tang et al., 2009. Interestingly, similar to Kv2.1, TASK-1 activity is also sensitive to hypoxia and the metabolic state of the cells. As stated, the stimulus for ET-1 biosynthesis is hypoxia. Focusing on the pathway by which ET-1 inhibits TASK-1 channel, ET-1 binds to ETA receptors, which then activates PLC to cause PIP2 hydrolysis producing diacylglycerol (DAG) and inositol phosphate-3 (IP_3). DAG further activates PKC, which then phosphorylates the serine and threonine residues of TASK-1, to inhibit TASK-1 activity. In contrast to the inhibitory action via the PKC pathway, the activity of TASK-1 in human PASMC is activated by the cyclic AMP (cAMP)-dependent phosphorylation induced by protein kinase A (PKA). For example, prostacyclin is a well-known vasodilator and the drug treprostinil (a stable prostacyclin analogue) activates TASK-1 via this pathway. When applying the cAMP analogue, 8-bromo-cAMP, an endogenous PKA activator, the same activation can also be achieved (Ma et al., 2013).

Lastly, Nagaraj et al (2013) have shown that TASK-1 colocalized with the Src family tyrosine kinase (SrcTk) (Nagaraj et al., 2013). During normoxia, the Src is phosphorylated at Tyr419 rendering an active Src, which then binds to TASK-1. This interaction is important for TASK-1 activity to maintain negative resting membrane potential in hPASMC. Under hypoxia, most Src will assume a closed configuration where its Tyr530 is phosphorylated and this prohibit its interaction with TASK-1. This causes a decrease in TASK-1 current, rise in intracellular Ca^{2+} concentration and subsequently PASMC depolarization.

In summary, TASK-1 orchestrates an important role in controlling the Ca^{2+} influx into PASMC and maintaining low vascular tone. Further experiments to reveal about the

function and regulation of this channel will provide insights to pathomechanisms of PH.

1.3 AMIGO proteins

1.3.1 Discovery of the AMIGO family

In order to look for genes that are involved in neurite outgrowth on HMGB1 (Amphoterin) substratum, Kuja-Panula et al, 2003 used ordered differential display (ODD) and discovered the amphoterin-induced gene and open reading frame (AMIGO) family (Chen et al., 2006; Kuja-Panula et al., 2003). As the name suggests, the expression of these genes is induced by amphoterin (HMGB1) substrate. They have hypothesized that the gene expression could be driven by the binding of HMGB1 to receptor of advanced glycation end products (RAGE), a well-known cell surface HMGB1 receptor (Chen et al., 2006).

AMIGO family comprises of AMIGO1, AMIGO2 and AMIGO3. Kuja-Panula et al, 2003 have identified AMIGO2 and AMIGO3 by using AMIGO amino acid sequence to look for other homologous proteins, with the homology between family members being 50-58% (Kuja-Panula et al., 2003). Meanwhile, two other groups have identified AMIGO2 independently and have designated it as Alivin1 and DEGA (Rabenau et al, 2004) respectively (Ono et al., 2003; Rabenau et al., 2004).

The AMIGO family encodes a type-I transmembrane protein with six leucine-rich repeats (LRR) motifs (explained below) and a single Ig domain (Figure 1.6 and Table 2). Figure 1.7 depicts the relationship between AMIGO family and other type 1 transmembrane LRR and Ig-like domain and/or FN-III domain containing proteins, together with a number of other brain-enriched LRR-containing proteins (such as OMgp, the Nogo-66 receptor paralogues NgR, NgR2 and NgR3 and Slit). The LRR motifs most closely resembles those in Slit (Whitford et al., 2002) and the Nogo receptor (Fournier et al., 2001) protein families, which are neuronal LRRs. The Ig domain is similar to the immunoglobulin V-set motifs that can be found in T-cell receptors and adhesion junction molecules (Kuja-Panula et al., 2003). The presence of

LRR and Ig domains, coupled with the fact that AMIGO1 is overexpressed during neurite outgrowth, suggest that AMIGO1 plays a role in cell adhesion and supports neurite outgrowth (Kuja-Panula et al., 2003; Ono et al., 2003; Rabenau et al., 2004).

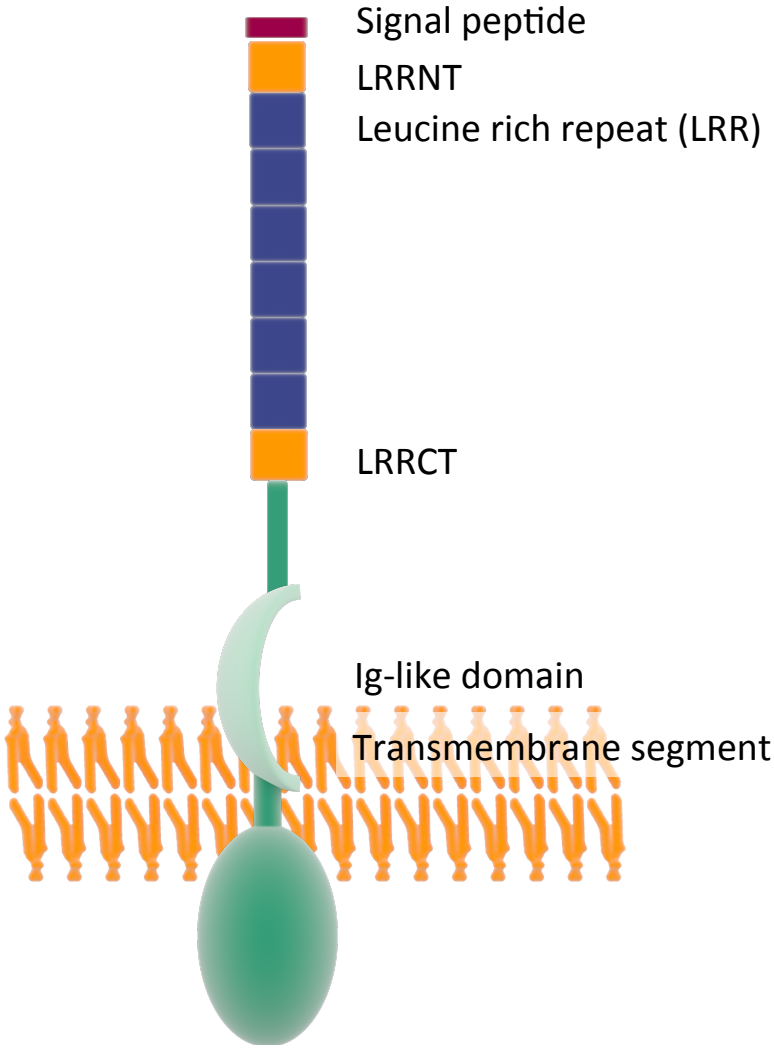

Figure 1.6: Schematic diagram of AMIGO1. Adapted from Chen et al., 2006.

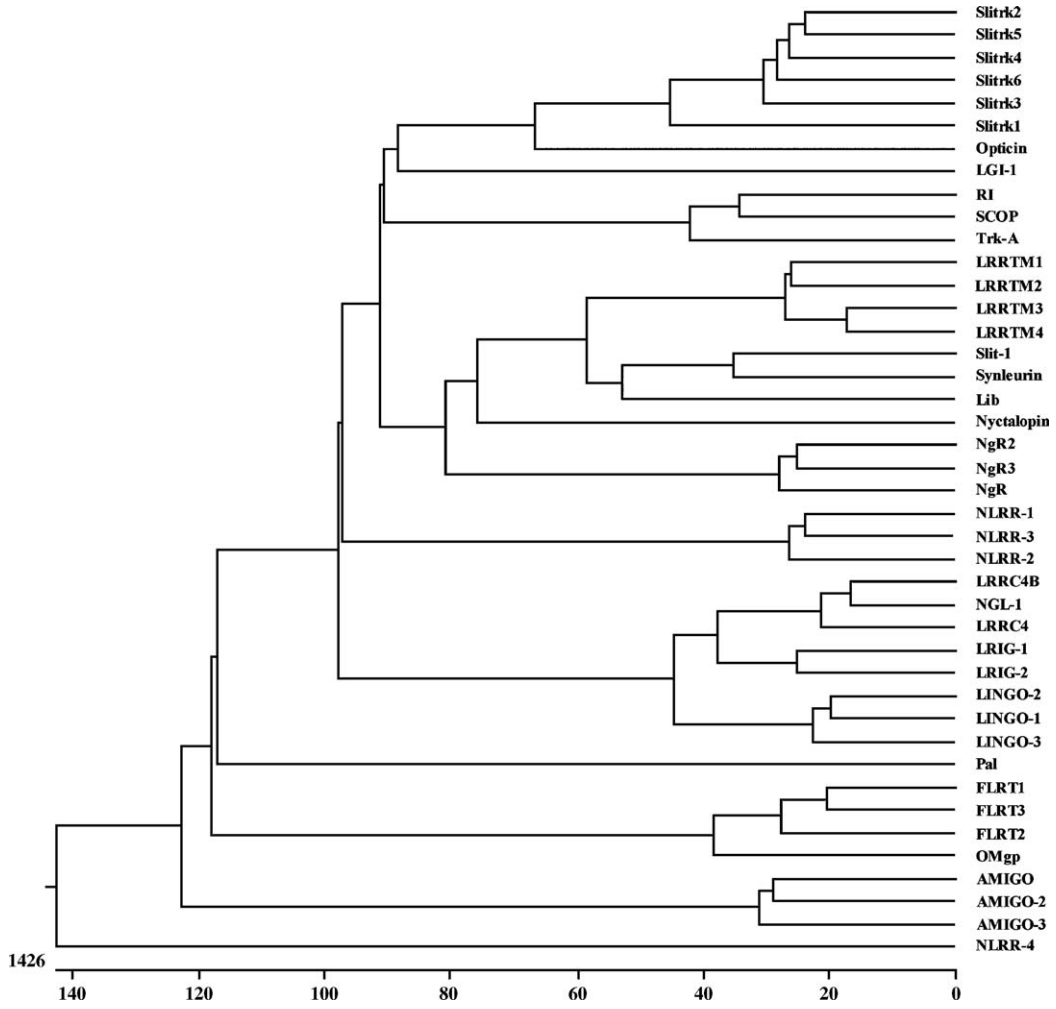

Figure 1.7: Nearest neighbour dendrogram showing the relationship between AMIGO family and the other type 1 transmembrane LRR and Ig-like domain and/or FN-III domain containing proteins, together with a number of other brain-enriched LRR-containing proteins (such as OMgp, the Nogo-66 receptor paralogues NgR, NgR2 and NgR3 and Slit). Nyctalopin (a gene mutated in congenital stationary night blindness) and suprachiasmatic nucleus circadian oscillatory protein (SCOP, a brain-enriched protein which interacts with K-Ras. Opticin is a small LRR proteoglycan expressed exclusively in the eye while synleurin is a ubiquitously expressed LRR-containing transmembrane protein which when ectopically expressed in cells intensifies their response to cytokines. LRRC4 (or NAG14) and LRRC4B (or HSM802162) are paralogues of NGL-1. Interestingly, LRRC4 has been shown to be exclusively expressed in the brain, is downregulated in brain tumor tissues and may have a role in suppression of CNS tumors. Ribonuclease inhibitor (RI) contains the prototypic LRR domain and is included for comparison. In the databases, one encounters various nomenclatures and annotations that may point to the same gene. According to the nomenclature of the Mouse Genome Informatics (MGI), NLRR1–NLRR3 corresponded to the genes officially annotated as LRRN1–LRRN3. LRRN4 (not shown) is similar in sequence with leucine-rich (LR) repeats and calponin homology (CH) domain containing 4 (LRCH4). LRRN5 is GAC-1 as mentioned in the text. LRRN6A is LINGO-1, LRRN6B is LINGO-3, and LRRN6C is LINGO-2 while LRRN6D is LINGO-4. A human NLRR-5 clone is actually LINGO-2. Adapted from Chen et al, 2006.

Interestingly, the short cytosolic tail (99 amino acids) has been well conserved during mammalian evolution, with the human AMIGO having 96% resemblance with the Placental and 90% with the Marsupial AMIGO sequences. This observation led Kuja-Panula et al, 2003, to believe that this cytoplasmic tail might have important function even though this function is yet to be determined. (Kuja-Panula et al., 2003)

	Discovery	Isoforms/ Paralogues/ Homologues	Tissue distribution	Known function in neurons/ Effect on neurons
AMIGO/ Alivin	Amphoterin and RAGE signalling induced transcript	AMIGO1, AMIGO2, and AMIGO3	All found in brains, AMIGO is more exclusively enriched in hippocampal formation	Substrate-bound AMIGO ectodomain promote neurite extension in hippocampal neurons
LINGO	Found to interact with NGR to form a ternary complex with p75 or TAJ/TROY	LINGO 1-4	LINGO-1 is enriched in CNS. LINGO 2-4 have wider distribution.	Neurite outgrowth inhibition (functioning together with NgR and p75/Taj)
NGL-1	Interaction with Netrin G1	LRRC4 (AF196976), LRRC4B (AL137451)	NGL-1 is exclusively enriched in brain	Substrate-bound NGL-1 stimulates growth of embryonic thalamic neurons
NLRR	Library screening with LRR domain probe	NLRRs 1-4	All found in brain, NLRR2 and NLRR3 exclusively brain-enriched	NLRR-3 upregulated in neuronal injury, NLRR-4 has role in hippocampal dependent memory retention
FLRT	Serendipitous discovery while screening for muscle extracellular matrix genes	FLRTs 1-3	All found in brain but only FLRT1 is exclusively brain-enriched	FLRT3 promotes neurite outgrowth of cerebellar granule neurons

Table 2: Site of expression and function of several LRR/Ig-domains containing protein families including AMIGO. Adapted from Chen et al, 2006

Kajander et al, 2011 has resolved the crystal structure of AMIGO1 and suggested that the AMIGO1 monomer has a curved structure, where the convex face is made of alpha-helices and the concave face is made of beta-sheets (Figure 1.8) (Kajander et al., 2011). AMIGO1 also exists as a dimer, where the concave face is the site of interaction (Figure 1.8). AMIGO1 is heavily glycosylated, where it has been proven to have five glycosylation sites, as predicted *in silico* (Kuja-Panula et al., 2003). These five sites (two sites from the LRR region and three sites from the Ig domain) are conserved from teleost to mammals (Kuja-Panula et al., 2003). The three glycosylation sites presumably serve to drive the protein into the right conformation for dimerization with another AMIGO1 (Kuja-Panula et al., 2003).

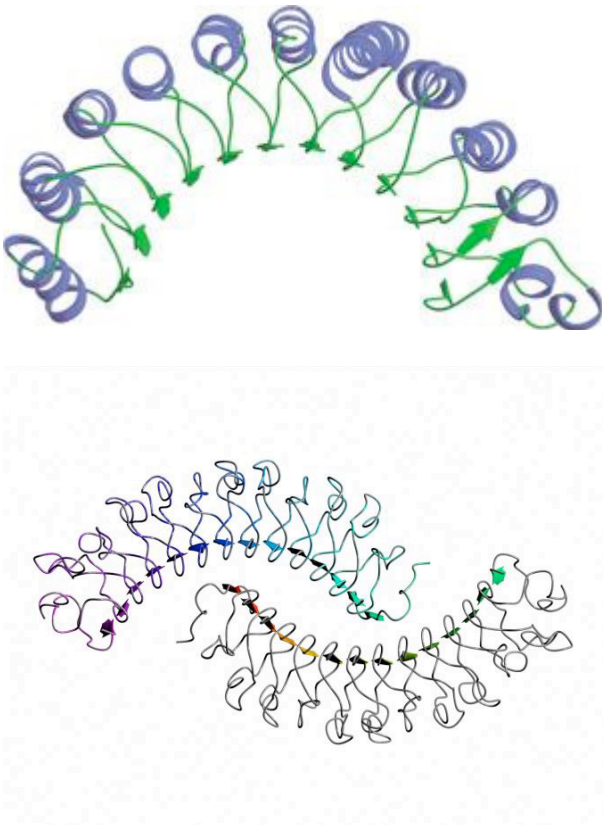

Figure 1.8: AMIGO1 monomer (Above), AMIGO1 dimer (Below). Adapted from Kajander et al, 2011.

1.3.2 Expression of the AMIGOs in mouse tissues

RT-PCR analysis performed in adult mouse tissues revealed that AMIGO1 is almost exclusively expressed in central nervous system (CNS) or nervous tissues (cerebellum, cerebrum, and retina) (Kuja-Panula et al., 2003). While AMIGO2 and AMIGO3 are also enriched in the brain, they have a wider distribution pattern (Kuja-Panula et al., 2003). AMIGO2 has the highest expression in lung, liver, cerebellum and retina and is present at a detectable level in cerebrum, kidney, small intestine, spleen, and testis (Kuja-Panula et al., 2003). Interestingly, AMIGO3 does not have a specific expression distribution compared to its counterparts (Kuja-Panula et al., 2003). Relevant to pulmonary hypertension, AMIGO2 and AMIGO3 are expressed in the lungs while AMIGO3 is expressed in the heart (Figure 1.9) (Kuja-Panula et al., 2003). Genomic sequence data suggest that these three proteins are probably present in the puffer fish *Fugu rubripes* (Kuja-Panula et al., 2003). The extracellular parts of AMIGO family has also been demonstrated to be similar to Kek protein family

(encoded by kekkon genes) found in *Drosophila* (Musacchio and Perrimon, 1996). Their extracellular parts consist of six LRR motifs with cysteine-rich LRRNT and LRRCT domains and one Ig domain near the transmembrane region. However, there is no homology in their cytoplasmic parts (Kuja-Panula et al., 2003). In addition, AMIGO2 also displays homology to Trk families (Kuja-Panula et al., 2003).

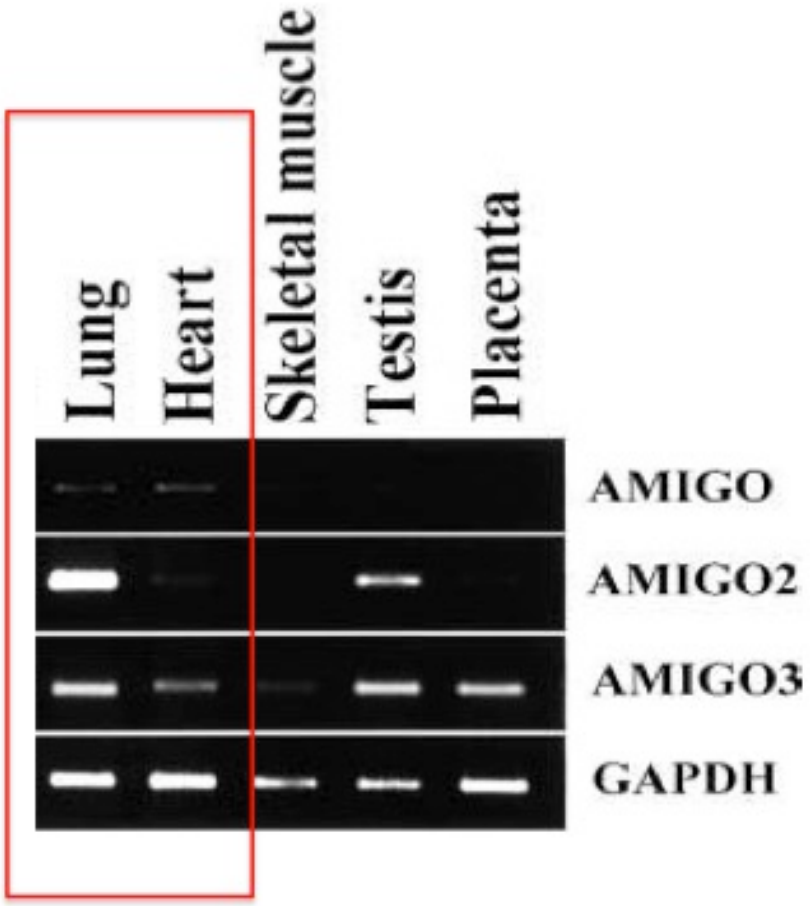

Figure 1.9: mRNA expression of AMIGO1-3 in various tissues. Red box indicates the site of expression of AMIGOs of interest in PH. Adapted from Kuja-Panula et al, 2003

1.3.3 AMIGO1

AMIGO1 expression was further studied at mRNA level using in situ hybridization and at protein level. Consistent with aforementioned, AMIGO antisense probe emitted a strong signal in both developing and adult nervous tissues (Kuja-Panula et al., 2003). The signal was already detected in the E13 rodent embryo, at dorsal root ganglia, trigeminal ganglion, and CNS (Kuja-Panula et al., 2003). AMIGO1 was highly expressed in brain (strongest signal in the hippocampus) at later stages of development and in adult (Kuja-Panula et al., 2003).

Polyclonal antisera against the extracellular 10-amino acid peptide sequence that is unique in AMIGO1 (not found in AMIGO2 and AMIGO3) were raised (Kuja-Panula et al., 2003). The anti-peptide antibodies identified the 75-kD AMIGO1-Ig fusion from *Drosophila* S2 cells and a 65-kD AMIGO1 polypeptide from crude brain extracts (Kuja-Panula et al., 2003).

AMIGO was identified in the search for a gene that is induced by amphoterin to promote neurite outgrowth in the hippocampal neurons (Kuja-Panula et al., 2003). Another clue that could further prove the hypothesis that AMIGO is directly involved in neurite extension is the presence of LRRs and Ig domains in the proteins, which are well-known motifs involved in this role (Kuja-Panula et al., 2003). Moreover, AMIGO is present *in vivo* in fibre tracts, where neurite growth is prominent (Kuja-Panula et al., 2003; Peltola et al., 2011; Zhao et al., 2014). Kuja-Panula et al, 2003, established that AMIGO is indeed involved, by showing that a fusion protein (containing the extracellular part of the AMIGO and a human IgG Fc part) immobilized to a microtitre well plate promotes the adhesion and neurite growth of hippocampal neurons, compared to the control where only the human IgG Fc portion was present. (Kuja-Panula et al., 2003) After 24 hours of culturing the rat hippocampal neurons *in vitro* onto the AMIGO extracellular matrix, neurite outgrowth was already evident (Kuja-Panula et al., 2003). When plated for four days, ‘fasciculation’, where neurites grow alongside each other by using pioneer axons as the substratum for their growth cones, occurs (Kuja-Panula et al., 2003). Interestingly, neurite outgrowth was inhibited in the presence of the soluble AMIGO-Ig fusion in the culture medium (Kuja-Panula et al., 2003). Therefore, there is a differential regulation of neurite outgrowth depending on the form of AMIGO (whether in an

immobilized matrix form or in soluble form). The same experiments were also repeated *in vivo* in Zebrafish CNS, where the knockdown of endogenous AMIGO or the dominant negative approach using the AMIGO ectodomain caused disrupted fasciculation of the medial longitudinal fasciculus (MLF) and post optic commissure (POC) fibre tracts, which are also sites where AMIGO is highly expressed during Zebrafish CNS development (Zhao et al., 2014). The reason for the difference in the ability of AMIGO1 to cause fasciculation when in ECM or soluble form might indicate that the protein is part of a signalling pathway, where downstream mediators of neurite extension are not activated if AMIGO1 is not forming a scaffold to support them (Kuja-Panula et al., 2003; Zhao et al., 2014).

Next, Kuja-Panula et al., 2003 determined whether the AMIGO proteins require a homophilic or heterophilic binding to support neurite outgrowth. Using the bead aggregation assay, they have demonstrated that inhibition of homophilic binding of the AMIGOs between adjacent neurites will cause defasciculation. However, the proteins also have heterophilic binding properties, which suggest that they might have a cooperative role during development and in adult mammals (Kuja-Panula et al., 2003).

1.3.3.1 Colocalization of AMIGO1 with Kv2.1

Staining of adult mouse CNS and mature in vitro hippocampal neurons with specific anti-AMIGO antibody showed that the AMIGO was found in cell soma and proximal part of neurites (Peltola et al., 2011). Closer observation revealed that AMIGO is expressed in punctate/ ring-like clusters (Peltola et al., 2011). Another protein that could have such peculiar staining pattern is Kv2.1 (Peltola et al., 2011). From this finding, Peltola et al, 2011 sought to double-stain the neurons with both AMIGO and Kv2.1 and they discovered that these two proteins are co-localized. The two proteins were also co-localized when they were expressed in heterologous system, confirming that they have similar temporal expression (Peltola et al., 2011). Dephosphorylation causes dispersion of Kv2.1 around cell membrane (Misonou et al., 2004). There are two notable stimuli which could induce dephosphorylation, namely hypoxia and glutamate treatment (Misonou et al., 2004). Misonou et al, 2004 have demonstrated

that CO_2 treatment induced a reduction in the molecular mass of Kv2.1, due to dephosphorylation of the protein. This is confirmed by the Western blotting of Peltola et al, 2011 where the size of Kv2.1 decreased from 125 to 100 kDa after being treated with CO_2 (Peltola et al., 2011). Strikingly, this does not prevent AMIGO protein from coimmunoprecipitating with the dephosphorylated, smaller form of Kv2.1 (Peltola et al., 2011). To visualize the dispersion pattern of Kv2.1 and to determine whether AMIGO1 will display the same expression pattern, brain slices from CO_2-treated mice were immunostained (Peltola et al., 2011). It was found that the AMIGO1 and Kv2.1 were diffused in cortical neurons, yet the staining of both proteins was still concentrated in the soma and the proximal part of neurites (Peltola et al., 2011).. This colocalization pattern was also preserved in cultured cortical neurons that have been treated with glutamate (Peltola et al., 2011). This shows that AMIGO1 and Kv2.1 are very tightly coupled regardless of stimuli-induced dephosphorylation of Kv2.1 (Peltola et al., 2011).

When studying the evolutionary conservation of AMIGO-Kv2.1 interaction from fish to mammals, Zhao et al, 2014 found that, AMIGO1 is mostly expressed in the anterior dorsal part of the forebrain area of 28-hour post fertilization Zebrafish larvae (Zhao et al., 2014). This is similar to the expression pattern of a 10^{th}-day mouse embryo. In adult zebrafish larvae (5-days post fertilization), AMIGO1 expression was detected in most brain areas that have functionally active neural circuits (Zhao et al., 2014). Again, this finding is similar to the situation in rodents, where AMIGO1 is found in postnatal brain during construction of the adult-type circuitry and is found in practically all areas of the CNS in most neurons and their fibers in young adults (Kuja-Panula et al., 2003; Peltola et al., 2011). These results could indicate that AMIGO1 is part of the Kv2.1 channel complex and this interaction has evolved since 450 million years ago (Kuja-Panula et al., 2003).

1.3.3.2 AMIGO1 changes voltage-gating properties of Kv2.1

After demonstrating that AMIGO1 and Kv2.1 are colocalized and this colocalization is even maintained following Kv2.1 dispersion due to stimulation by glutamate or dephosphorylation (Peltola et al., 2011), could AMIGO1 have an impact on the function of Kv2.1? Peltola et al, 2011 sought to address the possibility of AMIGO1 influencing the voltage-dependent activation of Kv2.1 and neuronal delayed rectifier current (Ik) (Peltola et al., 2011). They transfected HEK293 cells with either Kv2.1 alone or in combination with AMIGO1 and recorded currents in the whole-cell voltage-clamp configuration. They have assessed current amplitudes and IV relationships of Kv2.1 and Kv2.1/AMIGO1. While there are no changes in current amplitudes between the two at the maximal membrane depolarization voltage tested (+100mV), AMIGO1 dramatically increased the current at voltages from -40mV to +20mV (Peltola et al., 2011). The effect of AMIGO1 on Kv2.1 was most significant at the threshold of activation. When Kv2.1 was expressed alone, the cells were activated at around -20mV (Peltola et al., 2011). Similar to Kv9.3, AMIGO1 causes the Kv2.1 channels to be activated at a more hyperpolarized potential (Kerschensteiner, 2003; Peltola et al., 2011). Kv2.1/AMIGO1 current was already three-folds higher than Kv2.1 current at -20mV (Peltola et al., 2011). Control cells, which were transfected with Kv2.1 and a non-related type-1 transmembrane protein, NCAM, showed that currents were not affected by NCAM presence (Peltola et al., 2011).

The group further characterized the electrophysiological properties of Kv2.1 and AMIGO1 using a tail current protocol. Normalized conductance-voltage relationships reiterated their findings with the voltage-steps protocol, where AMIGO shifted the Kv2.1 activation to a more negative voltage (Peltola et al., 2011). It would be interesting to investigate if Kv2.1 channels will be activated even earlier when both AMIGO and Kv9.3 are present or when Kv9.3 is already heteromerized with Kv2.1, what effect will AMIGO have on the Kv2.1 current.

As highlighted earlier, the cytoplasmic tail of AMIGO was hypothesized to be important since it was evolutionarily-conserved yet its function is yet to be determined (Kuja-Panula et al., 2003). Peltola et al, 2011 have elucidated the role of

various parts of the AMIGO protein, namely the extracellular, transmembrane, and cytosolic domains by swapping each of them with NCAM counterparts to produce a fusion protein (Peltola et al., 2011). The effect of AMIGO in shifting the Kv2.1 current to a more hyperpolarized potential was abrogated when the transmembrane domain was swapped (Peltola et al., 2011). When the extracellular and cytoplasmic domains were swapped, AMIGO efficacy was reduced (Peltola et al., 2011). This suggests that the transmembrane domain could be the interaction site of Kv2.1 (Peltola et al., 2011). However, the extracellular and cytoplasmic domains are also important for the Kv2.1 modulation properties yet the mechanism through which they act is yet to be determined.

While the AMIGO1-Kv2.1 interaction is proven, there is a possibility that other factors could be involved to assist AMIGO1 in modulating Kv2.1 function. (Kuja-Panula et al., 2003; Peltola et al., 2011) Further experiments to address this would be necessary.

1.3.3.3 Inhibition of AMIGO1 in cultured neurons changes voltage-gated potassium currents

To provide the evidence that AMIGO1 is important in modulating the voltage-gated K^+ currents native cells, the group used short hairpin RNA/ inhibitory RNA in mature 14-day old *in vitro* cultured hippocampal neurons (Peltola et al., 2011). At potentials from -40 to -20mV, neurones where endogenous AMIGO1 is inhibited showed a 39-47% decrease in delayed rectifier current compared to controls (Peltola et al., 2011). At potentials over -10mV, the current closely resembles that of control. At -20mV, the average current densities of the AMIGO1-inhibited cells (5.13 ± 0.67 pA/pF) were also smaller than that in control cells (8.38 ± 1.25 pA/pF) (Peltola et al., 2011).

One might suspect that hippocampal neurones may contain several different Kv channels, which might contribute to the delayed rectifier current, instead of Kv2.1 alone (Peltola et al., 2011). To address this, the group treated the neurons with a specific Kv2.1 blocking agent named guangxitoxin (GxTX-1E) (Herrington et al.,

2006; Peltola et al., 2011). Similar to the inhibitory RNA experiment finding, the Kv currents were dramatically altered, confirming that the experimental setup of the group partially addressed this limitation (Peltola et al., 2011). The result obtained from neurons where AMIGO is inhibited is opposite to neurons with overexpression of AMIGO (Peltola et al., 2011). This confirmed the hypothesis that AMIGO is an auxiliary subunit of Kv2.1 (Peltola et al., 2011).

In experiments performed in Zebrafish, Zhao et al, 2014 looked at whether the inhibition of Kv2.1 in AMIGO1 knockdown morphants created using morpholino oligonucleotides could be rescued by restoring Kv2.1 protein expression by co-injecting Kv2.1 mRNA with the morpholino oligonucleotides. Although the rescue effect was not obvious in defects of early (1-5dpf) tract development, there were clear rescue effects in behavioural phenotypes indicative of functionally active neural circuitries (Zhao et al., 2014). Where Kv2.1 is restored, anatomical connectivity was restored to a level sufficient to perform normal sensorimotor functions (Zhao et al., 2014). The lack of rescue effect in the early tract development could be explained by the fact that AMIGO1 and Kv2.1 do not colocalize, even though they are both expressed, in early developing brain (Zhao et al., 2014). In mature brain however, these two proteins colocalize (Zhao et al., 2014).

1.3.3.4 AMIGO1 regulates Kv2.1 protein expression and voltage-gated potassium currents

Besides studying the AMIGO1-Kv2.1 interaction in heterologous expression system (HEK-293 cells) and in Zebrafish, this interaction has also been studied *in vivo* in mammals using an AMIGO-knockout mouse line (Peltola et al., 2016). The mice bred normally without any visible signs of defects in normal caged environment, with no appreciable difference observed in Luxol fast blue/cresyl violet staining and immunohistochemical staining with common markers for neurons and glia between knockout (KO) and wild type (WT) mice (Peltola et al., 2016). However, there is a remarkable reduction in Kv2.1 staining in adult mouse brain sections of KO mice (Peltola et al., 2016). The extent of staining was quantified to be 45% less in KO

mice when Western blotting with samples made from adult mouse brain membrane was performed (Peltola et al., 2016). As a control, Western blot was performed to quantify Kv1.2 band intensity and there was no difference between WT and KO (Peltola et al., 2016).

1.3.3.5 AMIGO1 KO mice displayed disrupted complex behavioural traits, possibly due to lack of AMIGO-Kv2.1 interaction

Similar to the findings in *in vitro* systems, Peltola et al., 2016 reported a reduction in the Kv currents at negative membrane potentials around the action potential threshold in AMIGO KO mice. As with the hippocampal neurons, there are several types of Kv channels expressed in the pyramidal neurons. The group suspected that the phenomenon where AMIGO KO mice exhibiting the current reduction can be explained by Kv2.1 dysfunction due to lack of AMIGO/Kv2.1 interaction (Peltola et al., 2016).

1.3.3.6 AMIGO1 knockout mice have altered complex behavioural traits that resemble schizophrenia

While AMIGO KO mice displayed normal traits in nociception and motor co-ordination, studies of more complex behavioural traits revealed some differences (Peltola et al., 2016). AMIGO KO mice travelled more (158%) in the open field test arena, in a given test period compared to their WT littermates which suggests that the AMIGO KO mice are hyperactive (Peltola et al., 2016). When AMIGO KO and WT mice were treated with a low dose of the psychotomimetic drug, MK-801, the hyperactivity phenotype was significantly increased in the KO mice, while there was no apparent difference in WT mice (Peltola et al., 2016). These observations were also confirmed in AMIGO-deficient Zebrafish larvae (3dpf). This could explain that compromised AMIGO-Kv2.1 interaction might lead to hyperactivity (Peltola et al., 2016).

Secondly, AMIGO1 KO mice showed reduced sensorimotor gating compared to WT mice (Peltola et al., 2016). Sensorimotor gating allows animals to automatically filter out non-related information from important information (Powell et al., 2012). This is important for animals to cope in a complex environment (Powell et al., 2012). This gating ability was be assessed by measuring the startle response of an animal during prepulse inhibition (PPI) (Powell et al., 2012). PPI is a phenomenon whereby a weaker prestimulus (prepulse) blocks the reaction of an organism towards a subsequent stronger startling stimulus (pulse) (Powell et al., 2012). Strikingly, the observation of PPI deficit is well-known in schizophrenia patients (Powell et al., 2012). This effect of PPI reduction can be remedied by the antipsychotic drug haloperidol (Kumari and Sharma, 2002). Treating the AMIGO1 KO mice with haloperidol shifted their PPI to normal values observed in their WT counterparts (Peltola et al., 2016).

In order to test the difference in social behaviours between WT and AMIGO1 KO mice, Peltola et al, 2016 have employed two tests; the resident intruder test and the tube test. The resident intruder test assesses how well the mice cope with social stress while the tube test determines dominant and subdominant behaviour (Peltola et al., 2016).. While WT and AMIGO1 KO mice showed no difference in the resident intruder test, AMIGO1 KO mice lost significantly more trials than WT mice, suggesting that AMIGO1 deficiency contributes to a subdominant behaviour (Peltola et al., 2016).

Lastly, the memory consolidation tests were performed to investigate the difference between WT and AMIGO1 KO mice (Peltola et al., 2016).. Initially, the group employed the Morris water maze for the purpose but upon finding no difference between WT and AMIGO1 KO mice, they proceeded to use an IntelliCage to study memory consolidation more closely (Peltola et al., 2016). IntelliCage allows the screening of several cognitive and behavioural traits of mice living in social groups (Peltola et al., 2016).. One of the tasks assessed was ‘patrolling’ where a mouse has to learn that the ‘correct’ corner is changed in a clockwise manner after every ‘correct’ visit (Peltola et al., 2016).. Similar to the 8-arm radial maze, ‘patrolling’ serves to measure behavioural flexibility and working memory (Too et al., 2014). Peltola et al.,

2016 reported that the AMIGO1 KO mice showed memory deficiency while performing this task.

1.3.3.7 Behavioural changes in AMIGO1-knockout mice resemble schizophrenia

Taken together, AMIGO1 KO mice displayed the four main behavioural features of schizophrenia, which are hyperactivity, PPI deficit, subdominant behaviour and memory deficiency (Gainetdinov et al., 2001; Huang et al., 2014; Papaleo et al., 2012). This is possibly not surprising considering that the mouse AMIGO2 (*ali1)* was mapped to a locus 55.3 cm from the centromere on chromosome 15 that is syntenic to positional candidate loci for familial Alzheimer's disease type 5 and Parkinson's disease 8 on human chromosome 12 (Ono et al., 2003).

This finding led Peltola et al., 2016 to speculate that the human AMIGO1 gene is a potential candidate gene for schizophrenia. In the adult human CNS, AMIGO might be an important component to fine-tune Kv2.1 function and loss of AMIGO and hence of Kv2.1, could lead to neurons overexcitability, which in turn could cause an overactive CNS (Peltola et al., 2016). Several research groups have published evidences that hyperactivity in different brain areas controlling different functions is linked with schizophrenia (del Pino et al., 2013; Huffaker et al., 2009; Suh et al., 2013). Coincidentally, Speca et al., 2014 have shown that Kv2.1 deficiency in mice also displayed hyperactive behaviours comparable to the ones observed in AMIGO1 KO mice. This further strengthens the notion that AMIGO1 mediates its function through Kv2.1.

While the role of AMIGO1 has been extensively researched in the brain, the roles of AMIGO2 and AMIGO3 remain underexplored. The electrophysiological and behavioural alterations due to interrupted AMIGO1-Kv2.1 interaction are striking. It would be interesting to probe as to whether disrupted AMIGO2- and AMIGO3-Kv2.1 could result in significant changes in the pulmonary vasculature.

1.3.4 AMIGO2

As mentioned above, Ono et al, 2003 discovered AMIGO2 separately from Kuja-Panula et al, 2003 and have designated AMIGO2 as Alivin1 (ali1), after "alive" and "activity-dependent leucine-rich repeat and Ig superfamily survival-related protein". Interestingly, the mRNA expression of ali1 in cultured cerebellar granule neurons are upregulated by high (25mM) KCl and/or NMDA concentrations and inhibited by low (5mM) KCl concentration in the culture medium, which triggered apoptosis (Ono et al., 2003). The upregulation could be explained by the observation that when cells were stimulated by 25mM KCl, Ca^{2+} influx through voltage-dependent L-type Ca^{2+} channels was permitted (Experimented using nifedipine, a specific antagonist for voltage- dependent L-type Ca^{2+} channels) (Ono et al., 2003). These results indicate that ali1 mRNA expression is tightly linked with the depolarization-dependent survival and/or NMDA-dependent survival state of the granule neuron (Ono et al., 2003).

Besides Ono et al, 2003, another group, Rabenau et al, 2004 also discovered AMIGO2 which they designated as DEGA, after "differentially expressed in human gastric adenocarcinomas". DEGA encodes a protein with a signal peptide, five leucine-rich repeat motifs, and a single IgG and transmembrane domain (Rabenau et al., 2004). Similar to the finding of Kuja-Panula et al., 2003 and Ono et al., 2003, they have reported that the function of the cytosolic domain of the protein is still unknown. Since an algorithm analysis revealed that approximately one-fifth of the residues are either serine or threonine, they have postulated that this might be a docking site for signalling pathway intermediates and thus AMIGO2 might be important for signal transduction via the phosphorylation pathway (Rabenau et al., 2004).

In Rabenau et al, 2004's studies, ~45% of tumor has reduced DEGA/AMIGO2 mRNA expression compared to normal tissue from gastric adenocarcinoma patients. To further confirm their observation, they have performed a gene-silencing study by establishing a DEGA/AMIGO-2 antisense construct in the gastric adenocarcinoma cell line (AGS) and found that cells where the AMIGO2 gene is silenced displayed morphology change, increased ploidy, chromosomal instability, reduced cell adhesion to and migration through collagen (Rabenau et al., 2004).

Interestingly, AMIGO2 suppression also led to inhibition of tumourigenicity in nude mice although the mechanism is not fully understood (Rabenau et al., 2004). A reason proposed by the group based on Kuja-Panula et al, 2003 and their findings is that AMIGO2 might be important for tumor adhesion since it acts as a cell adhesion signalling molecule. And when the adhesion process is jeopardized, the tumor fails to develop (Rabenau et al., 2004). This hypothesis drew similarity to the finding of Mafune and Ravikumar, 1992 where silencing of laminin-binding protein expression inhibits the adhesion and invasion in a human colon carcinoma cell line. Conversely, the loss of E-cadherin (also an adhesion molecule) in gastric cancer cells lead to metastasis (Rabenau et al., 2004). This could mean that AMIGO2 might be needed for metastasis (Rabenau et al., 2004). The third hypothesis stems from the fact that AMIGO2 silencing renders chromosomal instability, which could further inhibit several genes that are needed for tumorigenicity of AGS cells (Rabenau et al., 2004). An evidence supporting this would be the finding that cells with extra copies of the X chromosome and chromosome 18 that carry the ING and DCC tumor suppressors, respectively, fail to form tumors (Rabenau et al., 2004).

1.3.5 AMIGO3

It was widely believed that when myelin-derived inhibitory molecules bind to Nogo-Receptor (NgR1) and transmembrane receptor, p75/TROY or LINGO1, axon regeneration will be inhibited (Ahmed et al., 2013; Fournier et al., 2001; Whitford et al., 2002). Although, Chen et al, 2006, suggested that LINGO1 could be an interacting partner of NgR1/p75 complex (refer Table 2), a result published by Ahmed et al, 2015 indicated that AMIGO3 might the interacting partner instead of LINGO1. This is due to several reasons: 1) AMIGO3 mRNA and protein levels are significantly increased in dorsal root ganglion neuron (DRGN) and retinal ganglion cell following central axotomy while LINGO1 expression remains unchanged; 2) Using Immunoprecipitation and Western blot techniques, the interaction between AMIGO3 and NgR1 and p75/TROY is established; 3) AMIGO3 silencing is linked with dorsal column (DC) and optic nerve regeneration 4) Following simulation by appropriate neurotrophic factors (NTF), AMIGO3 silencing also promotes DRGN and RGC

neurite outgrowth in cultures where CNS myelin extracts (CME) have been initially added to inhibit such outgrowth (Ahmed et al., 2013). The finding that AMIGO3 promotes neuronal apoptosis is surprising, considering the fact that its other family members, AMIGO1 and AMIGO2, are involved in promoting neuronal survival.

Since AMIGO3 is expressed in both lung and heart (two anatomies important in pulmonary hypertension), AMIGO3 could have a role in the pathogenesis of PH (Kuja-Panula et al., 2003). The pro-apoptotic nature of AMIGO3 could be beneficial in the context of pulmonary vascular remodelling (Huang et al., 2010).

Another study by Ahn and colleagues (2015) investigated the anti-aging effect of rats treated with *Gryllus bimaculatus* extracts (which are extracts from *Gryllus bimaculatus* crickets that inhibits oxidation at DNA level, evident in the reduced level of 8-hydroxy-2'-deoxyguanosine (8-OHdG)). In contrast to untreated rats, rats treated with the extract showed upregulation of 1053 genes, including AMIGO3 (Ahn et al., 2015). Although it is difficult to conclude that AMIGO3 might be directly linked with the anti-oxidative response and hence the anti-aging effect, it is still tempting to speculate that the anti-oxidative property of AMIGO3 might be useful in PH (Ahn et al., 2015).

Aims and objectives

Chapter 3 aims to assess the regulation of Kv2.1 by Kv9.3 in tsA-201 cells using whole-cell voltage-clamp recording. This chapter also aims to investigate the effect of a reactive oxygen species generating enzyme, Nox4 on cells transiently transfected with Kv2.1 and Kv2.1/Kv9.3. Our hypotheses are that co-expression of Kv9.3 will increase the current amplitude of Kv2.1, causes Kv2.1 to be activated earlier, as well as prolong the time constant of deactivation of Kv2.1. With regards to the effect of Nox4, we hypothesize that Nox4 will reduce the current amplitude of Kv2.1 and Kv2.1/Kv9.3 since reactive oxygen species have been shown to inhibit Kv current. This chapter continues to investigate the effect of a Kv2 channel blocker, stromatoxin (ScTx), on Kv2.1, Kv2.1/Kv9.3, Kv2.1/Nox4, and Kv2.1/Kv9.3/Nox4. Our hypotheses are ScTx reduces the current amplitude of Kv2.1, Kv2.1/Kv9.3, Kv2.1/Nox4, and Kv2.1/Kv9.3/Nox4, causes the channels to be activated later and will shorten the time constant of inactivation of the channels.

Chapter 4 aims to assess the presence of Kv2.1 and Kv9.3 in rat lungs and hearts. We are interested in testing our hypothesis that both Kv2.1 and Kv9.3 are expressed in rat lungs and hearts. Since we are testing a novel commercial anti-Kv9.3 antibody, we only sought to answer if Kv9.3 channel is expressed in the rat lungs and hearts and which cell types express them using immunocytochemistry.

Chapter 5 aims to investigate the modulation of TASK-1 by Nox4 and chloramine T (Ch-T). In particular this chapter aims to investigate the regulation of WT TASK-1 and the gain-of-function K2N R3Q mutant TASK-1 by Nox4 under normoxic conditions. Since TASK-1 mutation which caused a reduction in function has been implicated in pulmonary arterial hypertension, we hypothesise that co-expression of Nox4, a reactive oxygen species producer, will reduce TASK-1 current amplitude. TASK-1 protein, when retained by a protein called COP1 in the endoplasmic reticulum, causes the channel to produce a very small current. The K2N R3Q mutant TASK-1, however, has its retention signal, KR, being mutated to NQ, thereby preventing COP1 from retaining the channel. Higher expression of the TASK-1 channel at the cell surface membrane increases the outward current carried by the channel. Our hypothesis is that K2N R3Q mutant could rescue TASK-1 current that is

inhibited by Nox4. This chapter also investigates the regulation of TASK-1 channels in the presence of a reactive oxygen species agent, Ch-T which produces singlet oxygen. Ch-T has been found to differentially affect other K2P channels such as TASK-2, TALK-1, and TALK-2 channels. We hypothesise that Ch-T will reduce WT-TASK-1 and K2N R3Q mutant TASK-1 currents.

Chapter 6 evaluates the modulation of Kv2.1, Kv2.1/Kv9.3, Kv2.1/Nox4, and Kv2.1/Kv9.3/Nox4 by various redox agents such as hydrogen peroxide (H_2O_2), DTT and DTNB. The effect of Ch-T on Kv2.1 and Kv2.1/Kv9.3 was also assessed. We tested the hypotheses that these redox agents will reduce the current amplitudes of Kv2.1 and Kv2.1/Kv9.3. We then consider how Kv2.1 and Kv9.3 can be differentially regulated by a family of cell adhesion molecules called amphoterin-induced gene and open reading frame (AMIGO) proteins. This study sought to probe what are the consequences in terms of current amplitude, activation threshold, and deactivation kinetics if AMIGO proteins are co-expressed with Kv2.1 and Kv2.1/Kv9.3. We hypothesized that AMIGO proteins will increase the current amplitude of Kv2.1 and Kv2.1/Kv9.3 and cause the channels to be activated earlier and decelerate the deactivation kinetics of these channels. In addition, AMIGO2 overexpression has been demonstrated to protect cells treated with hydrogen peroxide from cell death. Thus, the co-expression of AMIGO2 in the presence of H_2O_2 was also investigated. Our hypothesis for this study is that AMIGO2 will interact with H_2O_2 in regulating current through Kv2.1 and Kv2.1/9.3 channels.

Chapter 2: Materials and Methods

2.1 Plasmid preparation and sequencing

Plasmid preparation is performed to multiply the stock of DNA before it can be used for transient transfection. First, the DNA is transformed into *Escherichia coli* and as the bacteria multiply, the plasmid DNA that have been taken up are also multiplied. Plasmid vectors usually encode one or more antibiotic resistance genes to allow easy selection. This is because the bacterium that have taken up the plasmid DNA will grow in a culture where an antibiotic such as ampicillin or kanamycin has been added, while the bacterium void of the plasmid will not survive in the culture.

In order to extract the plasmid DNA, bacteria are lysed under alkaline conditions to denature the bacterial chromosomal DNA and protein. This is followed by neutralization and adjustment to high-salt binding conditions in one step. Lysates are cleared by centrifugation and are now ready for purification. Common commercial kits for purification are available and these kits are named according to the desired plasmid yield, such as miniprep, midiprep, maxiprep, megaprep, and gigaprep. Since the desired amount of plasmid DNA is small, the QIAprep Spin Miniprep kit (Qiagen, The Netherlands) is the most commonly used kit in our lab. A miniprep usually gives a plasmid DNA yield of 50 to 100μg. The DNA concentration was measured using the Nanodrop spectrophotometer (Implen, Germany) based on the absorbance at 260nm. This is because nucleic acids have absorbance maxima at this wavelength. The ratio of this absorbance maximum to the absorbance at 280nm, also known as the 260/280 ratio, is an indicator of DNA purity. In our experiments, a 260/280 ratio of ~ 1.8 was used as an indication that the DNA is 'pure'. The integrity of the plasmid DNA sequence was verified via sequencing. This is a common quality control step before the plasmid DNA is transfected into cells.

2.2 Cell culture

The tsA-201 cell line is a transformed human embryonic kidney-293 (HEK-293) cell line stably expressing an SV40 temperature-sensitive T antigen. This cell line is commonly used in functional expression assays and is ideal for expression of recombinant proteins. Mycoplasma has been removed from the cells at European Collection of Cell Cultures (ECACC). The identity of both tsA-201 and HEK-293 have been verified by short tandem repeat (STR) profiling.

Since the transfection efficiency decreases over a period of several months, a frozen stock is usually stored as reserve. Recovery of frozen cells from the -80°C freezer or liquid nitrogen is done by releasing the residual liquid nitrogen that is trapped in the ampoule, and then defrosting the cells in a 37°C water bath. The cells are then transferred into a tube containing pre-warmed media. The suspended cells are then centrifuged to remove any cryoprotectant (DMSO in our case). The supernatant is removed and the remaining cell pellet is resuspended in fresh media. The suspension is then transferred to a flask and incubated at 37°C overnight.

tsA-201 cells are routinely passaged either to be cultured into a new flask or grown as a monolayer on a poly-D-lysine-coated glass coverslip to be used for electrophysiology. Cells are ready to be passaged when they have reached 70-80% confluency. First, the morphology of the cells is checked to ensure that they are healthy. If the colour of the media has turned yellow, this is either a sign of contamination or that the cells are over confluent. The cells are dissociated from the flask wall using trypsin and are then re-suspended using media containing Dulbecco's modified eagle's medium (DMEM) (Sigma: #D5671, Germany) supplemented with 10% heat-inactivated fetal bovine serum (HIFBS) (Sigma #F9665, Germany), 1% penicillin and 10mg/ml streptomycin (Sigma #G1146, Germany), 1% non-essential amino acids Solution (NEAA) (Sigma #M7145, Germany), and 2mM L-Glutamine (Sigma #G7513, Germany). The solution is then centrifuged. The supernatant is removed, leaving the cells at the bottom of the tube undisturbed. The cells are then

suspended with fresh media and the suspension is either distributed into a new flask or cultured on a poly-D-lysine-coated glass coverslip.

2.3 Transfection

Transfection is the process of inserting nucleic acids by non-viral methods into a eukaryotic cell. In our experiments, cDNAs were introduced into tsA-201 cells via calcium phosphate precipitation method. Transfection can be stable or transient, where the nucleic acids transfected into the cell are not permanently incorporated into the cellular genome.

Nucleic acids can be delivered into a cell via viral or non-viral methods. The viral method exploits the virus's ability to inject its DNA into a host cell. Meanwhile, some of the well-known non-viral methods include calcium phosphate precipitation, electroporation or by lipofection. Since transfection is performed extensively in our lab, the calcium phosphate precipitation method is employed as it is a reliable and economical method. Besides, it has been documented that the calcium phosphate method is an effective transfection method for tsA-201 cells (Chen and Okayama, 1987).

The calcium phosphate method was devised by F. L. Graham and A. J. van der Eb in 1973. 4-(2-hydroxyethyl)-1-piperazineethanesulfonic acid (HEPES)-buffered saline solution, together with Na_2HPO_4 are combined with the $CaCl_2$ solution containing the DNA to be transfected. This results in the formation of calcium phosphate precipitate that binds the DNA on its surface (Graham and van der Eb, 1973). The fine precipitate is usually suspended in the solution and this suspension is then distributed to the cells that have been cultured on a glass coverslip in a four-well plate (Graham and van der Eb, 1973). When the precipitate adsorbed to the cells, the DNA uptake occurs during an incubation in a liquid medium at 37°C in the continued presence of extra calcium chloride (Graham and van der Eb, 1973). After 4-6 hours of incubation, the cells are washed with pre-warmed PBS (Graham and van der Eb, 1973). Fresh

media, as mentioned in the cell culture section above, are added and the cells are further incubated at 37°C overnight. The cells are now ready to be used.

The final amount of cDNAs of the Kv channels and GFP in each of the well of a four-well plate was 500ng. An example of calculation is as follows:
The following is prepared in tube A: The concentration of the Kv2.1 cDNA is 447ng/µl so, the volume of Kv2.1 cDNA that contains 500ng is 500/447 = 1.12µl. The concentration of the GFP cDNA is 232ng/µl so, the volume of GFP cDNA that contains 500ng is 500/232 = 2.16µl. The optimum final concentration of $CaCl_2$ is 225mM so the volume of $CaCl_2$ from the stock solution of 2M needed to achieve a final concentration of 225mM in a total volume of 25 µl is 2.81µl. Water is added until the volume in each well is 25µl.

The following is prepared in tube B: The phosphate-free buffer is a mixture of 280mM NaCl and 50mM HEPES, pH 6.95. A final concentration of Na_2HPO_4 of 1.8mM is optimum for transfection. Na_2HPO_4 is usually prepared from a stock solution with the concentration of 100mM. Therefore, the volume of Na_2HPO_4 needed from the stock solution to achieve 1.8mM is 0.45µl.

The content of tube A is added dropwise to tube B. The mixture is then incubated at room temperature for 5 to 15 mins to allow a $CaPO_4$/DNA precipitate to form. Contents of the tube is mixed by pipetting up and down gently, before being distributed dropwise into the well, onto the cells cultured on a glass coverslip. Cells are placed back into incubator for six hours. After six hours, PBS and media are warmed in water bath to 37ºC for 30 mins. Cells are washed twice with PBS and 0.5ml of media is added to each well. Cells are placed back in incubator overnight and ready to use for patch-clamping the next day.

Tube A	**Tube B**
1.12µl DNA (0.5 µg)	25 µl phosphate-free Buffer (HEPES)
2.16µl GFP (0.5 µg)	0.45 µl Na_2HPO_4
2.81µl $CaCl_2$ (2 M)	
18.91µl H_2O (up to 25 µl)	

Table 3: Example of calculation for the required volume of reagents in calcium phosphate transfection method of tsA-201 cells with Kv2.1 and GFP cDNAs.

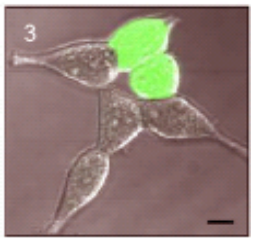

Figure 2.1: Image of tsA-201 cells transfected with gene of interest and green fluorescent protein (GFP). Two out of six tsA-201 cells are successfully transfected with the gene of interest and GFP appeared green under the light microscope. Scale bar is 10μm. Adapted from Thomas and Smart, 2005.

2.4 Patch-clamp electrophysiology

Patch-clamp electrophysiology is a technique that allows real-time measurements of ion channel function either through a single channel, also known as the cell-attached patch configuration, inside-out and outside-out configurations, and macroscopic currents from the whole-cell. It is worth noting that the data acquired from this technique can be interpreted quantitatively, making it a valuable technique for researchers (Akita et al., 2012).

Thanks to the improvisation by Hamill et al, 1981, measurement of membrane potential and currents from small cells was possible (Akita et al., 2012). This was done by pressing a patch electrode onto a cell surface to form a gigaohm seal with the cell membrane and by rupturing a piece of membrane that lies directly below the electrode by applying a negative pressure (i.e., suction). This causes the electrolyte in the microelectrode (internal solution in pipette) and the intracellular solution to become as one and this is what is called as whole-cell patch configuration. Such improvement also allowed the measurement of the cell capacitance (Neher and Marty, 1982).

Whole-cell recording occurs when the interior of the pipette becomes continuous with the cell cytoplasm, and this allows the measurement of the potential difference and current of the entire cell. Meanwhile, single channel recording, as the name suggests, allows the measurement current through a single channel at a given potential.

Voltage-clamp and Current clamp

Voltage-clamp electrophysiology controls the voltage across the membrane at a certain value so that the current flowing can be measured (Akita et al., 2012). Conversely, current-clamp injects current in order to measure the potential difference. When current is clamped at 0 (I= 0), the resting membrane potential is measured (Akita et al., 2012).

In voltage-clamp, there is an internal electrode which is in contacted with the inside of the cell and an amplifier that measures the membrane voltage (Vm) and an external electrode which serves as a reference electrode and is inserted in the bath solution (Akita et al., 2012). Meanwhile, the command voltage, Vc, is the desired membrane potential that is set by the researcher (Akita et al., 2012). In our system, we are using the same electrode to inject current and to measure the Vm.

The difference between Vm and Vc is measured by a comparator. If Vm is not equal to Vc, the comparator generates a 'difference signal' (Akita et al., 2012). Sensing the signal, the amplifier injects a current into the axon via a current-passing electrode in order to make Vm equal to Vc (Akita et al., 2012). This feedback circuit works almost instantaneously and keeps Vm as close to Vc as possible (Akita et al., 2012). The injected current that is needed to keep Vm as close to Vc can be recorded and measured. This means that as voltage-gated ion channel opens or closes over time in response to the change in Vm imposed by the voltage clamp, the current generated can be recorded and analyzed (Akita et al., 2012).

For example, say the Vc is clamped at 0mV and the Vm is at -65mV, a very brief capacitive current is seen, followed by a transient inward and outward currents depending on the ionic conductance at the voltage (Akita et al., 2012). The capacitive current is initiated because the step from one potential to another alters the charge separation, thus causing a potential difference across the membrane (Akita et al., 2012). Once the new potential is reached, there is no capacitive current (Akita et al., 2012). Thus, the capacitive current is a transient occurrence (Akita et al., 2012). Series resistance is the resistance due to components other than that of the cell membrane and consists mostly of component of the pipette shank and a component of the pipette tip that contains some broken patch membranes (Akita et al., 2012). The

presence of series resistance prevents Vm from getting closer to the Vc as the larger series resistance and cell capacitance, the longer is the time needed to reach Vc since the time constant for slow capacitive surge, τ = series resistance $\times$ cell capacitance (Akita et al., 2012). Secondly, a voltage drop across series resistance will occur, yielding an error in the Vc, when a large current in generated in the whole-cell mode (Akita et al., 2012). Even when constant Vc is applied, the varying current amplitude and series resistance will cause Vm to vary accordingly (Akita et al., 2012). In short, the presence of series resistance prevents accurate voltage-clamping. Series resistance can be compensated by tuning the potentiometer linked to the current output (indicated with SR compensation on the monitor) (Akita et al., 2012). The whole-cell, voltage-clamp setup is used in all the electrophysiological experiments described in this thesis.

Whole-cell currents were recorded using an Axopatch 200A amplifier (Axon Instruments, USA). Currents were digitized using a Digidata 1200 Interface (Axon Instruments, USA), and analyzed using pClamp 10.2 software (Axon Instruments, USA). Pipettes were fabricated from borosilicate glass using the micropipette puller. Pipettes are polished to a final resistance of 4-6MΩ. The external bath solution contained the following: NaCl, 145 mM; KCl, 2.5 mM; $CaCl_2$, 1 mM; $MgCl_2$, 3 mM; HEPES, 10 mM; pH adjusted to pH 7.4 with NaOH. The internal pipette solution contained KCl, 150 mM; $MgCl_2$ 3mM; EGTA, 5 mM; HEPES, 10 mM; pH adjusted to pH 7.4 with KOH.

Protocols:

- **Standard voltage-step protocol**

The standard voltage-step protocol in this study consist of a voltage-step and a repolarization step (Figure 2.2). However, this project is only interested in the analysis of currents measured at the voltage-step and the time constant measured at the repolarization step. The holding potential was -60mV. Test pulses to potentials ranging from -100mV to +50mV for a duration of 500ms each sweep was applied in 10mV increments. In order to better visualize the difference between Kv2.1 and

Kv2.1/Kv9.3, Nox4/Kv2.1, and Nox4/Kv2.1/Kv9.3, the ratio of current measured at each step to current at +50mV is also determined.

The first variant of protocol repolarized from every potential (-100mV till +50mV) to -80mV. However, modification was made when the currents were repolarized to -50mV for two reasons: 1) to allow measurement of time constant of inactivation and 2) direct comparison with the data from Zhong et al, 2010.

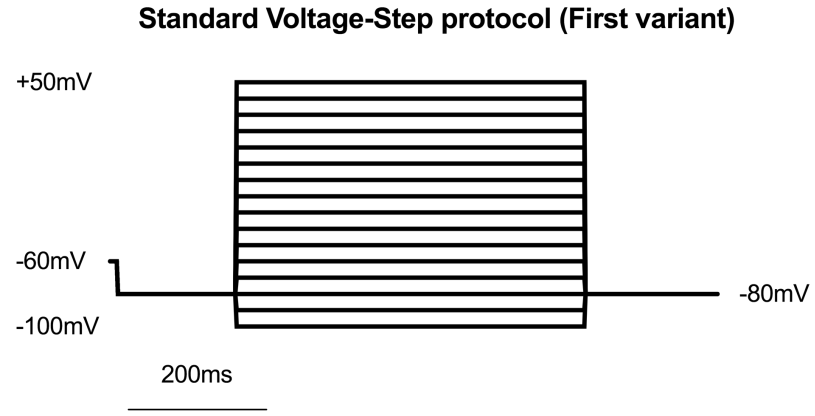

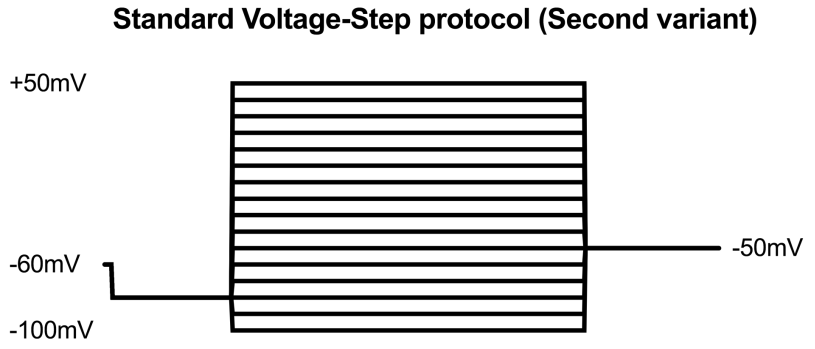

Figure 2.2: Standard voltage-step protocol. The main steps in this protocol are the voltage-step and the repolarization step. Test pulses to potentials ranging from -100mV to +50mV for a duration of 500ms each sweep was applied in 10mV increments before being repolarized to -80mV in the first variant or to -50mV in the second variant of the protocol. The holding potential was -60mV.

- **Open-state inactivation protocol**

Test pulses to depolarize the membrane to potentials of high open probability (+40mV) were given for 32s. Ratio of current measured at the end to current measured at the end of the pulse (Ipn/Ip) is determined. The holding potential was -60mV.

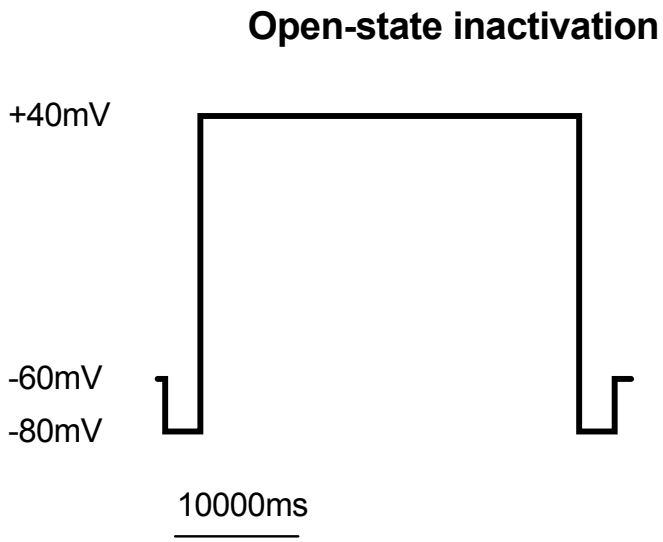

Figure 2.3: Open-state inactivation protocol. Cell membrane was held at -60mV and then depolarized to -80mV. Test pulse to +40mV to depolarize the membrane to high open probability was given for 32s. Membrane is then repolarized to -80mV before being returned to holding potential of -60mV.

- **Closed-state inactivation protocol**

Test pulses to +40mV were given at the beginning and end of each sweep. The length of time at which the second pulse is given after the first is increased by 2s for every sweep. For example, the first trace comprised of the test pulse of +40mV given at the beginning and another pulse is given two seconds later. In the second trace, the first pulse is given at the beginning and then four seconds later. This continued for each subsequent trace and the last trace comprised of a test pulse at the beginning and at 28s later. The ratio of the current at the second pulse to that of the first (Ipn/Ip) is determined and is proportional to the number of channels that did not inactivate (Figure 2.4). Since we are mostly interested in the current at the first pulse and the last pulse, a short version of the protocol which include the first trace and the last trace, was also created (Figure 2.4).

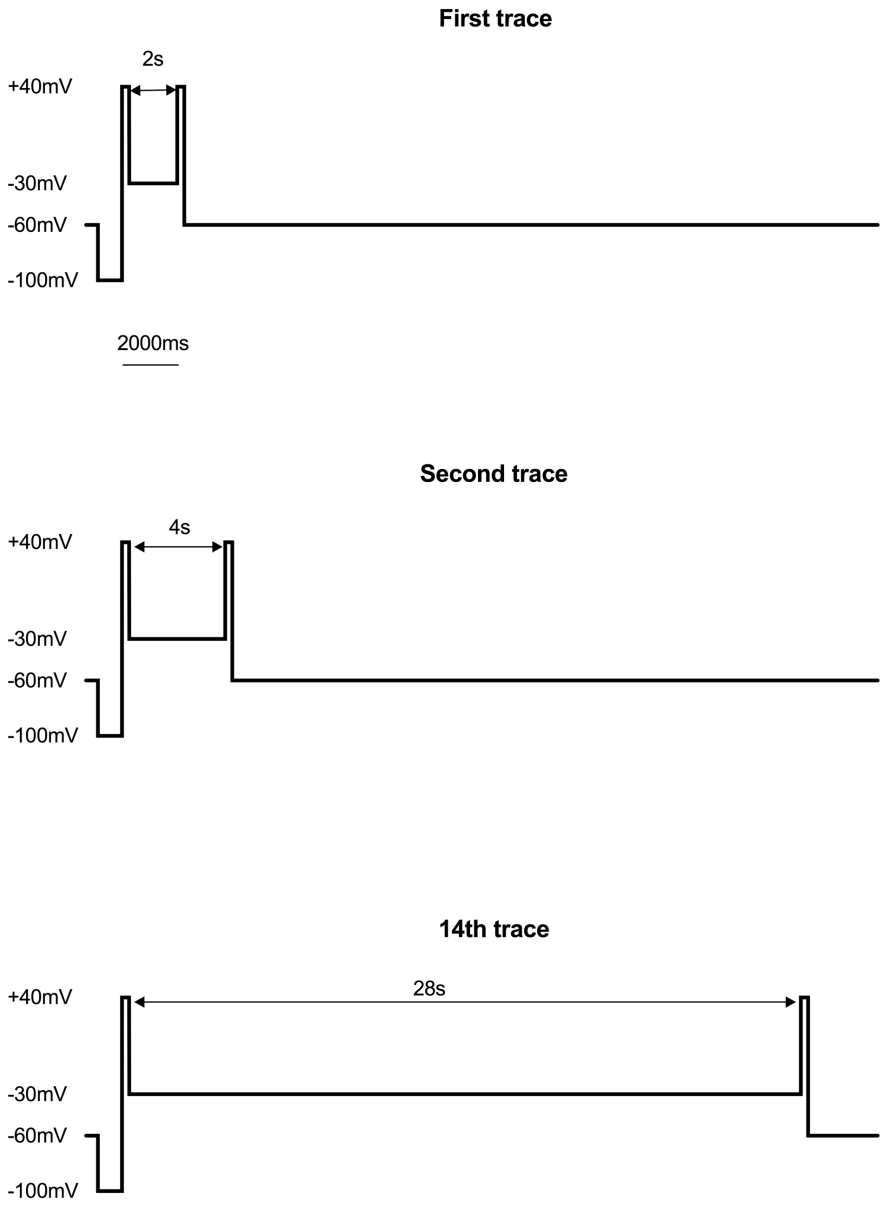

Figure 2.4: Closed-state inactivation protocol. In the first trace, a test pulse to +40mV were given at the beginning and a second pulse was given two seconds later. In the second trace, the second pulse were given four seconds after the first. In every subsequent trace, the period from the first pulse is increased by two seconds. This continued until the 14th trace, where the period between the first pulse and the second pulse is 28s. The ratio of the current at the second pulse to that of the first (Ipn/Ip) is determined and is proportional to the number of channels that did not inactivate. A shorter version of the protocol comprising of the first and 14th trace is created since we are mostly interested in the current of the second pulse at the beginning and at the end of the pulse.

- **TASK-1 channel protocol**

The electrophysiology protocol has a voltage-step and a voltage-ramp part. Only currents measured in the voltage-step part will be considered. Currents were measured at the resting membrane potential, -80mV, and at the stimulating pulse of -40mV, which was given for 500ms (Figure 2.5). The difference between the current measured at -40mV and at -80mV is calculated.

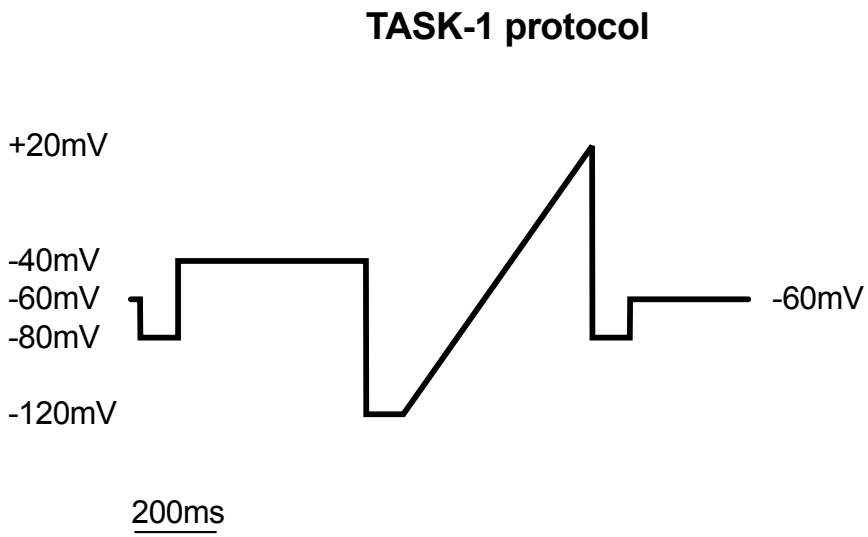

Figure 2.5: TASK-1 protocol. Membrane is hyperpolarized from -60mV to -80mV and is then depolarized to -40mV for a duration of 500ms. Then the membrane is hyperpolarized to -120mV and is subjected to a voltage ramp to +20mV, before being hyperpolarized to -80mV again. The cell is then depolarized to -60mV again. Difference between currents measured at the voltage-step at -40mV and at -80mV at the start of the protocol is calculated.

2.5 Data analysis and statistical tests

Data were expressed as mean ± SEM. To analyze the difference in absolute current across different voltages, two-way ANOVA followed by the appropriate posthoc method was used. Data were analyzed using two-way ANOVA, followed by Tukey's significant difference method when comparing several cell populations across different voltages. Dunnett's test was chosen instead of Tukey's test if one of the cell populations is chosen as a control group. Two-way ANOVA is usually used when

comparing three or more groups. Therefore, when there is a need to compare only data from two populations across different voltages, two-way ANOVA followed by Bonferroni method was chosen. Bonferroni is the suitable method for comparing two populations and this method does not assume independence, which is the case in our paired data (For example, readings taken from cells exposed to external solution, followed by redox agent).

When comparing data (say normalized current) from two cell populations at one voltage, two-tailed, unpaired Student's t-test with Welch's correction was used. Welch's correction was chosen because the sample sizes are unequal. If there were three or more populations, say comparing the slow component of time constant of deactivation (tslow) of several groups, data were analyzed by one-way ANOVA followed by either Tukey's test (if there is no group being chosen as a control group) or Dunnett's test (if one of the groups was chosen as control group).

Chapter 3: Modulation of Kv2.1 by Kv9.3, Nox4, and stromatoxin (ScTx-1)

3.1 Introduction

Kv2.1, along with Kv1.5, are the most studied ion channels in PH (Archer et al., 1998). Kv2.1 is present in virtually every cell and is expressed abundantly in the pulmonary vasculature (Archer et al., 2004, 1998; Park et al., 2010). It is hypothesized to underlie the delayed rectifier current in the PASMC and several studies have shown that hypoxia inhibits Kv channel. It is likely that Kv2.1 (probably in association with Kv9.3) is a main channel subunit subjected to such inhibition (Patel et al., 1999, 1997). Kv2.1 is one of three components contributing to functional Kv currents in the arteries, the other two being Kv1.2 plus Kv1.5 with Kvβ1.2 subunits; and Kv7.4 subunits (Park et al., 2010). Kv2.1 has been established as a target protein of reactive oxygen species and oxidation of Kv2.1 has been demonstrated to increase excitability of cells, subsequently increasing vulnerability to apoptotic cell death (Peers and Boyle, 2015). For example, Kv2.1 oxidation is a reported to contribute to neuropathy in conditions such as Alzheimer's disease. (Cotella et al., 2012; Yu et al., 2016). This has led to speculation that Kv2.1 might act as an oxygen sensor. However, there is no evidence of oxygen-sensing property being present in Kv2.1, suggesting this property might be conferred by an interacting partner.

Kv2.1 can interact with electrically silent Kv (KvS) subunits Kv5−Kv6 and Kv8−Kv9, forming functional heterotetrameric Kv2/KvS channels (Stas et al, 2015). The association of Kv2.1 with Kv9.3 (Patel et al., 1997, 1999, Kerschensteiner and Stocker, 1999, Zhong et al, 2010, Cox and Fromme, 2016) is perhaps the most well-documented in the context of PH. As mentioned, Kv9.3 is a silent subunit but its association with Kv2.1 has been shown to modulate the biophysical and pharmacological properties of Kv2.1, where Kv9.3 increases Kv2.1 current amplitude (Zhong et al, 2010). Meanwhile, coexpression of Kv9.3 with Kv2.1 decelerates Kv2.1's open-state inactivation and accelerates closed-state inactivation, thereby

causing Kv2.1 to preferentially exhibit closed-state inactivation (Kerschensteiner and Stocker, 1999). Such a mode of inactivation has been indicated to regulate membrane excitability through the modulation of repetitive firing and back-propagation of action potentials in neurons as well as the repolarization of cardiac action potentials (Kerschensteiner and Stocker, 1999). Such modulation might also control the PA myocytes action potential duration as the effect of Kv9.3 in slowing down the deactivation of Kv2.1 is particularly prominent in the voltage range corresponding to the resting membrane potential of PA myocytes (Patel et al., 1997). Pharmacologically, their co-expression resulted in the reduction in sensitivity to the K channel blockers, 4-AP and TEA (Kerschensteiner and Stocker, 1999; Kerschensteiner, 2003).

Concurrent with the suggestion that Kv2.1/Kv9.3, instead of homomeric Kv2.1, is the main contributor to the delayed rectifier current in the PASMC, it has been reported that both Kv2.1 and Kv9.3 (along with Kv1.2 and Kv1.5) protein expressions were upregulated in cultured PASMC exposed to 18 hours of hypoxia and this might be mediated by hypoxia-inducible factor (HIF)-1 binding to erythropoietin enhancer fragments (Dong et al., 2012; Zhong et al., 2010).

The heteromeric Kv2.1/Kv9.3 channels are activated by intracellular ATP and are reversibly inhibited by hypoxia and the extent of these modulations are different from Kv2.1 alone, suggesting that both subunits have unique characteristics and are distinguishable from each other (Patel et al, 1997 and 1999). This has led to the speculation that Kv2.1/Kv9.3 activities are tightly connected to the glycolytic pathway/ metabolic status of the PASMC. There are four separate findings which supported their connection with the metabolic state of the cells. Firstly, Rounds and McMurty (1981) discovered that inhibitors of oxidative phosphorylation and glycolysis caused a transient pressor responses in perfused rat lung (Patel et al., 1997). 2-deoxyglucose and carbonyl cyanide p-trifluoromethoxyphenylhydrazone (FCCP) have been shown to inhibit Kv channels, raised cytoplasmic Ca^{2+} concentration, and lead to PASMC contraction (Patel et al., 1997). Another separate finding has shown rotenone and antimycin A (inhibitors of activated oxygen species biosynthesis from the electron transport chain and ATP synthesis) elicited the same effects (Patel et al., 1997). Fourthly, Evans et al., 1994 showed that rise in

intracellular ATP levels elevated the amplitude of the delayed rectifier K^+ current amplitude in rabbit PASMC (Patel et al., 1997).

Of all the Nox proteins present in the mouse lung tissue (NOX1, NOXA1, NOXO1, p22phox, p47phox, p40phox, p67phox, NOX2, and NOX4), only Nox4 mRNA were upregulated in the pulmonary artery vessel of mice kept in hypoxic (10% O_2) conditions for 21 days (Mittal et al., 2012). Interestingly, silencing of Nox4 reduced generation of reactive oxygen species and reduced PASMC proliferation. These observations were also replicable in humans where lungs from idiopathic PAH patients were reported to have a 2.5-fold upregulation of Nox4 protein in the vessel media. For these reasons, Nox4 has been postulated to be an oxygen sensor in PASMC. Furthermore, Nox4 is upregulated in hypoxia-induced pulmonary hypertension in both rats and mice and probably drive PASMC proliferation via the phosphorylation of retinoblastoma protein (Mittal et al., 2012). This implies that Nox4 has a link with the pulmonary vascular remodelling process. Since Nox4 upregulation in the hypoxic condition coincides with Kv2.1 and Kv9.3 upregulation, there is a possibility that Nox4 might associate with either Kv2.1, Kv9.3 or both, to bring about hypoxic pulmonary vasoconstriction.

While it is known that, Nox4 silencing or the decrease of Nox4 function using a reactive oxygen species scavenger apocynin, reversed the inhibitory effect of hypoxia on Kv current density (without affecting the Kv protein level expression), it largely remains unknown which Kv channel Nox4 interacted with. There have been data provided by Mittal et al, 2012, whereby Nox4 gave rise to oxidation of cysteine residues in Kv1.5 channels, which subsequently lead to 55% of reduction in Kv current. However, the possible effect of Nox4 on Kv2.1 cannot be ruled out (Mittal et al., 2012).

The absence of a specific Kv channel blocker has hindered the investigation into the role of Kv2.1 as a delayed current rectifier in several types of cells (Chen et al., 2010; Shiau et al., 2003). The identification of spider toxins as specific Kv2 inhibitors has been helpful in resolving this. Hanatoxins were the first spider venom peptide to be demonstrated as a specific Kv2.1 channel blocker. Hanatoxins bind C-terminal

residues of the S3 segment of Kv2.1 and alter the channel gating towards its depolarized state (Shiau et al., 2003).

Besides hanatoxins, other more novel spider toxins such as stromatoxin-1, ScTx-1 from the African tarantula (*Stromatopelma calceata*) and heteroscordratoxins, HmTx1 and HmTx2 from *Heteroscordra maculate* have also been proven as effective Kv2.1 inhibitors (Shiau et al., 2003). Inhibitory effects of ScTx-1 and HmTx-1 have been reported to be as strong as Hanatoxins (Shiau et al., 2003).

An example pointing to the relevance of the use of ScTx-1 is a study performed by Tsantoulas et al., 2014, which showed that dorsal root ganglion cells treated with ScTx-1 had reduced Kv2 current. This is measured by the reduced refractory period, which corresponds to smaller after-hyperpolarization duration and thus shortened inter-spike intervals during repetitive discharge (Tsantoulas et al., 2014). In short, Kv2 dysfunction could cause action potential to be conducted in the presence of sustained input to cause dorsal root ganglion hyperexcitability. Therefore, Kv2 serves as a braking mechanism in such condition. If such mechanism is compromised in the PASMC, this could lead to PASMC excitability and increased arterial tone, which could be debilitating in PAH.

In another study done by Hristov et al., 2012, ScTx-1 reduced the amplitude of the Kv current in freshly isolated guinea pig detrusor smooth muscle cells. Although ScTx-1 did not alter the steady-state activation and inactivation curves, it reduced the activation time-constant of the Kv current at positive voltages (Hristov et al, 2012). They have postulated that the major contributor of this Kv current is heterotetramer of Kv2.1 and a silent Kv channel, by comparing the biophysical characteristics of ScTx-1-sensitive current with the current profile of such heterotetramer (Hristov et al., 2012).

In diabetic vascular smooth muscle cells isolated from high fat diet mice, the reduction in the Kv current in cells treated with ScTx-1 corresponds to the decreased Kv2.1 mRNA and protein levels also interfered with the regulation of the arterial tone. Nieves-Cintrón et al., 2015 further added that the event of Kv2.1 inhibition occurs prior to suppression of the large-conductance Ca^{2+}- activated channel subunits

and the latter is also observed in the event of chronic hyperglycemia. Taken together, their study implicated the function of Kv2.1 in regulating the arterial tone in diabetes (Nieves-Cintrón et al., 2015).

Interestingly, Zhong et al., (2010) have found that Kv2.1/Kv9.3 heteromer in HEK-293 cells have a longer deactivation time compared to Kv2.1 homomer. This can be seen by the steeper curve due to repolarization to -50mV from various step voltages (Zhong et al., 2010). Secondly, Zhong et al, 2010 have shown that the rat middle cerebral arteries (RMCA) current, which is ScTx-1-sensitive, more closely resembled the Kv2.1/Kv9.3 current as it has slower deactivation kinetics, rather than the Kv2.1 current. This led them to hypothesize that Kv2.1/Kv9.3 is the major contributor of the delayed rectifier current in RMCA.

In the light of these findings, the current study aims to elucidate the modulation of Kv2.1 by Kv9.3. This relationship was probed using several electrophysiology protocols. It is also of interest to determine if the presence of Kv9.3 will affect interaction of Nox4 with Kv2.1. Following from their research which demonstrated the use of ScTx-1 in distinguishing Kv2.1 and Kv2.1/Kv9.3 (Zhong et al., 2010), this chapter also aims to probe the effect of this venom on these channels and the results from this study would hopefully be extrapolated for future research on native PASMC. For the experiments to test the modulation of Kv2.1 by Kv9.3 and Nox4, tsA-201 cells are transiently transfected with the respective combination of cDNAs-Kv2.1, Kv2.1/Kv9.3, Kv2.1/Nox4, and Kv2.1/Kv9.3/Nox4. Electrophysiology protocols used were the standard voltage-step protocol, and open-state inactivation and closed-state inactivation protocols. With regards to the experiments to test the effect of ScTx-1, a non-perfused setup whereby the toxin was added to the bath instead of perfusing the cells with the toxin. This setup was chosen due to the high cost of the ScTx-1. An initial set of experiments was performed with Kv2.1 and Kv2.1/Kv9.3 in external bath solution, in a non-perfused setup to see if this setup affected the deactivation time constants.

3.2 Results

Kv2.1 produces functional current while Kv9.3 is a silent channel

Cells were transfected with respective cDNAs and GFP cDNA is used as a reporter gene. The standard voltage-step protocol was used for recordings and data were expressed as mean ± SEM. Data were analyzed using Student's t-test with Welch's correction to examine the difference between the two mean values at a certain voltage and Welch's correction was chosen because of unequal variances in the two populations. Two-way ANOVA and Tukey-Kramer (known as Tukey's honestly significant difference (HSD) on GraphPad Prism 7, USA) as post-hoc analysis, were also used. The Tukey-Kramer method was chosen as a follow up for the two-way ANOVA because I was interested in comparing every mean with every other mean and this method also allows for possibility of unequal sample sizes (Kim, 2015).

Current traces showed that Kv2.1 cells have a high functional current compared to either tsA-201 cells expressing Kv9.3, transfected with GFP only or untransfected cells (Figure 3.1). A current density against voltage plot also showed that the Kv2.1 current density (41.5 ± 11 pA/pF) is significantly higher than that of Kv9.3 (7.5 ± 4 pA/pF) at -20mV. Kv9.3 current density is comparable to untransfected cells (2.1 ± 0.5 pA/pF) or cells transfected only with GFP (5.5 ± 2.2 pA/pF) at -20mV (Figure 3.2). These findings are consistent with the findings of Patel et al., 1997 and Kerschensteiner, 2003, who demonstrated that Kv9.3 is electrically silent.

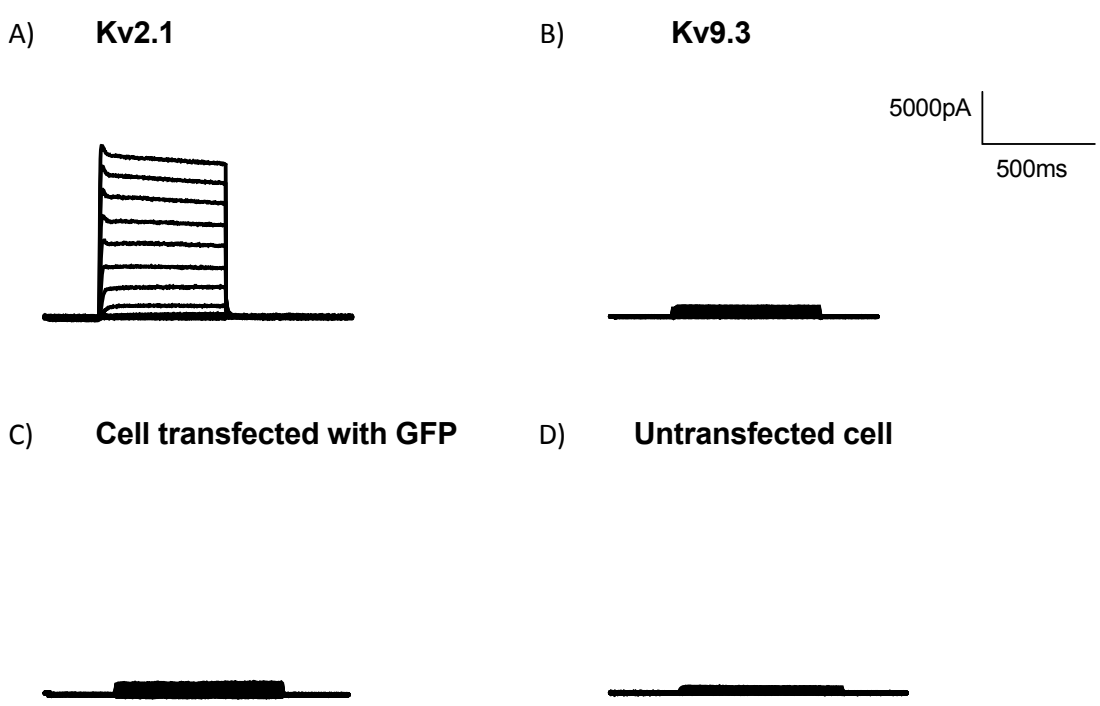

Figure 3.1: Kv2.1 produces functional current while Kv9.3 is a silent channel. Representative traces of cells transfected with A) Kv2.1, B) Kv9.3, C) cell transfected with GFP, and D) untransfected cell.

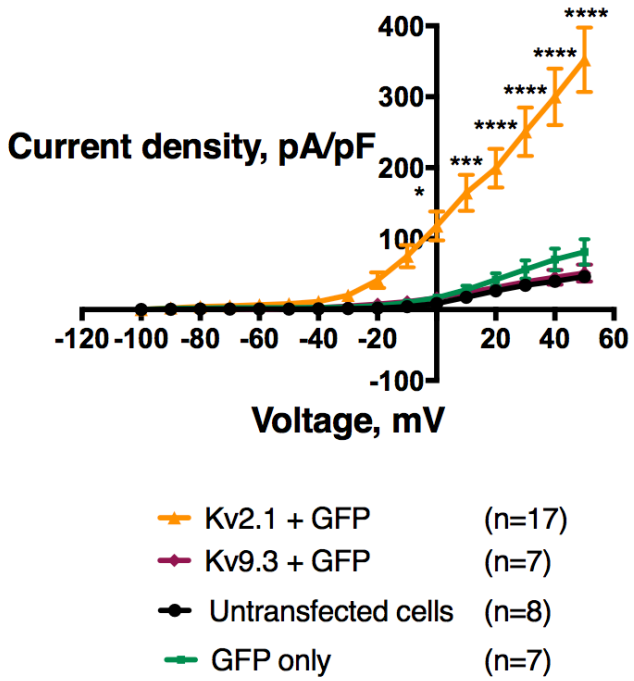

Figure 3.2: Current density of Kv2.1, Kv2.1/Kv9.3, untransfected cells, and cells transfected with GFP only plotted against voltage. Data were acquired from the standard voltage-step protocol, where currents were activated by application of test pulses at various potentials, ranging from -100mV to +50mV for a duration of 500ms each step, with an increment of 10mV in each voltage step. tsA-201 cells were transfected with Kv2.1 and GFP, or Kv9.3 and GFP, GFP only, or untransfected. Current density plotted against voltage showed that the current density of Kv2.1 is significantly higher than untransfected cells or cells transfected with Kv9.3 or GFP only from a membrane potential of -20mV onwards. Data were analyzed using two-way ANOVA and Tukey's honestly significant difference method was chosen as the post-hoc, it was found that current density of Kv2.1 was statistically-significant different from untransfected cells from 0mV to +50mV, with * indicating $p \leq 0.05$, ** indicating $p \leq 0.01$, *** indicating $p \leq 0.001$, and **** indicating $p < 0.0001$. When Kv2.1 is compared with cells transfected with Kv9.3+GFP and GFP only, the difference between current density from 0mV to +50mV were also statistically significant, with p-value of at least ≤ 0.05.

Kv9.3 does not affect the endogenous current

The current density of cells expressing Kv9.3 alone (51.3 ± 11.9 pA/pF at 50mV) is comparable to untransfected cells (46.5 ± 8.9 pA/pF) and cells transfected with GFP only (81.1 ± 17.8 pA/pF) (Figure 3.3). Data analysis performed using two-way

ANOVA, with Tukey's multiple comparisons test chosen for post-hoc analysis revealed that there is no statistically significant difference between the populations. This is a clear indication that when Kv9.3 is expressed alone, the channel does not interfere with the endogenous current from the tsA-201 cells that are used in these experiments.

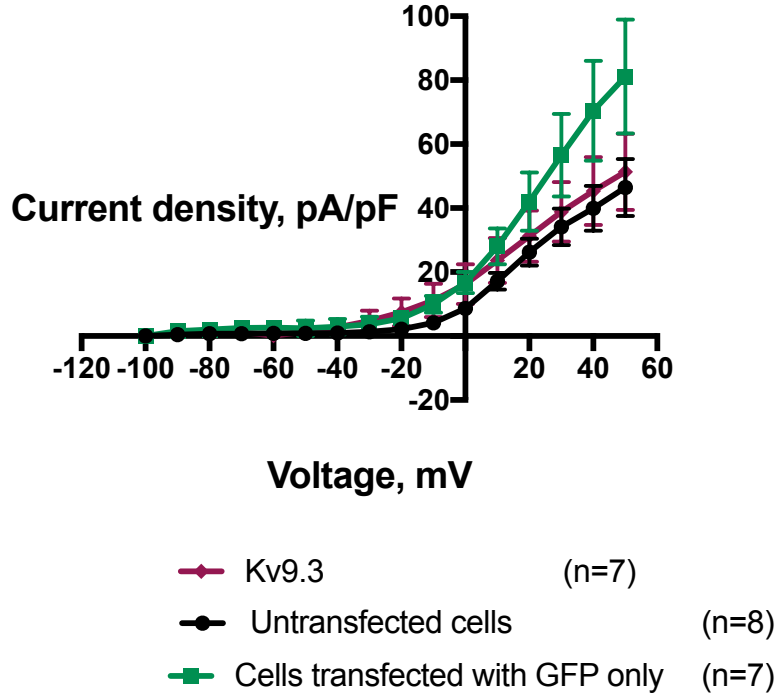

Figure 3.3: Kv9.3 does not affect the endogenous current. Current density plotted against voltage for tsA-201 cells expressing Kv9.3, untransfected cells, and cells transfected with GFP only. Data were acquired from the standard voltage-step protocol, where currents were activated by application of test pulses at various potentials, ranging from -100mV to +50mV for a duration of 500ms each step, with an increment of 10mV in each voltage step. The current density for each type of cells were comparable, as indicated by overlapping mean values and error bars. Data were analyzed using two-way ANOVA and Tukey's honestly significant difference method was chosen as post-hoc analysis, and it was found that the differences between the populations are not statistically significant.

Modulation of Kv2.1 by co-expression of Kv9.3

When Kv9.3 is expressed with Kv2.1, the absolute current increased starting from potentials where the cells are activated. This is in agreement with the finding of Patel et al., 1997, where they reported that Kv2.1/Kv9.3 has higher current amplitude (17μ

A at +100mV) than Kv2.1 homomers (5μA at +100mV). Forster resonance energy transfer (FRET) suggested that the stoichiometry of the Kv2.1/Kv9.3 heterotetramer consists of three Kv2.1 subunits and one Kv9.3 α-subunit (Kerschensteiner et al., 2005). Figure 3.4 depicts two important findings: 1) Kv2.1/Kv9.3 is activated earlier (at a more negative potential) compared with Kv2.1; 2) The absolute current of Kv2.1/Kv9.3 cells were significantly higher than that of Kv2.1 cells from -20mV to +50mV, with a p value of at least ≤ 0.05, when analyzed with two-way ANOVA with Sidak method chosen for post-hoc analysis. The Sidak method was chosen because it is appropriate for comparison of means of two cell populations, and the readings for Kv2.1 and Kv2.1/Kv9.3 were obtained independently (in other words, not paired). This method also offers higher statistical power which reduces the chance of committing a Type 1 (false positive) statistical error.

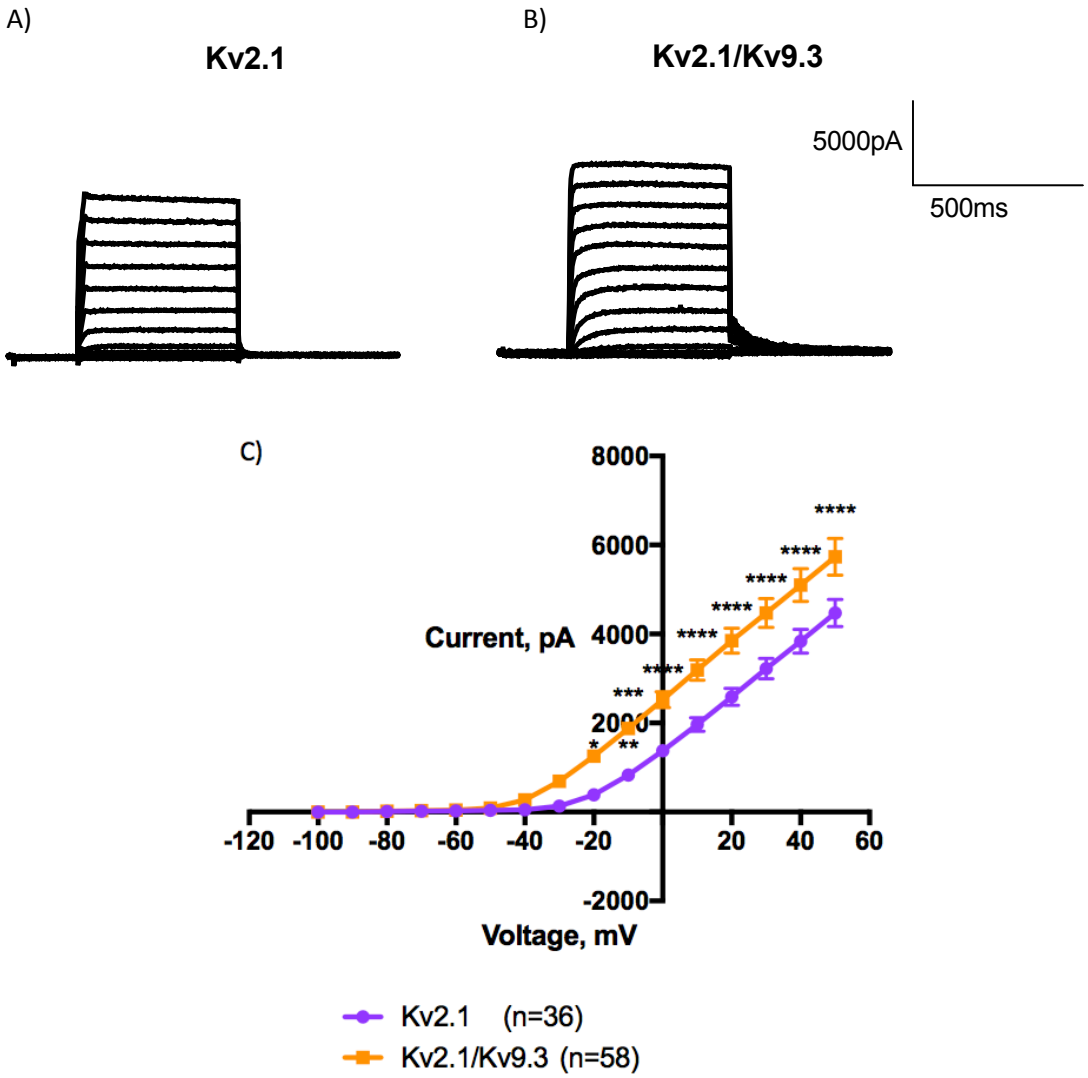

Figure 3.4: Co-expression of Kv9.3 with Kv2.1 increases the Kv2.1 current amplitude. Current traces of A) Kv2.1 and B) Kv2.1/Kv9.3. C) Absolute current of Kv2.1 and Kv2.1/Kv9.3 against test potential ranging from -100mV to +50mV. The current of the Kv2.1 and Kv2.1/Kv9.3 cells were analyzed using two-way ANOVA with Sidak method. The analysis revealed that current amplitudes of Kv2.1/Kv9.3 were significantly higher than Kv2.1 from -20mV to +50mV, with * indicating $p \leq 0.05$, ** indicating $p \leq 0.01$, *** indicating $p \leq 0.001$, **** indicating $p < 0.0001$.

In order to better distinguish the activation thresholds of Kv2.1 and Kv2.1/Kv9.3, the current density at each potential was normalized to the highest current density (current density measured at +50mV). The activation threshold is given as the potential at which the gradient of the slope is the highest. The rationale behind this is that, when the current rises significantly from the baseline at a certain potential, that potential is considered as the activation threshold. For example, the activation

threshold for Kv2.1 is -20mV because this is the point where it is apparent that the current started to rise significantly from the baseline. The co-expression of Kv9.3 with Kv2.1 shifts the activation threshold to -40mV (Figure 3.5 and Figure 3.6). The normalized current of Kv2.1/Kv9.3 at -30mV is significantly higher than that of Kv2.1 (Figure 3.5 and Figure 3.6).

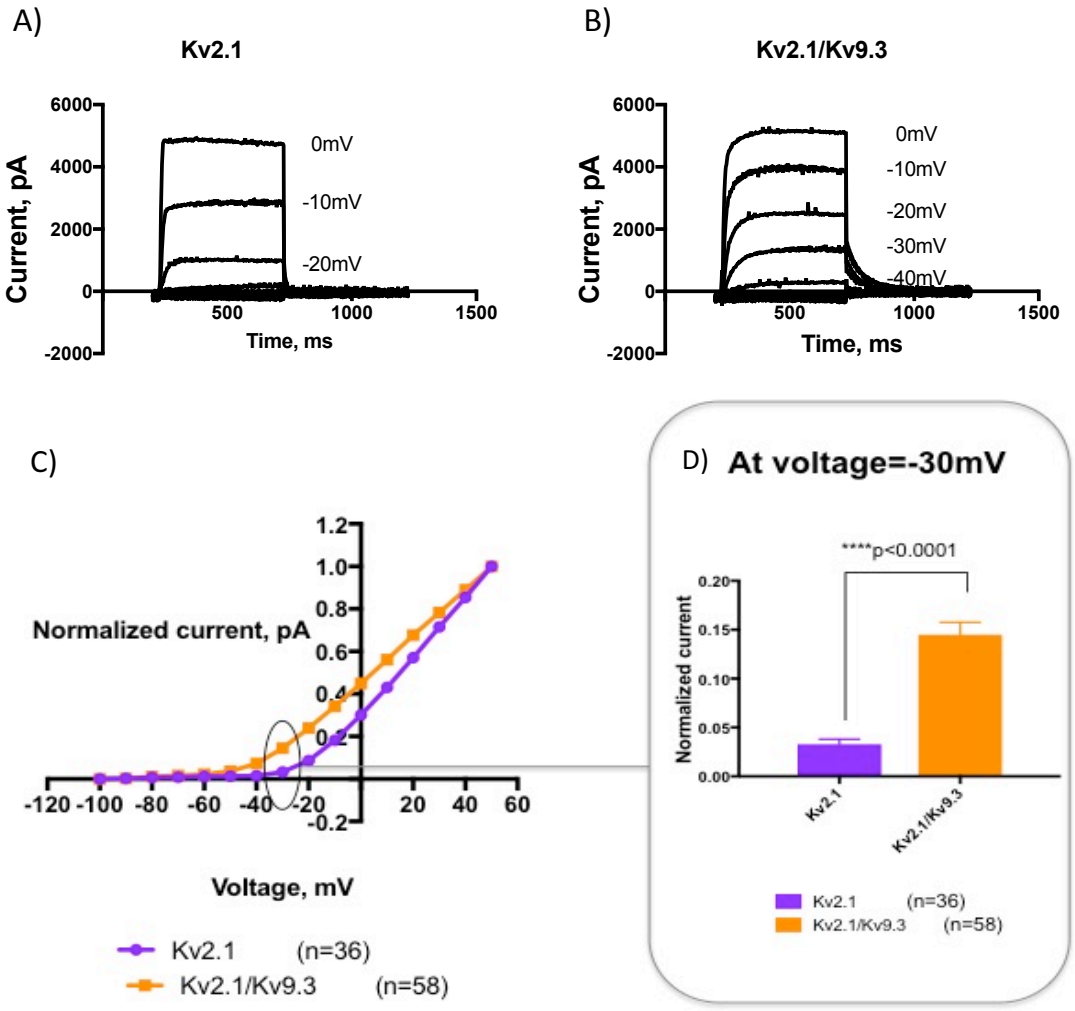

Figure 3.5: Kv9.3 shifts the activation threshold of Kv2.1 to a more negative potential. Magnified current traces of cells transiently transfected with A) Kv2.1 and B) Kv2.1/Kv9.3 resulting from currents being activated at various potentials. Kv2.1 channels are activated at -20mV, while Kv2.1/Kv9.3 activated at an earlier potential, -40mV. Two-tailed, unpaired Student's t-test with Welch's correction was used to analyze the difference between normalized current of Kv2.1 and Kv2.1/Kv9.3 at -30mV and there is statistically-significant difference between them.

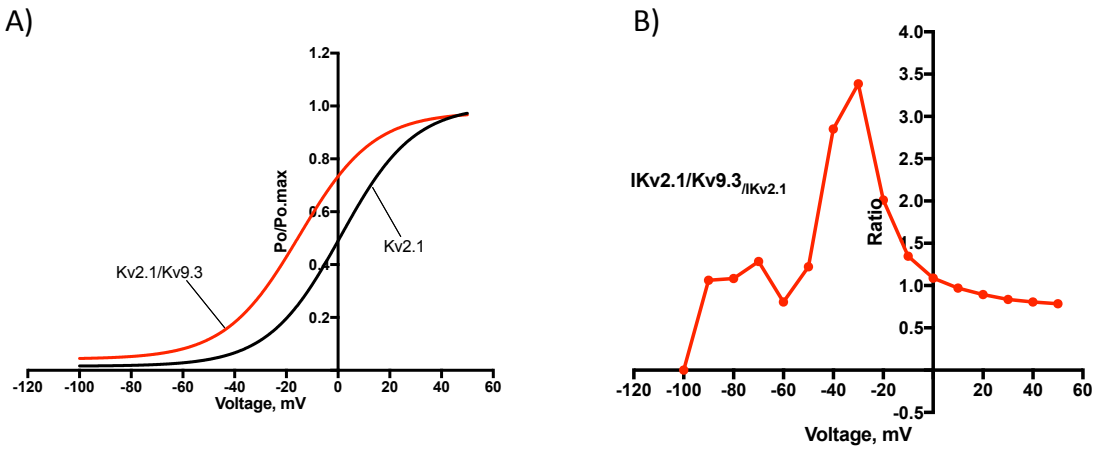

Figure 3.6: Comparison of Kv2.1/Kv9.3 with Kv2.1. A) To assess the steady-state activation, conditioning pulses from -100mV to +50 mV (increment: 10 mV) were applied. After each voltage step, voltage was clamped to -80mV. The relative open probabilities derived from the initial currents were plotted against the voltages of the depolarizing step and fitted with a Maxwell-Boltzmann function (Refer Equation 2 below). B) Ratio of sustained outward currents at different membrane potentials from Kv2.1/Kv9.3 cells to Kv2.1 cells.

$$\frac{Po}{Po.max} = Conductance\ (Bottom) + \frac{Conductance\ (Top) - Conductance\ (Bottom)}{1 + \exp\left(\frac{V1/2 - Vm}{\frac{RT}{zF}}\right)}$$

Equation 2: Boltzmann fit function. This equation describes the fraction of channels that are activated (Po/ Po.max) as a function of the membrane potential, Vm. $V_{1/2}$ is the potential at which conductance is halfway between the Conductance (Bottom) and Conductance (Top) and was calculated to be 1.11 ± 2.1 mV for Kv2.1 and -14.98 ± 2.1 mV for Kv2.1/Kv9.3. Conductance (Bottom) and Conductance (Top) are made into constants equal to 0.0 and 1.0, respectively. R is the universal gas constant, T is temperature in °K, F is the Faraday constant, and z is the valence. Adapted from Kerschensteiner and Stocker, 1999.

Effect of co-expression of Nox4 with Kv2.1 or Kv2.1/Kv9.3

When Nox4 is present with Kv2.1, the current amplitude closely resembled that of Kv2.1 homomer (Figure 3.7). Furthermore, co-expression of Nox4 with Kv2.1/Kv9.3 did not affect the current amplitude of the Kv2.1/Kv9.3 heteromer (Figure 3.7). Considering that Nox4 is a major reactive oxygen species producer in the PASMC and that reactive oxygen species cause deleterious effect via inhibition of Kv currents, the initial hypothesis would be that co-expression of Nox4 with either the homomer or

the heteromer will reduce the current amplitude. However, this effect is not seen in the results. In Chapter 6, we were interested to test the hypothesis that Nox4 overexpression sharpened the response of cells transiently transfected with Kv2.1 and to various reactive oxygen species.

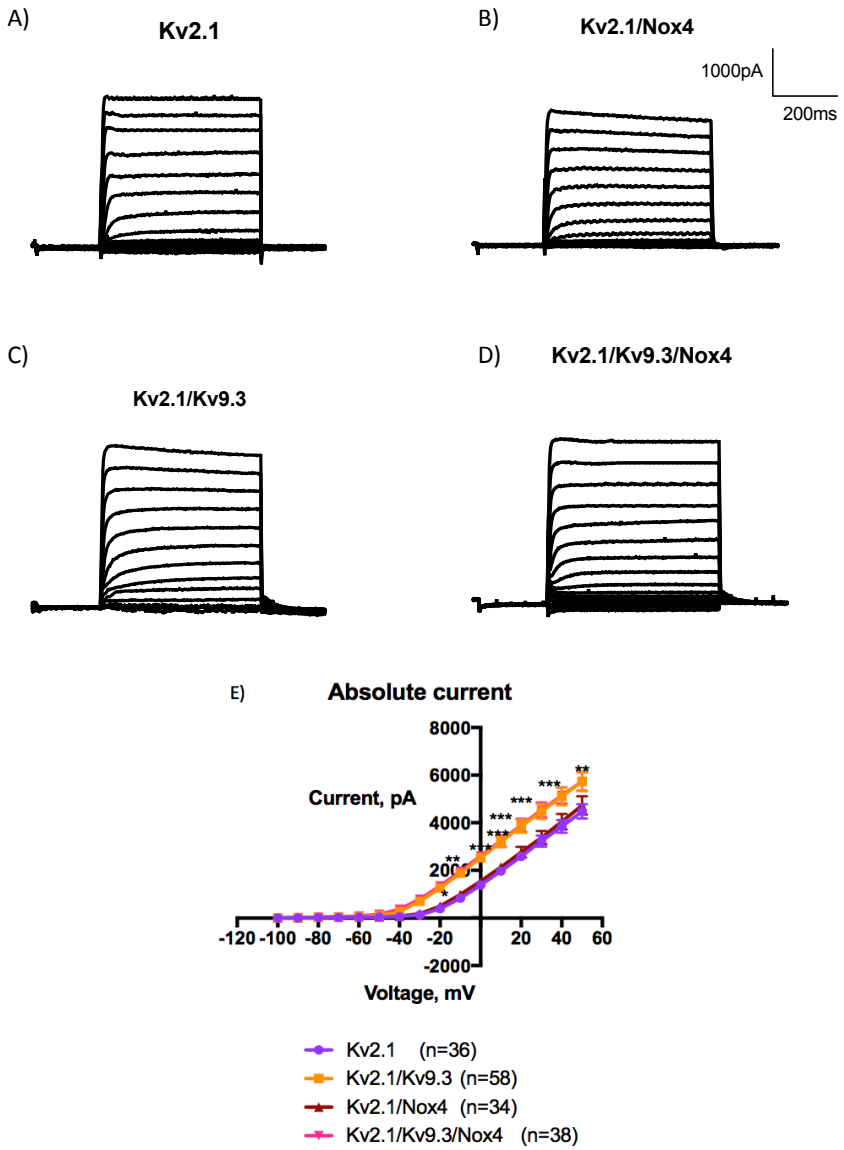

Figure 3.7: Co-expression of Nox4 with Kv2.1 or Kv2.1/Kv9.3 does not affect the current amplitude. Representative traces of A) Kv2.1 and B) Kv2.1/Nox4; C) Kv2.1/Kv9.3 and D) Kv2.1/Kv9.3/Nox4; E) Absolute current of Kv2.1, Kv2.1/Kv9.3, Kv2.1/Nox4, and Kv2.1/Kv9.3/Nox4 against test potential ranging from -100mV to +50mV. Two-way ANOVA followed by Tukey honestly significant difference method was used to analyze the difference between Kv2.1, Kv2.1/Kv9.3, Kv2.1/Nox4, and Kv2.1/Kv9.3/Nox4 and it was found that the there is no significant difference between Kv2.1 and Kv2.1/Nox4 and between Kv2.1/Kv9.3 and Kv2.1/Kv9.3/Nox4. Similar to Kv2.1 and Kv2.1/Kv9.3, the difference between Kv2.1/Nox4 and Kv2.1/Kv9.3/Nox4 is also statistically significant, with * indicating $p \leq 0.05$, ** indicating $p \leq 0.01$, *** indicating $p \leq 0.001$.

Kv2.1/Kv9.3/Nox4 cells show two types of steady-state activation trend

Initial set of experiments were performed where recordings were obtained for five cells transiently transfected with Kv2.1/Nox4 and Kv2.1/Kv9.3/Nox4. Taking -30mV as the test potential to be analyzed, the normalized current of the first five Kv2.1/Kv9.3/Nox4 cells recorded is significantly lower than that of the 20 Kv2.1/Kv9.3 cells recorded at the same time (Figure 3.8 A). Meanwhile, the normalized current of Kv2.1/Kv9.3/Nox4 cells recorded at a later stage is similar to that of Kv2.1/Kv9.3 (Figure 3.8 B). The two trends will be explained separately later in Figure 3.9 and Figure 3.10.

Whether co-expression of Nox4 with Kv2.1/Kv9.3 abolishes the effect of Kv9.3 in modulating Kv2.1 by causing the cells to be activated at a more negative potential remains elusive. This could be down to the transient effect of Nox4 or the unstable nature of the superoxide that Nox4 generates compared to the application of H_2O_2, which is constantly being perfused onto cells. Another argument would be that recombinant system might not the be the best way to study the effect of Nox4 as the function of Nox4 could be governed many other factors such as physical factors (stretch, shear stress, and pulsatile strain) and humoral factors (growth factors, cytokines, and vasoactive agents) in native settings. Moreover, the presence of regulatory proteins which might be important for Nox4 to propagate its effect might be missing as we are using heterologous expression system, and the absence of the regulatory protein(s) might prevent Nox4 from generating superoxide.

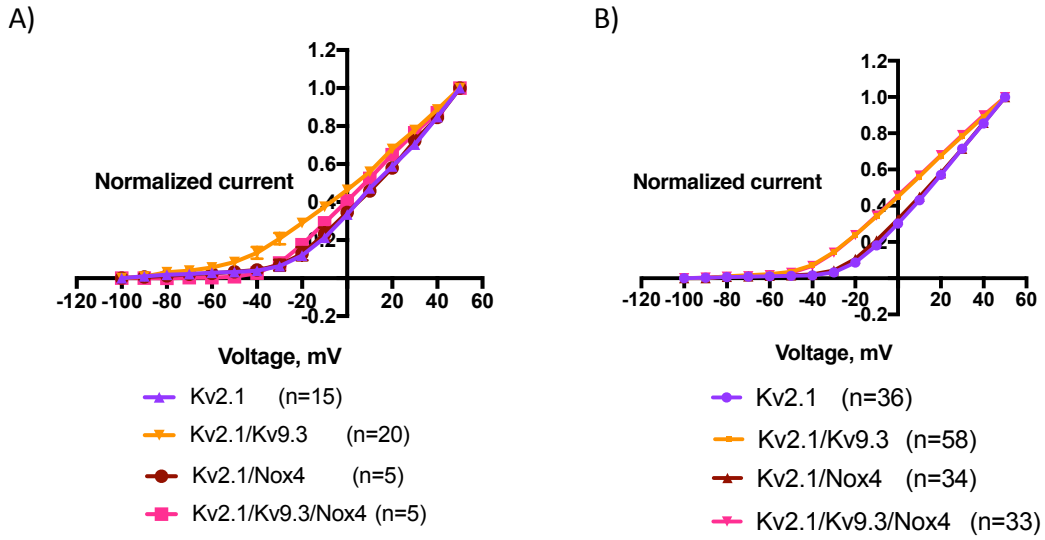

Figure 3.8: Kv2.1/Kv9.3/Nox4 cells show two types of steady-state activation trend. Plot of normalized current against various step voltages. A) Kv2.1/Kv9.3/Nox4 appears to have similar trend to Kv2.1 and Kv2.1/Nox4, indicating that Nox4 abolishes the effect of Kv9.3 on Kv2.1. B) Kv2.1/Kv9.3/Nox4 seems to show similar trend to Kv2.1/Kv9.3, indicating that Nox4 does not have any effect on either Kv2.1 or Kv9.3.

Nox4 abolishes the effect of Kv9.3 in shifting the activation threshold of Kv2.1 to a more polarized potential in one series of experiments

Kv2.1/Kv9.3 is activated at a more negative potential compared with Kv2.1 and Kv2.1/Nox4. Observing a subset of cells expressing Kv2.1/Kv9.3/Nox4, the heterotetramer lost the property of Kv2.1/Kv9.3 and instead displayed a similar trend to Kv2.1 (Figure 3.8 A and Figure 3.9). The normalized current at -30mV were analyzed using one-way ANOVA followed by Tukey's multiple comparison test to see if there is a difference between all the groups. The statistical analysis revealed that there is a significant difference between Kv2.1 and Kv2.1/Kv9.3 and also between Kv2.1/Nox4 and Kv2.1/Kv9.3 but there is no difference between Kv2.1/Kv9.3/Nox4 and Kv2.1/Kv9.3, with the p value being 0.0586, which is quite close to the threshold p value that is taken to be significant. The normalized currents at -30mV were also analyzed using one-way ANOVA followed by Dunnett's test with Kv2.1/Kv9.3 set as the control group, to see if there is a difference between the other groups compared with Kv2.1/Kv9.3. The statistical analysis revealed that there is a significant

difference between all the groups compared with Kv2.1/Kv9.3 (Figure 3.9). This could indicate that Nox4 abolishes the Kv9.3's effect on Kv2.1 activation threshold.

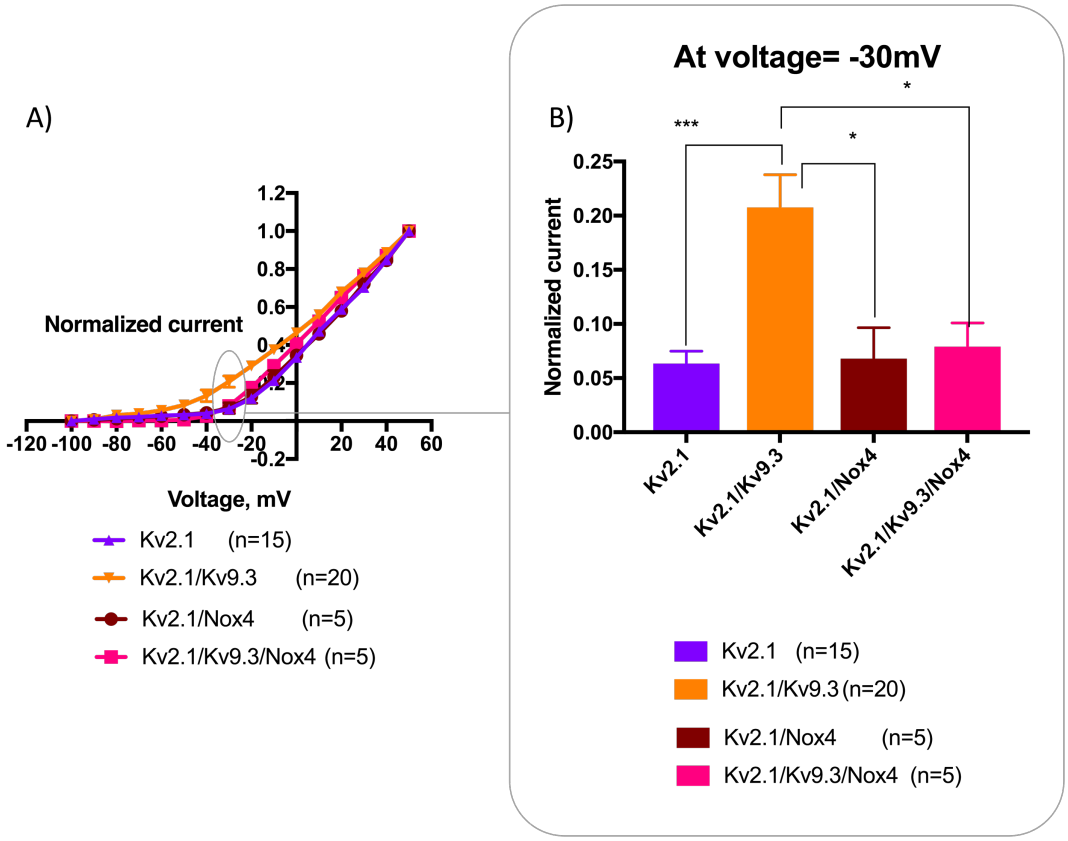

Figure 3.9: Nox4 abolishes the effect of Kv9.3 on the activation threshold of Kv2.1. A) Plot of normalized current for Kv2.1, Kv2.1/Kv9.3, Kv2.1/Nox4, and Kv2.1/Kv9.3/Nox4. B) Bar chart depicting the normalized current at V=-30mV for the respective cells, and Kv2.1/Kv9.3 has the highest normalized current at that potential, indicating that the heteromer channels are activated earlier than the rest. The difference between the normalized currents at -30mV for Kv2.1, Kv2.1/Nox4, and Kv2.1/Kv9.3/Nox4 were compared to that of Kv2.1/Kv9.3, using one-way ANOVA with Dunnett's method was also used to analyze if there is a difference between the normalized current of Kv2.1/Kv9.3 with other groups. It revealed that there is a statistical significant difference of between Kv2.1 and Kv2.1/Kv9.3 (with *** indicating $p \leq 0.001$), between Kv2.1/Kv9.3 and Kv2.1/Nox4 (with * indicating $p \leq 0.05$), and between Kv2.1/Kv9.3 and Kv2.1/Kv9.3/Nox4 (with * indicating $p \leq 0.05$).

Nox4 does not abolish the effect of Kv9.3 in shifting the activation threshold of Kv2.1 to a more polarized potential in another series of experiments

In another subset of Kv2.1/Kv9.3/Nox4 cells, the trend is similar to that of Kv2.1/Kv9.3 (Figure 3.8 B and Figure 3.10). This, instead, indicates that Nox4 does not have any effect on Kv9.3 or Kv2.1. When the data were analyzed using one-way

ANOVA with Dunnett's method, with Kv2.1/Kv9.3 being set as the control group as it is of interest to know if the other cell groups are different from Kv2.1/Kv9.3, it revealed that only Kv2.1 and Kv2.1/Nox4 are significantly different while the difference between Kv2.1/Kv9.3/Nox4 and Kv2.1/Kv9.3 is not significant (Figure 3.10B)

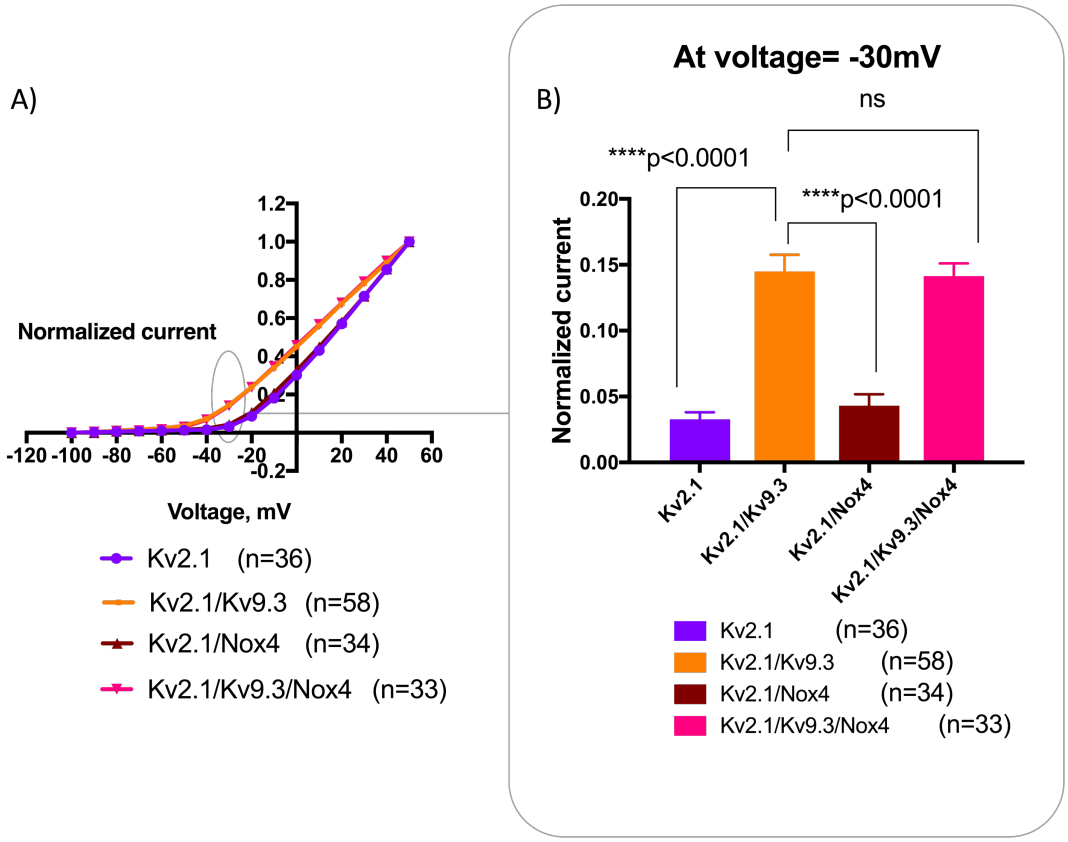

Figure 3.10: Nox4 does not abolish the effect of Kv9.3 in shifting the activation threshold of Kv2.1 to a more polarized potential. A) Plot of normalized current for Kv2.1, Kv2.1/Kv9.3, Kv2.1/Nox4, and Kv2.1/Kv9.3/Nox4. B) Bar chart depicting the normalized current at V=-30mV for the respective cells, and there is no significant difference between the normalized current of Kv2.1/Kv9.3 and Kv2.1/Kv9.3/Nox4, indicating that Nox4 does not abolish the Kv9.3 effect on Kv2.1's activation threshold. The difference between the normalized currents at -30mV for Kv2.1, Kv2.1/Nox4, and Kv2.1/Kv9.3/Nox4 were compared to that of Kv2.1/Kv9.3, using one-way ANOVA followed by Dunnett's test, with Kv2.1/Kv9.3 being set as the control group, with **** indicating $p < 0.001$.

Deactivation time constants of Kv2.1: effect of Kv9.3

Consistent with the findings of Zhong et al, 2010, the difference in the slope resulting from the repolarization to -50mV from various step voltages for Kv2.1 and Kv2.1/Kv9.3 was also observed in our experiments. The steps taken to analyze the

slopes for Kv2.1 and Kv2.1/Kv9.3 are depicted in Figure 3.11 and Figure 3.12, respectively. Although we observed that most of the current slopes resulting from the repolarization to -50mV occurred for every step voltage, we have chosen to current slope from +20mV, which corresponds to the 13th trace. This is for the ease of comparison with the current trace from the same voltage step that was chosen by Zhong et al., 2010. This slope/curve was fitted with a two-phase exponential function on pClamp 10.2 software (Axon Instruments, USA), with the recommended fitting method, Chebyshev. In addition, we have selected the option for forced positive of the measurement of time constants, τ and the number of terms were fixed to be 2, in order to calculate tfast and tslow. The two-phase exponential equation is given below (Equation 3). This fit also solves for the current amplitude, A and the constant y-offset, C for each component *i*. The longer deactivation kinetics of Kv2.1/Kv9.3 are apparent in the current traces shown in Figure 3.13 C, where the steeper slope of the current trace for Kv2.1 corresponds to a faster deactivation kinetic compared to that of Kv2.1/Kv9.3. The steepness of the slope for Kv2.1/Nox4 is almost similar to that of Kv2.1, indicating that the presence of Nox4 does not alter the deactivation kinetic.

$$f(t) = \sum_{i=1}^{n} A_i e^{-t/\tau_i} + C$$

Equation 3: Two-phase exponential function used in the fitting of curve resulting from the repolarization from +20mV to -50mV. A is the current amplitude, C is the constant y-offset, *i* is the component, and τ is the time constant for component *i*.

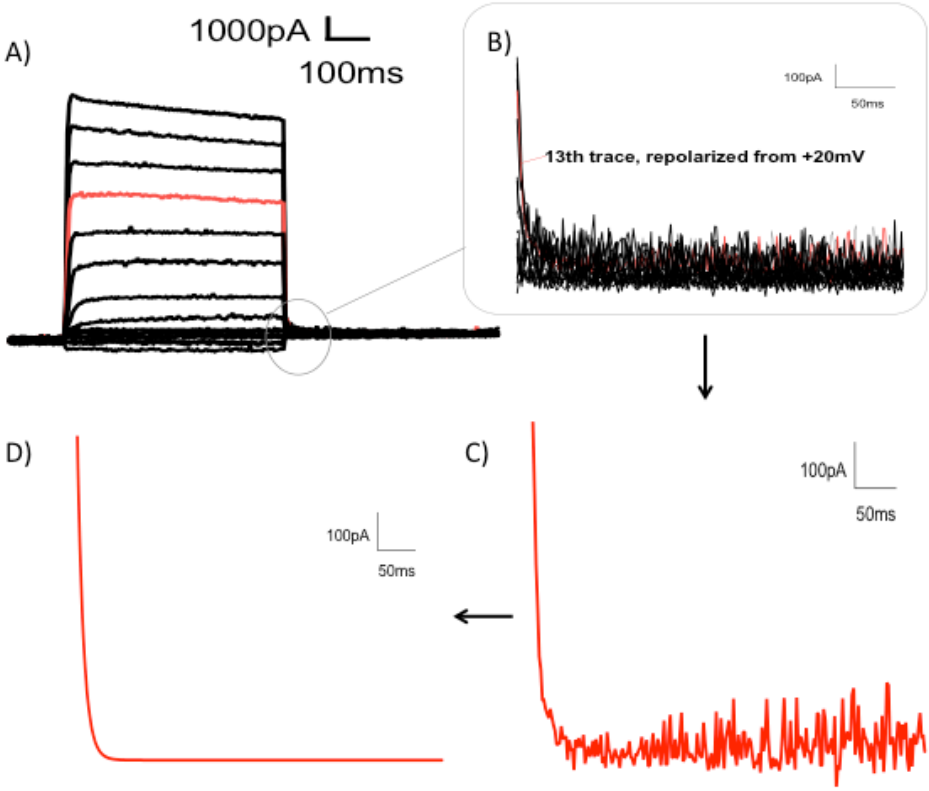

Figure 3.11: Steps to determine the slow and fast deactivation time constants (tslow and tfast) of current traces from a Kv2.1 cell. A) Overview of the voltage steps and the slopes resulting from repolarization from various potentials to -50mV. B) Magnification of the slopes, with the 13th trace, which corresponds to repolarization from +20mV, highlighted in red. C) The trace corresponding to repolarization from +20mV that was chosen for analysis. D) The trace corresponding to repolarization from +20mV that was fitted using the two-phase exponential equation using the Chebyshev method on pClamp 10.2 software, and the number of terms were fixed to be two, so that tslow and tfast can be determined.

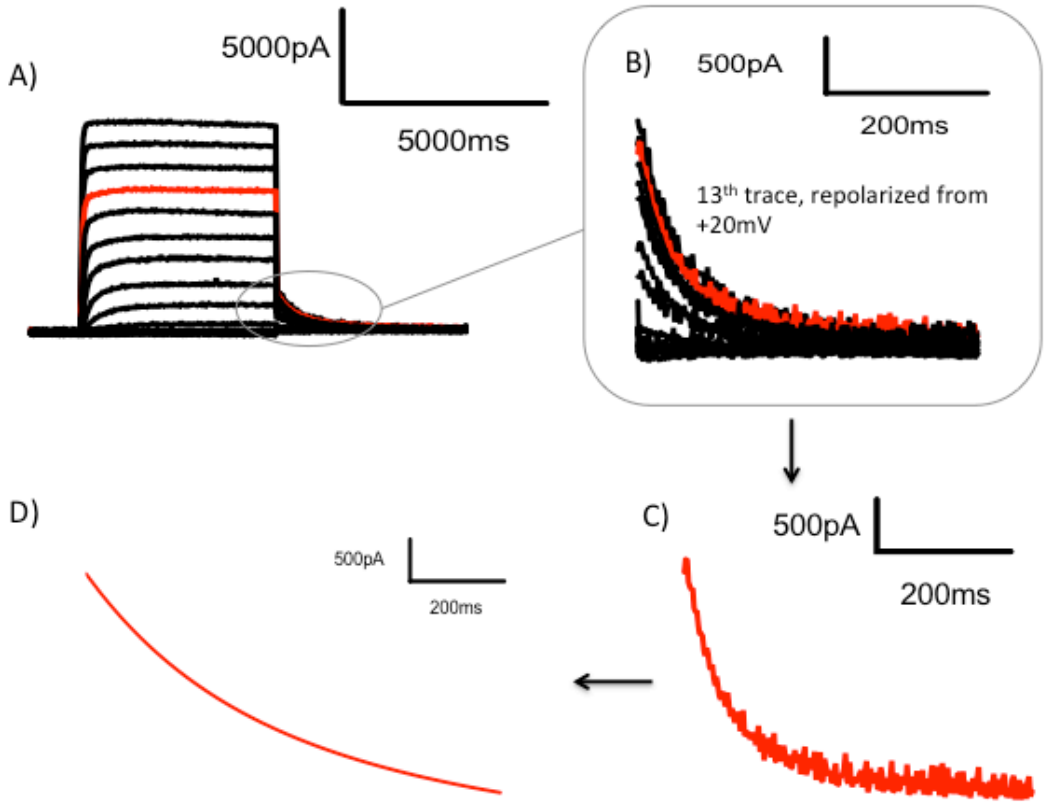

Figure 3.12: Steps to determine the slow and fast deactivation time constants (tslow and tfast) of current traces from a Kv2.1/Kv9.3 cell. A) Overview of the voltage steps and the slopes resulting from repolarization from various potentials to -50mV. B) Magnification of the slopes, with the 13th trace, which corresponds to repolarization from +20mV, highlighted in red. C) The trace corresponding to repolarization from +20mV that was chosen for analysis. D) The trace corresponding to repolarization from +20mV that was fitted using the two-phase exponential equation using the Chebyshev method on pClamp 10.2 software, and the number of terms were fixed to be two, so that tslow and tfast can be determined.

The decay of the tail current resulting from repolarization to -50mv from +20mV was measured and the slope is fitted with bi-exponential functions which then allowed for calculation of the slow and fast components. Co-expression with Kv9.3 increases the tslow and tfast of Kv2.1, evident in the reduction in steepness of the current decay slope of cells transfected with Kv2.1/Kv9.3 compared with Kv2.1 (Figure 3.13C). The results were quantified in a bar chart also supported this finding, where the time constants for Kv2.1 were (tslow = 63.7 ± 4.2 ms, tfast = 9.0 ± 0.8ms, n=12) compared with Kv2.1/Kv9.3 (tslow = 120.1 ± 5.5 ms, tfast = 31.0 ± 2.0 ms, n=15) (Figure 3.13D) and the Student's t-test performed to analyze the difference between cells

transfected with Kv2.1 compared with Kv2.1/Kv9.3 revealed that there is a statistical difference between them. Measurement of the deactivation time constant is a method to distinguish Kv2.1 and Kv2.1/Kv9.3. The observation here is in line with the results published by other researchers ((Hristov et al., 2012; Zhong et al., 2010). Kv2.1/Nox4 displayed fast deactivation kinetics, similar to the trend seen in Kv2.1 cells while Kv2.1/Kv9.3/Nox4 cells showed a more similar trend to Kv2.1/Kv9.3 (Figure 3.13E and Figure 3.13F).

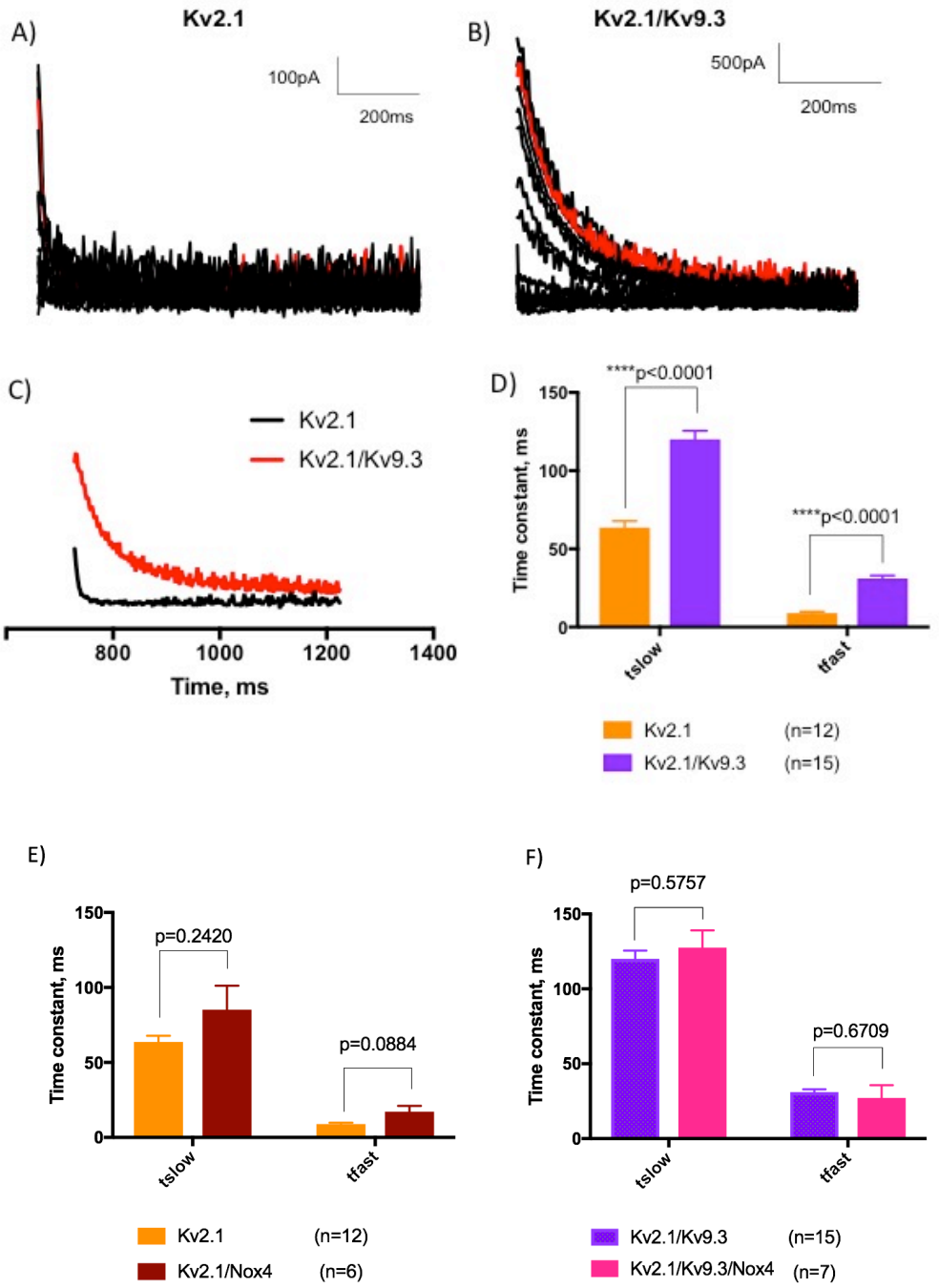

Figure 3.13: Kv9.3 prolongs the slow component of the deactivation time constant (tslow) of Kv2.1 but Nox4 does not have any effect on the deactivation kinetics of Kv2.1 and Kv2.1/Kv9.3. Current traces at the slope where the repolarization from various voltage steps to -50mV occurs for A) Kv2.1 and B) Kv2.1/Kv9.3. C) The 13th trace resulting from repolarization from +20mV for Kv2.1 (Black) and Kv2.1/Kv9.3 (Red). D) Bar chart depicting the two components of the deactivation time constant (tslow and tfast) of Kv2.1 and Kv2.1/Kv9.3, where time constants for Kv2.1 were (tslow = 63.7 ± 4.2 ms, tfast = 9.0 ± 0.8ms, n=12) compared with Kv2.1/Kv9.3 (tslow = 120.1 ± 5.5 ms, tfast = 31.0 ± 2.0 ms, n=15). Student's t-test with Welch's correction was used to analyze whether the difference between the two populations were statistically significant, with $p \leq 0.05$ taken as the threshold value. Student's t-test revealed that the differences in both tslow and tfast were statistically significant, with **** indicating that $p < 0.0001$. Cells expressing the channels were patched with external solution perfusion. Bar chart depicting the two components of the deactivation time constant (tslow and tfast) of E) Kv2.1 compared with Kv2.1/Nox4 (tslow = 85.2 ± 15.9 ms, tfast = 17.2 ± 3.9 ms, n=6), and Student's t-test revealed that there is no statistically significant difference between them and F) Kv2.1/Kv9.3 vs Kv2.1/Kv9.3/Nox4 (tslow = 127.5 ± 11.6 ms, tfast = 27.2 ± 8.5 ms, n=7), and there is no significant difference between them.

Modulation of Kv2.1 in terms of open-state and closed-state inactivation

Kv9.3 decelerates the open-state inactivation of Kv2.1

According to Kerschensteiner et al, 2003, co-expression of Kv9.3 with Kv2.1 will cause a deceleration of the open-state inactivation. This state of inactivation can be tested by applying a test pulse at +40mV for 32s to see how the current decay compared to the current at the starting point of the pulse. The representative traces in Figure 3.14A and Figure 3.14B confirmed the observation of Kerschensteiner et al, 2003, where Kv2.1/Kv9.3 showed a slower decay of current by the end of the pulse compared with Kv2.1. However, when the results were plotted as normalized current (current at the end of the pulse, IPn, normalized to current at the start of the pulse, IP) over time, the Kv2.1/Kv9.3 trend was not significantly different from that of Kv2.1 (Figure 3.14C).

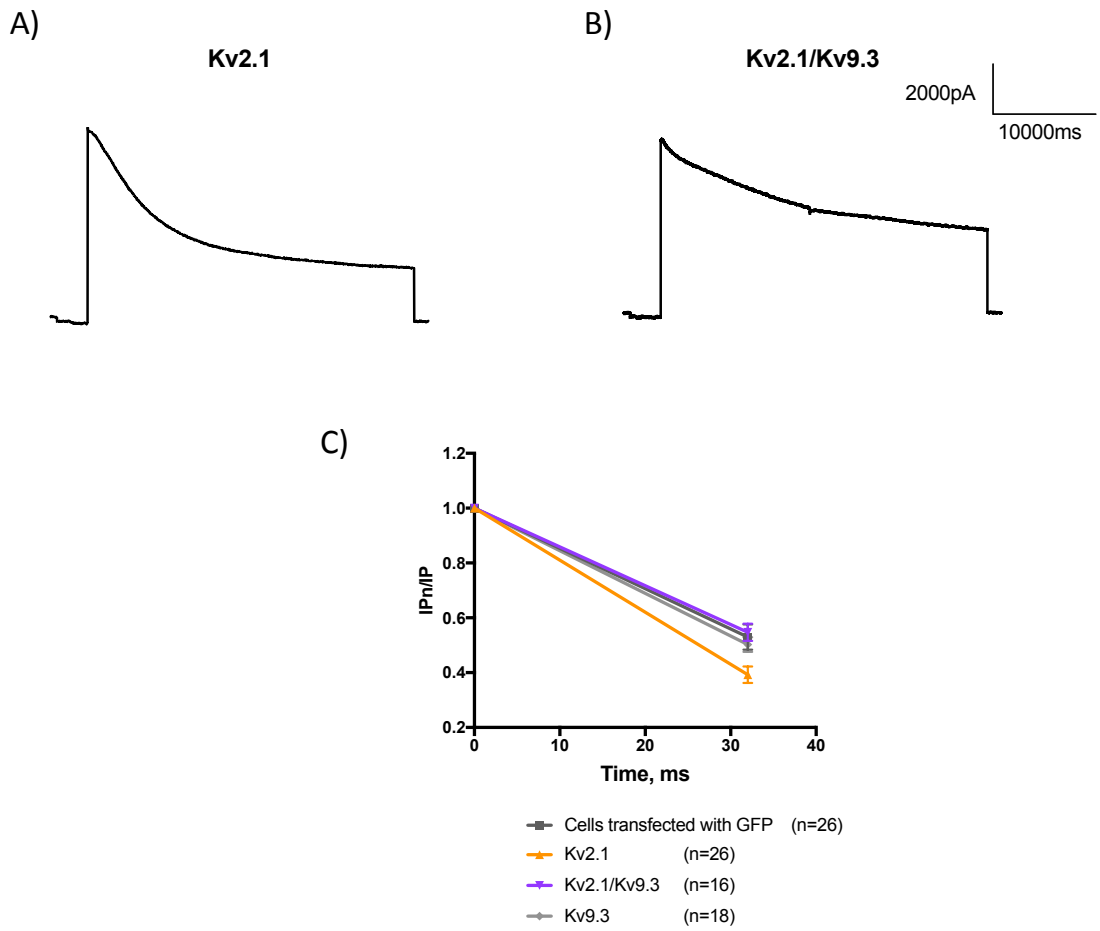

Figure 3.14: Kv9.3 slows the open-state inactivation of Kv2.1. Recordings were obtained using the open-state inactivation protocol outlined in Chapter 2. Cells were injected with a test pulse at +40mV for 32s, then repolarized to -80mV before being returned to the holding potential -60mV. Representative traces for A) Kv2.1 and B) Kv2.1/Kv9.3. C) Normalized current, IPn/IP plotted against holding time for cells transfected with GFP, Kv2.1, Kv2.1/Kv9.3 and Kv9.3 cells. Although the error bars of Kv2.1 did not overlap with that of Kv2.1/Kv9.3, Student's t-test with Welch's correction performed on the difference in the normalized current at the end point showed that there is no statistically-significant difference between them.

Kv9.3 accelerates Kv2.1 closed-state inactivation

Interestingly, it has also been published that co-expression of Kv9.3 with Kv2.1 accelerates the closed-state inactivation of Kv2.1. Closed-state inactivation can be determined by giving two test pulses, in which the holding time between the two pulses increases in every sweep. It had been found that the current density of the cells transfected with Kv2.1 decreases as the period at which the second test pulse is given increases. When Kv9.3 is expressed with Kv2.1, the current density decreases faster, as can be seen in the representative traces (Kv2.1 in Figure 3.15A compared to Kv2.1/Kv9.3 in Figure 3.15B). This effect is also shown when the results were quantified in a plot of current ratio at the end of the pulse compared with start of the pulse, Ipn/IP against holding time, where from the third test pulse onwards there is non-overlapping readings and error bars for Kv2.1 and Kv2.1/Kv9.3 (Figure 3.15C). The reduction of current at different holding time between the first and second pulse was analysed using two-way ANOVA, followed by Sidak test as post-hoc. I have chosen Sidak as post-hoc because the cell readings for Kv2.1 are independent from those of Kv2.1/Kv9.3, hence making it a suitable post-hoc and this method has higher statistical power than the commonly used Bonferroni test. The analysis revealed that when the holding time between the first and second pulse was 16s, 20s, and 28s, there is a significant difference between the current ratio (IPn/IP) for Kv2.1 and Kv2.1/Kv9.3. This result is consistent with that established by Kerschensteiner et al, 2003.

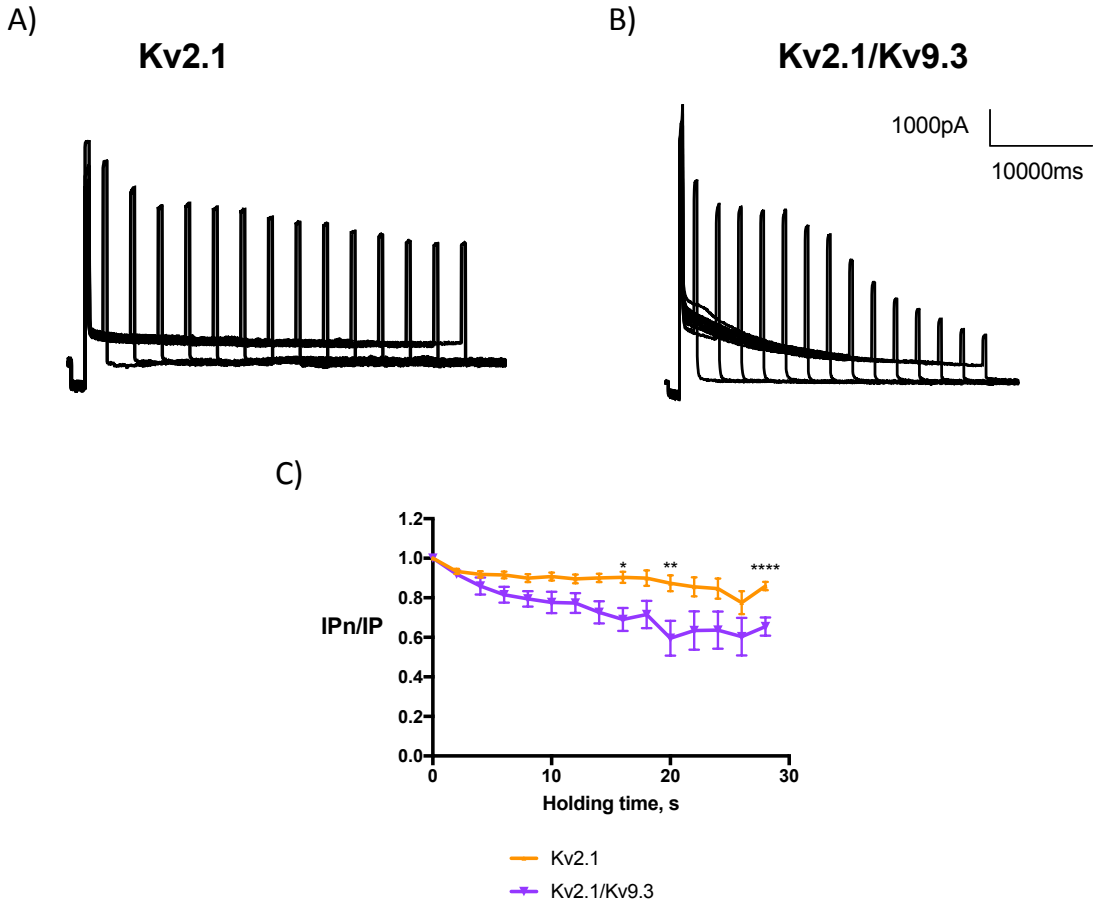

Figure 3.15: Kv9.3 accelerates Kv2.1 closed-state inactivation. Recordings were obtained using the closed-state inactivation protocol outlined in Chapter 2. Cells were hyperpolarized to -100mV before being injected with a test pulse at +40mV twice and then returned to the holding potential of -60mV. For the first sweep, the gap between the first test pulse and the second test pulse was 2s. The gap between the test pulses were increased by 2s in subsequent sweep, meaning the gap was 4s in the second sweep, 6s in the third sweep and so on. Representative current traces for A) Kv2.1 and B) Kv2.1/Kv9.3 in the closed-state inactivation protocol. C) Plot of current ratio at the second pulse compared with first pulse, IPn/IP against holding time. The current ratio IPn/IP is proportional to the number of channels that did not inactivate. Two-way ANOVA followed by Sidak test to analyse the current ratio when the gap between first and second pulse at every holding time revealed that there is a statistically-significant difference for Kv2.1 and Kv2.1/Kv9.3 when the holding time is 16s, 20s, and 28s. * indicated $p \leq 0.05$, ** indicated $p \leq 0.01$, and **** indicated that $p < 0.0001$.

Modulation of Kv2.1, Kv9.3, and Nox4 by stromatoxin (ScTx-1)

To assess the effect of ScTx-1 on Kv2.1, Kv2.1/Kv9.3, Kv2.1/Nox4 and Kv2.1/Kv9.3/Nox4 cells, tsA-201 cells were transfected with the respective combination of cDNAs and electrophysiology recordings were obtained in the absence and presence of 100nM ScTx-1. According to Escoubas et al., 2002, this is the concentration that permits ~90% inhibition of Kv2.1/Kv9.3 current based on observation in experiments performed using expressed channel. Due to the high cost of ScTx-1, patch clamp electrophysiology was performed on cells cultured on a coverslip that was immersed in external solution with ScTx-1 added, without being perfused. In a normal experiment setup, cells are perfused with external solution or external solution with redox agents added. Standard voltage-step protocol, as described in Chapter 2 (Materials and Methods), was used.

Effect of ScTx-1 on current amplitude and activation threshold

In line with the published results of other research groups, ScTx-1 does indeed act as a Kv2.1 blocker by reducing the current amplitude as the difference between current amplitude at 30mv, 40mV, and 50mV for Kv2.1 and Kv2.1/ScTx-1 is statistically significant (Figure 3.16 C). However, ScTx-1 does not have any impact on the activation threshold of Kv2.1 (Figure 3.16 D).

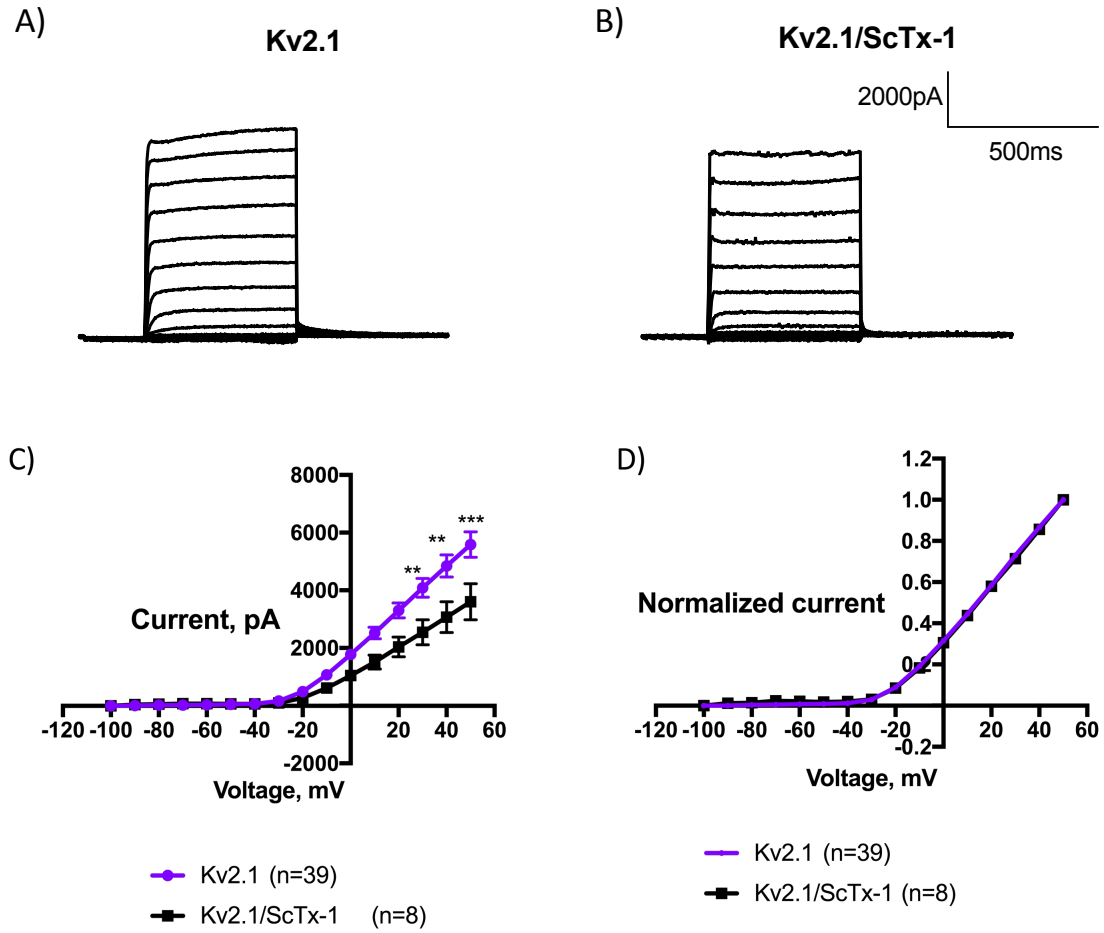

Figure 3.16: ScTx-1 decreases the current amplitude of Kv2.1 but does not affect the activation threshold of Kv2.1. tsA-201 cells were transiently transfected with Kv2.1. Electrophysiology recordings were obtained using the standard voltage-step protocol. 100nM ScTx-1 was used for treated cells. Representative current traces of A) Kv2.1 and B) Kv2.1/ScTx-1; C) IV relationship of Kv2.1 (purple) and Kv2.1/ScTx-1 (black); D) Normalized current against voltage plot for Kv2.1 (purple) and Kv2.1/ScTx-1 (black). Two-way ANOVA followed by Sidak as post-hoc was used to analyze the difference between the current from the tsA-201 cells transfected with Kv2.1 without ScTx-1 treatment (purple) and with ScTx-1 treatment (black) at every voltage. ** indicates $p \leq 0.01$ and *** indicates $p \leq 0.001$.

Surprisingly, the presence of Kv9.3 renders the effect of ScTx-1 on current amplitude of Kv2.1 ineffective (Figure 3.17 C). This is contrary to the results published by Zhong et al, 2010 who proposed that the ScTx-1-sensitive RMCA current has a more similar profile to Kv2.1/Kv9.3 current, in terms of longer deactivation kinetics and a shift in the activation threshold towards a more negative membrane potential. However, it must be emphasized that they have compared native RMCA with Kv2.1/Kv9.3 cells, both in the presence of ScTx-1 (Zhong et al., 2010). The Kv2

blocker also does not have any effect on the activation threshold of Kv2.1/Kv9.3 (Figure 3.17 D).

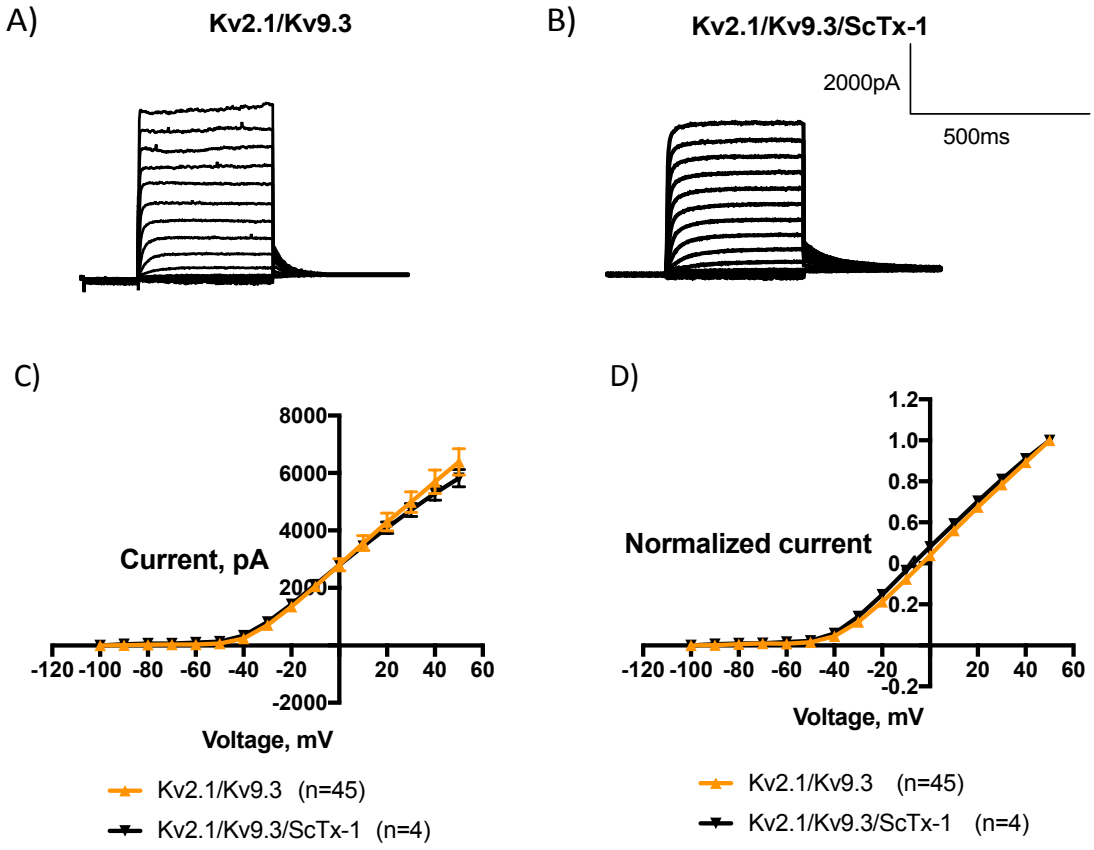

Figure 3.17: ScTx-1 does not have an impact on the current amplitude and activation threshold of Kv2.1/Kv9.3. tsA-201 cells were transiently transfected with Kv2.1/Kv9.3. Electrophysiology recordings were obtained using the standard voltage-step protocol. 100nM ScTx-1 was used for treated cells. Representative current traces of A) Kv2.1/Kv9.3 and B) Kv2.1/Kv9.3/ScTx-1; C) IV relationship of Kv2.1/Kv9.3 (orange) and Kv2.1/Kv9.3/ScTx-1 (black); D) Normalized current against voltage plot for Kv2.1/Kv9.3 (orange) and Kv2.1/Kv9.3/ScTx-1 (black). Two-way ANOVA followed by Sidak test was used to analyze the difference between the current from the tsA-201 cells transfected with Kv2.1/Kv9.3 without ScTx-1 treatment (orange) and with ScTx-1 treatment (black) at every voltage. There is no statistically significant difference between the current of Kv2.1/Kv9.3 without or with ScTx-1 treatment at every voltage.

Similar to the results where ScTx-1 reduces the current amplitude of Kv2.1, the Kv2 blocker is also effective despite the presence of Nox4. This effect is apparent in the representative current traces comparing Kv2.1/Nox4 (Figure 3.18 A) and Kv2.1/Nox4/ScTx-1 (Figure 3.18 B) and also the IV graph (Figure 3.18 C). The current amplitudes at 30mV, 40mV, and 50mV were statistically significant when comparing Kv2.1/Nox4 in the absence and presence of ScTx-1 (Figure 3.18C). It is surprising as to why the presence of Kv9.3 renders ScTx-1 ineffective in reducing Kv2.1 current yet the presence of Nox4 does not have any effect on ScTx-1. Perhaps, this further confirms that Nox4 does not regulate Kv2.1 (as has been demonstrated earlier) and therefore, its presence does not change the interaction of Kv2.1 with ScTx-1. The Kv2 blocker also does not alter the activation threshold of Kv2.1/Nox4 and this observation is parallel to the one with Kv2.1 alone (Figure 3.18 D).

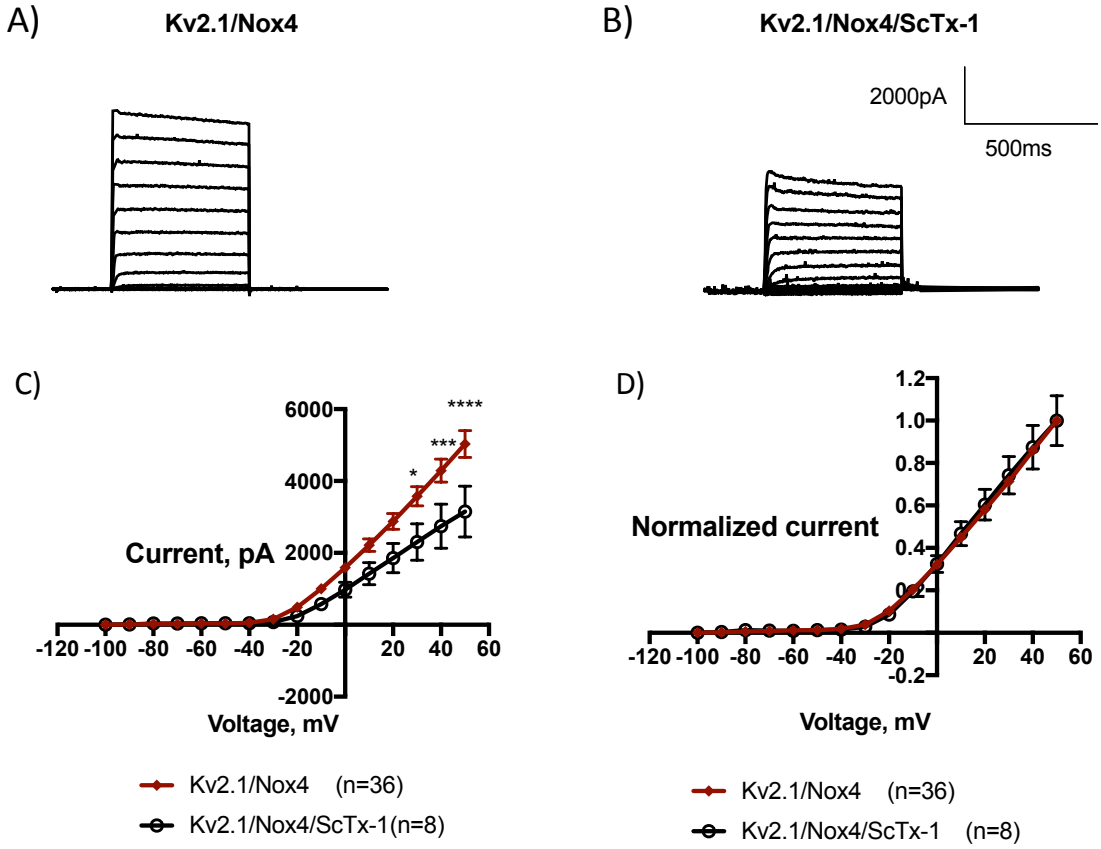

Figure 3.18: ScTx-1 decreases the current amplitude of Kv2.1/Nox4 but does not affect the activation threshold of Kv2.1. tsA-201 cells were transiently transfected with Kv2.1/Nox4. Electrophysiology recordings were obtained using the standard voltage-step protocol. 100nM ScTx-1 was used for treated cells. Representative current traces of A) Kv2.1/Nox4 and B) Kv2.1/Nox4/ScTx-1; C) IV relationship of Kv2.1/Nox4 (brown) and Kv2.1/Nox4/ScTx-1 (black); D) Normalized current against voltage plot for Kv2.1/Nox4 (brown) and Kv2.1/Nox4/ScTx-1 (black). Two-way ANOVA followed by Sidak test was used to analyze the difference between the current from the tsA-201 cells transfected with Kv2.1/Nox4 without ScTx-1 treatment (brown) and with ScTx-1 treatment (black) at every voltage. The analysis revealed that the current amplitudes at 30mV, 40mV, and 50mV were statistically significant for Kv2.1/Nox4 and Kv2.1/Nox4/ScTx-1. * indicates $p \leq 0.05$, *** indicates $p \leq 0.001$, and **** indicates $p < 0.0001$.

Since ScTx-1 does not have any effect on the current amplitude and activation threshold of Kv2.1/Kv9.3, it is not surprising that the toxin does not affect Kv2.1/Kv9.3/Nox4 (Figure 3.19 C and Figure 3.19 D). Concurrent with the observation with Kv2.1/Nox4, the presence of Nox4 does not have any impact on Kv2.1/Kv9.3, further strengthening the claim that Nox4 does not regulate Kv2.1 or Kv2.1/Kv9.3.

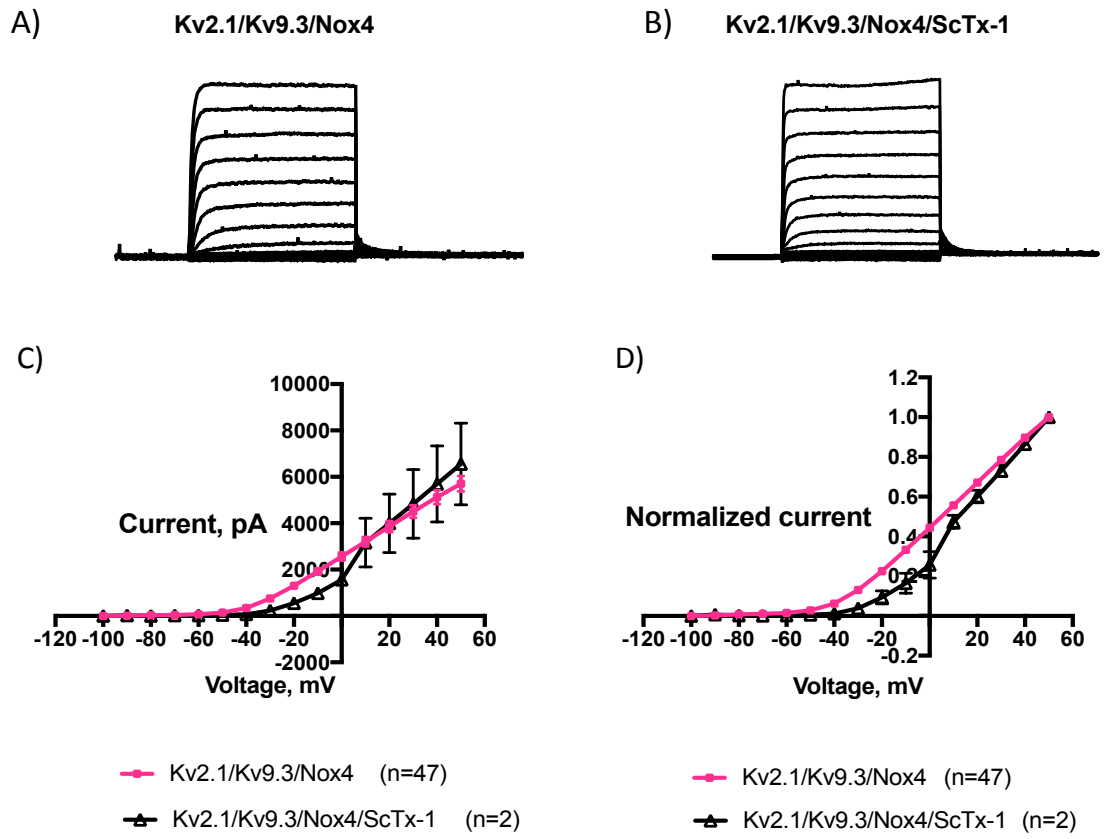

Figure 3.19: ScTx-1 does not have an impact on the current amplitude and activation threshold of Kv2.1/Kv9.3/Nox4. tsA-201 cells were transiently transfected with Kv2.1/Kv9.3/Nox4. Electrophysiology recordings were obtained using the standard voltage-step protocol. 100nM ScTx-1 was used for treated cells. Representative current traces of A) Kv2.1/Kv9.3/Nox4 (pink) and B) Kv2.1/Kv9.3/Nox4/ScTx-1 (black); C) IV relationship of Kv2.1/Kv9.3/Nox4 (pink) and Kv2.1/Kv9.3/Nox4/ScTx-1 (black); D) Normalized current against voltage plot for Kv2.1/Kv9.3/Nox4 (pink) and Kv2.1/Kv9.3/Nox4/ScTx-1 (black). Two-way ANOVA followed by Sidak test was used to analyze the difference between the current from the tsA-201 cells transfected with Kv2.1/Kv9.3/Nox4 without ScTx-1 treatment (pink) and with ScTx-1 treatment (black) at every voltage. There is no statistically significant difference between the current of Kv2.1/Kv9.3/Nox4 without or with ScTx-1 treatment at every voltage.

Effect of ScTx-1 on time constants of deactivation

Consistent with the finding of Zhong et al., 2004 and the results in Figure 3.13D, the tslow of Kv2.1/Kv9.3 heteromer is significantly longer than that of Kv2.1 homomer (Figure 3.20) even in non-perfused setup. Since it is postulated that Kv channels in PASMC are mostly expressed as Kv2.1/Kv9.3 heteromers, this finding could have implications on how slow deactivation kinetics are favoured in the PASMC, allowing more K^+ ions efflux, to dampen the cell excitability.

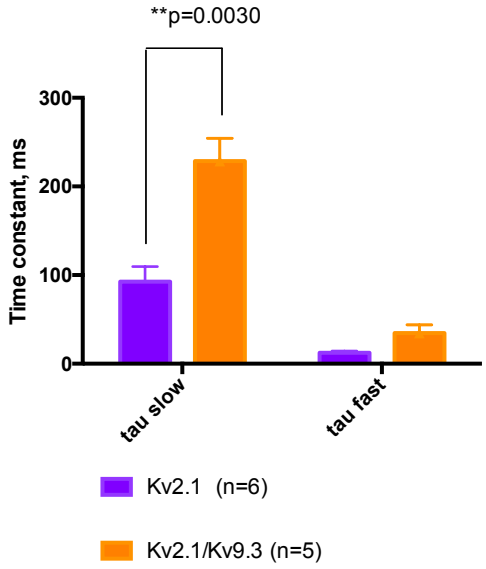

Figure 3.20: Kv2.1/Kv9.3 has a significantly longer tslow compared with Kv2.1 in non-perfused setup. tsA-201 cells were transiently transfected with Kv2.1 or Kv2.1/Kv9.3. Electrophysiology recordings were obtained using the standard voltage-step protocol. The current slope resulted from repolarization from +20mV to -50mV were fitted using the bi-exponential function, with the Chebyshev method and number of terms were fixed at 2, to allow for calculation of tslow and tfast. Bar chart showing tslow and tfast for Kv2.1 (purple) and Kv2.1/Kv9.3 (orange). Student's t-test was used to analyze the difference between tslow and tfast of Kv2.1 and Kv2.1/Kv9.3, with $p \leq 0.05$ taken as statistically significant value. t-test revealed that tslow of Kv2.1/Kv9.3 is significantly higher than that of Kv2.1, with p=0.0030.

As demonstrated in the current traces, the gradient of the slopes remained unchanged in the absence or presence of 100nM ScTx-1 (Figure 3.21A, Figure 3.21 B, Figure 3.21 C). The slopes were fitted with a bi-exponential function using the recommended Chebyshev method, and number of terms were fixed at two in order to quantify the slow and fast components of the deactivation kinetics, tslow and tfast. The bar chart showed that there is no difference in the tslow and tfast of Kv2.1, Kv2.1/Kv9.3, and Kv2.1/Nox4 in the absence and presence of ScTx-1 (Figure 3.21 D, Figure 3.21 E, Figure 3.21 F). This could indicate that ScTx-1 does not affect the deactivation kinetics of the channels.

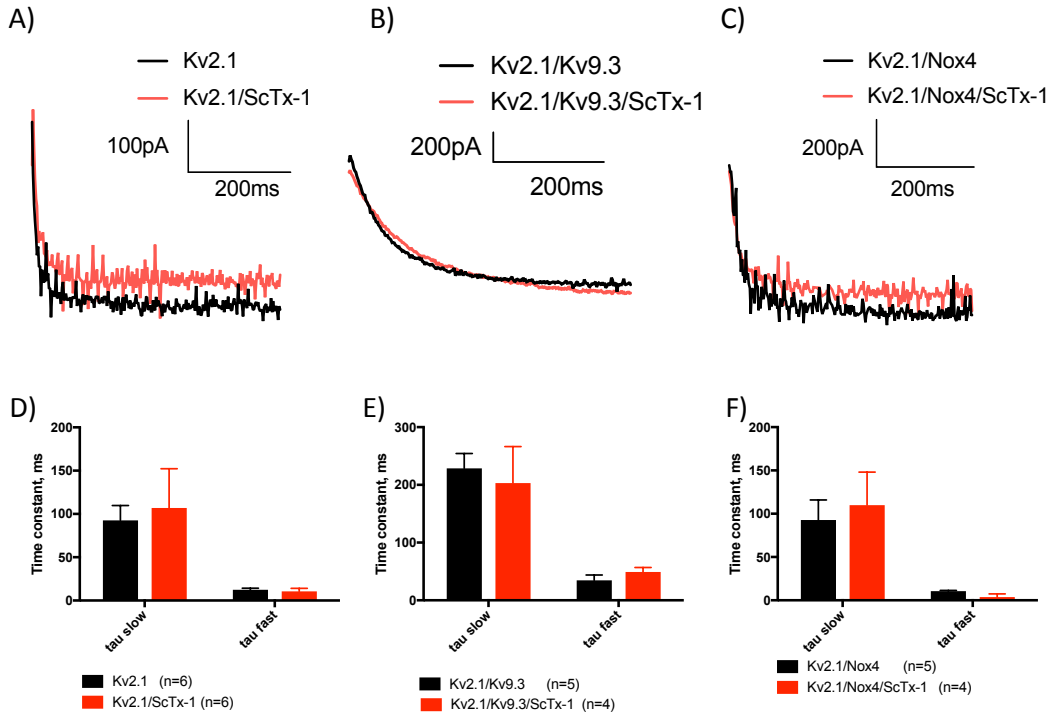

Figure 3.21: Addition of ScTx-1 does not alter the tslow or tfast of Kv2.1, Kv2.1/Kv9.3, and Kv2.1/Nox4. tsA-201 cells were transiently-transfected with the respective cDNAs and recordings were obtained using the standard voltage-step protocol. Current traces during repolarization to -50mV, from +20mV of A) Kv2.1 with and without ScTx-1, B) Kv2.1/Kv9.3 with and without ScTx-1, C) Kv2.1/Nox4 with and without ScTx-1; Current traces (slopes) were fitted with bi-exponential function using the recommended Chebyshev method and number of terms were fixed at two to allow calculation of tslow and tfast. Bar charts depicting the mean ± SEM of tslow and tfast for D) Kv2.1 and Kv2.1/ScTx-1; E) Kv2.1/Kv9.3 and Kv2.1/Kv9.3/ScTx-1; and F) Kv2.1/Nox4 and Kv2.1/Nox4/ScTx-1. Student's t-test was used to analyze the difference between Kv2.1 with and without ScTx-1, Kv2.1/Kv9.3 with and without ScTx-1, Kv2.1/Nox4 with and without ScTx-1. Student's t-test did not reveal any significant difference between the cell populations, indicating that ScTx-1 treatment does not have any effect on the deactivation kinetics of the cells.

3.3 Discussion

Results presented here on the modulation of Kv2.1 by Kv9.3 agree with the research that has been published by other groups. In terms of Kv9.3 increasing the current amplitude of Kv2.1, Patel et al, 1997 and Zhong et al, 2010 have reported similar findings. Interestingly, co-expression of Kv9.3 with Kv2.1 also causes Kv2.1 to be activated earlier (at a more negative/hyperpolarized potential) compared with Kv2.1 homomers. Such modulation might have positive impacts in PH as it will allow more K^+ ions to leave the cell at a given potential (therefore higher Kv2.1 current) and a longer time for the efflux to occur since the channels are opened earlier. Functional interaction of Kv2.1 and Kv9.3 agrees with the finding of Zhong et al, 2010 who concluded that the predominant ion channels expressed in the PASMC are likely to be Kv2.1/Kv9.3 heteromers instead of Kv2.1 homomers.

Kv9.3 also delays the open-state inactivation while accelerating the closed-state inactivation of Kv2.1. This means that the Kv2.1/Kv9.3 favours the closed-state inactivation, allowing for speedier recovery before the next action potential. When resolving the current decay to study two components of the deactivation kinetics, namely the slow and fast deactivation time constants, it was found that Kv9.3 prolongs both components. This could probably have positive consequences in PH since the time taken for the channels to deactivate is lengthened thus slowing down depolarization, thereby reducing excitability of the PASMC.

RNA expression levels for Kv2.1, Kv9.3, and Nox4 are upregulated during hypoxia (Archer et al, 2004, Mittal et al, 2007, Mittal et al, 2011). It is interesting to note that although Kv2.1 and Kv9.3 are upregulated, hypoxia decreases the sustained outward current (Dong et al., 2012). This could be perhaps due to a modulating factor that inhibits the channels in hypoxia. There are countless of debates as to where Reactive oxygen species are derived, the mitochondria or NADPH oxidase (Harrison et al., 2007; Lee et al., 2013; Mittal et al., 2012, 2007). Our hypothesis was reactive oxygen species are derived from NADPH oxidase and thus Nox4 would be the candidate of interest. This is because Nox4 is abundantly expressed in lung tissues and is the only

NADPH oxidase subunit that was significantly upregulated in PASMC in response to chronic hypoxia in PASMC derived from rats and mice lung tissue. Nox4 has also been shown to contribute to pulmonary vascular remodelling in systemic vasculatures and pulmonary arteries (Brandes et al., 2010; Mittal et al., 2012). Although Mittal et al, 2011 argued that Nox4 colocalizes with Kv1.5 but not Kv2.1, we were interested to see if the co-expression of Kv9.3 with Kv2.1 would change that, in other words, if Kv9.3 is needed for interaction of Nox4 with Kv2.1. Consistent with this argument, my study found that Nox4 does not significantly alter the electrophysiological properties of Kv2.1 homomers, either in terms of current amplitude, activation threshold, and deactivation kinetics. In one series of experiment, it was found that the co-expression of Nox4 with Kv2.1/Kv9.3 abolished the effect of Kv9.3 in shifting the activation threshold (meaning the behaviour was more similar the Kv2.1 rather than the Kv2.1/Kv9.3). However, in another series of experiment, Kv2.1/Kv9.3/Nox4 cells displayed a similar behaviour to Kv2.1/Kv9.3. The five cells in the first series of experiment that displayed a similar behaviour to Kv2.1 could indicate that the presence of Nox4 is interrupting the Kv2.1-Kv9.3 interaction. We hypothesized that Nox4 is binding to the site of Kv2.1-Kv9.3 interaction, or that presence of Kv9.3 helped Nox4 docked to a site which allows Nox4 to interfere with the Kv2.1-Kv9.3 interaction. Alternatively, Nox4 might directly modulate Kv9.3, thereby inhibiting it from modulating Kv2.1. However, in the latter series of experiment, Kv2.1/Kv9.3/Nox4 cells behaved more similarly to Kv2.1/Kv9.3 cells. Although Kv9.3 is a silent channel, it is structurally similar to Kv2.1, which perhaps explains why they are able to heteromultimerize in the first place (Kerschensteiner, 2003). This being said, if Nox4 has been shown not to modulate Kv2.1, then even the presence of Kv9.3 that can 'potentially' bring Nox4 into a close proximity to Kv2.1 will not cause any difference to the Kv2.1 properties. As to the possibility that Nox4 directly modulates Kv9.3 thereby interfering with Kv9.3-Kv2.1 interaction, the likelihood is small since Nox4 fails to regulate Kv2.1.

While most researchers proposed Nox4 as the only predominant NADPH oxidase subunit upregulated in hypoxia, Buttigieg et al, 2012 concluded that Nox2 is the predominant oxygen sensor that modulates activity of Kv channels in H146 cells, which is a model system for native pulmonary neuroepithelial bodies (NEB). The authors demonstrated that Nox2 was coupled with Kv3.3 and Kv4.3 and that these

complexes colocalized at the plasma membrane. This feature of being expressed in the membrane would be expected if the ion channels or the NADPH oxidase subunit were to be an airway-based sensor (Buttigieg et al., 2012). By using Nox2 siRNA, they showed that hypoxic-response in H146 cells was severely reduced (Buttigieg et al., 2012). In contrast, when Nox4 siRNA were used, cells retained a residual hypoxic response (Buttigieg et al., 2012). They concluded that Nox2 is the predominant oxygen sensor while Nox4 plays a minor role in hypoxia-sensing (Buttigieg et al., 2012). It must be emphasized that while H146 cell, and by inference pulmonary NEB, is a good model system to dissect the hypoxic responses mediated by different Nox/K^+ channel complexes in airway chemoreceptors (Buttigieg et al., 2012), it might not be a good representative model of the whole pulmonary vasculature as it lacks Kv2.1 and Kv9.3, which are abundantly expressed in lung and heart (Archer et al., 2004; Patel et al., 1999). To date, it has never been shown whether Nox2 can form complexes with either Kv2.1 or Kv2.1/Kv9.3. Taken together, there is a possibility that Nox2, instead of Nox4, could be the protein regulating Kv2.1 and Kv9.3, and these unique Nox/Kv channel combinations might play different roles in different anatomy (Buttigieg et al., 2012).

Although there are several pieces of evidence supporting the role of Nox proteins in hypoxia-sensing, Patel and Honore, 2001, proposed that NADPH oxidase subunits are not a universal oxygen-sensor. For example, the finding of Archer et al, 1999 which showed that hypoxic inhibition of K^+ cells in PASMC was still observed in Nox2 knock-out animals, is contradictory to the observation of Buttigieg et al, 2012. Thus, Nox proteins are likely not to be the only regulatory subunits that confer oxygen-sensitivity upon Kv channels.

The redox regulation of different cell types might also explain the discrepancy of which Nox subunit or Kv channels are the main players in hypoxia-sensing (Buttigieg et al., 2012; Conforti et al., 2000). For example, Kv2.1 has been constantly reported to be sensitive to hypoxic inhibition in cDNA-transfected L cells, but such inhibition is only observed in a subset of transfected COS cells and not detected at all in Kv2.1 mRNA-injected *Xenopus* oocytes (Conforti, et al, 2000, Patel et al, 1997, Hulme et al, 1999, Patel and Honore, 2001). Collectively, these results indicate that the same Kv channel can be subjected to different regulation by redox status depending on the

different regulatory proteins present in the host cells. Therefore, with regards to the discrepancy in results from the two series of experiment performed in this study, summarizing that Kv2.1/Kv9.3/Nox4 showed two trends of steady-state activation, it is likely that the regulatory proteins present in the tsA-201 cells in one series of experiment was not present in another. In the case of tsA-201 cells, it was found that a large subset of Kv2.1/Kv9.3 cells is not susceptible to modulation by Nox4.

Parallel to the observation of other research groups, the Kv2 blocker, ScTx-1 reduces the current amplitude of both Kv2.1 and Kv2.1/Nox4. This might suggest that Nox4 does not regulate or interact with Kv2.1. In other words, the presence of Nox4 does not affect the interaction of Kv2.1 with ScTx-1. However, it is surprising that the co-expression of Kv9.3 with Kv2.1 renders the toxin ineffective in reducing the Kv2.1 current amplitude. This is contradictory to the results published in the Supplementary Material section of Zhong et al, 2010's paper titled 'Stromatoxin-sensitive, heteromultimeric Kv2.1/Kv9.3 channels contribute to myogenic control of cerebral arterial diameter: Heteromultimeric Kv2.1/Kv9.3 channels and cerebral myogenic response', where the inhibitory effect was already evident in the presence of 30nM ScTx-1. Furthermore, they have also shown that the native RMCA current which is sensitive to ScTx-1 has a similar profile to Kv2.1/Kv9.3 channels which are heterologously expressed in HEK-293 cells, in terms of deactivation kinetics and voltage-dependence of activation. The native RMCA current and Kv2.1/Kv9.3 channels have longer deactivation kinetic profiles and a negative shift in their activation thresholds, compared with homotetrameric Kv2.1 channels, which have an accelerated current decay during deactivation and are activated at a more positive voltage.

The reason for the discrepancy between observation in this study and the published result might be due to the effect of Kv9.3 increasing the Kv2.1 current amplitude, which might offset the current reduction effect of ScTx-1. The discrepancy in results of this experiment with what has been published could also arise due to difference in how the experiments have been performed, where in our experiment the tsA-201 cells were not perfused with 100nM ScTx-1, but instead the cells were constantly in the bath containing 100nM ScTx-1. This non-perfusion setup whereby the cells are constantly in contact with ScTx-1 might have affected the results of experiments by

desensitizing the channels to the inhibitory effect of the venom. In both experiments measuring the current amplitude, activation threshold, and time constants of deactivation, our initial data have consistently showed that there is no difference between the cells recorded in perfused and non-perfused setup. For example, the observation that Kv2.1/Kv9.3 having a significantly longer tslow compared with Kv2.1 in a non-perfused setup matched the observation made in Chapter 3, where perfused cells are used. Given that now a difference is being seen in our results compared to what have been published by other authors, results from the small number of trials of non-perfused cells might be misleading and perhaps the trials should be repeated to establish if there is a change in results due to the setup.

Another reason explaining this phenomenon could be that the inhibitory effect of ScTx-1 on Kv2.1/Kv9.3 is transient and therefore constant application of ScTx-1 could mean the effect was not captured or recorded. There are several examples where after a certain toxin stimulated an inhibition or activation effect on an ion channel, the channel is returned to its resting state (baseline) and then the current going through the channel is either further increased or decreased, exceeding the baseline level. An example would be the effect of Aristolochic acid on TREK1 and TREK2 channels. The compound activates the channels but after the compound is washed off, the current is initially restored to the baseline but then dropped off to a level lower than the baseline. Overall, the result regarding the neutral effect of ScTx-1 on Kv2.1/Kv9.3 is inconclusive and warrants further experiments.

Despite having an effect on the current amplitudes of Kv2.1 and Kv2.1/Nox4, the toxin does not cause an alteration to the activation thresholds. It must be emphasized that the comparison of activation thresholds between control cells (absence of ScTx-1) and cells in the presence of ScTx-1 were not done in the publication of Zhong et al, 2010. Thus, the result presented in this chapter provided a new insight as to the different action of ScTx-1 on Kv2.1, where the venom causes current reduction without causing the channel to be activated earlier or later.

The observation that there is a slower deactivation kinetic in Kv2.1/Kv9.3 compared with Kv2.1 alone is consistent with the findings of Zhong et al, 2010. This difference is clearly observed in the current traces of representative cells. The attempt to quantify the deactivation kinetics was done by fitting the slopes with two exponential

components to allow calculation of tslow and tfast. Student's t-test performed to investigate as to whether there are differences between the tslow of Kv2.1 and Kv2.1/Kv9.3 revealed that tslow of Kv2.1/Kv9.3 is significantly higher than Kv2.1 ($p=0.0030$). However, there is no significant difference with tfast between Kv2.1 and Kv2.1/Kv9.3. When testing whether ScTx-1 has an effect in shortening or prolonging the time constants of deactivation of the channels, it was found that ScTx-1 does not have any impact on the deactivation kinetics of the channels.

One of the objectives of the experiments carried out above was to assess whether ScTx-1 is a good pharmacological tool to distinguish between Kv2.1 and Kv2.1/Kv9.3, Kv2.1/Nox4, and Kv2.1/Kv9.3/Nox4.

Results highlighted from this study showed that the toxin is indeed a Kv2.1 blocker, but its effect on Kv2.1/Kv9.3 is rather inconclusive. Patch clamp data from other publications showed that the biophysical characteristics of the ScTx-1-sensitive current is similar to the one of heterotetrameric Kv2.1/silent Kv channels (likely Kv2.1/Kv9.3) (Chen et al., 2010; Druzin et al., 2011; Hristov et al., 2012; Nieves-Cintrón et al., 2015; Zhong et al., 2010). However, experiments by these groups were done in native systems and they have mentioned that presence of homotetrameric Kv2.1 channels cannot be ruled out and it is difficult to deduce that ScTx-1 is acting exclusively on Kv2.1/Kv9.3 or on Kv2.1 (Chen et al., 2010; Hristov et al., 2012). Therefore, it might be difficult to conclude that ScTx-1 differentially regulates Kv2.1 and Kv9.3. Perhaps it might be better to increase the number of trials, or to adhere to the perfused setup during whole cell recording when it is economically feasible, before doing whole cell recording on native PASMC to compare the current profile with the heterologously- expressed Kv2.1 and Kv2.1/Kv9.3 channels.

Chapter 4: Protein expression of Kv2.1 and Kv9.3 in rat lungs and heart

4.1 Introduction

After performing the functional studies to understand how Kv9.3 can modulate the electrical behaviour of Kv2.1, it was of interest to determine the distribution of these ion channels in the lung and heart tissue. Zhong et al, 2010 attempted to dissect the expression of Kv2.1 and Kv9.3 in dissociated single rat medial cerebral arteries myocytes by using proximity ligation assay and they have confirmed the colocalization of both ion channels. They used the proximity ligation assay due to the scarcity of a reliable commercial anti-Kv9.3 antibody that can be used for immunohistochemistry. In this chapter, we have used a novel anti-Kv9.3 antibody from Alomone Labs, Israel. Kv9.3 mRNA has been reported to be widely expressed in several tissues, such as brain, cochlear nucleus, lungs and PASMC but Kv9.3 protein expression has so far only been demonstrated in cerebral artery smooth muscle cells (Zhong et al., 2010) and placenta (Bocksteins, 2016; Shepard and Rae, 1999). Using immunohistochemistry, I sought to find out whether Kv2.1 and Kv9.3 are expressed in rat lung and heart cells and if they are found to be present, it was of interest to know which type of cells are immunopositive. In contrast to Western blotting, immunohistochemistry allows the visualization of where these proteins are present, providing more specific insights of the types of cells. By counting the cells that are positively-stained by the antibodies we will have an insight as to what proportion of cells express the respective ion channels.

4.2 Materials and Methods

Tissue preparation and Immunohistochemistry

Rabbit polyclonal anti-Kv2.1 and anti-Kv9.3 antibodies were acquired from Alomone Labs, Israel. Sprague Dawley male rats, aged P30, with average weight of 225g, were decapitated using spine-dislocation method. A total of 10 rats were used. All animal procedures were conducted in Charles River, Margate, UK, in accordance with guidelines of the Animal Welfare and the Humane Treatment of Animals policy. By inserting a syringe needle filled with phosphate-buffered saline (PBS) into the trachea, the lungs were washed with PBS till the lungs appeared pale. The lungs and heart were isolated and fixed with 10% neutral buffered formalin (NBF) for 48 hours on a shaker. Next, the organs were dehydrated by immersing them in 50% ethanol for two hours, twice; 70% ethanol for one hour, followed by 90% ethanol for 2 hours, and 100% ethanol for one hour, twice. The organs are blotted dry with tissue paper before being immersed with xylene/xylol (Thermo Fisher Scientific) for one hour, twice.

The organs were then infiltrated with molten paraffin (Thermo Fisher Scientific) for one hour, twice and then left at room temperature to cool overnight. Paraffinization was performed using the Leica embedding centre (Leica Biosystems, Germany). Briefly, the organs were stored in the warming compartment for about 15 mins to allow the excess wax to be melted. Then a thin slice of the organ was cut off using a blade. The tissue slice was placed in the centre of a metal cassette and molten paraffin was dispensed on the tissue slice and a plastic cassette placed on top. The tissue slice was left to cool at 4°C for 30 min and then at room temperature overnight. The metal part was removed leaving the tissue embedded in paraffin within the plastic cassette. The embedded tissue slice was sliced to a thickness of 3 micrometres using Leica RM2255 fully automated rotary microtome (Leica Biosystems, Germany). The tissue slices were then mounted on glass slides (Superfrost Ultraplus Adhesion slides, Thermo Fisher Scientific). Deparaffinization was performed by putting the glass slides in the 60°C incubator, for one hour, to melt the excess paraffin.

The tissue slices were rehydrated in xylene/xylol for 10mins, three times; blotted dry

with tissue paper; re-immersed in 100% ethanol for 5 mins, twice; 96% ethanol for 5 mins, once and in 70% ethanol for 5 mins, once. Antigen retrieval is done by boiling the tissue slices with 1X Rodent Decloaker (Biocare Medical), for 25 mins. In order to prevent non-specific staining due to presence of endogenous peroxidase, the samples were treated with a solution consisting of methanol and ice-cold hydrogen peroxidase in a ratio 1:1, for 20 mins. The samples were then washed in water for 5mins, and in 1X Tris-buffered saline (TBS), pH7.2, (Zytomed, Germany) for 5mins, twice. The samples were treated with 1X proteinase K (Biocare Medical, US) for 15 mins. Then the samples were washed with distilled water for 5mins, and then twice with 1X TBS on a shaker. Non-specific binding sites were blocked with 10% bovine serum albumin (BSA) (Sigma Aldrich, Germany) for one hour. BSA was diluted in PBS prior to use. Then, samples were washed with TBS on a shaker for five times, 5mins each. To block rodent's IgG, samples were treated with Rodent Block M (Biocare Medical, US) for 30mins. The samples were subjected to five washes with TBS for 5mins each time, on the shaker.

Primary antibodies were prepared in the correct dilution using the antibody diluent (Biocare Medical, US), where the optimum concentration of rabbit polyclonal anti-KV2.1 was determined to be 1:50 whereas anti-Kv9.3 was 1:1000. The diluted antibodies were vortexed before use. The protocol for determining the optimum antibody dilution is outlined below in 'Optimization protocols and negative controls'. The area to be stained on the slide was marked with ImmEdge hydrophobic barrier pen (Vector Labs, US). Slides were blotted dry quickly and 50µl of primary antibody was spotted on the sample area. Samples were incubated at 4°C overnight in the dark.

The samples were washed with TBS for seven times, 20mins each. Samples were treated with alkaline phosphatase (BioCare Medical, US) for 30mins at room temperature. Then the slides were washed in TBS for four times, 5mins each. In order for the staining to develop, Vulcan Fast Red (Warp Red Chromogen Kit, BioCare Medical, US) was spotted on the samples. After 4-6 mins, formation of a bright fuchsin-red precipitate will be noticed and the glass slides were examined on the microscope. When the signal of staining is intense enough, the slides were submerged in water to quench the reaction. Care must be taken to ensure that the staining was not

over-developed. Nuclear counterstaining was performed by spotting the samples with haematoxylin (Invitrogen, US) for 1min. The samples were then washed with distilled water, followed by TBS for 3-5 min and finally in tap water for 10min on the shaker. Dehydration was done by submerging the slides in 100% ethanol, three times, and xylol for two times. The slides were then blotted dry and mounted with Pertex (HistoLab, Sweden).

Image acquisition

The sections were examined using the Leica DM 2500 microscope (Leica Biosystems, Germany). Images were acquired using Leica DFC290 HD digital camera and Leica QWin imaging software with identical image system settings (Zhu et al., 2008) (Leica Biosystems, Germany). There might be variations in every tissue section, even if the tissue section was taken from the same rat. Therefore, it is necessary to capture multiple distinct ROI (region of interest) of a tissue section. The ROIs were captured randomly to ensure that not only the regions where the cells were positively-stained were captured but instead the ROIs should be representative of the tissue section. Depending on the area of the tissue section, the number of ROIs that were needed to be captured was determined.

Cell counting and statistical analyses

Cell counting was performed using the ImageJ software (National Institutes of Health, US) to determine the percentage of cells that are positive for either Kv2.1 or Kv9.3 (stained red) vs total number of cells (representative of nuclear staining). Cells are stained blue due to the binding of haematoxylin to the nucleus of the cells. If the cell is stained blue and red, as the detection method used was Vulcan Fast Red, this signified that the cell is positively-stained by either the Kv2.1 or Kv9.3 antibody (Figure 4.1 gives an indication of a positively-stained cell and a negatively-stained cell). Data are presented as the mean ± standard error of mean (SEM). Graphical and statistical analyses were conducted using GraphPad Prism7 (GraphPad, US). Statistical comparisons between two groups were performed using an unpaired

Student's t-test with Welch correction, and p-value ≤ 0.05 was considered to be statistically significant.

Percentage of immunopositive cells in were determined by the following formula:

$$\frac{Number\ of\ immunopositive\ cells}{Total\ number\ of\ cells} \times 100\ (\%)$$

The average of percentage of immunopositive cells in a particular organ of 'n' number of rats is determined. The reason that we have decided not to use a software to estimate the positively-stained area is due to the risk of false positive (type 1 error) as there might be artefacts which are stained red but not blue (essentially not a cell) and get counted as a cell. Besides, counting the number of immunopositive cells per square area assumes that each square area has the same density of cells.

For example, for a tissue section with an area of 1000mm^2, ten fields of images of 10X resolution were captured. In these ten fields, there were an average of 40,000 cells and out of this, 4000 immunopositive cells were observed. Data are presented as the average of the total number of positively-stained cells over total number of cells present ± SEM. The results are depicted in a bar chart.

An example of how the calculation was done is as follows: For a section of Rat 2 Left lung that was stained with Kv2.1, ten fields of images were captured. The total number of cells in these ten fields is 41,584 cells. Out of this total, 4303 cells were stained red (immunopositive). Thus the percentage of immunopositive cells compared with total cells present would be 10.35%. Meanwhile, in Rat 3 Left lung, 11 fields were captured (because the section area was slightly bigger than Rat 2's left lung), and total number of cells is 45,879 and out of this total, 2604 cells were immunopositive. So, the percentage of immunopositive cells is 5.68%. The average of the percentages from the nine rats analyzed was calculated and variation in the percentage readings between the rats is given as SEM.

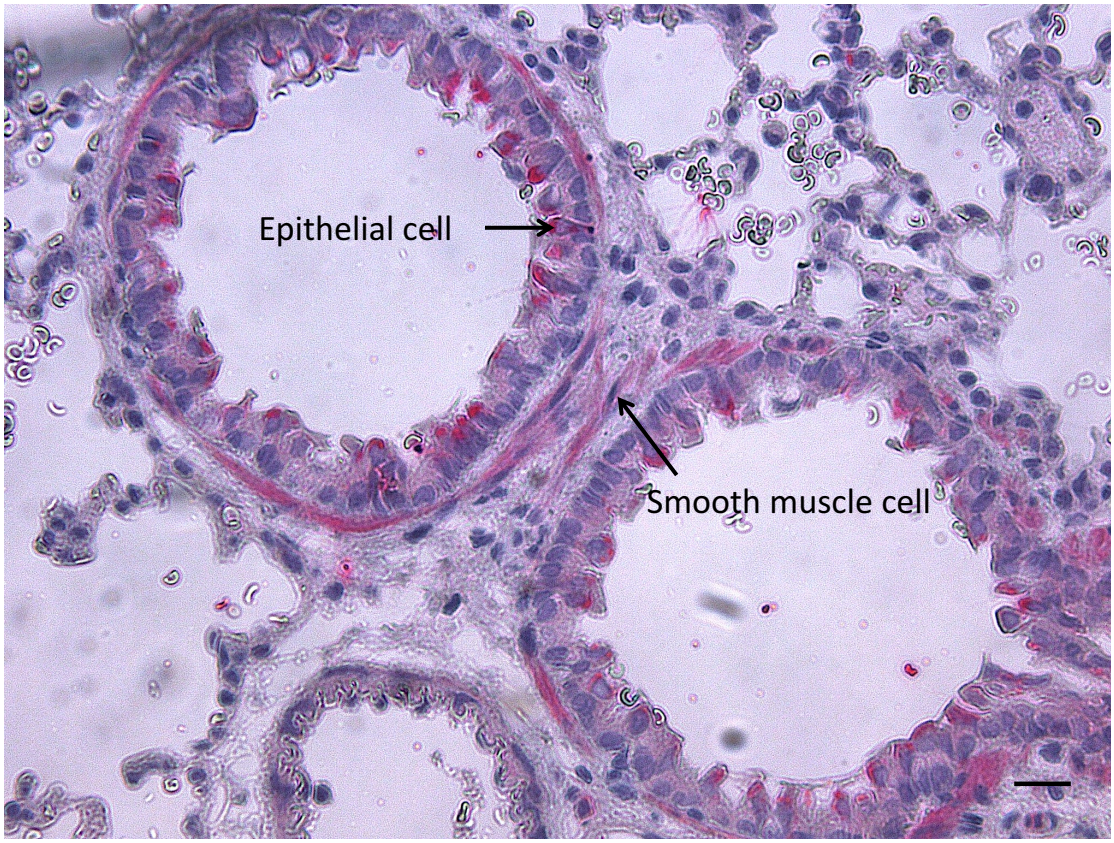

Figure 4.1: Image of rat lung cells taken at 40X resolution using Leica DM 2500 microscope (Leica Biosystems, Germany). All cells were stained blue as haematoxylin is a stain that targets the cell nucleus. The black arrow indicates a cell that was both stained blue and red. The antibody used in this experiment was against Kv2.1, thus the cell was then considered to be expressing the Kv2.1 protein. Scale indicates 242μm. Kv2.1 is mainly expressed in epithelial cells and smooth muscle cells.

Optimization protocol and negative controls

The primary antibodies used were rabbit polyclonal anti-Kv2.1, catalogue number: APC-012, and anti-Kv9.3, catalogue number: APC-133 (both from Alomone Labs, Israel). In order to determine the optimum concentration of these primary polyclonal antibodies, tissue slices were first stained with the antibody of the following dilutions:

Anti-Kv2.1 antibody- 1:50, 1:100, 1:200, 1:500, and 1:1000
Anti-Kv9.3 antibody- 1:50, 1:100, 1:200, 1:500, 1:1000, and 1:2000

The concentrations above have been used in other reference papers recommended by the antibody provider, Alomone Labs and were used as a guideline for our experiments (Costigan et al., 2010; Richardson and Kaczmarek, 2000; Shepard and Rae, 1999). Since there might be differences in our protocols compared to other published papers (such as in development methods used), it is a good practice to establish the optimum conditions according to our needs. The optimum primary antibody concentration would be the one which allows us to clearly discriminate a positively-stained cell from a cell that has only been stained blue by haematoxylin and more importantly, one which does not stain in a specific fashion (meaning all the cells are stained, unless it has been published to be an antigen that is ubiquitously expressed in the cells) or produce a lot of background staining (also known as background noise). Referring to Figure 4.2 and Figure 4.3, the optimum concentrations of Kv2.1 was found to be 1:50 and that for Kv9.3 was 1:1000. This process of distinguishing positively-stained and negatively-stained cells can also be aided by performing negative control experiments which omit primary antibody application in the protocol.

The optimum development period where the Vulcan Fast Red (Warp Red Chromogen Kit) is applied on the tissue is established during this optimization session. The optimum development time for slides stained with Kv2.1 primary antibody was established to be 4 minutes while slides stained with Kv9.3 primary antibody was 6 minutes.

4.3 Results

Optimization of IHC protocol

There are two reasons to perform the optimization of IHC protocol- 1) To establish the optimum concentration of antibody so that the immunopositive cells can be distinguished, yet the amount of background staining is minimal; 2) To determine the time duration of development of stain with Vulcan Fast Red. As shown in Figure 4.2 and Figure 4.3, the ideal dilutions of antibody to be used were found to be 1:50 for Kv2.1 and 1:1000 for Kv9.3.

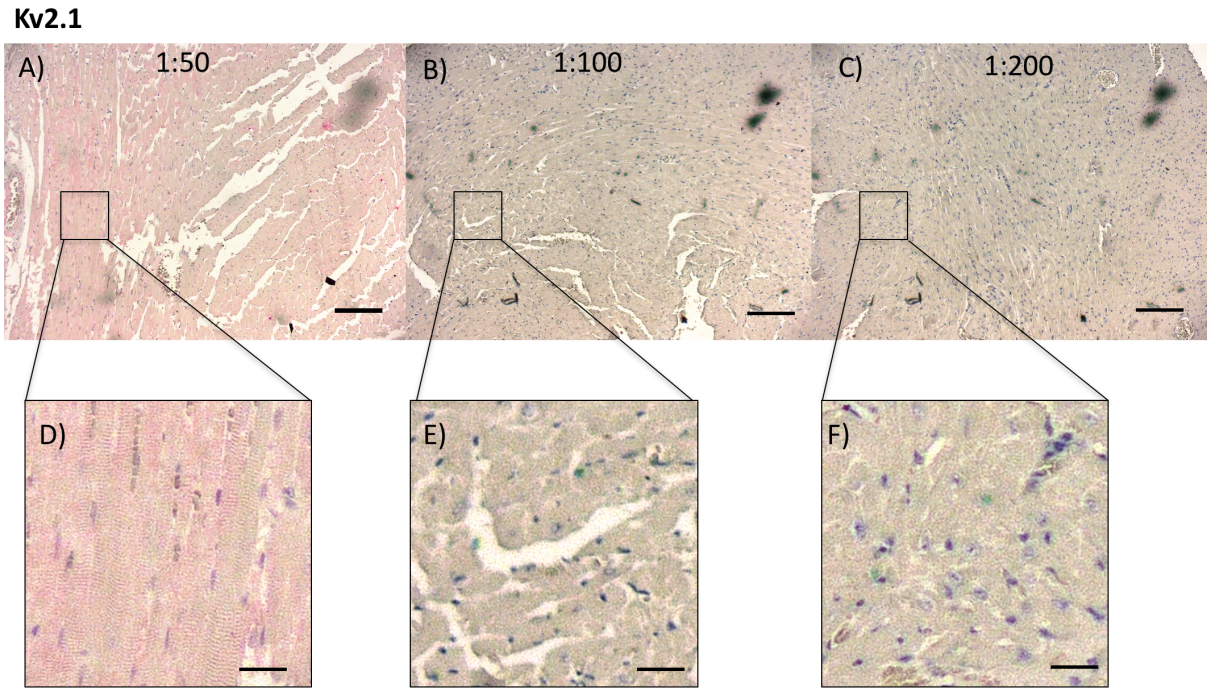

Figure 4.2: Optimization protocol to determine the appropriate concentration of Kv2.1 to be used to stain tissues. Heart tissues stained with polyclonal Kv2.1 antibody in the following dilutions- A) 1:50, B) 1:100, and C) 1:200, where scale indicates 140µm. The square sections of these images are enlarged as follows- D) 1:50, E) 1:100, and F) 1:200, where scale indicates 23.3µm. It is clear that the cells in D are stained red when a dilution of 1:50 of the antibody is used whereas the cells in E and F are not stained in red.

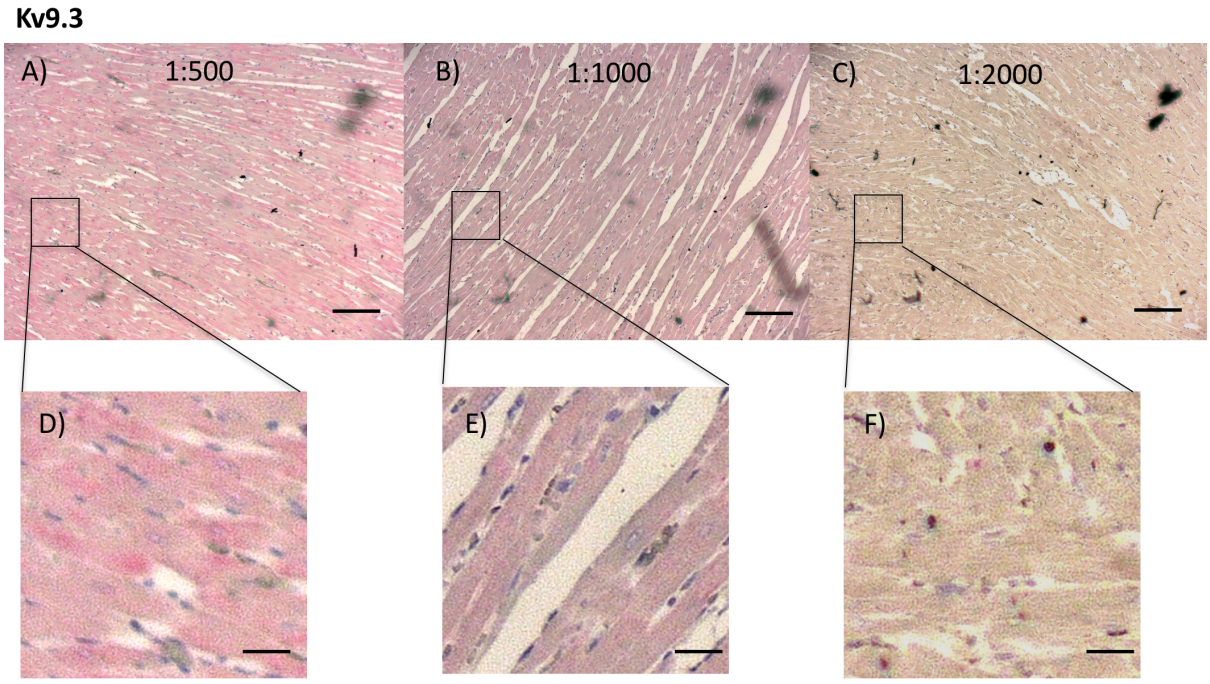

Figure 4.3: Optimization protocol to determine the appropriate concentration of Kv9.3 to be used to stain tissues. Heart tissues stained with polyclonal Kv9.3 antibody in the following dilutions- A) 1:500, B) 1:1000, and C) 1:2000, where scale indicates 140µm. The square sections of these images are enlarged as follows- D) 1:50, E) 1:1000, and F) 1:2000, where scale indicates 23.3µm. The cells in D) and E) are both stained red whereas cells in F) are not. To prevent false positive result, the antibody dilution of 1:1000 is chosen since the image E) showed that this dilution will result in clear staining of cells.

Cells that are positively-stained with the antibodies are compared with negative controls

Negative controls are slides of rat heart and lungs tissues which are not stained with the primary antibodies. It is clear in Figure 4.4 and Figure 4.5 that the rat heart and lung tissues that act as negative controls only have cells stained in blue due to haematoxylin, indicating the presence of nucleus, but are not stained in red.

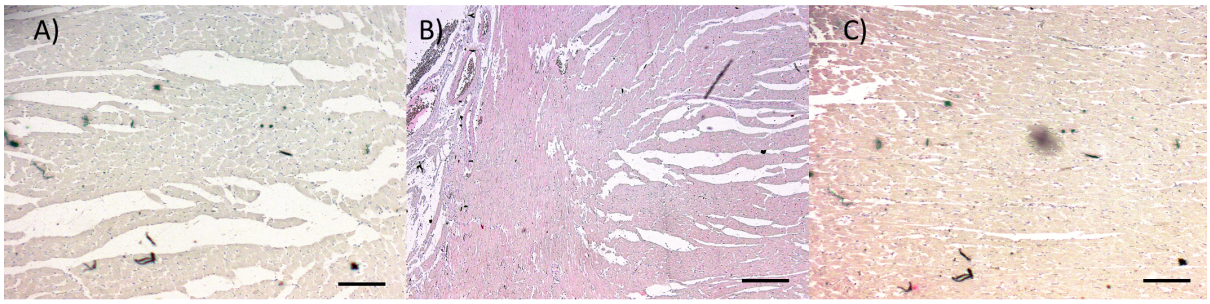

Figure 4.4: Rat heart cells that are positively-stained with the antibodies are compared with negative controls. A) Negative staining, Rat heart cells stained with B) polyclonal anti-Kv2.1 antibody, 1:50 dilution and C) polyclonal anti-Kv9.3 antibody, 1:1000 dilution (right). The negative staining in A) shows that while the cells are stained blue with haematoxylin, they are not stained red as in B) and C). Scale indicates 140μm.

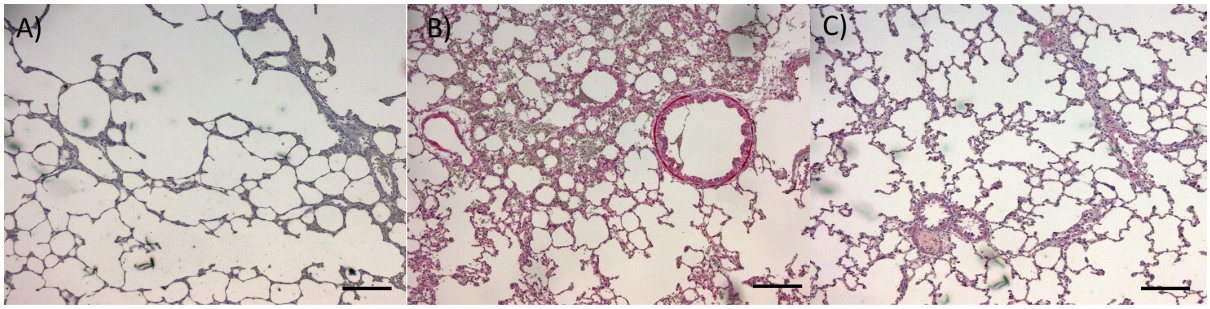

Figure 4.5: Rat right lung cells that are positively-stained with the antibodies compared with negative controls. A) Negative staining, Rat right lung cells stained with B) polyclonal anti-Kv2.1 antibody and C) polyclonal anti-Kv9.3 antibody (right). The negative staining in A) shows that while the cells are stained blue with haematoxylin, they are not stained red as in B) and C). Scale indicates 140μm.

Distribution of Kv2.1 in rat left lung, right lung, and heart

Kv2.1 is mainly expressed in the epithelium, especially in goblet cells, and smooth muscle cells of the lung (Figure 4.1, Figure 4.6 A and B). As evident in Figure 4.6 C, all heart cells in all six animals appeared to be expressing Kv2.1 and therefore there are no error bars plotted in the bar chart column (Figure 4.6D). Cells from several rats were counted and data were expressed as mean percentage of positively-stained cells ± SEM.

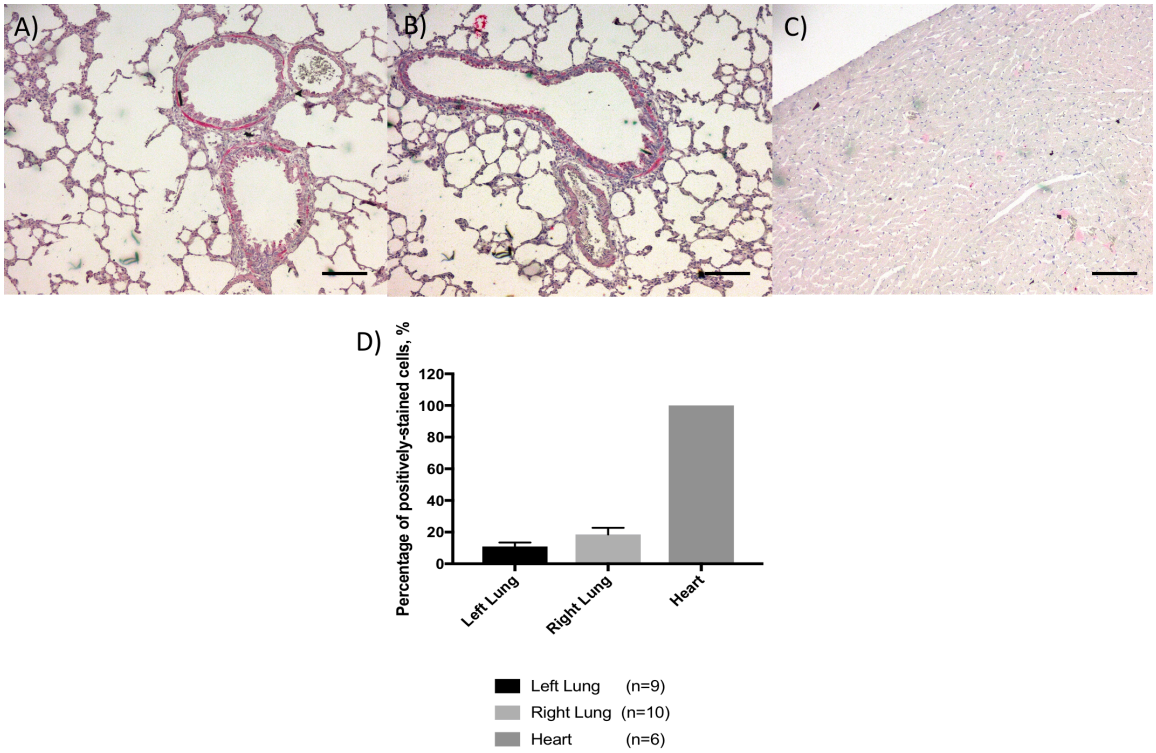

Figure 4.6: Protein expression of Kv2.1 in rat A) left lung, B) right lung, and C) heart. Scale indicates 140µm. D) Bar chart showing the percentage of cells expressing Kv2.1 in the rat left lung, right lung, and heart. 'n' indicated in the bar chart represents the number of animals used and therefore denotes the number of independent trials of the experiments.

Distribution of Kv9.3 in rat left lung, right lung, and heart

Similar to Kv2.1, Kv9.3 is also expressed in epithelium and smooth muscle cells in the lung (Figure 4.7 A and B). All the heart cells are stained red, indicating immunopositivity for Kv9.3 (Figure 4.7 C). Cells from several rats were counted and

data were expressed as mean percentage of positively-stained cells ± SEM, as plotted in Figure 4.7D.

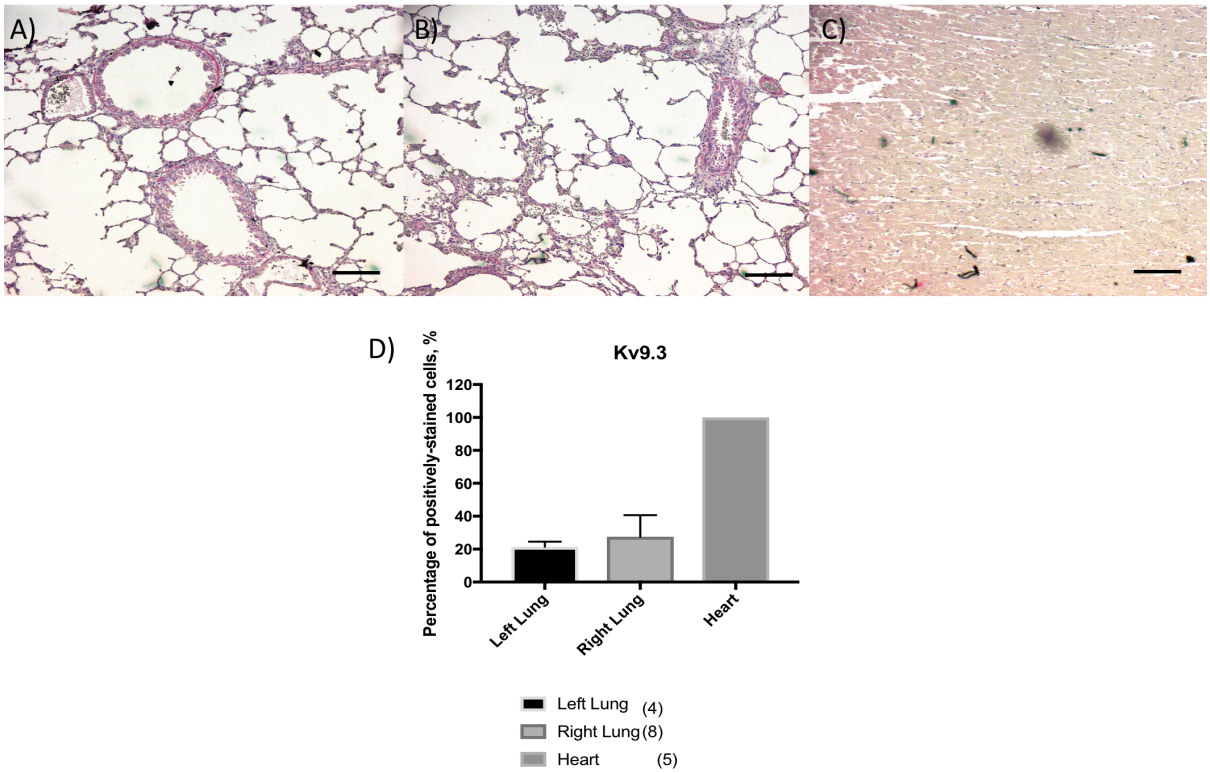

Figure 4.7: Protein expression of Kv9.3 in rat A) left lung, B) right lung, and C) heart. Scale indicates 140µm. D) Bar chart showing the percentage of cells expressing Kv2.1 in the rat left lung, right lung, and heart. 'n' indicated in the bar chart represents the number of animals used and therefore denotes the number of independent trials of the experiments.

Presence of Kv2.1 with Kv9.3 in rat left lung, right lung, and heart

As highlighted in the bar charts above (Figure 4.6 D and Figure 4.7 D), Kv2.1 and Kv9.3 are expressed at the same levels in rat lungs and hearts. Figures below allow the visualization of the compartments where these two proteins are expressed and we can infer that they are expressed in approximately the same compartments in the left lung (Figure 4.8), right lung (Figure 4.9), and heart (Figure 4.10). Further immunohistochemistry experiments with serial sections (series of sections of the same organ from the same rat) should be performed to investigate whether Kv2.1 and Kv9.3 are co-expressed.

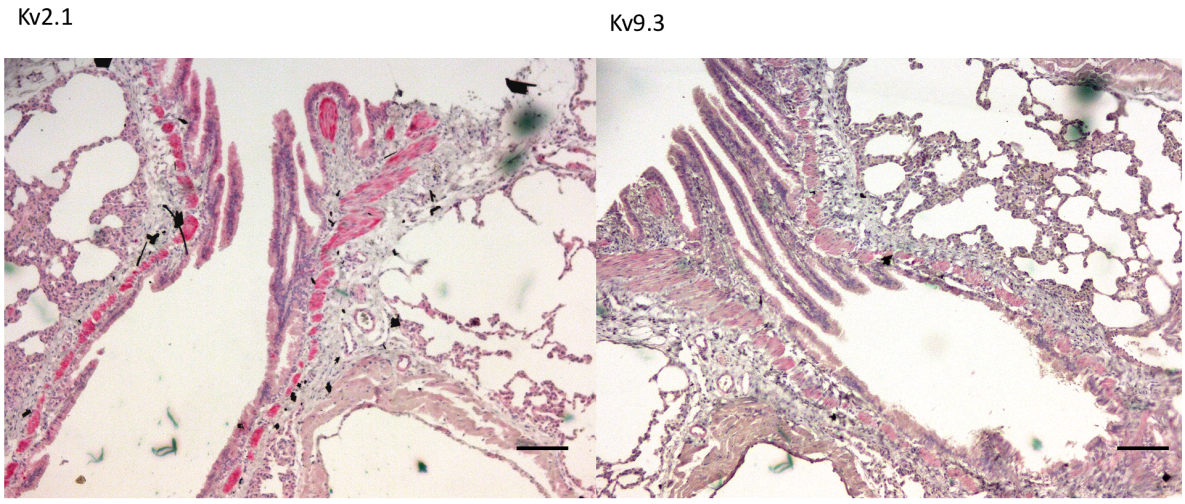

Figure 4.8: Presence of Kv2.1 and Kv9.3 in rat left lungs. Positive staining of epithelial cells and smooth muscle cells in the rat left lungs with anti-Kv2.1 antibody (left) and anti-Kv9.3 antibody (right). Scale indicates 100μm.

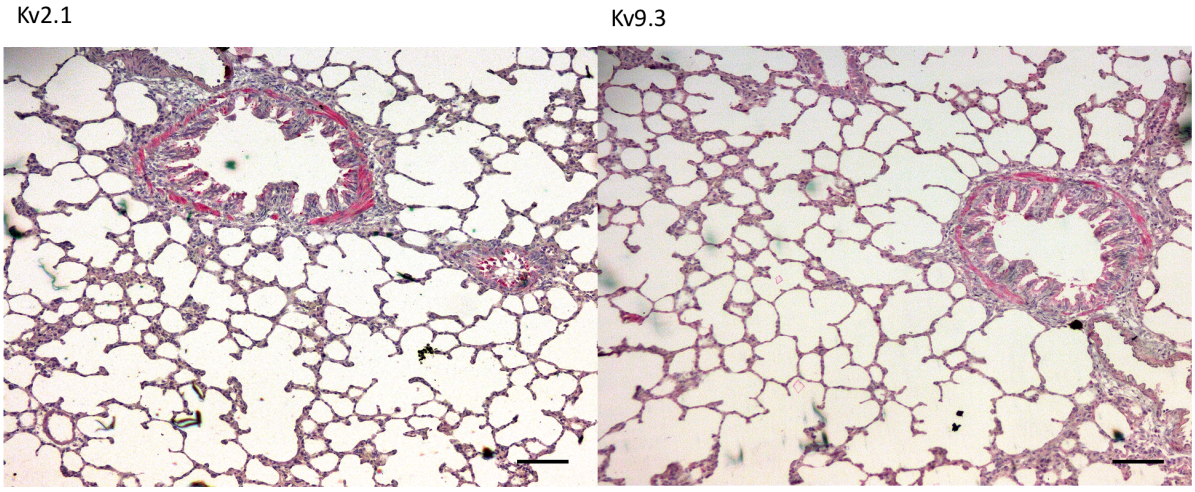

Figure 4.9: Presence of Kv2.1 and Kv9.3 in rat right lungs. Positive staining of epithelial cells and smooth muscle cells in the rat right lungs with anti-Kv2.1 antibody (left) and anti-Kv9.3 antibody (right). Scale indicates 100μm.

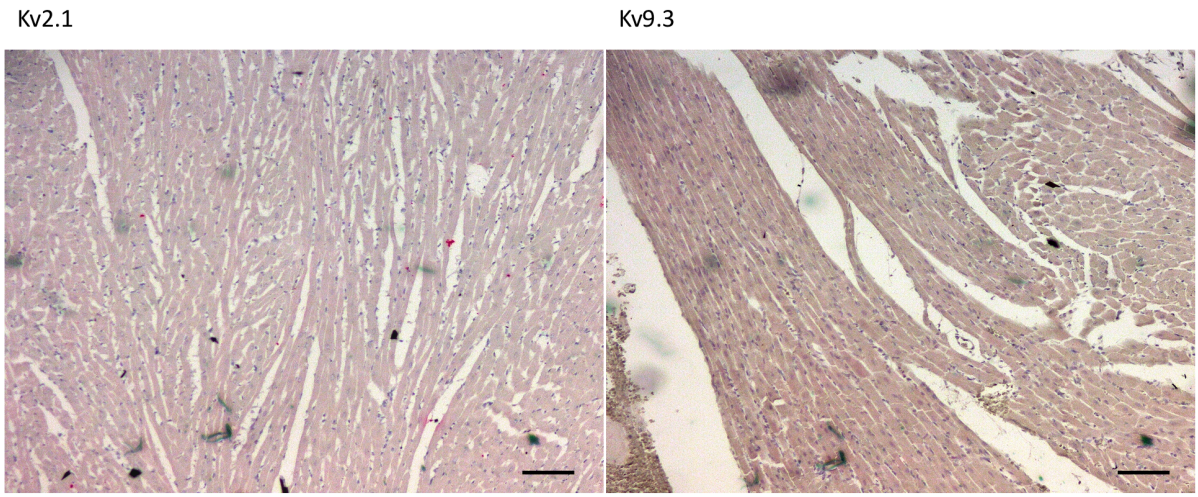

Figure 4.10: Presence of Kv2.1 and Kv9.3 in rat hearts. Positive staining of rat heart cells with anti-Kv2.1 antibody (left) and anti-Kv9.3 antibody (right). Scale indicates 100μm.

4.4 Discussion

The expression of Kv2.1 in rat PASMC is well-documented and the results from this experiment found that Kv2.1 is indeed present in rat lungs and hearts. In terms of the breakdown of cell types, it has been found that adult murine myocardium consists of approximately 56% myocytes, 27% fibroblasts, 7% endothelial cells, and 10% vascular smooth muscle cell (Banerjee et al., 2007).

Although Kv9.3 has been shown to regulate Kv2.1 function, the protein expression of Kv9.3 in rat heart and lung has never been demonstrated using immunohistochemistry due to the non-availability of a reliable, commercial primary antibody. I have used the rabbit polyclonal anti-Kv9.3 antibody from Alomone Labs, Israel but the reliability of the antibody remains inconclusive. In future experiments, staining using sm22 or α-smooth muscle cell actin, which target smooth muscle cells, and CD31, which targets endothelial cells, should be carried out to confirm that the anti-Kv9.3 antibody is really targeting these cell types. By performing these additional staining for endothelial and smooth muscle cells, we would be able to carry out cell counting to determine the proportion of cell types expressing Kv2.1 and Kv9.3 and see whether these cell types express the ion channels in different amount. Another control experiment that could be used to confirm the specificity of the anti-Kv2.1 and anti-

Kv9.3 antibodies would be staining of the tsA-201 cells transiently-transfected with the Kv2.1 and Kv9.3 cDNAs.

Several authors have published the high level of mRNA expression of Kv2.1 and Kv9.3 in smooth muscle cells (Archer et al., 2004; Patel et al., 1997; Platoshyn et al., 2004). Zhong et al, 2010 confirmed the co-expression of the two proteins in rat middle cerebral artery myocytes using proximity ligation assays. While the results in this chapter could indicate that Kv9.3 is expressed abundantly in rat hearts and lungs, the colocalization of Kv2.1 and Kv9.3 cannot be confirmed. In future experiments, staining of serial tissue sections with both antibodies should have been carried out, which will then enable us to compare whether these proteins are expressed in the same cell types or are expressed at close proximity to each other. Double staining using both antibodies conjugated with different fluorescent dyes could also be done but the complexity of the procedure might be higher.

Chapter 5: Modulation of TASK-1 by Nox4 and chloramine-T (Ch-T)

5.1 Introduction

There are several pieces of evidence implicating TASK-1 in PH. TASK-1 mutations have been identified in PH patients (Ma et al., 2013) and Antigny et al. (2016) provided further evidence that the expression of TASK-1 (KCNK3 gene) is reduced and the function of the channel is compromised in both human PAH and monocrotaline-induced PH in rats. During the development of monocrotaline-induced PH, TASK-1 current in freshly isolated PASMC and PAEC was found to decrease and this led to membrane depolarization (Antigny et al., 2016). Chronic inhibition of TASK-1 also gives rise to neomuscularization and early haemodynamic signs of PH (Antigny et al., 2016). These are associated with excess proliferation of PAEC, PASMC, adventitial fibroblasts, and pulmonary and systemic inflammation, eventually leading to pulmonary vascular remodelling (Antigny et al., 2016). By restoring TASK-1 function using a pharmacological activator, monocrotaline-induced PH is dramatically reversed in rats (Antigny et al., 2016). Navas Tejedor et al, 2017 identified two further mutations in TASK-1 channels which supported the claim that compromised TASK-1 functions could lead to cell depolarization and eventually causing pulmonary vasoconstriction.

Mutations in several genes have been included in the PAH panel of genes for clinical testing. 70% of hereditary PAH and 10-40% of idiopathic PAH cases have been linked to mutations in bone morphogenetic protein receptor 2, BMPR2 gene (Ma and Chung, 2017). Gene mutations such as activin receptor-like type 1, endoglin, SMAD9, TBX4, EIF2KA4, and caveolin 1 have also been associated with PAH (Ma and Chung, 2017). Interestingly, the finding of Navas Tejedor et al., 2017 demonstrated that patients having missense mutation in TASK-1 but do not carry a mutation in BMPR2, TBX4, and EIF2KA4, are still susceptible to PAH (Navas

Tejedor et al., 2017). Although TASK-1 mutation is very rare, it might be worthwhile to consider it as a standard in PAH diagnosis in the future.

Another interesting finding which links TASK-1 to PH is the colocalization of TASK-1 with Nox4. It is hypothesized that there is a possible interaction between them since they are expressed together (Lee et al, 2006, Buttigieg et al, 2012, Mittal et al, 2012). It is widely known that TASK-1 current can be inhibited by low extracellular pH and hypoxia (Mathie et al., 2010a). The fact that TASK-1 channels can be inhibited by hypoxia makes it seem plausible that TASK-1 channels are expressed in oxygen-sensing cells such as pulmonary neuroepithelial bodies (NEB) (Lee et al., 2006). Since TASK-1 per se is not capable of sensing oxygen, this capability must be conferred by a regulatory protein which interacts with TASK-1 (Lee et al., 2006). It was proposed that this interacting partner is Nox4 (Lee et al., 2006). The group went on to validate via confocal microscopy experiments that Nox4 does indeed colocalizes with TASK-1 in the plasma membrane (Lee et al., 2006). Interestingly, co-expression of Nox4 with TASK-1 dramatically magnified the effect of hypoxia on reducing TASK-1 current and this effect is abolished when siRNA and NADPH oxidase inhibitors targeting Nox4 are present (Lee et al., 2006). Co-immunoprecipitation data from several groups confirmed that Nox4 interacts with TASK-1 (Lee et al., 2006, Cutz et al., 2009 and Buttigieg et al, 2012). It has also been shown that Nox2 formed molecular complexes with Kv3.3 and Kv4.3 but not with TASK-1, indicating that different affinity of Nox proteins to different K^+ channels could confer different physiological functions (Lee et al., 2006). In contrast to the data where the inhibition of TASK-1 current by hypoxia is augmented by the presence of Nox4 (Lee et al, 2006), other studies concluded that Nox2 is the predominant oxygen sensor as this isoform, but not Nox4, suppressed hypoxia-induced serotonin release (Cutz et al, 2009). In addition, downregulation of Nox2 mRNA also inhibited the hypoxia-sensitive outward current (Cutz et al., 2009). These conflicting data warrant deeper further investigation into the functional relationship of TASK-1 and Nox4.

TASK-1 current is very small in mammalian expression system. This is because WT TASK-1 contains a dibasic motif KR at N-terminus and a tribasic motif KRR at the C-terminus, which act as retention signals (O'Kelly and Goldstein, 2008; Zuzarte et al., 2009). These motifs are binding sites of a chaperone protein, COP1, which retain

TASK-1 in the endoplasmic reticulum, causing reduced surface expression, and thus reduced whole-cell current (O'Kelly and Goldstein, 2008; Zuzarte et al., 2009). However, binding of another chaperone protein, 14-3-3, will sterically hinder these sites from interacting with COP1, thus supporting the trafficking of TASK-1 channels to the plasma membrane (O'Kelly and Goldstein, 2008; Zuzarte et al., 2009). There are several ways to increase the surface expression of TASK-1 such as ablation of the dibasic motif at the N-terminus (O'Kelly and Goldstein, 2008) and phosphorylation of the serine residue (-RRSSV) at the C-terminus to prevent COP1 binding even in the absence of 14-3-3 (Kilisch et al, 2016).

A small outward TASK-1 current might make it difficult to detect any changes of the current due to the presence of an activator or an inhibitor. Therefore the experiments in this chapter have additionally used a TASK-1 variant, where the KR residues specifically at position 2 and 3 of the N-terminus have been mutated to NQ (K2N R3Q) (O'Kelly and Goldstein, 2008). Ablation of this retention signal has been reported to increase surface expression by 2.7 fold (Zuzarte et al., 2009).

ROS production escalates in many pathophysiological states such as apoptosis and in diseases where inflammation is involved such as PH (Binder et al., 1999). It is thus of interest to study how ROS modulate TASK-1 channels in the absence and presence of Nox4. Duprat et al., 2005 have shown that chloramine-T (Ch-T), which produces a ROS known as singlet oxygen, strongly activates TALK-1 (104.9±8.4%) and TALK-2 (70.7±15.3%), while inhibiting TASK-2 (46.5±2.5%,). This shows that the sensitivity of TALK family to ROS is dependent of their redox status (Duprat et al., 2005). Ch-T affects TASK-2 and TALK-1 at all potentials. However, Ch-T did not affect current kinetics of TALK-1 but Ch-T causes TASK-2 to be activated earlier (129.5±2.7ms) in comparison with control (140.4 ± 7.5ms) (Duprat et al., 2005).

Noteworthy, ROS seem to have specific targets. For example, the most commonly described ROS, superoxide, affects the gating properties of channels from the same family in different ways (Duprat et al., 2005). Superoxide activates TALK-2 and TASK-2, but inhibits TALK-1 (Duprat et al., 2005). Interestingly, TALK-2 is almost silent at rest but ROS induce a high level of activation (Duprat et al., 2005). While xanthine/ xanthine oxidase or rose bengal has a bigger effect on TASK-2 than on

TALK-1, Ch-T has a stronger effect on TALK-1 (Duprat et al., 2005). This again exemplifies that ROS have specific modes of action on the channels and it would be interesting to establish whether TASK-1 is subjected to ROS actions.

5.2 Results

Presence of a leak current in cells transfected with WT TASK-1 is confirmed

tsA-201 cells were transfected with WT-TASK-1 + GFP, Nox4 + GFP, GFP only, or were untransfected. The electrophysiology protocol used to obtain recordings has a voltage-step and a voltage-ramp part. Only currents measured in the voltage-step part will be considered. Currents were measured at the resting membrane potential, -80mV, and at the stimulating pulse of -40mV, which was given for 500ms. Cells were then hyperpolarized to -120mV before being ramped up to +20mV. The cells are then repolarized to -80mV before returning to the holding potential of -60mV. Functional current is defined as the difference between the current at -40mV (the activation potential) and -80mV (resting membrane potential). The current at respective points were measured using pClampfit 10.2. Results were stated as Mean ± SEM.

The current from WT TASK-1-transfected cells (167.4 ± 29 pA) is significantly higher than that in control cells, such as untransfected cells (77.5 ± 17.9 pA) or cells transfected with GFP (86.4 ± 5.1 pA) or Nox4 + GFP only (70.4 ± 8.9 pA) when data were analyzed with one-way ANOVA followed by Dunnett's test. In this analysis, all the groups compared with WT TASK-1 because we are interested to see if the other groups are different from WT TASK-1 and it was found that the differences between these groups compared with WT TASK-1 were statistically significant, $p \leq 0.05$. When all the groups were analyzed using one-way ANOVA followed by Tukey's test, it was found that untransfected cells and cells transfected with Nox4 were significantly different from WT-TASK-1 but cells transfected with GFP were not statistically significant, with the p value (0.0544) near the cut-off point that we have set which was $p \leq 0.05$. This control experiment also showed that expression of Nox4 alone does not affect the endogenous current of the cells (Figure 5.1).

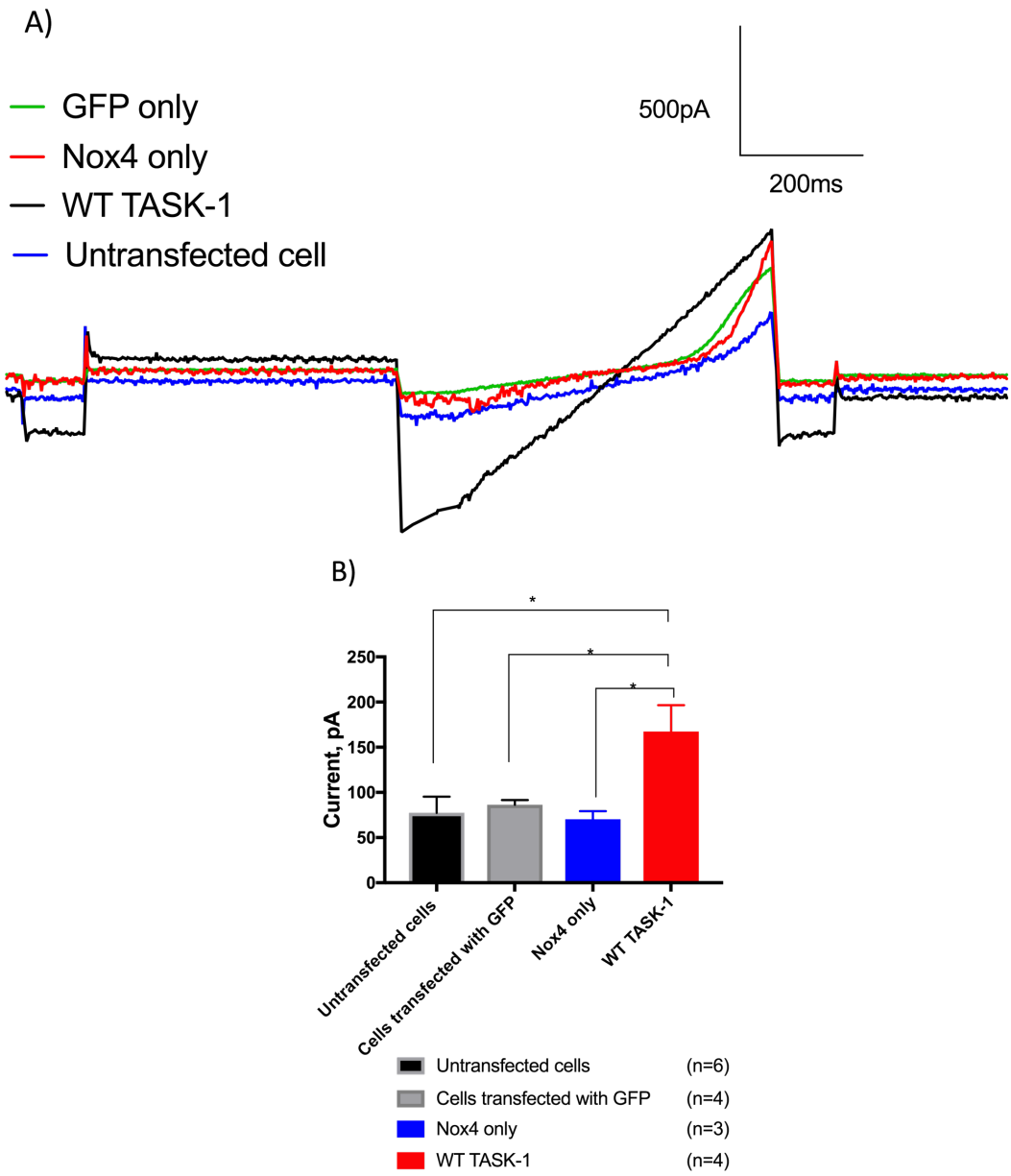

Figure 5.1: Presence of a leak current in cells transfected with WT TASK-1. A) Representative current traces for WT TASK-1, cells transfected with GFP only or Nox4 only, and untransfected cell. Cells transfected with the respective cDNAs were recorded using the protocol where cells were hyperpolarized to -80mV, and a stimulating pulse at -40mV were given for 500ms. Functional current is defined as the difference between the current at -40mV (the activation potential) and -80mV (resting membrane potential). B) Bar chart showing the functional current of untransfected cells, cells transfected with GFP, Nox4 only, and WT TASK-1. Data were expressed as mean ± SEM and were analyzed using one-way ANOVA followed by Dunnett's test as we were interested to know whether there is a difference between all the other groups compared with TASK-1. It was found that the differences were statistically significant, with * indicating $p \leq 0.05$. However, when the data were analyzed using one-way ANOVA followed by Tukey's multiple comparison test, the differences between WT-TASK-1 and untransfected cells and cells transfected with Nox4 are still statistically significant, but the difference with cells transfected with GFP only was near the threshold ($p = 0.0544$).

Gain-of-function mutant TASK-1, K2N R3Q produces significantly higher current than that of WT TASK-1

The K2N R3Q mutant TASK-1 channel (also referred to as mutant TASK-1) is a mutant where the retention signal, KR, at the N-terminus has been ablated by changing the KR residues to NQ. This prohibits the binding of COP1 to TASK-1, thereby inhibiting COP1 from retaining the TASK-1 protein in the endoplasmic reticulum. This allows the trafficking of the TASK-1 channel to the surface membrane. In effect, the higher number of channels expressed on the membrane causes the increase in outward current. In line with the conclusions drawn by O'Kelly and Goldstein, 2008 and Zuzarte et al, 2009, the current of cells transfected with K2N R3Q mutant TASK-1 (389.6 ± 6.6 pA) is approximately 2.7-fold higher than those with WT TASK-1 (167.5 ± 29 pA) (Figure 5.2).

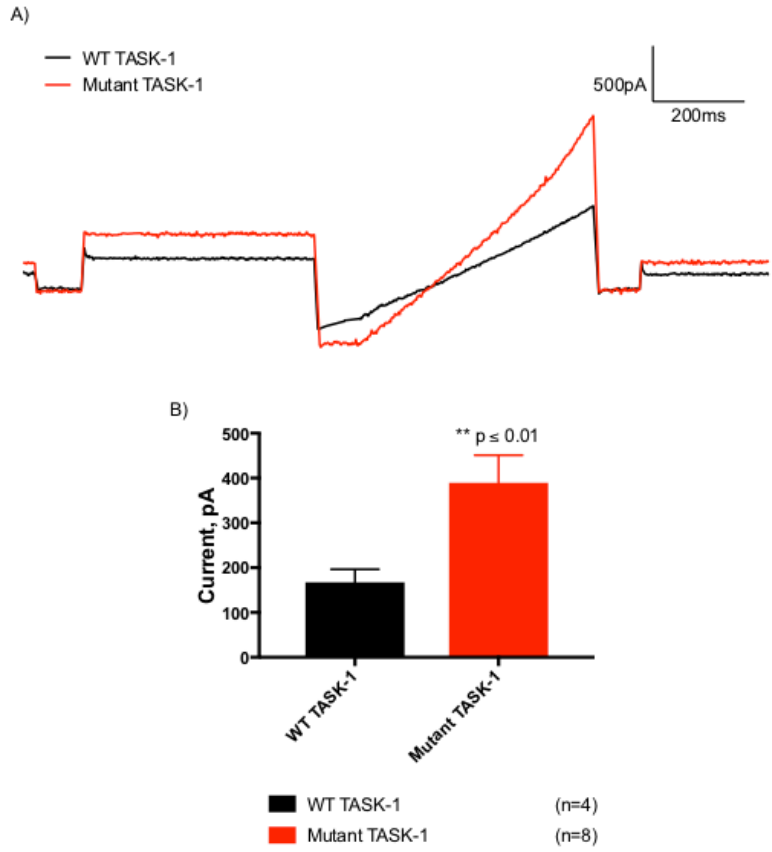

Figure 5.2: Current produced by K2N R3Q gain-of-function mutant TASK-1 is significantly higher than that of WT TASK-1. tsA-201 cells were transfected with WT TASK-1 + GFP and Mutant TASK-1 + GFP and electrophysiology recordings were obtained with a protocol where the cells were first hyperpolarized to -80mV from a holding potential of -60 mV. The cells were then given a test pulse at -40mV for 500ms. Cells were then hyperpolarized to -120mV before being ramped up to +20mV. The cells are then repolarized to -80mV before returning to the holding potential of -60mV. Functional current was taken to be the difference between the current measured at -80mV and at +40mV. The difference between the functional currents produced by the cells were analyzed using Student's t-test with Welch correction due to presence of unequal variances. A) Representative traces for WT TASK-1 and K2N R3Q Mutant TASK-1 cells. B) Bar chart depicting current of WT TASK-1 compared with K2N R3Q Mutant TASK-1; ** indicates that the K2N R3Q Mutant TASK1 current is significantly higher than that of WT TASK-1, p = 00093 ($p \leq 0.01$), indicated by **.

Nox4 does not have any effect on the current of WT or mutant TASK-1 under normoxia

Lee et al, (2006) have demonstrated that Nox4 inhibits WT TASK-1 under hypoxic conditions. This project aims to investigate whether this is true with K2N R3Q mutant

TASK-1 under normoxic conditions. Figure 5.3 shows that the effect of Nox4 on WT and mutant TASK-1 is not significant.

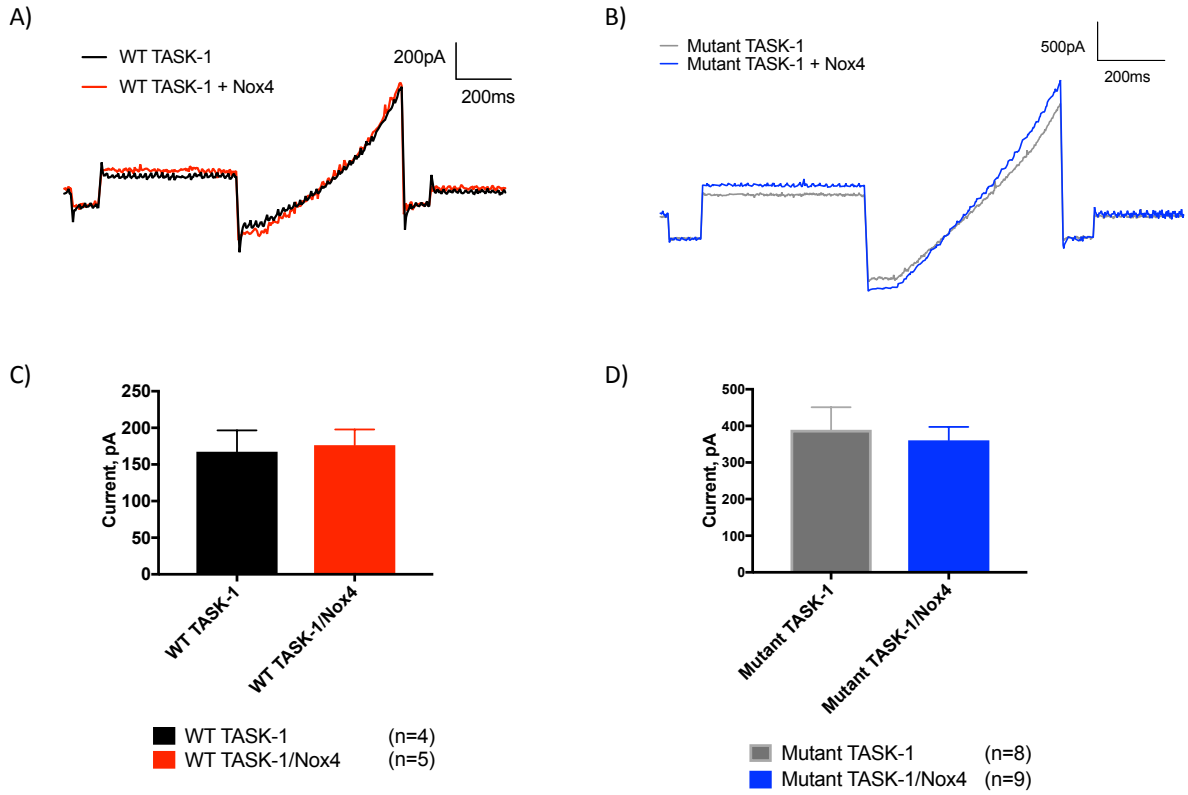

Figure 5.3: Nox4 does not have any effect on the current of WT or K2N R3Q mutant TASK-1 under normoxia. A) Representative traces for WT TASK-1 and WT TASK-1/Nox4 cells. B) Representative traces for K2N R3Q Mutant TASK-1 and K2N R3Q Mutant TASK-1/Nox4 cells. Bar charts comparing C) current of WT TASK-1 (167.5 ± 29 pA) compared with WT TASK-1/Nox4 (176.3 ± 21.6 pA) (p=0.3730) and D) current of K2N R3Q mutant TASK-1 (389.6 ± 61.6 pA) compared with K2N R3Q mutant TASK-1/Nox4 (360.8 ± 36.5 pA) (p=0.5334). Functional current was taken to be the difference between the current measured at -80mV and at +40mV. The difference between the functional currents produced by the cells were analyzed using Student's t-test with Welch correction due to presence of unequal variances.

Following from the results above which suggest that Nox4 does not regulate TASK-1, we were interested to find out if Nox4 acts as an oxygen sensor only at hypoxic condition, in other words, in the presence of a ROS agent. Although Nox4 is constitutively active, results in Chapter 3 demonstrated that co-expression of this protein with either Kv2.1 or Kv2.1/Kv9.3 did not affect the current amplitude, activation threshold or the deactivation kinetics. This led to the speculation that Nox4

could act as an oxygen sensor in the presence of a ROS agent and not in normoxic conditions.

In order to test the hypothesis that Ch-T affects the K2N R3Q mutant TASK-1 co-expressed with Nox4, cells transfected with K2N R3Q mutant TASK-1 and Nox4 cDNAs were perfused with 1mM Ch-T. As mentioned previously and demonstrated in the results above (Figure 5.2), there is a very low current going through the WT TASK-1 channel and in order to detect any changes in the current due to the presence of Ch-T, we used the gain-of-function K2N R3Q mutant TASK-1 instead. Another modification has been made in the protocol is the use of the high K^+ external buffer (25mM KCl), instead of the usual low K^+ external buffer (2.5mM KCl), following from the observation made by Lee et al, 2006, to increase the outward current through the gain-of-function K2N R3Q mutant TASK-1 channel.

Ch-T does not affect the current of K2N R3Q mutant TASK-1/Nox4 cells

As evident in Figure 5.4, the current traces showed that Ch-T does not have a significant effect on the current activated by K2N R3Q Mutant TASK-1 co-expressed with Nox4. When the functional currents were analyzed for K2N R3Q mutant TASK-1 in the absence and presence of Ch-T (553.4 ± 60.7 pA vs 545.5 ± 62.2 pA) and K2N R3Q mutant TASK-1/Nox4 in the absence and presence of Ch-T (525.6 ± 96.2 pA vs 469.6 ± 95.3 pA), the bar chart showed that Ch-T does not alter the current.

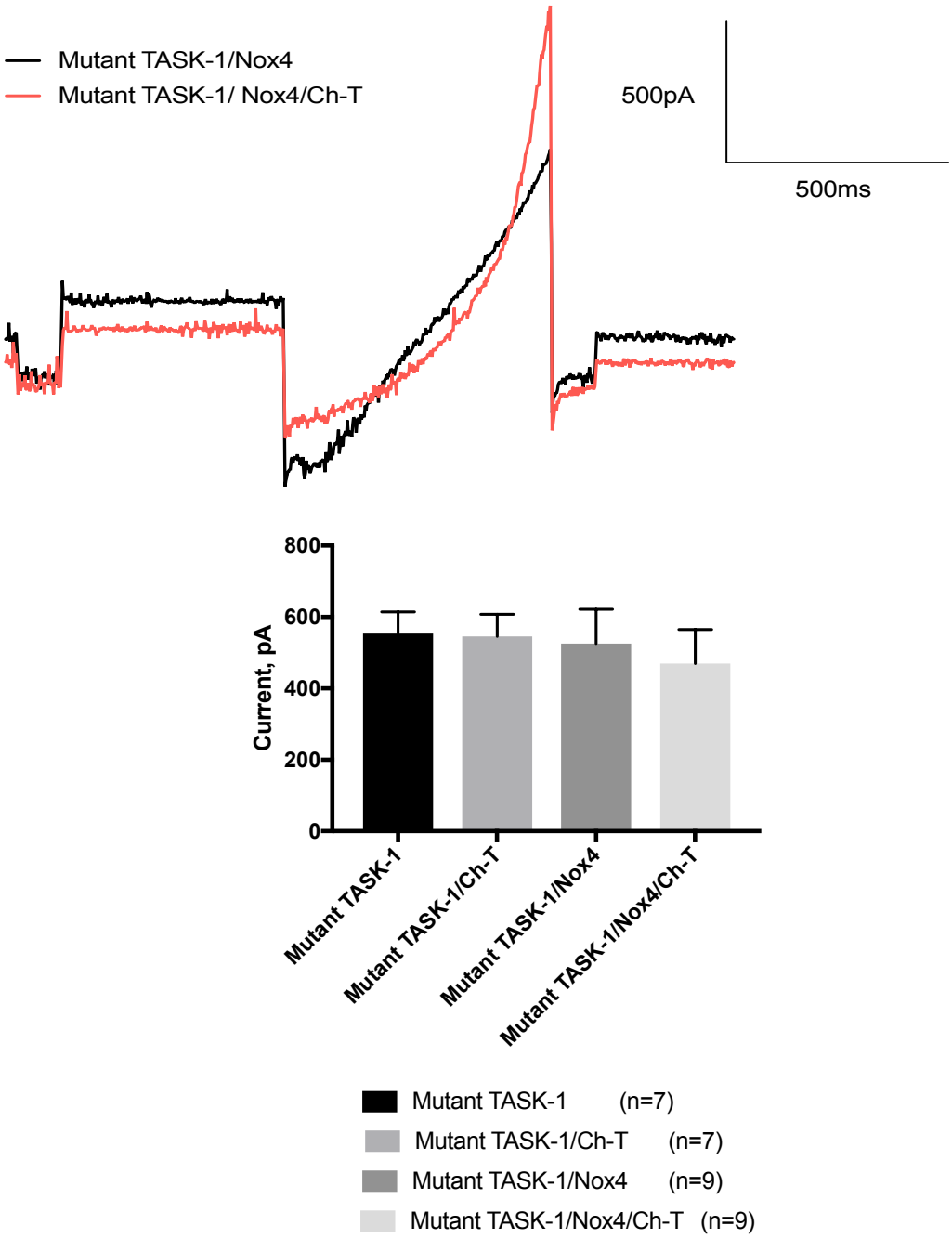

Figure 5.4: Ch-T does not affect the current of mutant TASK-1/Nox4 cells. Cells were transfected with the respective cDNAs or combination of cDNAs. The electrophysiology protocol used were the same as the one described above. During recordings, cells were first perfused with external solution for 15 sweeps and then with Ch-T for the other 15 sweeps. Representative current trace of Mutant TASK-1 in the absence and presence of 1mM Ch-T. Bar chart showing the mean current ± SEM of Mutant TASK-1 in the absence vs presence of Ch-T (553.4 ± 60.7 pA vs 545.5 ± 62.2 pA), Mutant TASK-1/Nox4 and Mutant TASK-1/Nox4 in the absence vs presence of Ch-T (525.6 ± 96.2 pA vs 469.6 ± 95.3 pA). One-way ANOVA with Tukey HSD post-hoc analysis revealed that there is no statistically significant difference between the cell populations.

5.3 Discussion

TASK-1 mutations have been identified in PH patients, implicating the channel in the pathological state of PH (Ma et al., 2013). For years, BMPR2, activin receptor-like type 1, endoglin, SMAD9, TBX4, EIF2KA4, and caveolin 1 have been used as the standard gene mutations for diagnosis of PH patients (Guignabert et al., 2015). In addition to loss of function TASK-1 mutations, reduction in TASK-1 expression could also compromise the function of this channel (Antigny et al., 2016). Research on monocrotaline-induced PH in rats showed that reduction in TASK-1 current caused membrane depolarization, which further led to neomuscularization and early haemodynamic events (Antigny et al, 2016). Recently, Navas Tejedor et al, 2017 have demonstrated that patients having missense mutation in TASK-1 but do not carry mutation in BMPR2, TBX4, and EIF2KA4, are still susceptible to PAH. This observation further strengthens the implication of TASK-1 in the disease.

The relationship between TASK-1 and Nox4 is well documented. Nox4 has been shown to be upregulated in hypoxia and it colocalizes with TASK-1 (Lee et al, 2006, Mittal et al, 2007, Mittal et al, 2011, Buttigieg et al, 2012). Although TASK-1 is present in specialized cells that have oxygen-sensing properties, such as carotid bodies, neuroepithelial bodies, and PASMC, TASK-1 *per se* is not an oxygen sensor (Lee et al., 2006). Thus, it is postulated that an interacting partner of the ion channel is the one conferring such property. Nox4 has been shown to colocalize and regulate the function of TASK-1 in hypoxia (Lee et al, 2006).

Results from this current study confirmed that K2N R3Q gain-of-function mutant TASK-1 has higher current than WT TASK-1, whereby the mutation of the retention signal KR to NQ in the N-terminus (O'Kelly and Goldstein, 2008; Zuzarte et al., 2009), improves the trafficking of the channel to the membrane, thereby increasing current that flows through the channel. Since the difference in current at -80mV and at -40mV is very small in WT TASK-1, any inhibition to the current might be difficult to visualize, especially if the inhibition effect is very small. Therefore, we decided to measure the effect of Nox4 on the K2N R3Q mutant TASK-1 and compare it with the WT TASK-1. In line with the results published by Lee et al, 2006, Nox4 does not

inhibit either the WT or K2N R3Q mutant TASK-1 current in normoxia. We initially hypothesized that since Nox4 colocalizes with TASK-1 and that Nox4 is constitutively active, the ROS generated from Nox4 might be sufficient to create the hypoxic inhibition effect on TASK-1. From this study, we can conclude that this is not the case. This agrees with several results that have been published where Nox4 only acts as an oxygen sensor when there is a change from normoxic to hypoxic conditions (20% O_2 to 1% O_2) (Lee et al, 2006, Mittal et al, 2011). This showed that the colocalization of Nox4 with an ion channel is not enough to affect the ion channel and that a stimulus (hypoxia) must be present. This is consistent with the findings of Lee et al, 2006, where they showed that Nox4 does not affect Kv1.5 current in normoxia even though they colocalize together. On the other hand, Mittal et al, 2011 showed that Nox4 does inhibit Kv1.5 current in rat PASMC isolated from rats exposed to chronic hypoxia for three weeks. In short, these arguments might suggest that Nox4 functions as an oxygen sensor in hypoxia and it might be that Nox4 inhibit TASK-1 current by inducing a conformational change during binding or by any other manner, as simply generating ROS (such as H_2O_2) is not enough to affect TASK-1 current. This is further supported by the observation that 326 mM H_2O_2 applied to cell-attached or outside-out patches does not affect TASK-1, TASK-3 and TASK-1/3 heteromer transiently-transfected on HeLa cells although 16mM H_2O_2 applied to inside-out patches activated these channels (Papreck et al., 2012). From this experiment, it was concluded that ROS does not affect TASK activity and ROS are likely not the hypoxic signal that increases membrane excitability due to inhibition of TASK channels (Papreck et al., 2012). The latter could suggest that Nox4 is responding to other factors that causes hypoxia and not to ROS.

It is tempting to speculate that restoration of BMPR2 (mutation associated with large percentage of PH patients) and/or TASK-1 function could alleviate PH. Bone morphogenetic protein (BMP) synthesis is prioritized in bones that support weight, like tibia and as a result, lighter bones (possibly ribs or bone structures that protects the heart and lungs) do not heal well (Palencia-Desai et al., 2015). The issues with restoration of BMP by injection are its high cost and that it might stimulate too much bone growth, and oftentimes at undesirable places (Tannoury and An, 2014). Levin, 2013 has suggested that while most focus has been dedicated to understanding the transcriptional and biochemical regulation of cell proliferation and differentiation,

bioelectrical properties could also have a profound impact on these processes (Levin, 2013, Adams et al, 2016). This could mean that the function of TASK-1 goes beyond controlling K^+ ion movement across the cells to control vasoconstriction, as TASK-1 could very well affect gene expression or the bioelectrical crosstalk that could have downstream effects in controlling cell behaviour and morphogenesis which could lead to pulmonary vascular remodelling. This is in agreement with the study of Leithner et al., 2016 which showed that TASK-1 is pro-proliferative. While being pro-proliferative is not normally viewed as a beneficial function in the case of PH, as pulmonary vascular remodelling occurs due to uncontrollable cell proliferation of certain cell types that causes lumen obstruction, TASK-1 could be supporting the proliferation of cells that can help with clearing aberrant inflammatory cells, or to increase the proportion of cells that can provide a negative feedback loop to stop the proliferation of the problematic cell types (such as PAEC and collagen). These speculations await deeper research into the understanding of TASK-1 function and its associated partners.

The effect of singlet oxygen produced by Ch-T on TASK-2 (Duprat et al., 2005) piqued our interest as to what effects this ROS agent might have on TASK-1 channel coexpressed with an oxygen-sensor protein, Nox4. It might not be surprising that no change in current is observed in the K2N R3Q mutant TASK-1, either expressed alone or with Nox4, in the presence of Ch-T. This is because TASK-1 and TASK-2, despite having similar names, actually belong to different families (Enyedi and Czirjak, 2004). TASK-2 belongs to the TALK family instead of the TASK family. (Enyedi and Czirjak, 2004). Moreover, the modes of action of ROS are very specific (Duprat et al., 2005). The singlet oxygen produced by Ch-T affects K^+ channels belonging to the same family in different ways, as it inhibits TASK-2 while strongly activating TALK-1 and TALK-2 (Duprat et al., 2005). More interestingly, different ROS agents regulate these channels in different manner (Duprat et al., 2005). The most commonly known ROS, superoxide, affects both TASK-2 and TALK-2, but not TALK-1 (Duprat et al., 2005). The fact that TASK-1 is unaffected compared with the TALK channels could also indicate that TASK-1 has a different physiological function.

Chapter 6: Modulation of Kv2.1, Kv9.3, and Nox4 by hydrogen peroxide (H_2O_2), dithiothreitol (DTT), 5-5'-dithiobis-2-nitrobenzoic acid (DTNB), chloramine-T (Ch-T), and amphoterin-induced gene and open reading frame (AMIGO) proteins

6.1 Introduction

Hydrogen peroxide (H_2O_2) is a well-known ROS in the pulmonary vasculature (Harrison et al., 2007). The question as to whether the main producer of H_2O_2 in the pulmonary vasculature is Nox4 or mitochondria still remains unanswered (Brandes et al., 2010; Harrison et al., 2007; Lee et al., 2013; Mittal et al., 2012). The hypothesis that Nox4 is the primary H_2O_2 producer will be studied. In contrast with other Nox proteins (Nox1−Nox3 and Nox5), Nox4 produces H_2O_2 instead of superoxide (Nisimoto et al., 2014). However, this result has also been debated because the possibility of Nox4 producing superoxide and compartmentalizing it in the membrane, thereby preventing detection, cannot be ruled out (Nisimoto et al., 2014).

Although there is much evidence pointing to the harmful effects of ROS to biological processes which could lead to inflammation and hypertension (Harrison et al., 2007; Touyz, 2004), there is also evidence substantiating the role of H_2O_2 as a signalling molecule in the presence of other harmful stimuli in order to initiate a counter balancing mechanism to take place (S. W. Park et al., 2015)

One of the potential targets of H_2O_2 is Kv channels. However, it still remains controversial as to whether H_2O_2 activates Kv channels and therefore acts as a vasodilator or it inhibits target channels and acts as a vasoconstrictor (S. W. Park et al., 2015). This is because there has been evidence supporting either sides of the argument and some even reporting that both are true (S. W. Park et al., 2015). Reasons that could account for these different findings could be the experimental design and the vascular bed or vessels used in research (S. W. Park et al., 2015).

In short, the effect of H_2O_2 on Kv channels still remains controversial. Therefore, it would be interesting to explore the effects of H_2O_2 on Kv2.1. Whether co-expression of Kv9.3 with Kv2.1 abolishes or modulates the effect of H_2O_2 is unknown but was explored. Thus, it is of interest to see how Nox4 regulates both Kv2.1 and Kv9.3 in the presence of H_2O_2. In Chapter 3, it was found that Nox4 does not inhibit Kv2.1 and Kv2.1/Kv9.3 current amplitude and does not have any effect on their activation threshold. Perhaps, this was due to the fact that the experiments were performed in normoxia and hence the effect of Nox4 was not visible.

Various studies have confirmed the relationship between the redox status of the cells and the effect on Kv channels (Archer et al., 2004; Park et al., 1997, Ward and McMurty, 2009). Park et al, 1997 showed that the reducing agent dithiothreitol (DTT) decreased Kv current while oxidizing agent, 2,2'-dithio-bis(5-nitropyridine), DTNBP increased Kv current. DTT also accelerated the inactivation kinetics while DTNBP accelerated activation kinetics (Park et al., 1997).

However, this argument that, when the cell is oxidized or reduced will activate or inhibit Kv channels respectively, has been debated as other research has shown that oxidizing agent and reducing agent do not always have opposing effect on Kv current. The reason as to why remains elusive. To illustrate this point, Park et al., 1997, have studied the effect of DTT and DTNBP on the activation and inactivation time course of Kv current in the PASMC (Park et al., 1997). For the activation time course experiments, DTNBP reduced the time constant significantly while DTT had no effect on the activation time constants of Kv currents in the PASMC. However, DTT does not have an exactly opposing effect to that of DTNBP, because DTT increased the time constants at potentials <10mV but decreased the time constants at potentials >40mV (Park et al., 1997). In terms of inactivation time course, DTT decreased the fast component of time constant but it does not affect the slow component. DTNBP does not have any effect in either of the time constant components (Park et al., 1997).

In our studies, we are interested in the effects of reducing (DTT) and oxidizing (5,5'-dithiobis-2-nitrobenzoic acid (DTNB)) agents on Kv2.1, Kv2.1/Kv9.3 channels. In addition, the effect of these agents on the co-expression of Nox4 with Kv2.1 or Kv2.1/Kv9.3 was also probed.

Similar to the pulmonary vasculature, ROS such as superoxide, hydroxyl radical, hypochlorous acid (HOCl), and hydrogen peroxide play a pathogenic role in the colonic tissues (Prasad and Goyal, 2004). These ROS are usually generated following the polymorphonuclear neutrophils oxidative burst and they can combine with ammonia (NH_3), which is abundant in the colon (10-70 mM luminal), to produce colon-specific amine-based oxidants such as monochloramine (NH_2Cl) (Prasad and Goyal, 2004). Chloramine-T (Ch-T) is known for the generation of the ROS, singlet oxygen molecule (Duprat et al., 2005). Unlike other oxidizing agents such as H_2O_2 and DTNB which specifically oxidizes cysteine residues, chloramine-T and NH_2Cl can oxidize both cysteine and methionine residues (Prasad and Goyal, 2004).

In mouse colonic myocytes, there are two major components of Kv currents known as transient outward K^+ current (I_{to}) and sustained delayed rectifier K^+ current (I_{dr}) (Koh et al., 1999; Prasad and Goyal, 2004). Ito has fast activation and inactivation kinetics at subthreshold potentials and is blocked by external 4-aminopyridine. Idr activates above -10mV, but does not inactivate and is suppressed by tetraethylammonium (Prasad and Goyal, 2004). It has been shown that I_{to} is conducted by Kv4.1, Kv4.2 and Kv4.3 (Koh et al., 1999).

Interestingly, both Ch-T and NH_2Cl inhibit I_{to} while enhancing I_{dr} at the same time, whereas the cysteine-specific oxidizing agents have no effect on I_{dr} but cause a partial and slow inhibition of Ito by inducing the channel to open at a more negative potential (about 18mV earlier) (Prasad and Goyal, 2004).

Secondly, cysteine-specific reducing agents such as DTT and GSH abolished the effect of H_2O_2 and DTNB on I_{to} but they did not reverse the effect of NH_2Cl and Ch-T on either Idr or Ito (Prasad and Goyal, 2004). This shows that chemically-distinct oxidizing agents can modulate Kv channels in a different way. Since the cysteine-specific H_2O_2 and DTNB have no effect on Idr, this suggests that modification of Idr by Ch-T and NH_2Cl could result from methionine oxidation alone (Prasad and Goyal, 2004). Meanwhile, suppression of Ito could result from oxidation of cysteine or methionine or both (Prasad and Goyal, 2004).

In relation to pulmonary hypertension, Tanaka et al., 1998 suggested that suppression

of Ito channels (native A-type channels) could be explained by oxidation and this then can lead to a pathogenic effect such as arrhythmias in the heart.

Since there is an established link between Ch-T and Kv current in colonic cells, it would be interesting to investigate whether Ch-T, which produces singlet oxygen, affects Kv2.1 and such regulation might be crucial in PH.

Amphoterin-induced gene and open reading frame (AMIGO)-1 was discovered by Kuja-Panula et al, 2003 and has been shown to colocalize with Kv2.1. This led to the speculation that AMIGO1 could be an interacting partner of Kv2.1 (Kuja-Panula et al., 2003). Peltola et al, 2011, demonstrated that AMIGO1 changes the voltage-gating properties of Kv2.1 by increasing the current at voltages from -40mV to +20mV and causing the channel to be activated at more negative potentials, and influences the expression level of Kv2.1 in mammals. AMIGO1-Kv2.1 interaction has been shown to be essential, as mice lacking such interaction (due to AMIGO1 KO) displayed altered complex behavioural traits that resemble schizophrenia (Peltola et al., 2016). Interestingly, a separate study found that Kv9.3 mRNA levels in prefrontal cortical parvalbumin neurons were significantly lower (in situ hybridization reported 23% lower while microarray revealed 40% lower) in schizophrenia subjects (monkeys) (Georgiev et al., 2014). The group hypothesized that Kv9.3 is responsible for the precise detection of coincident excitatory synaptic inputs to parvalbumin neurons, which is important for the synchronization of cortical neural networks in γ-oscillations and therefore vital for cognitive functions (Georgiev et al., 2014). The relationship of Kv9.3 and Kv2.1 has been established by several authors and has been confirmed in Chapter 3 (Kerschensteiner, 2003; Patel and Honoré, 2001; Patel et al., 1997, 1999). However, it has never been addressed what are the modes of regulation that will result when both AMIGO1 and Kv9.3 are co-expressed with Kv2.1 and what are the impacts of such modulation in the context of PH.

Since AMIGO1 has been demonstrated to interact with Kv2.1, we are interested to probe whether AMIGO2 is also an auxiliary subunit of Kv2.1 even though the similarity between AMIGO1 and AMIGO2 is only 48% (Kuja-Panula et al., 2003; Peltola et al., 2016, 2011; Zhao et al., 2014). While most studies pinpointed the role of AMIGO2 in promoting cell survival (Chen et al., 2012; Hossain et al., 2011;

Rabenau et al., 2004), the benefits of AMIGO2 in the context of PVR remains elusive. PVR occurs due to overgrowth of PASMC and PAEC and one of the stimuli that causes PVR is hypoxia (Huang et al., 2010; Kuhr et al., 2012). Hossain et al, 2011, showed that AMIGO2 expression is sensitive to hypoxia and AMIGO2 overexpression protected endothelial cells from cell death when the cells are treated with 50mM of H_2O_2 for five days. As discussed in Introduction, promotion of apoptosis is beneficial in PVR as overgrowth of PAEC will cause the lumen to be stiff and increases the resistance to blood flow (Huang et al., 2010; Kuhr et al., 2012). However, it could also be argued that it is the inappropriate accumulation of inflammatory cells or failure of the proteasome to clear dysfunctional cells plays a more important role in promoting PVR (Guignabert et al., 2015). Pro-proliferation mechanisms to maintain the survival of normal, functional endothelial cells in the pulmonary vasculature should not bring adverse effects. Secondly, whether H_2O_2 inhibits or activates K^+ channels and thus act as a vasoconstrictor or a vasodilator, respectively is unclear (S. W. Park et al., 2015). Some researchers have even reported that H_2O_2 could act as both vasoconstrictor and vasodilator, depending on the concentration (<10mol/L elicits vasoconstrictor effect, while higher concentration will elicit the opposite) (Archer et al., 2004; S. W. Park et al., 2015). One of the hypotheses that could explain this phenomenon could be the absence of a regulatory protein that will allow H_2O_2 to have an effect on Kv2.1. In a nutshell, it is a challenge to decipher whether the role of AMIGO2 in protecting endothelial cells is favourable in PVR. It is noteworthy that AMIGO2 has never been shown to co-express with Kv2.1 *in vitro*, hence how and whether AMIGO2 regulates Kv2.1 is not known. This study sought to address what are the implications of co-expression of AMIGO2 with Kv2.1 and Kv2.1/Kv9.3, in the absence and presence of H_2O_2.

It is rather unanticipated that AMIGO3 promotes neuronal apoptosis, an effect that is opposite from its family members, AMIGO1 and AMIGO2 (Ahmed et al., 2013). In a study assessing the anti-aging effects of rats treated with extracts from *Gryllus bimaculatus* crickets, it has been demonstrated that AMIGO3 is one of the genes that was upregulated in rats with reduced level of 8-hydroxy-2'-deoxyguanosine (8-OHdG) (Ahn et al., 2015). The authors suggested that the anti-oxidative effects were a consequence of AMIGO3 upregulation (Ahn et al., 2015). Accordingly, the effect of

AMIGO3 co-expression with Kv2.1 is being investigated in this study so that more understanding of how AMIGO3 could regulate Kv2.1 can be gained.

6.2 Results

Effect of H_2O_2 on current amplitude and activation threshold

The representative traces without or with the addition of 1mM H_2O_2 appeared similar and the quantification of the current of several cells confirmed that this redox agent does not exert an effect on the current amplitude (Figure 6.1). The standard voltage-step protocol was used to obtain recordings, where cells were depolarized from -100 mV to +50mV in increment of 10mV every sweep. Current measurement taken at the voltage-step from -100 to +50mV revealed that H_2O_2 does not make a difference to the current amplitude of Kv2.1 (Figure 6.1). Furthermore, analysis of normalized current also demonstrated that H_2O_2 does not have an impact on the activation threshold of Kv2.1 (Figure 6.1).

Data were expressed as mean current amplitude ± SEM in the plot of current against voltage, and as mean normalized current ± SEM in the plot of normalized current against voltage. In terms of comparing the differences in current amplitude across all voltages, two-way ANOVA was used as I was examining two factors, which are presence of 1mM of H_2O_2 and voltages. Bonferroni method was chosen to accompany the two-way ANOVA as I was only analyzing two means each time and this method does not assume independence. The reason I have not used the Sidak method, despite it providing a higher statistical power and was the method recommended by the GraphPad Prism software, was that this method assumes that each comparison is independent of the others, in other words, cells that are perfused with external solution cannot be perfused with 1mM H_2O_2. Since the recordings were paired, meaning the same cell was used to obtain recording for external solution and 1mM H_2O_2, the Bonferroni method is appropriate in this case (Kim, 2015). Data analysis for normalized current were carried out using the Student's t-test to examine the difference between cells without and with 1mM H_2O_2 at -30mV. The Welch's correction method was used because of unequal variances.

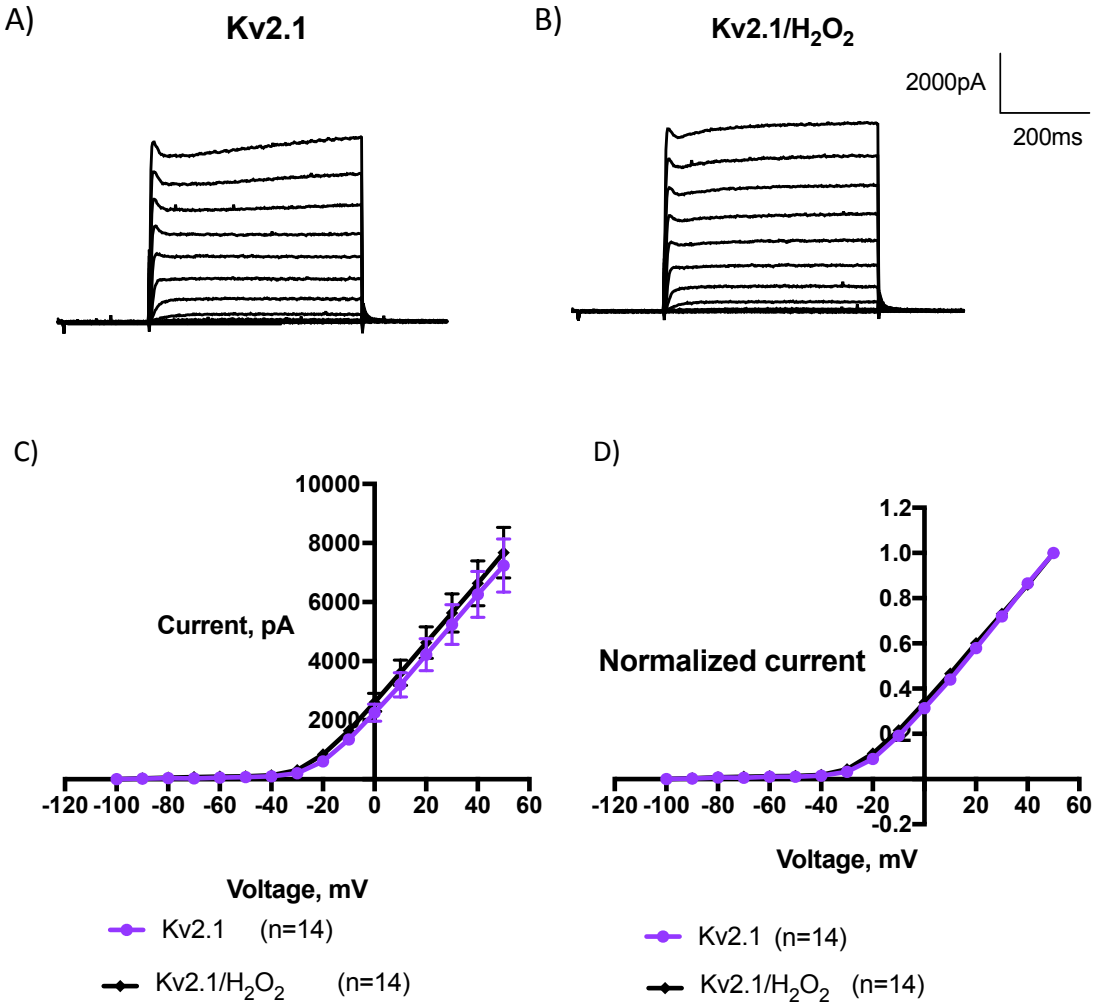

Figure 6.1: H_2O_2 does not affect the current amplitude and activation threshold of Kv2.1. tsA-201 cells were transfected with Kv2.1+GFP and the standard voltage-step protocol was used. Cells were perfused with external solution (Kv2.1) and then 1mM of H_2O_2 (Kv2.1/ H_2O_2). Representative traces for A) Kv2.1 and B) Kv2.1/H_2O_2. C) Plot of current against voltage for Kv2.1 and Kv2.1/$_2O_2$. D) Normalized current vs Voltage plot for Kv2.1 and Kv2.1/H_2O_2. Data were expressed as mean ± SEM. Two-way ANOVA with Bonferroni method to analyze the difference in current amplitude across all voltages did not reveal a statistically-significant difference between cells perfused without or with 1mM H_2O_2. Student's t-test with Welch's correction was used to analyze the difference between normalized current of Kv2.1 and Kv2.1/H_2O_2 at -30mV because the variances were unequal and it revealed that there was no statistically-significant difference between cells perfused with external solution and H_2O_2.

There is no apparent difference in the current traces of Kv2.1/Kv9.3 in the absence and presence of H_2O_2 (Figure 6.2 A and B). Analysis of the currents at each voltage

step confirmed this finding (Figure 6.2 C). As demonstrated in Chapter 3 (Figure 3.5 and Figure 3.6), the activation of Kv2.1/Kv9.3 (-40mV) occurs at a more negative potential than Kv2.1 (-20mV). Addition of H_2O_2 does not abolish the effect of Kv9.3 on Kv2.1, as the activation threshold did not shift to a more similar trend to Kv2.1 (Figure 6.2 D).

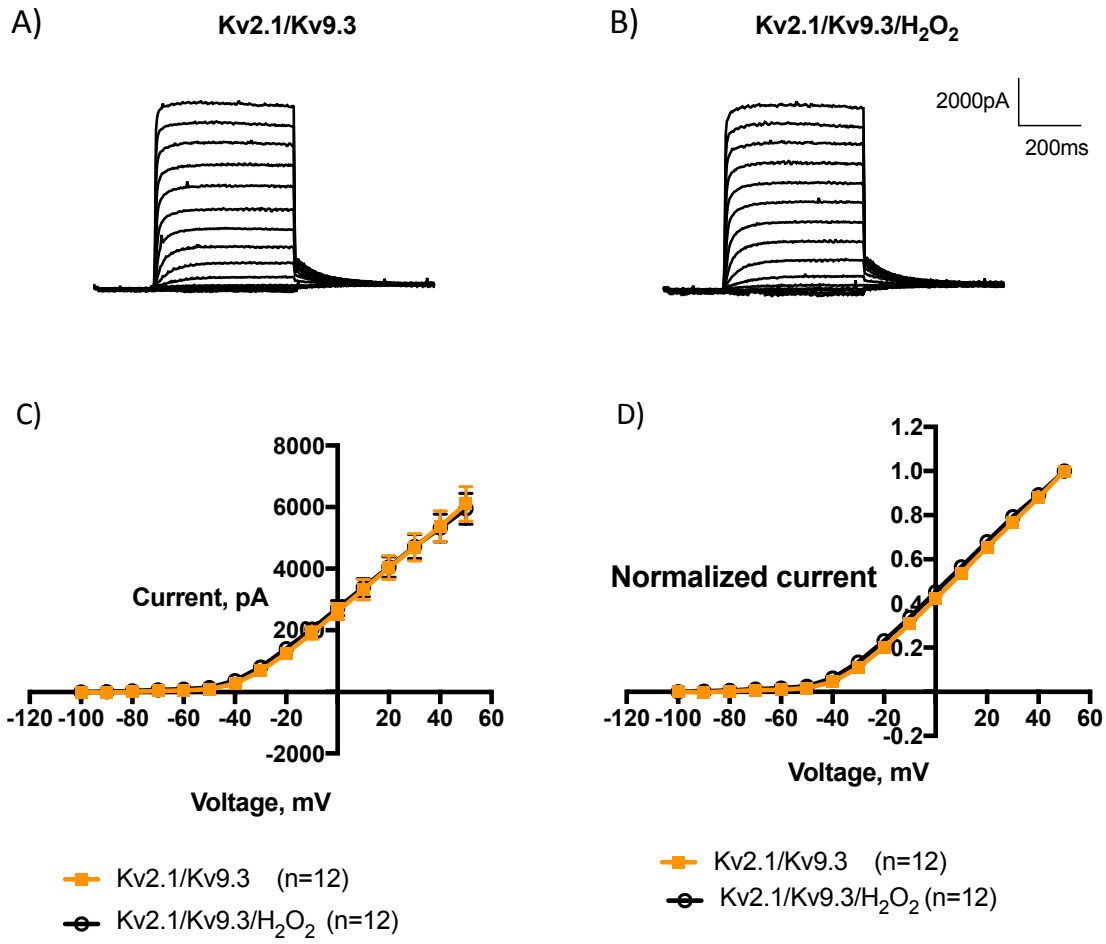

Figure 6.2: H_2O_2 does not affect the current amplitude and activation threshold of Kv2.1/Kv9.3. tsA-201 cells were transfected with Kv2.1/Kv9.3 + GFP and the standard voltage-step protocol was used. Cells were either perfused with external solution (Kv2.1/Kv9.3) or 1mM of H_2O_2 (Kv2.1/Kv9.3/H_2O_2). Representative traces for A) Kv2.1/Kv9.3 and B) Kv2.1/Kv9.3/H_2O_2. C) Plot of current against voltage for Kv2.1/Kv9.3 and Kv2.1/Kv9.3/H_2O_2. D) Normalized current vs Voltage plot for Kv2.1/Kv9.3 and Kv2.1/Kv9.3/H_2O_2. Data were expressed as mean ± SEM. Two-way ANOVA with Bonferroni method to analyze the difference in current amplitude across all voltages did not reveal a statistically-significant difference between cells perfused without or with 1mM H_2O_2. Student's t-test with Welch's correction was used to analyze the difference between normalized current of Kv2.1/Kv9.3 and Kv2.1/Kv9.3/H_2O_2 at -30mV because the variances were unequal and it revealed that there was no statistically-significant difference between cells perfused with external solution and H_2O_2.

Nox4 is thought to be an H_2O_2 producer in the pulmonary vasculature (Mittal et al., 2007, Nisimoto et al., 2014). However, results in Chapter 3 showed that Nox4 does not regulate Kv2.1. Therefore, it is not surprising that Nox4 does not facilitate or mediate the effect of H_2O_2 on Kv2.1. Results in Figure 6.3 showed that H_2O_2 does not affect the current amplitude or activation threshold of Kv2.1/Nox4.

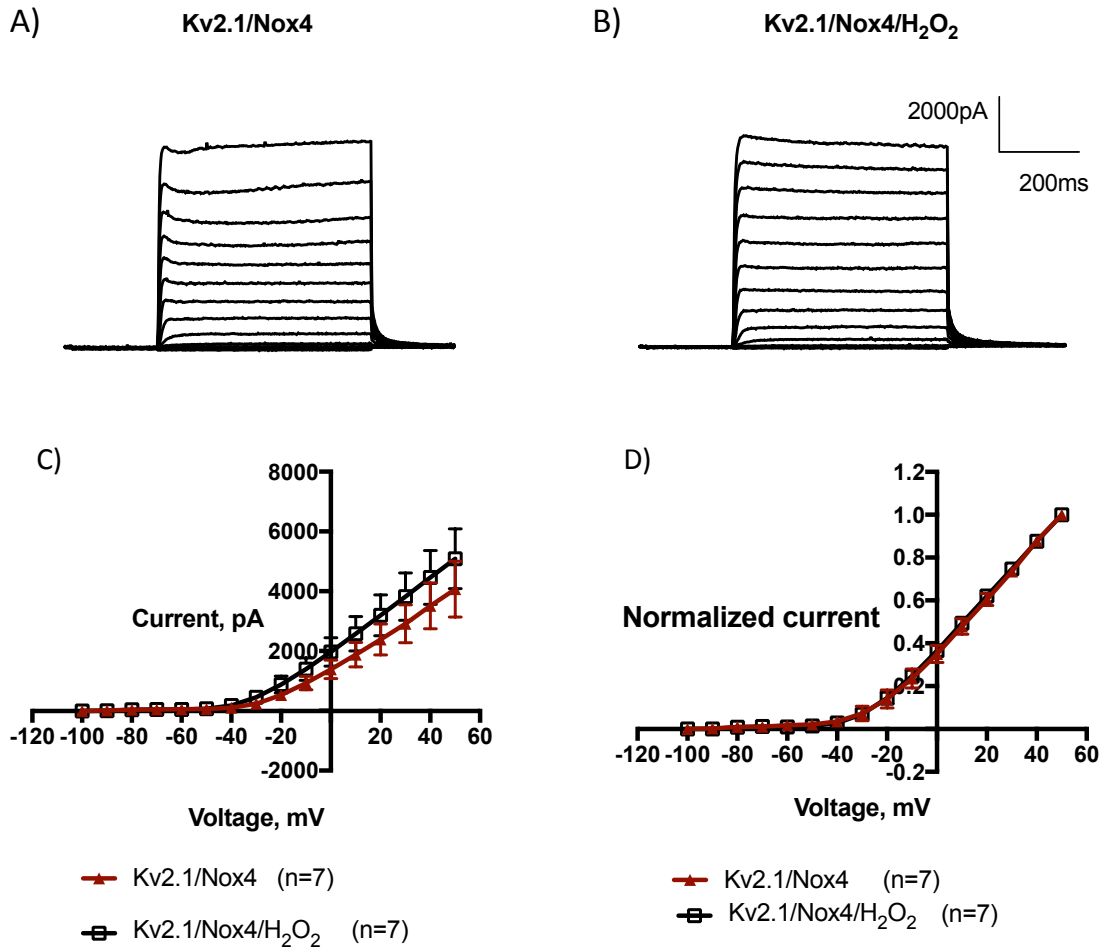

Figure 6.3: The presence of H_2O_2 does not have any effect on the current amplitude and activation threshold of Kv2.1/Nox4. Cells were either perfused with external solution (Kv2.1/Nox4) or 1mM of H_2O_2 (Kv2.1/Nox4/H_2O_2). Representative traces for A) Kv2.1/Nox4 and B) Kv2.1/Nox4/H_2O_2. C) Current vs Voltage plot for Kv2.1/Nox4 and Kv2.1/Nox4/H_2O_2. D) Normalized current vs Voltage plot for Kv2.1/Nox4 and Kv2.1/Nox4/H_2O_2. Data were expressed as mean ± SEM. Two-way ANOVA with Bonferroni method to analyze the difference in current amplitude across all voltages did not reveal a statistically-significant difference between cells perfused without or with 1mM H_2O_2. Student's t-test with Welch's correction was used to analyze the difference between normalized current of Kv2.1/Nox4 and Kv2.1/Nox4/H_2O_2 at -30mV because the variances were unequal and it revealed that there was no statistically-significant difference between cells perfused with external solution and H_2O_2.

H_2O_2 does not alter the current amplitude or the activation threshold of Kv2.1/Kv9.3/Nox4

The presence of H_2O_2 does not have any effect on the current amplitude of Kv2.1/Kv9.3/Nox4 (Figure 6.4). Moreover, it does not abolish the effect of Kv9.3 on the Kv2.1/Nox4 in shifting the activation threshold to a more negative (polarized) potential (Figure 6.4).

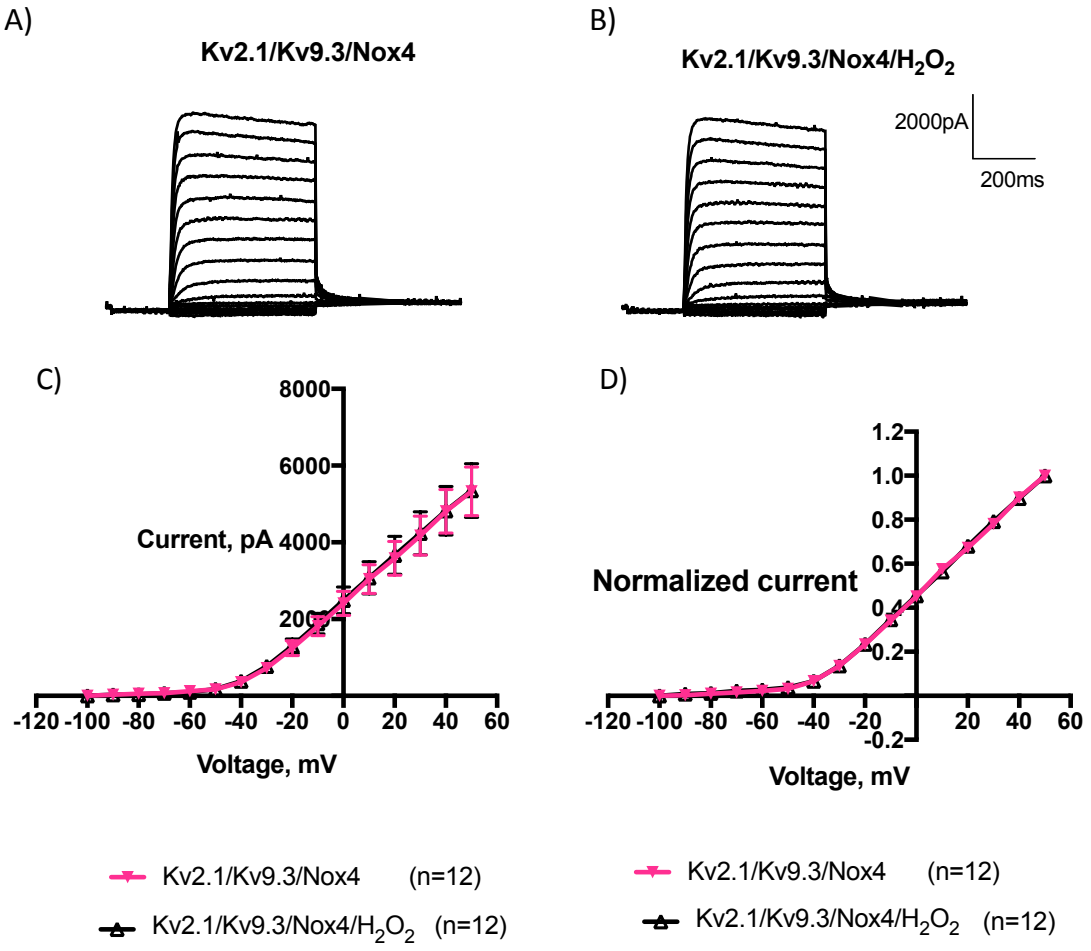

Figure 6.4: H_2O_2 does not alter the current amplitude or the activation threshold of Kv2.1/Kv9.3/Nox4. Cells were either perfused with external solution (Kv2.1/Kv9.3/Nox4) or 1mM of H_2O_2 (Kv2.1/Kv9.3/Nox4/H_2O_2). Representative traces for A) Kv2.1/Kv9.3/Nox4 and B) Kv2.1/Kv9.3/Nox4/H_2O_2. C) Current vs Voltage plot for Kv2.1/Kv9.3/Nox4 and Kv2.1/Kv9.3/Nox4/H_2O_2. D) Normalized current vs Voltage plot for Kv2.1/Kv9.3/Nox4 and Kv2.1/Kv9.3/Nox4/H_2O_2. Data were expressed as mean ± SEM. Two-way ANOVA with Bonferroni method to analyze the difference in current amplitude across all voltages did not reveal a statistically-significant difference between cells perfused without or with 1mM H_2O_2. Student's t-test with Welch's correction was used to analyze the difference between normalized current of Kv2.1/Kv9.3/Nox4 and Kv2.1/Kv9.3/Nox4/H_2O_2 at -30mV because the variances were unequal and it revealed that there was no statistically-significant difference between cells perfused with external solution and H_2O_2.

Effect of H_2O_2 on deactivation kinetics

After assessing the effect of H_2O_2 on the current amplitude and activation threshold and finding that the effects are not apparent, another method to assess whether H_2O_2 has any effect on Kv2.1, Kv9.3, and Nox4 was used. The slow and fast components of the time constant of deactivation, tslow and tfast, were measured. The current traces in Figure 6.5 showed that the gradient of the slope resulting from repolarization to -50mV from a step potential of +20mV (the 13th trace) is similar for Kv2.1, Kv2.1/Kv9.3, Kv2.1/Nox4, and Kv2.1/Kv9.3/Nox4 regardless of the presence of H_2O_2. The bar charts showed that the tslow and tfast of the respective cells did not change in the absence or presence of H_2O_2. Data were expressed as mean ± SEM and Student's t-test with Welch's correction was used to compare the tslow or tfast for cells with or without H_2O_2. Two-way ANOVA was also used to analyze the difference in the means, because we are testing two factors which are the presence of H_2O_2 and the time constants (tslow and tfast). The multiple comparison tests were done using the Bonferroni method. Bonferroni is the most commonly used method as it is easy to understand, and confidence intervals can be computed. Since we are only analyzing two means each time, Bonferroni is appropriate. Furthermore, since the recordings were paired, meaning the same cell was used to obtain recording for external solution and 1mM H_2O_2, I have chosen the Bonferroni method, which does not assume independence.

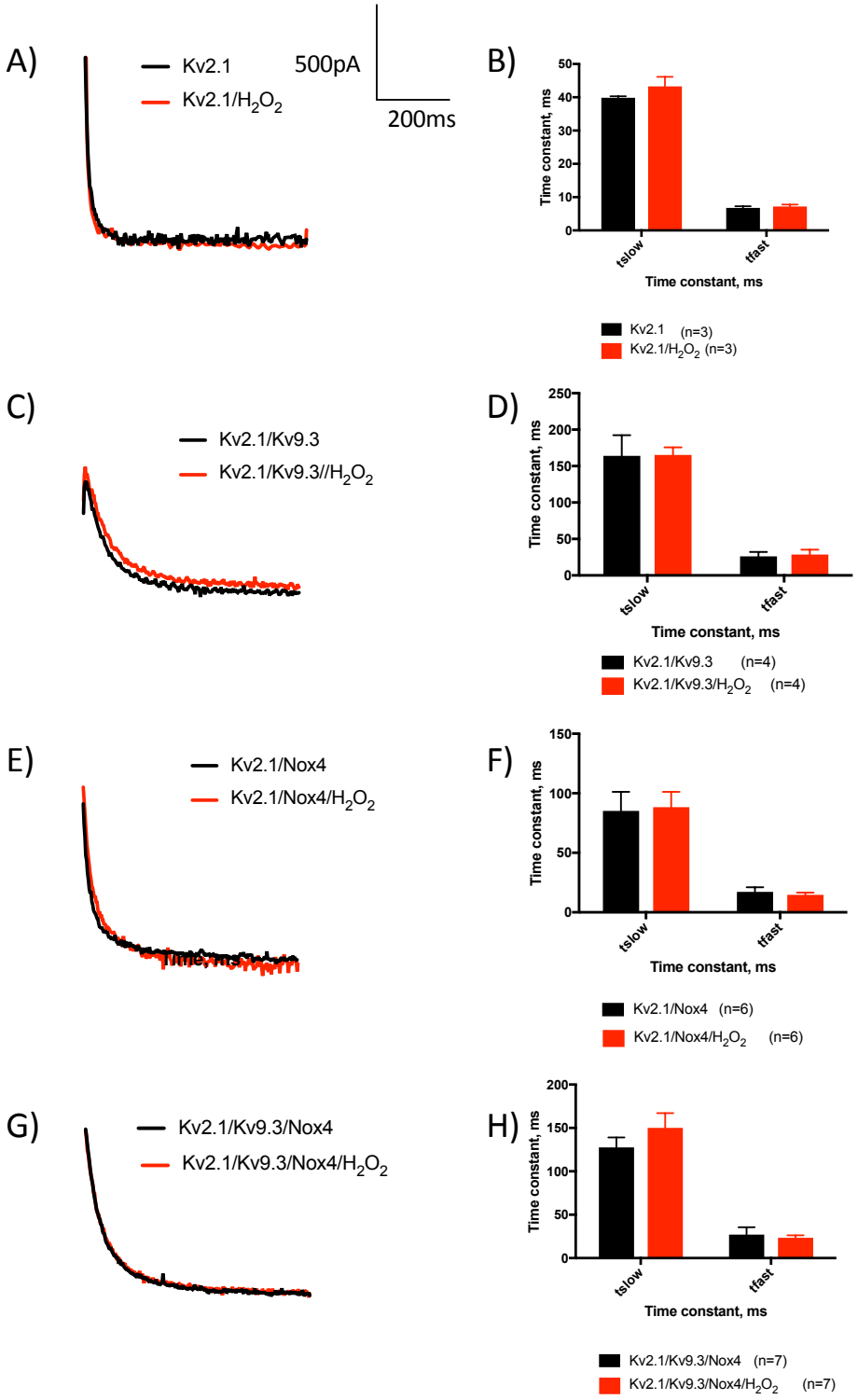

Figure 6.5: H_2O_2 does not alter the deactivation kinetics of Kv2.1, Kv2.1/Kv9.3, Kv2.1/Nox4, and Kv2.1/Kv9.3/Nox4.Current traces of the slope resulting from repolarization to -50mV from a step potential of +20mV for A) Kv2.1 vs Kv2.1/ H_2O_2, C) Kv2.1/Kv9.3 vs Kv2.1/ Kv9.3/H2O2, E) Kv2.1/Nox4 vs Kv2.1/Nox4/H_2O_2, G) Kv2.1/Kv9.3/Nox4 vs Kv2.1/Kv9.3/Nox4/$_2O_2$. Bar charts depicting the tslow and tfast from the slopes for B) Kv2.1 vs Kv2.1/ H_2O_2, D) Kv2.1/Kv9.3 vs Kv2.1/ Kv9.3/H2O2, F) Kv2.1/Nox4 vs Kv2.1/Nox4/H_2O_2, H) Kv2.1/Kv9.3/Nox4 vs Kv2.1/Kv9.3/Nox4/$_2O_2$. In the bar charts, data were expressed as mean ± SEM. Student's t-test with Welch's correction was used to analyze the difference between cells perfused with external solution and H_2O_2 in terms of tslow and tfast and it was found that there is no statistically significant difference between both time constants of cells perfused with external solution or H_2O_2. Two-way ANOVA with Bonferroni test showed that the differences in time constants for cells perfused with external solution and H_2O_2 are not statistically significant.

Effect of DTT on current amplitude and activation threshold

Cells were transfected with either Kv2.1, Kv2.1/Kv9.3, Kv2.1/Nox4, or Kv2.1/Kv9.3/Nox4 cDNAs and GFP cDNA was used as a reporter. Cells were either perfused with external solution or 5mM DTT when recordings were obtained using the standard voltage-step protocol outlined in Chapter 2. Data were expressed as mean current amplitude ± SEM or mean normalized current ± SEM across all voltages. Student's t-test with Welch's correction was used to analyze the difference between the normalized current of cells at -30mV, without and with 5mM DTT, as the variances were unequal. Multiple comparison test to compare differences in current amplitude across all voltages were done using two-way ANOVA and Bonferroni method. Since I was only comparing two populations (for example, Kv2.1 cells without or with 5mM DTT) at a time, Bonferroni method is recommended as it can compute confidence intervals and it does not assume independence. I have excluded the Sidak method even though it has a higher statistical power because this method requires samples to be independent, meaning cells that are used for reading without 5mM DTT cannot be used for recordings with 5mM DTT. Since the readings are paired in the experiments, Sidak method would not be appropriate (Kim, 2015).

Although it has been shown that DTT decreased the Kv current in rabbit PASMC (Park et al., 1997), results from this chapter demonstrated that DTT has no effect on the current amplitude of Kv2.1 (Figure 6.6). Consistent the findings of (Park et al., 1997), results in Figure 6.6 showed that 5mM DTT has no significant effect on the steady-state activation, whereby the activation threshold of Kv2.1 were not altered despite the presence of DTT. Park et al., 1997 have also shown that DTT does not have any effect on the steady-state inactivation of Kv current. The experiments to investigate the steady-state inactivation of Kv2.1 and or Kv9.3 were not performed in this chapter and therefore a comparison with the studies performed by another group cannot be done.

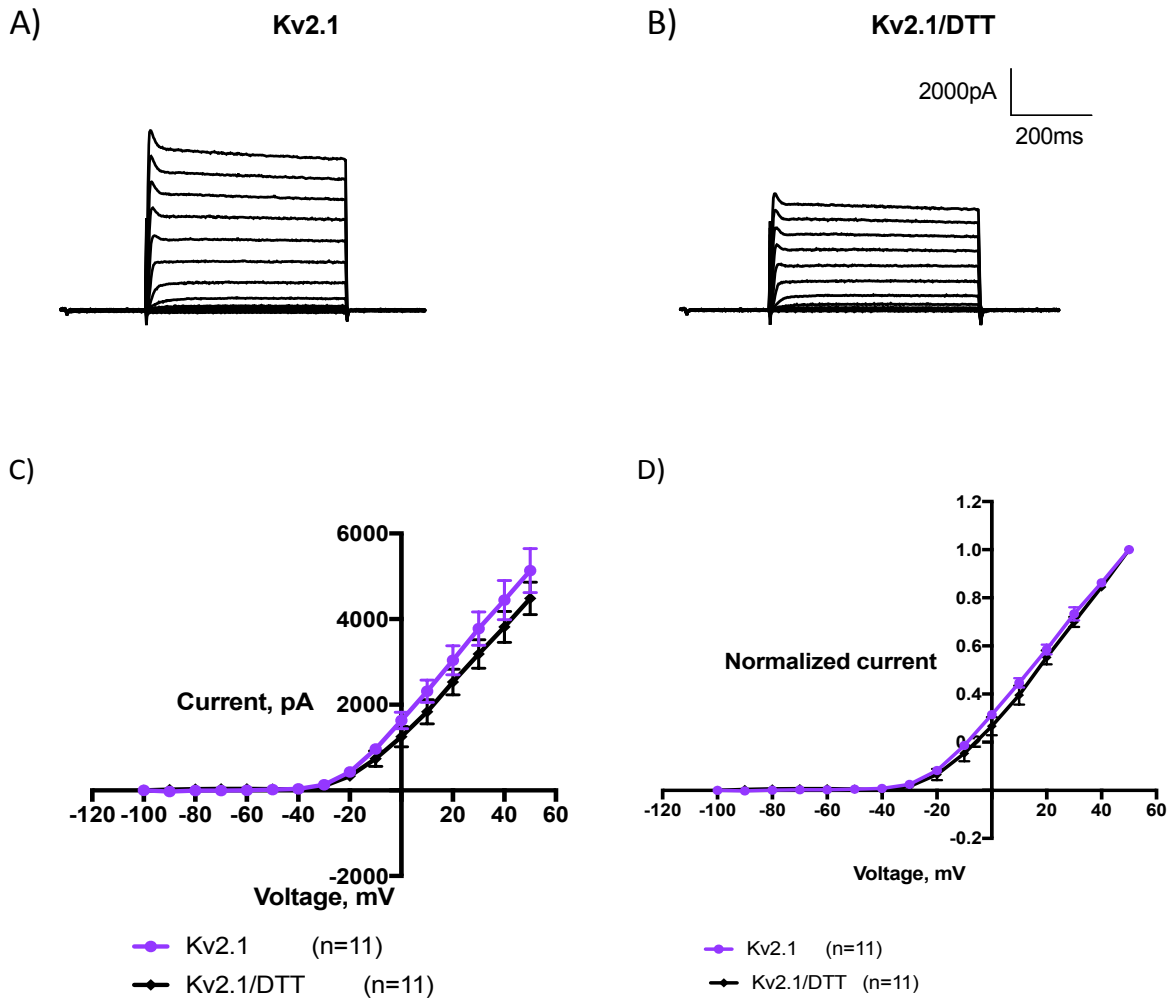

Figure 6.6: DTT does not alter the current amplitude and activation threshold of Kv2.1. Cells were transfected with Kv2.1 + GFP. The standard voltage-step protocol was used to obtain recordings and cells were either perfused with external solution (Kv2.1) or with 5mM DTT (Kv2.1/DTT). Representative current traces for A) Kv2.1 and B) Kv2.1 with DTT. C) Current vs Voltage plot for Kv2.1 and Kv2.1/DTT. D) Normalized current vs Voltage plot for Kv2.1 and Kv2.1/DTT. Data were expressed as mean ± SEM. Two-way ANOVA with Bonferroni method to analyze the difference in current amplitude across all voltages did not reveal a statistically-significant difference between cells perfused without or with 5mM DTT. Student's t-test with Welch's correction was used to analyze the difference between normalized current of Kv2.1 and Kv2.1/DTT at -30mV because the variances were unequal and it revealed that there was no statistically-significant difference between cells perfused with external solution and 5mM DTT.

In addition to the finding that DTT does not alter the activation threshold of Kv2.1, results displayed in Figure 6.7 revealed that DTT does not have any impact on the current amplitude and activation threshold of Kv2.1/Kv9.3. Although Kv9.3 is a silent subunit, its co-expression with Kv2.1 has been shown to modulate the latter, as shown

in Chapter 3, Figure 3.8 and Figure 3.9. However, in the presence of DTT, Kv2.1/Kv9.3 still has a similar trend to Kv2.1/Kv9.3 cells in control buffer.

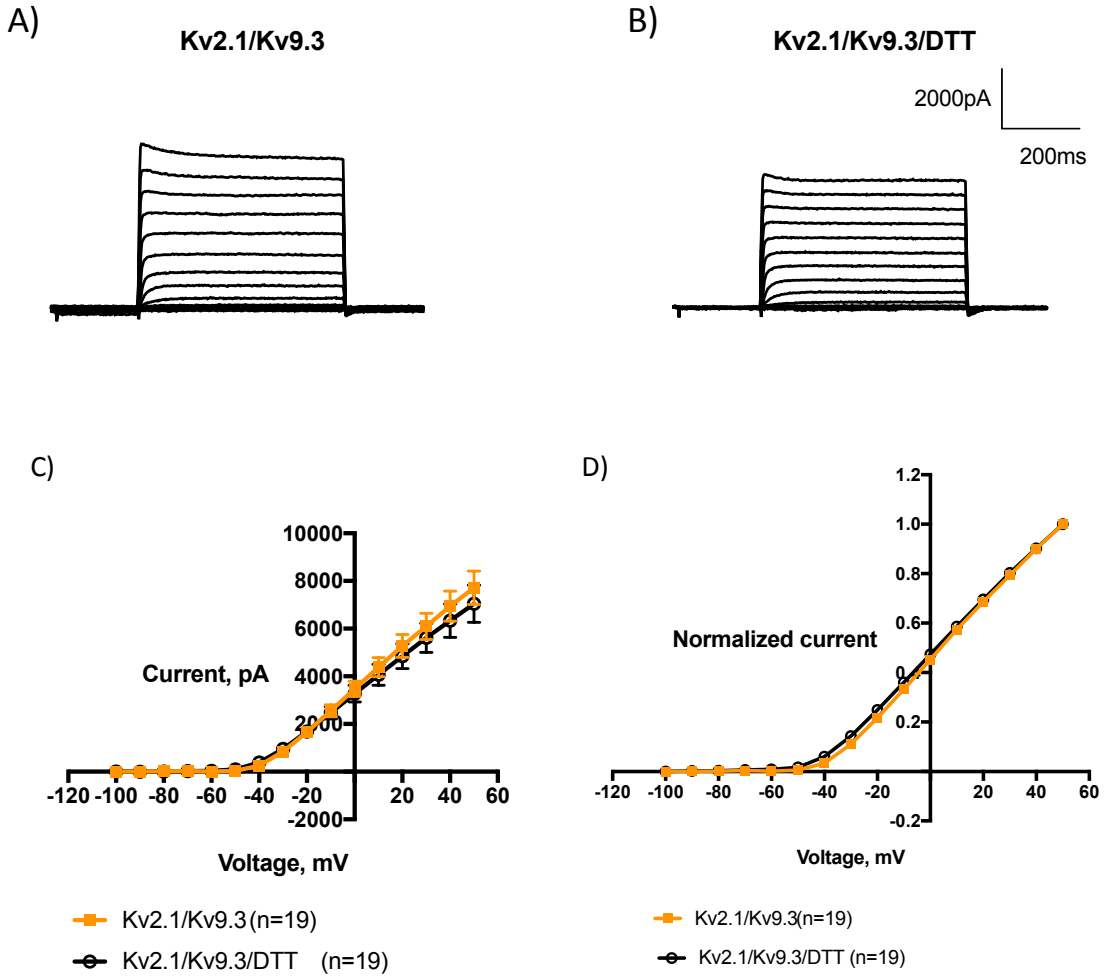

Figure 6.7: DTT does not alter the current amplitude and activation threshold of Kv2.1/Kv9.3. Cells were transfected with Kv2.1/Kv9.3 + GFP. The standard voltage-step protocol was used to obtain recordings and cells were either perfused with external solution (Kv2.1/Kv9.3) or with 5mM DTT (Kv2.1/Kv9.3/DTT). Representative current traces for A) Kv2.1/Kv9.3 and B) Kv2.1/Kv9.3 with DTT. C) Current vs Voltage plot for Kv2.1/Kv9.3 and Kv2.1/Kv9.3/DTT. D) Normalized current vs Voltage plot for Kv2.1/Kv9.3 and Kv2.1/Kv9.3/DTT. Data were expressed as mean ± SEM. Two-way ANOVA with Bonferroni method to analyze the difference in current amplitude across all voltages did not reveal a statistically-significant difference between cells perfused without or with 5mM DTT. Student's t-test with Welch's correction was used to analyze the difference between normalized current of Kv2.1/Kv9.3 and Kv2.1/Kv9.3/DTT at -30mV because the variances were unequal and it revealed that there was no statistically-significant difference between cells perfused with external solution and 5mM DTT.

The current traces in Figure 6.8 showed that the presence of DTT does not affect Kv2.1/Nox4. In the current vs voltage plot, DTT does not have any impact on Kv2.1/Nox4 current amplitude. Moreover, the activation threshold of Kv2.1/Nox4 remains the same despite the addition of DTT.

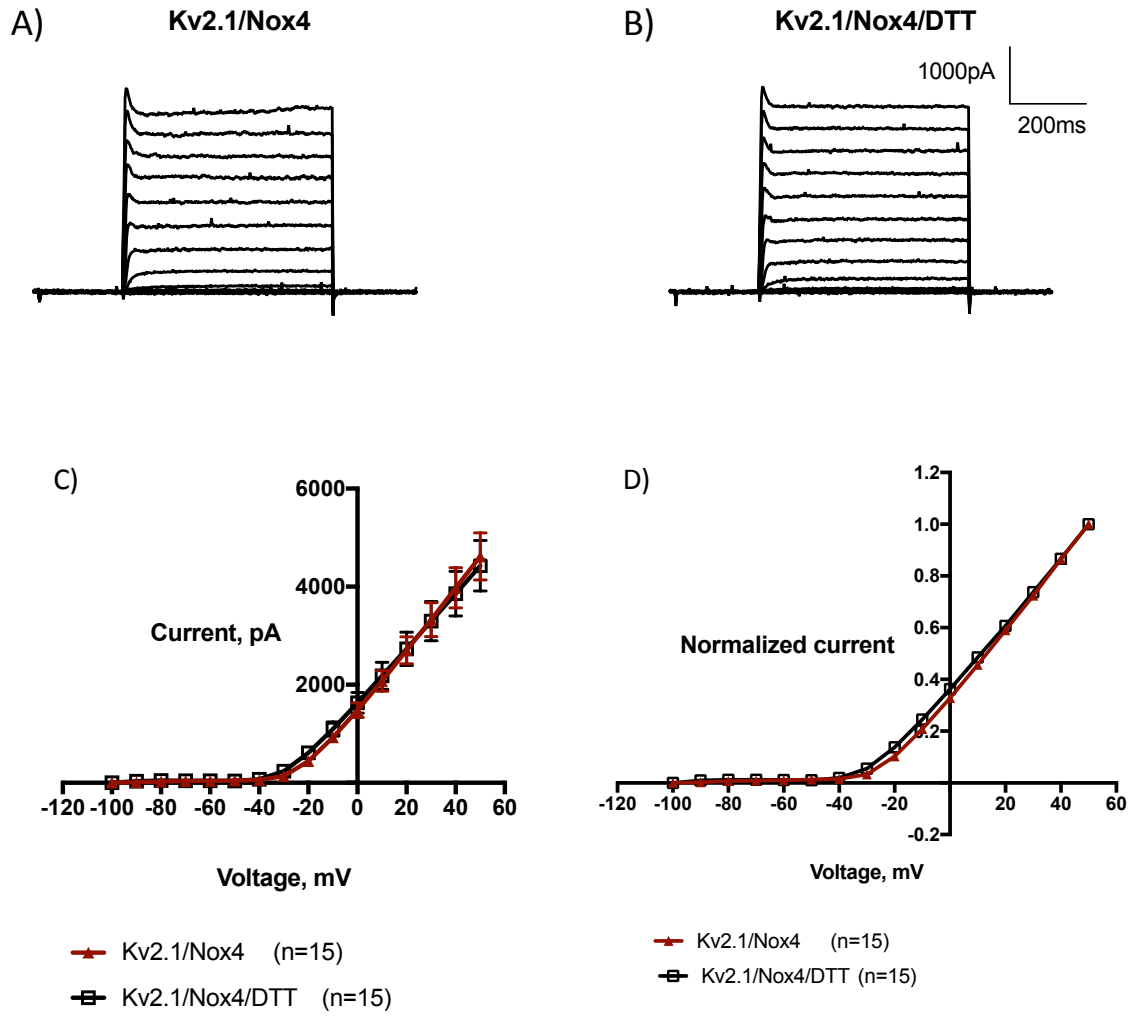

Figure 6.8: DTT does not reduce the Kv2.1/Nox4 current or shift the activation threshold. Cells were transfected with Kv2.1/Nox4 + GFP. The standard voltage-step protocol was used to obtain recordings and cells were either perfused with external solution (Kv2.1/Nox4) or with 5mM DTT (Kv2.1/Nox4/DTT). Representative current traces for A) Kv2.1/Nox4 and B) Kv2.1/Nox4 with DTT. C) Current vs Voltage plot for Kv2.1/Nox4 and Kv2.1/Nox4/DTT. D) Normalized current vs Voltage plot for Kv2.1/Nox4 and Kv2.1/Nox4/DTT. Two-way ANOVA with Bonferroni method to analyze the difference in current amplitude across all voltages did not reveal a statistically-significant difference between cells perfused without or with 5mM DTT. Student's t-test with Welch's correction was used to analyze the difference between normalized current of Kv2.1/Nox4 and Kv2.1/Nox4/DTT at -30mV because the variances were unequal and it revealed that there was no statistically-significant difference between cells perfused with external solution and 5mM DTT.

The co-expression of Nox4 with Kv2.1/Kv9.3 does not change the interaction of the Kv channels with DTT. Figure 6.9 showed that the current traces of Kv2.1/Kv9.3/Nox4 are similar despite the presence of DTT and the current vs voltage plot also revealed that DTT does not inhibit Kv2.1/Kv9.3/Nox4 current. The normalized current vs voltage plot showed that DTT does not cause activation of Kv2.1/Kv9.3/Nox4 to occur earlier or later.

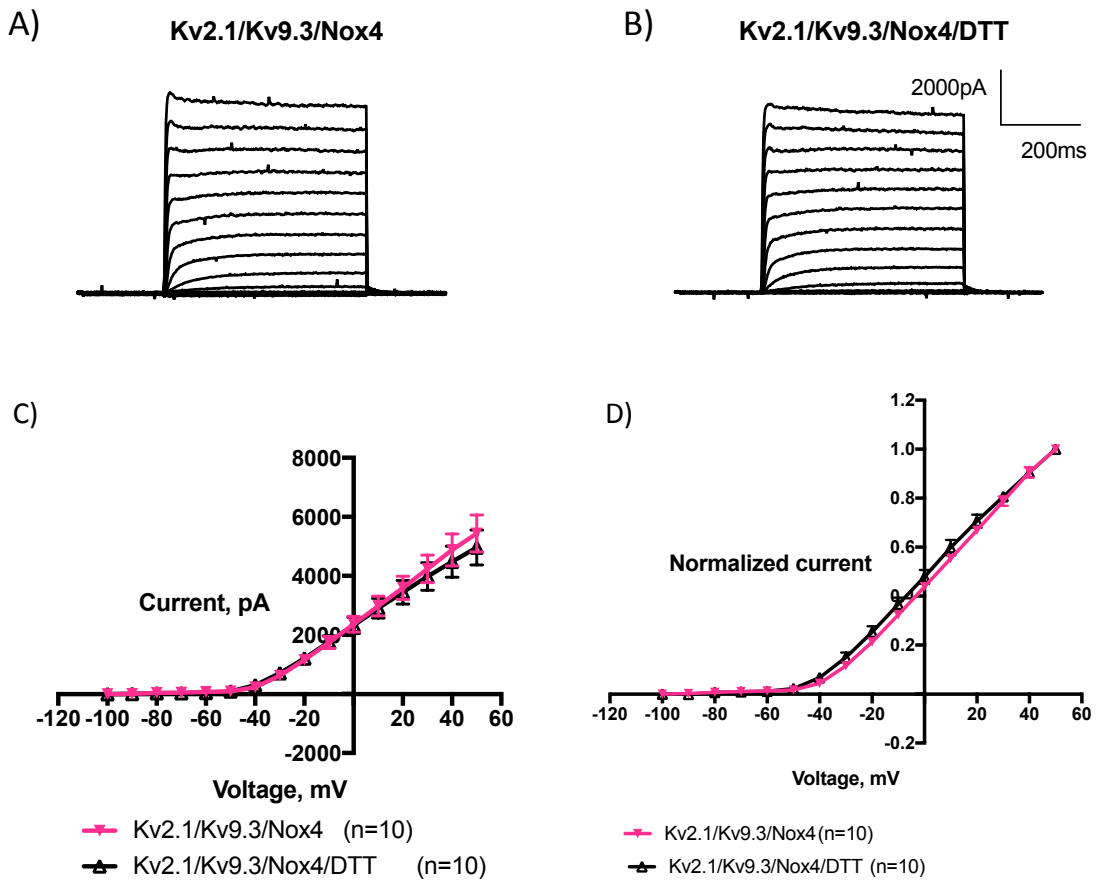

Figure 6.9: DTT does not have an impact on Kv2.1/Kv9.3/Nox4 current amplitude and activation threshold. Cells were transfected with Kv2.1/Kv9.3/Nox4 + GFP. The standard voltage-step protocol was used to obtain recordings and cells were either perfused with external solution (Kv2.1/Kv9.3/Nox4) or with 5mM DTT (Kv2.1/Kv9.3/Nox4/DTT). Representative current traces for A) Kv2.1/Kv9.3/Nox4 and B) Kv2.1/Kv9.3/Nox4 with DTT. C) Current vs Voltage plot for Kv2.1/Kv9.3/Nox4 and Kv2.1/Kv9.3/Nox4/DTT. D) Normalized current vs Voltage plot for Kv2.1/Kv9.3/Nox4 and Kv2.1/Kv9.3/Nox4/DTT. Two-way ANOVA with Bonferroni method to analyze the difference in current amplitude across all voltages did not reveal a statistically-significant difference between cells perfused without or with 5mM DTT. Student's t-test with Welch's correction was used to analyze the difference between normalized current of Kv2.1/Kv9.3/Nox4 and Kv2.1/Kv9.3/Nox4/DTT at -30mV because the variances were unequal and it revealed that there was no statistically-significant difference between cells perfused with external solution and 5mM DTT.

Effect of DTNB on current amplitude and activation threshold

Cells were transfected with either Kv2.1, Kv2.1/Kv9.3, Kv2.1/Nox4, or Kv2.1/Kv9.3/Nox4 cDNAs and GFP cDNA was used as a reporter. Cells were either perfused with external solution or 2mM DTNB when recordings were obtained using the standard voltage-step protocol outlined in Chapter 2. Data were expressed as mean current amplitude ± SEM or mean normalized current ± SEM across all voltages. Student's t-test with Welch's correction was used to analyze the difference between the normalized current of cells without and with 2mM DTNB as the variances were unequal. Multiple comparison test to compare differences in either current amplitude or normalized current across all voltages were done using two-way ANOVA and Bonferroni method. Since I was only comparing two populations (for example, Kv2.1 cells without or with 2mM DTNB) at a time, Bonferroni method is recommended as it can compute confidence intervals and it does not assume independence. I have excluded the Sidak method even though it has a higher statistical power because this method requires samples to be independent, meaning cells that are used for reading without 2mM DTNB cannot be used for recordings with 2mM DTNB. Since the readings are paired in the experiments, Sidak method would not be appropriate.

The oxidizing agent, DTNB does not have any impact on the current amplitude of Kv2.1 (Figure 6.10). In the normalized current vs voltage plot, the trends for Kv2.1 in the absence and presence of DTNB overlap, indicating that DTNB does not affect the activation threshold of Kv2.1 (Figure 6.10).

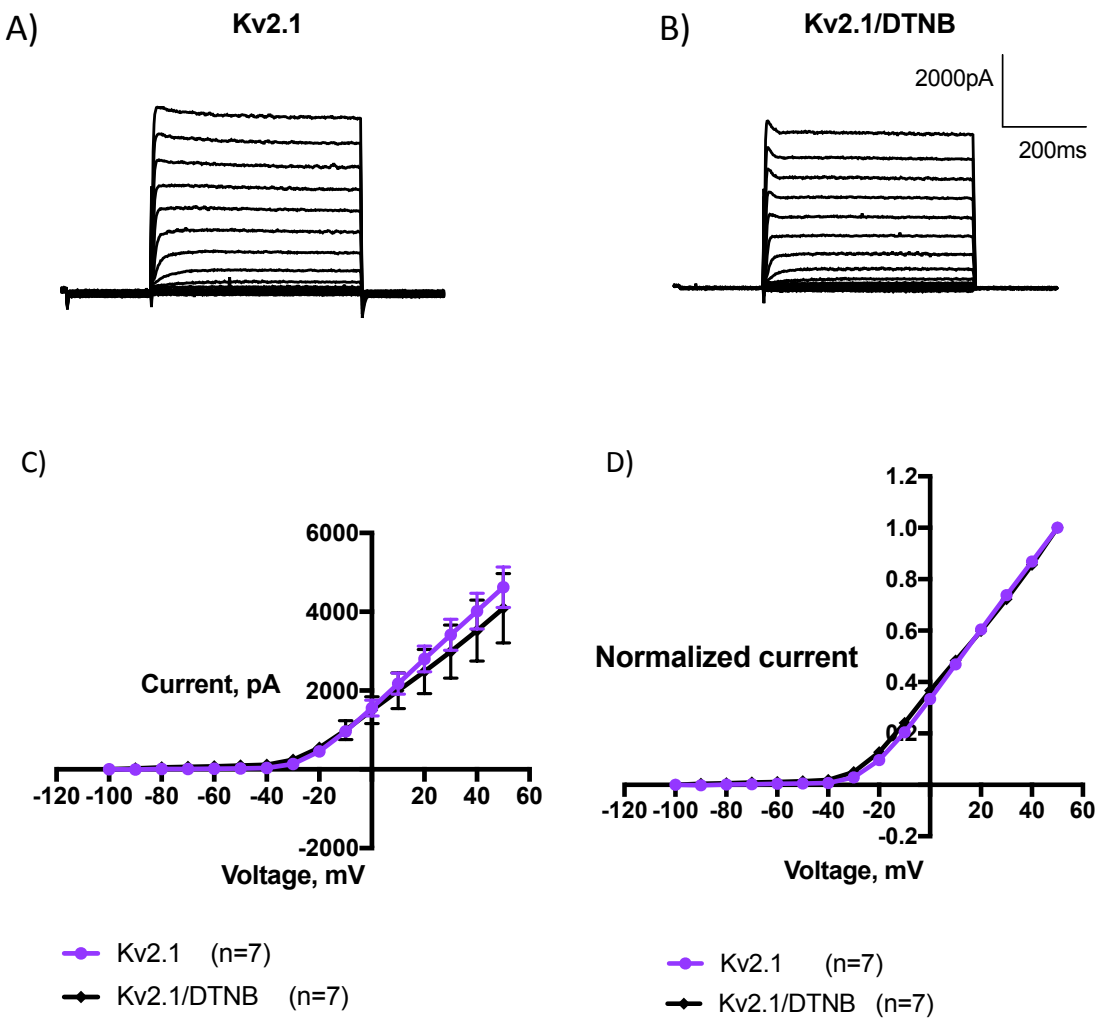

Figure 6.10: DTNB does not alter the current amplitude and activation threshold of Kv2.1. Cells were transfected with Kv2.1 + GFP. The standard voltage-step protocol was used to obtain recordings and cells were either perfused with external solution (Kv2.1) or with 2mM DTNB (Kv2.1/DTNB). Representative current traces for A) Kv2.1 and B) Kv2.1 with DTNB. C) Current vs Voltage plot for Kv2.1 and Kv2.1/DTNB. D) Normalized current vs Voltage plot for Kv2.1 and Kv2.1/DTNB. Two-way ANOVA with Bonferroni method to analyze the difference in current amplitude across all voltages did not reveal a statistically-significant difference between cells perfused without or with 2mM DTNB. Student's t-test with Welch's correction was used to analyze the difference between normalized current of Kv2.1 and Kv2.1/DTNB at -30mV because the variances were unequal and it revealed that there was no statistically-significant difference between cells perfused with external solution and 2mM DTNB.

DTNB also fails to exert any effect on Kv2.1/Kv9.3. The current amplitude of Kv2.1/Kv9.3 is not reduced in the presence of DTNB (Figure 6.11). The activation threshold of the cells is the same regardless of the presence of DTNB (Figure 6.11).

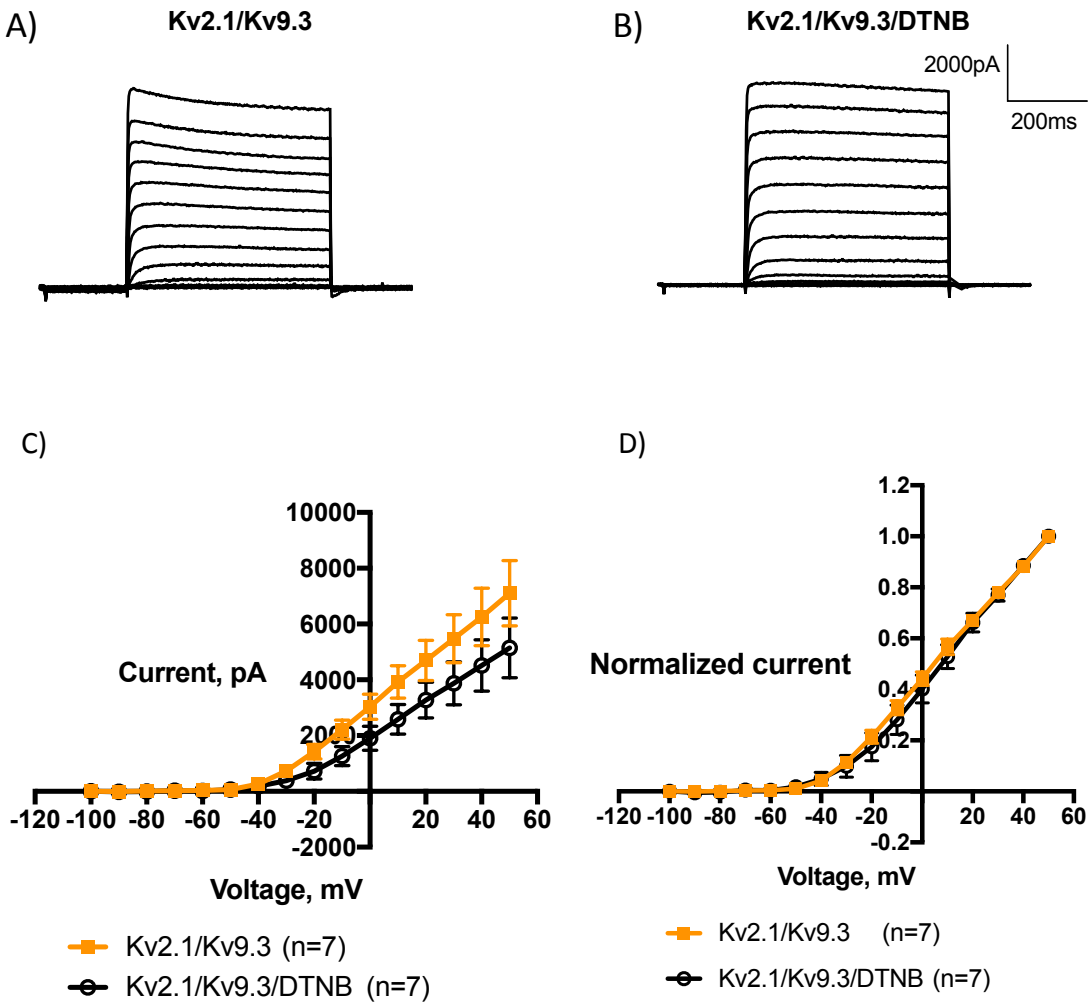

Figure 6.11: DTNB does not affect the Kv2.1/Kv9.3 current and activation threshold. Cells were transfected with Kv2.1/Kv9.3 + GFP. The standard voltage-step protocol was used to obtain recordings and cells were either perfused with external solution (Kv2.1/Kv9.3) or with 2mM DTNB (Kv2.1/Kv9.3/DTNB). Representative current traces for A) Kv2.1/Kv9.3 and B) Kv2.1/Kv9.3 with DTNB. C) Current vs Voltage plot for Kv2.1/Kv9.3 and Kv2.1/Kv9.3/DTNB. D) Normalized current vs Voltage plot for Kv2.1/Kv9.3 and Kv2.1/Kv9.3/DTNB. Two-way ANOVA with Bonferroni method to analyze the difference in current amplitude across all voltages did not reveal a statistically-significant difference between cells perfused without or with 2mM DTNB. Student's t-test with Welch's correction was used to analyze the difference between normalized current of Kv2.1/Kv9.3 and Kv2.1/Kv9.3/DTNB at -30mV because the variances were unequal and it revealed that there was no statistically-significant difference between cells perfused with external solution and 2mM DTNB.

The presence of DTNB does not alter Kv2.1/Nox4 current amplitude (Figure 6.12). The activation threshold of Kv2.1/Nox4 in the presence of DTNB is identical to that in the absence of DTNB (Figure 6.12). These results indicate that the presence of Nox4 does not facilitate the interaction between Kv2.1 and DTNB.

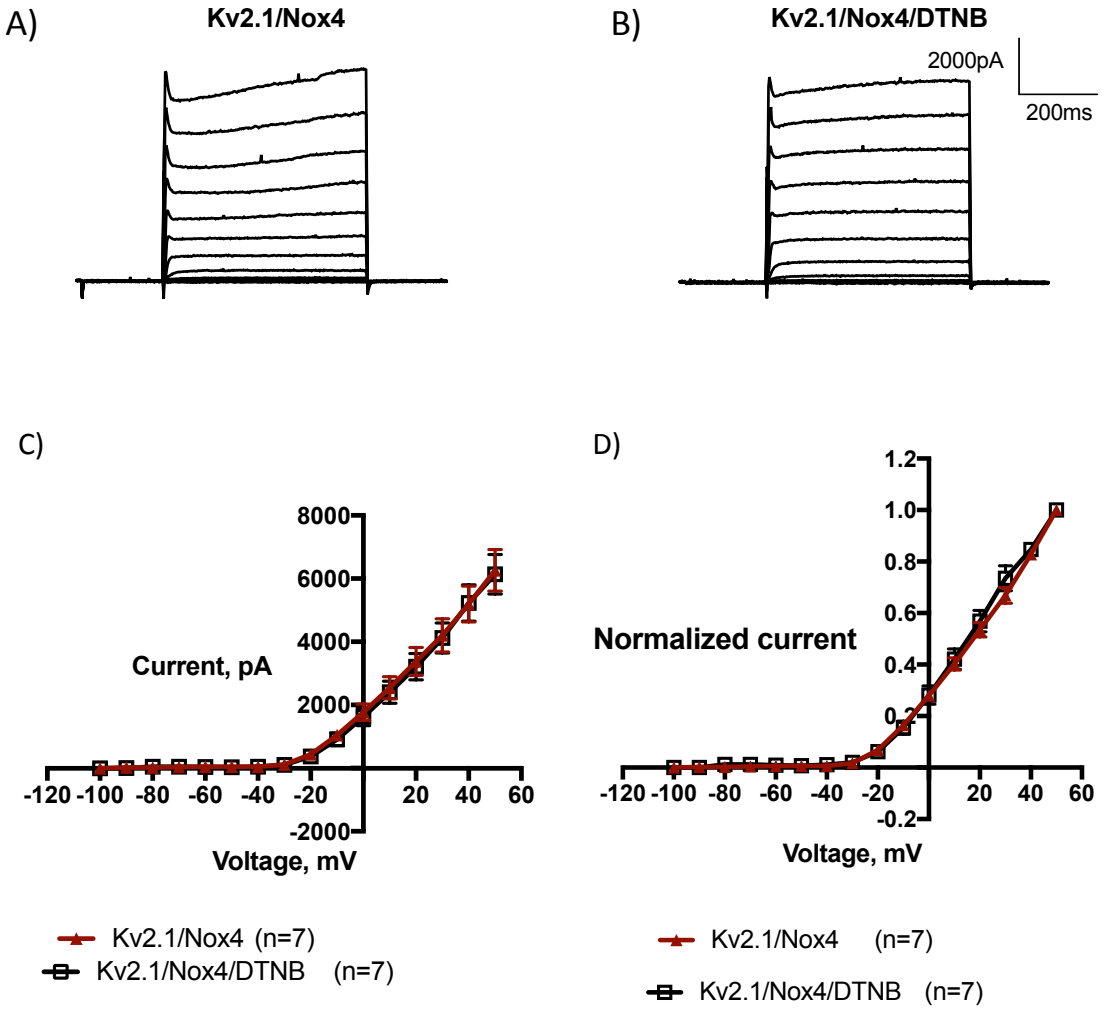

Figure 6.12: DTNB does not affect Kv2.1/Nox4 current and has no impact on the activation threshold. Cells were transfected with Kv2.1/Nox4 + GFP. The standard voltage-step protocol was used to obtain recordings and cells were either perfused with external solution (Kv2.1/Nox4) or with 2mM DTNB (Kv2.1/Nox4/DTNB). Representative current traces for A) Kv2.1/Nox4 and B) Kv2.1/Nox4 with DTNB. C) Current vs Voltage plot for Kv2.1/Nox4 and Kv2.1/ Nox4/DTNB. D) Normalized current vs Voltage plot for Kv2.1/Nox4 and Kv2.1/ Nox4/DTNB. Two-way ANOVA with Bonferroni method to analyze the difference in current amplitude across all voltages did not reveal a statistically-significant difference between cells perfused without or with 2mM DTNB. Student's t-test with Welch's correction was used to analyze the difference between normalized current of Kv2.1/Nox4 and Kv2.1/Nox4/DTNB at -30mV because the variances were unequal and it revealed that there was no statistically-significant difference between cells perfused with external solution and 2mM DTNB.

DTNB decreases the current amplitude of Kv2.1/Kv9.3/Nox4 (Figure 6.13) and the effect is statistically significant at 50mV. It is surprising that DTNB does not have any effect on other cells (Kv2.1, Kv2.1/Kv9.3, and Kv2.1/Nox4) but has an effect

when both Kv9.3 and Nox4 are co-expressed with Kv2.1. One of the hypotheses could be that the presence of both Kv9.3 and Nox4 somehow facilitates the interaction of DTNB on Kv2.1. However, the activation threshold of Kv2.1/Kv9.3/Nox4 in the presence of DTNB remains unchanged (Figure 6.13).

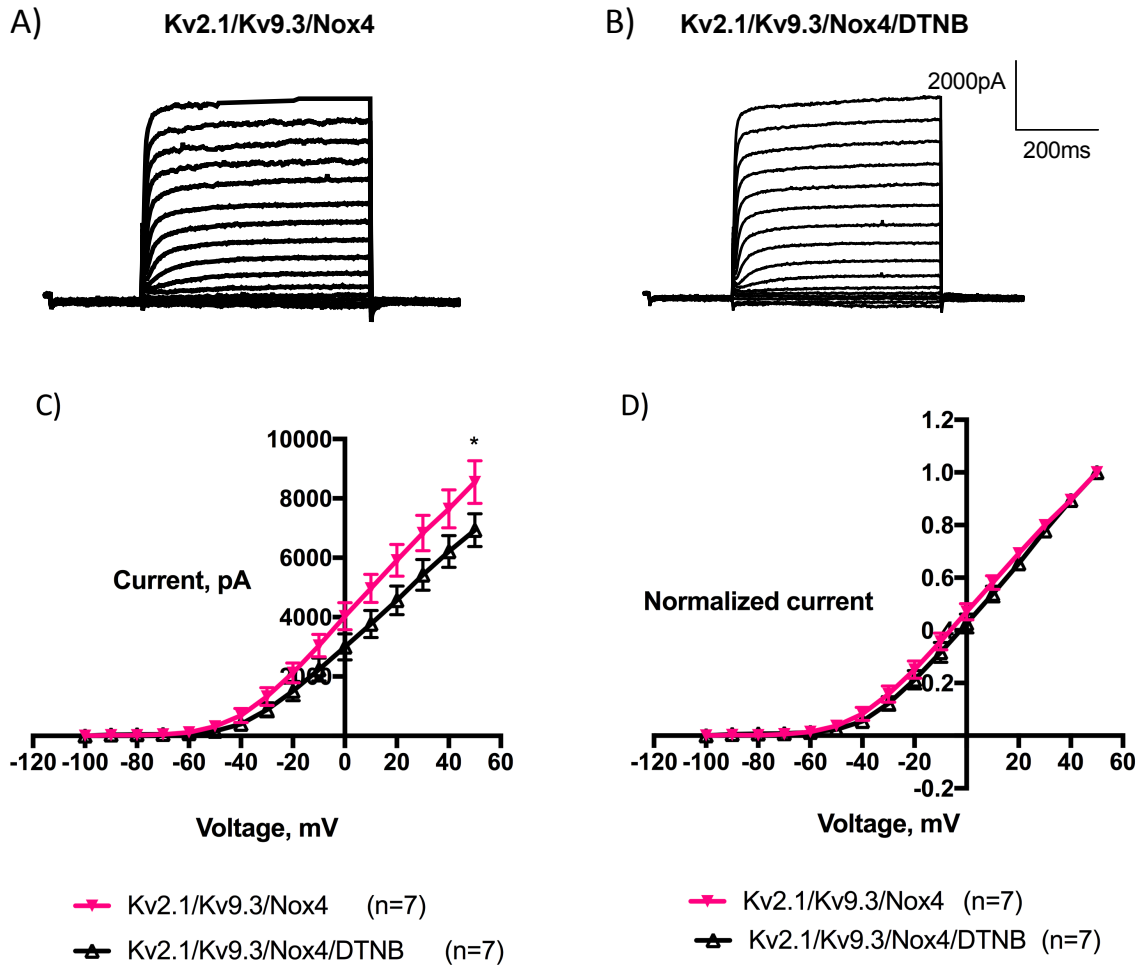

Figure 6.13: DTNB significantly decreases Kv2.1/Kv9.3/Nox4 current but has no impact on the activation threshold. Cells were transfected with Kv2.1/Kv9.3/Nox4 + GFP. The standard voltage-step protocol was used to obtain recordings and cells were either perfused with external solution (Kv2.1/Kv9.3/Nox4) or with 2mM DTNB (Kv2.1/Kv9.3/Nox4/DTNB). Representative current traces for A) Kv2.1/Kv9.3/Nox4 and B) Kv2.1/Kv9.3/Nox4/DTNB. C) Current vs Voltage plot for Kv2.1/Kv9.3/Nox4 and Kv2.1/Kv9.3/Nox4/DTNB. The p-value for the current at V=50mV for the cells was calculated to be 0.0199 (* indicates $p \leq 0.05$), indicating that the difference in current is significant. D) Normalized current vs Voltage plot for Kv2.1/Kv9.3/Nox4 and Kv2.1/Kv9.3/Nox4/DTNB. Two-way ANOVA with Bonferroni method revealed that there is no statistically-significant difference in the current amplitudes for all voltages, except at 50mV, where the $p = 0.0315$, so $p \leq 0.05$ indicated by *. In terms of normalized current at -30mV, Student's t-test with Welch's correction showed that there is no statistically-significant difference between cells perfused without or with 2mM DTNB.

Effect of chloramine-T on current amplitude and activation threshold

Recordings of transiently-transfected cells were done using standard voltage-step protocol. Data were expressed as mean ± SEM and the current amplitudes at 50mV were first analyzed using Student's t-test with Welch's correction due to unequal variances. Two-way ANOVA was used to compare all readings of current amplitudes and normalized currents across all voltages. This is followed by Bonferroni procedure to examine whether they are differences between cells perfused with external solution and 1mM Ch-T.

In contrast to the inhibitory effect of Ch-T on transient outward K^+ current (Ito) or enhancing effect on sustained delayed rectifier K^+ current (Idr) (Prasad and Goyal, 2004), Ch-T does not affect the Kv2.1 current (Figure 6.14). This could probably suggest that Kv2.1 might not be an important delayed rectifier current contributor in the colon. Another reason for such discrepancy is that Kv2.1 has a different activation kinetic compared to mouse Kv4.1, mouse Kv4.2 and mouse Kv4.3, which were tested in the experiments of Prasad and Goyal, 2004. And it is also possible that the methionine residues on Kv2.1 are not susceptible to oxidation. Agreeing with what has been reported by Prasad and Goyal, 2004, Ch-T does not alter the activation kinetics of the Kv2.1 current as indicated in Figure 6.14.

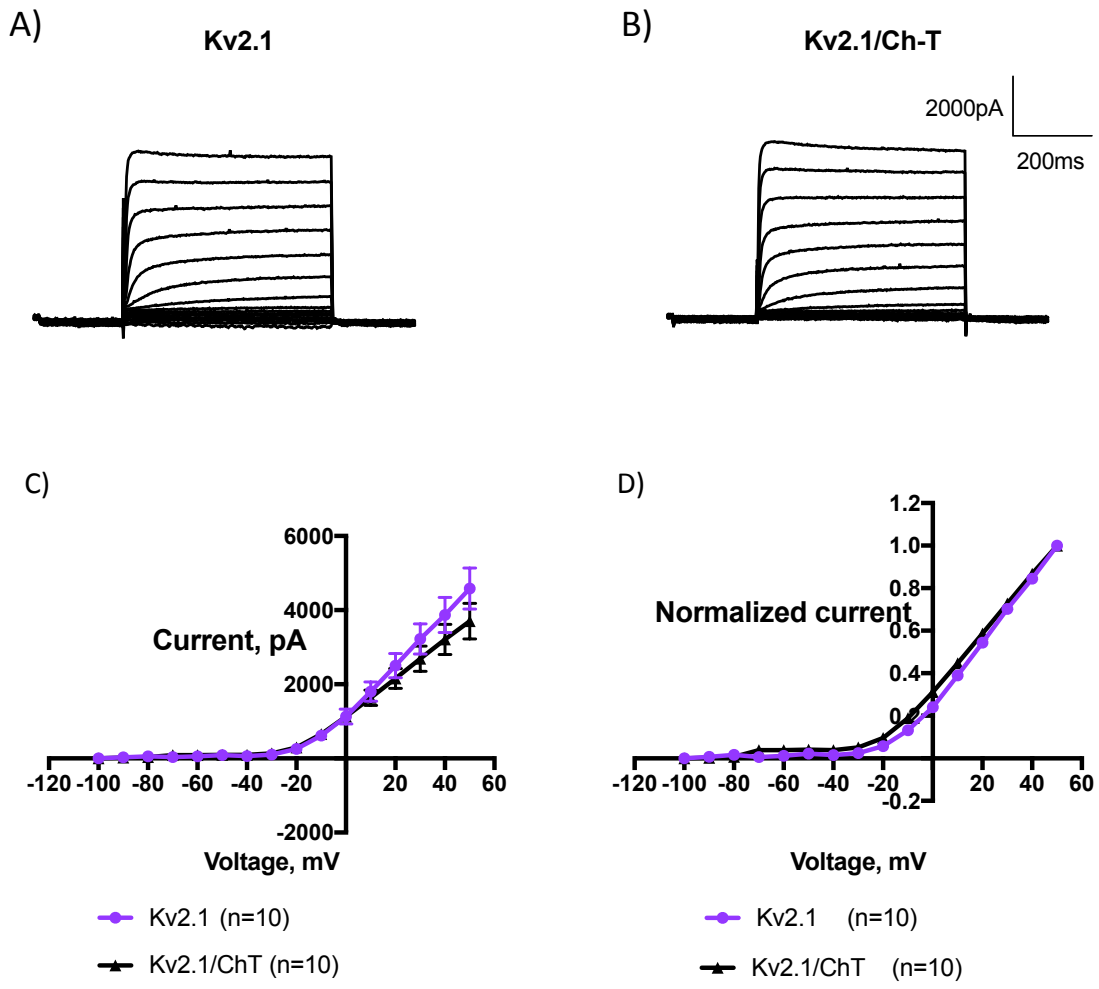

Figure 6.14: Chloramine-T does not have any effect on the current amplitude of Kv2.1 homomer and has a very moderate effect on the activation threshold. Cells were transfected with Kv2.1 + GFP. The standard voltage-step protocol was used to obtain recordings and cells were perfused with external solution (Kv2.1) and then with 1mM Ch-T (Kv2.1/Ch-T). Representative traces for A) Kv2.1 and B) Kv2.1 with Ch-T. C) Current vs Voltage plot for Kv2.1 and Kv2.1/Ch-T. D) Normalized current vs Voltage plot for Kv2.1 and Kv2.1/Ch-T. Two-way ANOVA with Bonferroni method to analyze the difference in current amplitude across all voltages did not reveal a statistically-significant difference between cells perfused without or with 1mM Ch-T. Student's t-test with Welch's correction was used to analyze the difference between normalized current of Kv2.1 and Kv2.1/Ch-T at -30mV because the variances were unequal and it revealed that there was no statistically-significant difference between cells perfused with external solution and 1mM Ch-T.

Similar to Kv2.1, Ch-T does not have any effect on Kv2.1/Kv9.3 current amplitude and activation threshold (Figure 6.15). This could indicate that neither homotetrameric Kv2.1 nor heterotetrameric Kv2.1/Kv9.3 is an important contributor

of the delayed rectifier current in the colon. The modulation effects of Kv9.3 on Kv2.1 did not alter Kv2.1 response to Ch-T.

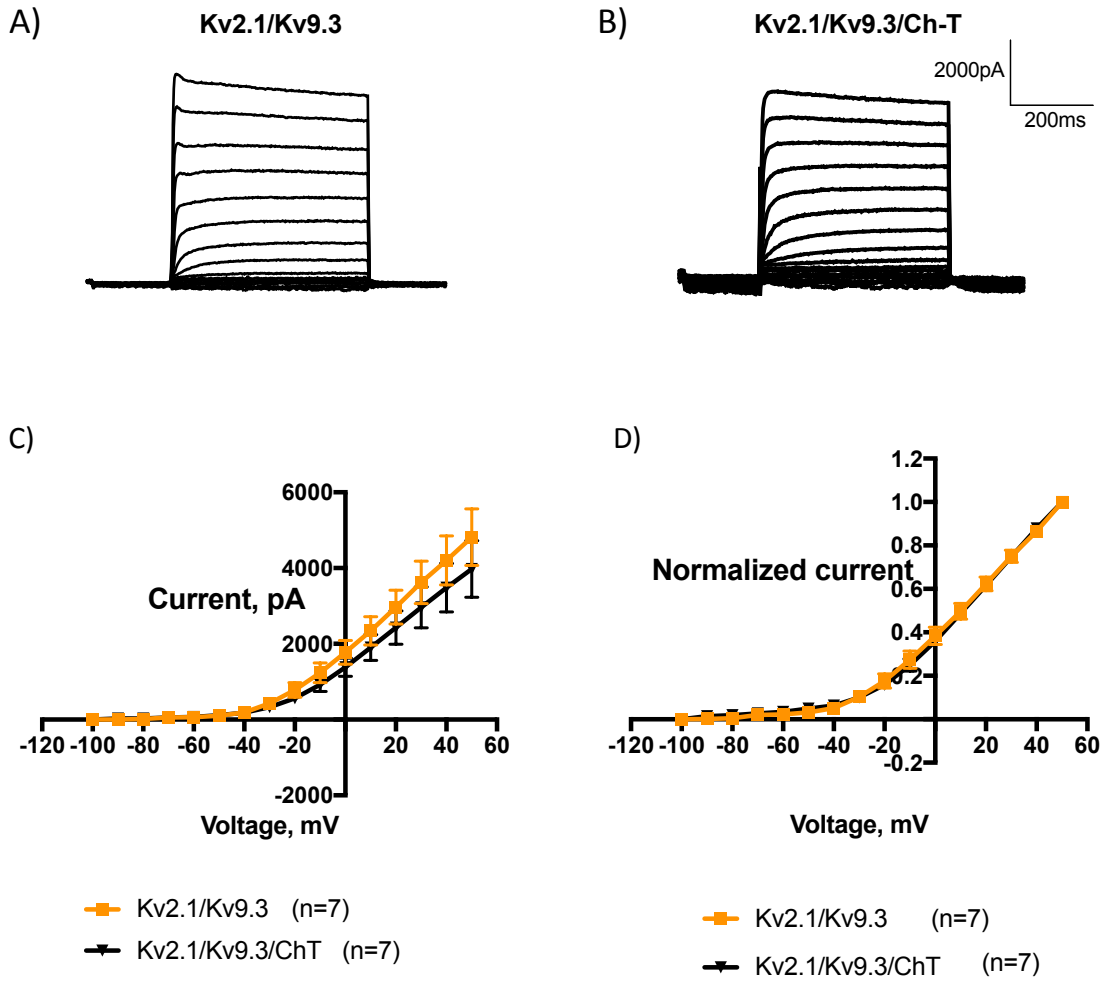

Figure 6.15: Chloramine-T does not alter the current amplitude and activation threshold of Kv2.1/Kv9.3. Cells were transfected with Kv2.1/Kv9.3 + GFP. The standard voltage-step protocol was used to obtain recordings and cells were perfused with external solution (Kv2.1/Kv9.3) and then with 1mM Ch-T (Kv2.1/Kv9.3/Ch-T). Representative traces for A) Kv2.1/Kv9.3 and B) Kv2.1/Kv9.3 with chloramine-T. C) Current vs Voltage plot for Kv2.1/Kv9.3 and Kv2.1/Kv9.3/Ch-T. D) Normalized current vs Voltage plot for Kv2.1/Kv9.3 and Kv2.1/Kv9.3/Ch-T. Two-way ANOVA with Bonferroni method to analyze the difference in current amplitude across all voltages did not reveal a statistically-significant difference between cells perfused without or with 1mM Ch-T. Student's t-test with Welch's correction was used to analyze the difference between normalized current of Kv2.1/Kv9.3 and Kv2.1/Kv9.3/Ch-T at -30mV because the variances were unequal and it revealed that there was no statistically-significant difference between cells perfused with external solution and 1mM Ch-T.

Effect of AMIGO proteins on the current amplitude and activation threshold of Kv2.1

To assess the effect of AMIGO1, AMIGO2, and AMIGO3 proteins on Kv2.1 and Kv2.1/Kv9.3 cells, tsA-201 cells were transfected with the respective combination of cDNAs and electrophysiology recordings were obtained using the standard voltage step and repolarization protocols. During the patch clamp experiments, cells were perfused using external solution.

While co-expression of AMIGO3 does not affect Kv2.1 current amplitude, AMIGO1 decreases the current significantly from 0mV to 50mV, while AMIGO2 reduces current from 40mV to 50mV (Figure 6.16). This result could suggest that AMIGO1 is associated with Kv2.1 as it is modulating Kv2.1 function. However, this result is in contrast to the finding by Kuja-Panula et al, 2003, where the researchers found that AMIGO1 increased the Kv2.1 current at voltages from -40mV to +20mV. The effect of AMIGO1 was most significant at the threshold of activation (Peltola et al., 2011). Whether this could further suggest that another interacting partner besides AMIGO1 needs to be present in order for us to observe the same effect as Kuja-Panula et al, 2003's group awaits further experimentation. Another reason that could lead to such discrepancy could be that the other researchers used a mouse AMIGO1 while human AMIGO1 was used in our experiment. The difference in the repolarization protocol right after the voltage-step could also have contributed to the discrepancy in results.

In terms of activation threshold, one-way ANOVA with Dunnett's test was used to analyze the difference in normalized current of Kv2.1, Kv2.1/AMIGO1, Kv2.1/AMIGO2, and Kv2.1/AMIGO3 at -30mV. The voltage -30mV is chosen because this is the voltage used for comparison in Chapter 3. The analysis revealed that there is statistical significant difference between the normalized current of Kv2.1 and Kv2.1/AMIGO2 at -30mV (Figure 6.16). Since the currents at different voltages were normalized to the current at 50mV resulting in all the normalized current to approach the value of 1.0, it will be inappropriate to analyze all the readings at every voltage using two-way ANOVA.

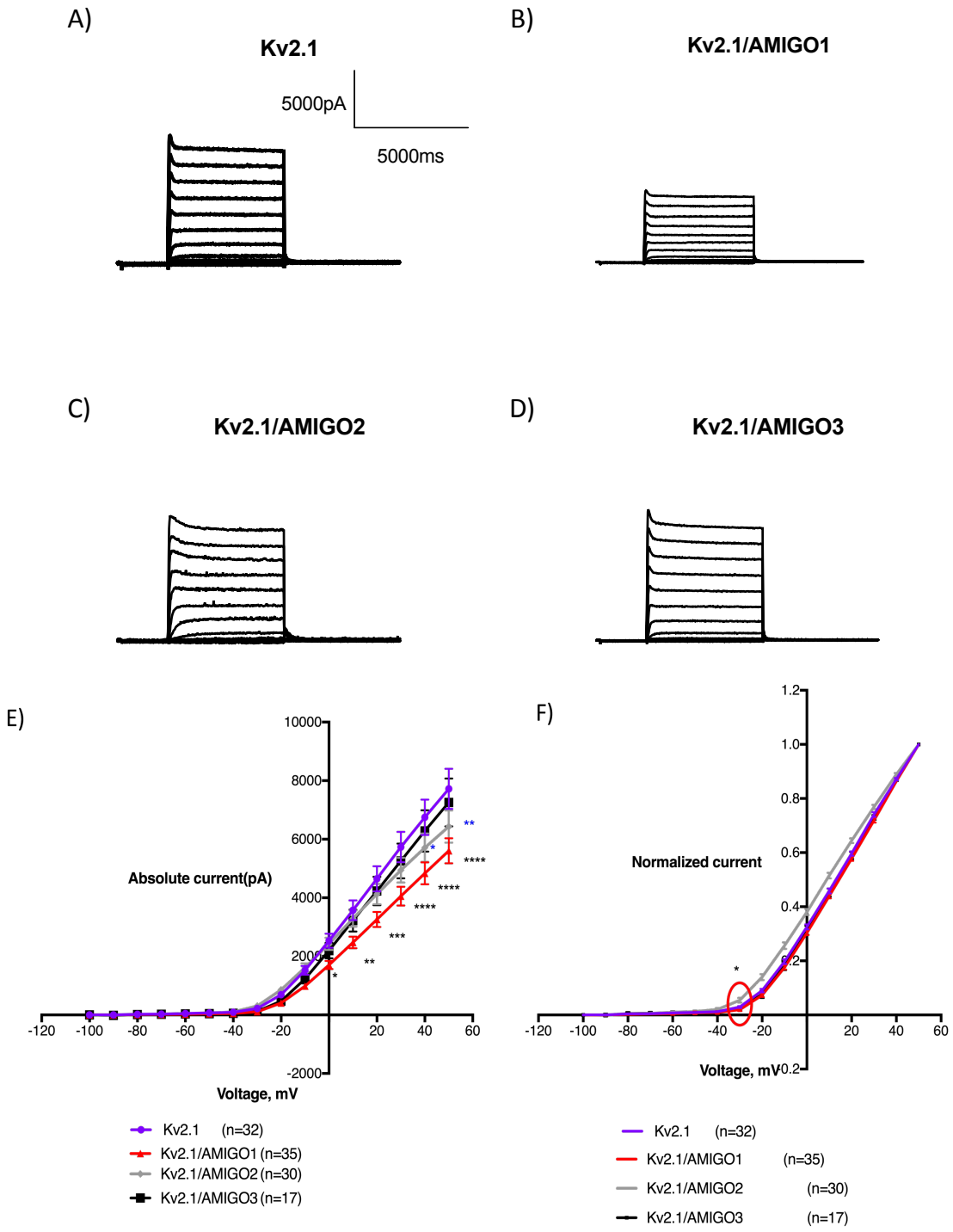

Figure 6.16: Effect of AMIGO proteins on current amplitude and activation threshold of Kv2.1. Current traces of A) Kv2.1, B) Kv2.1/AMIGO1, C) Kv2.1/AMIGO2, D) Kv2.1/AMIGO3. E) IV relationship of Kv2.1 in the presence of AMIGO1, AMIGO2, and AMIGO3 compared with Kv2.1 alone. Two-way ANOVA followed by Dunnett's test with Kv2.1 as control group showed that AMIGO1 reduces Kv2.1 current amplitude and this effect is statistically significant from 0mV to 50mV, with * indicating $p \leq 0.05$, ** indicating $p \leq 0.01$, *** indicating $p \leq 0.001$, **** indicating $p < 0.0001$. Current reduction effect due to coexpression of Kv2.1 with AMIGO2 is smaller, but is statistically significant at 40mV and 50mV, with * indicating $p \leq 0.05$ and ** indicating $p \leq 0.01$. F) Normalized current of Kv2.1 in the presence of AMIGO1, AMIGO2, and AMIGO3 compared with Kv2.1 alone. One-way ANOVA followed by Dunnett's test with Kv2.1 set as control group to analyze the difference in the normalized current at -30mV revealed that there is statistical significant difference between the Kv2.1/AMIGO2 and Kv2.1.

Effect of AMIGO proteins on the current amplitude and activation threshold of Kv2.1/Kv9.3

Similar to the finding above, AMIGO1 has been found to reduce the current of the Kv2.1/Kv9.3 (Figure 6.17). Data were analyzed using two-way ANOVA followed by Dunnett's test with Kv2.1/Kv9.3 as control group. The analysis showed that AMIGO1 reduces Kv2.1/Kv9.3 current amplitude and this effect is statistically significant from -10mV to 50mV (Figure 6.17). Current reduction effect due to coexpression of Kv2.1/Kv9.3 with AMIGO2 is statistically significant from 0mV to 50mV (Figure 6.17).

It is interesting to note that co-expression of AMIGO1 with Kv2.1/Kv9.3 resulted in a lower current amplitude (4717.9±662 pA, n=25) compared with Kv2.1/AMIGO1 (5604.6±4230 pA, n=35) at 50mV (Figure 6.16E and Figure 6.17E). This could indicate that the effect of AMIGO1 is enhanced when Kv2.1 is present together with Kv9.3 as the percentage of reduction of current amplitude is about 15.8%. While AMIGO2 significantly reduced Kv2.1 homomer current at 40mV and 50mV, AMIGO2 significantly reduced the current of Kv2.1/Kv9.3 heteromer (Figure 6.17) from 0mV onwards. This observation could signify that Kv9.3 is needed for the interaction of AMIGO2 with Kv2.1. On the other hand, co-expression of AMIGO3 with Kv2.1/Kv9.3 displayed a similar I-V relationship to Kv2.1/Kv9.3, indicating that AMIGO3 does not affect the current amplitude (Figure 6.17).

AMIGO2 also shifts the Kv2.1/Kv9.3 heteromer's activation threshold to a more depolarized potential (Figure 6.17). However, the extent of the effect is greater than on Kv2.1 homomer, judging by the p-value obtained from analyzing the current at -30mV (Figure 6.17F vs Figure 6.16F). This observation is in agreement with the notion that the effect of AMIGO2 is more visible in the presence of Kv9.3.

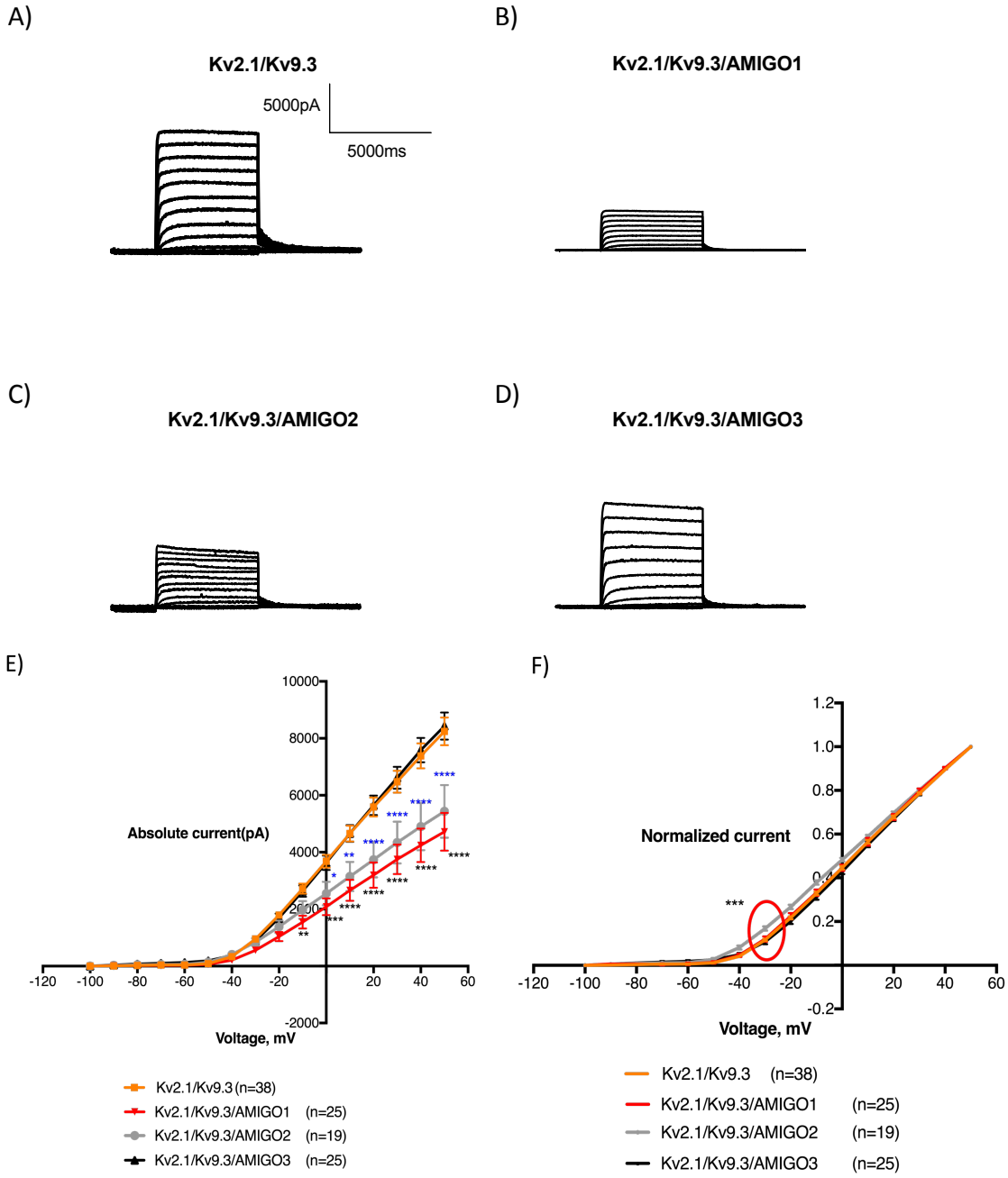

Figure 6.17: Effect of AMIGOs on current amplitude and activation threshold of Kv2.1/Kv9.3. AMIGO1 and AMIGO2 reduce the current amplitude of Kv2.1/Kv9.3. Current traces of A) Kv2.1/Kv9.3, B) Kv2.1/Kv9.3/AMIGO1, C) Kv2.1/Kv9.3/AMIGO2, D) Kv2.1/Kv9.3/AMIGO3. E) IV relationship of Kv2.1/Kv9.3 in the presence of AMIGO1, AMIGO2, and AMIGO3 compared with Kv2.1 alone. Two-way ANOVA followed by Dunnett's test with Kv2.1/Kv9.3 as control group showed that AMIGO1 reduces Kv2.1/Kv9.3 current amplitude and this effect is statistically significant from -10mV to 50mV, with ** indicating $p \leq 0.01$, *** indicating $p \leq 0.001$, **** indicating $p < 0.0001$. Current reduction effect due to coexpression of Kv2.1/Kv9.3 with AMIGO2 is statistically significant from 0mV to 50mV, with * indicating $p \leq 0.05$, ** indicating $p \leq 0.01$, **** indicating $p < 0.0001$. F) Normalized current of Kv2.1/Kv9.3 in the presence of AMIGO1, AMIGO2, and AMIGO3 compared with Kv2.1/Kv9.3 alone. One-way ANOVA followed by Dunnett's test with Kv2.1/Kv9.3 as control group to analyze the difference in the normalized current at -30mV revealed that there is statistical significant difference between the Kv2.1/Kv9.3/AMIGO2 and Kv2.1/Kv9.3.

AMIGO2 increases the tslow and tfast of Kv2.1

AMIGO2 was found to have profound effects on both the slow and fast inactivation kinetics of Kv2.1, evident both in the current trace resulting from repolarization to -50mV from +20mV and in the bar charts depicting the tslow and tfast (Figure 6.18). AMIGO2 delayed both the slow and fast components of the Kv2.1 deactivation time (Figure 6.18). When assessing the effects of AMIGO2 on current amplitude, the current reduction effect appeared at a hyperpolarized potential when AMIGO2 is coexpressed with Kv2.1/Kv9.3 than with Kv2.1 (starting at 10mV for Kv2.1/Kv9.3/AMIGO2 and at 40mV for Kv2.1/AMIGO2) (Figure 6.16E and Figure 6.17E). Therefore, assessment of the deactivation kinetics might be a different method to characterize the presence of AMIGO2 protein. This observation could also suggest that AMIGO2 is causing the Kv2.1 channel to be inactivated for longer without affecting current amplitude or causing the channel to be activated earlier. Overall, this effect on delaying the deactivation kinetics will result in longer time for the next action potential to be transduced. This is because the channel has to recover from inactivation before the next action potential can be generated.

Interestingly, AMIGO1 was shown to reduce Kv2.1 current amplitude (Figure 6.16) yet it does not have any effect on the deactivation kinetics (Figure 6.18). The reason as to why the AMIGO1 and AMIGO2 proteins have reversed effects, with the former affecting current amplitude yet does not affect the tslow and tfast of Kv2.1 and the latter reducing Kv2.1 current at a more depolarized potential yet have a profound effect in deactivation kinetics, is not known. AMIGO1 and AMIGO2 presumably interact with Kv2.1 in a different manner. On the other hand, AMIGO3 does not exhibit any influence on Kv2.1 deactivation kinetics (Figure 6.18).

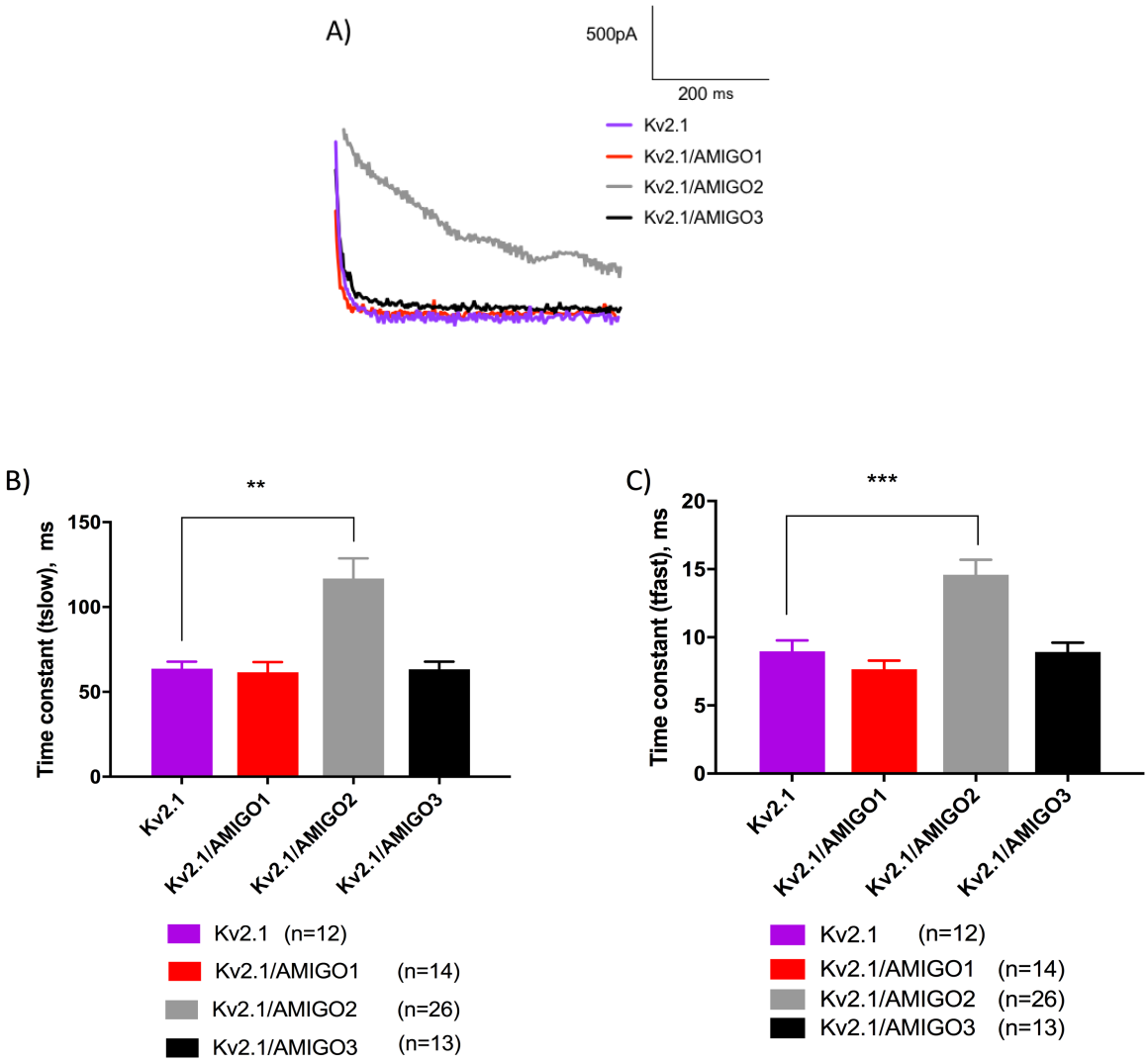

Figure 6.18: AMIGO2 increases the tslow and tfast of Kv2.1. A) Current traces resulting from the depolarization to -50mV from +20mV for Kv2.1, Kv2.1/AMIGO1, Kv2.1/AMIGO2, and Kv2.1/AMIGO3. Bar chart showing the B) slow deactivation kinetics (tslow) and C) fast deactivation kinetics (tfast) of Kv2.1, Kv2.1/AMIGO1, Kv2.1/AMIGO2, and Kv2.1/AMIGO3. One-way ANOVA with Dunnett's test revealed that there is a statistically-significant difference between tslow and tfast of Kv2.1 and Kv2.1/AMIGO2, with ** indicating $p \leq 0.01$ and *** indicating $p \leq 0.001$.

AMIGO2 increases the tslow of Kv2.1/Kv9.3 while AMIGO1 decreases the tfast of Kv2.1/Kv9.3

Although AMIGO2 exerts its effect on the tslow of Kv2.1/Kv9.3, AMIGO2 has no effect on the tfast of Kv2.1/Kv9.3 (Figure 6.19). Surprisingly, AMIGO1 accelerates the fast component of inactivation kinetics of Kv2.1 when Kv9.3 is present (Figure 6.19). The effect of AMIGO1 on the tfast of Kv2.1/Kv9.3 revealed that AMIGO1 might interact with Kv9.3, although AMIGO1 does not affect the activation threshold of Kv2.1/Kv9.3 (Figure 8.6). The difference in inactivation times observed when different AMIGO proteins are co-expressed with the Kv2.1/Kv9.3 heteromer could prove that the characterization of different AMIGO proteins associated with Kv2.1/Kv9.3 based on calculation of inactivation times gave insights into how the channels are differentially regulated by different AMIGO proteins.

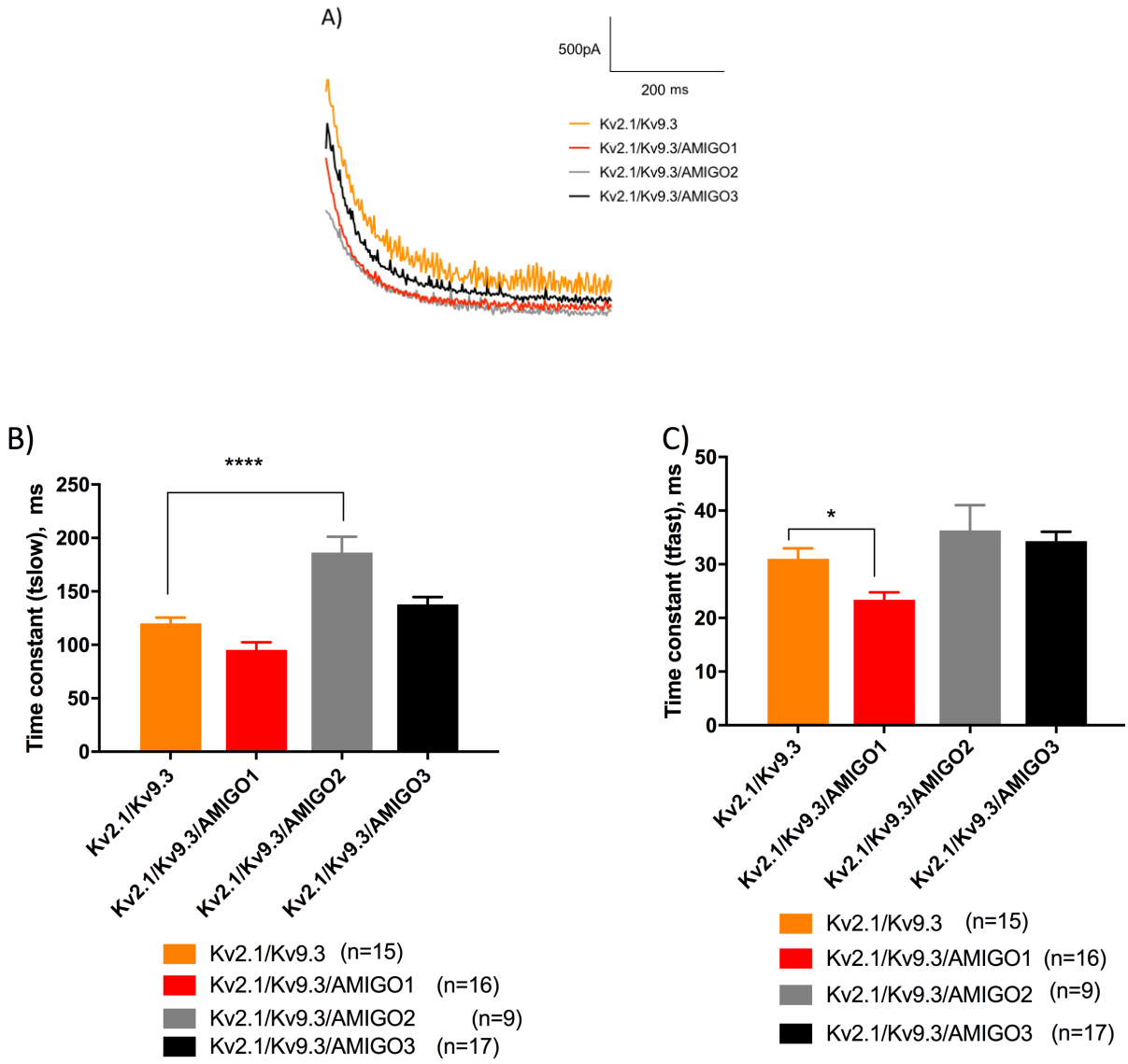

Figure 6.19: AMIGO2 increases the tslow of Kv2.1/Kv9.3 while AMIGO1 decreases the tfast of Kv2.1/Kv9.3. A) Current traces resulting from the depolarization to -50mV from +20mV for Kv2.1/Kv9.3, Kv2.1/Kv9.3/AMIGO1, Kv2.1/Kv9.3/AMIGO2, and Kv2.1/ Kv9.3/AMIGO3. Bar chart showing the B) slow deactivation kinetics (tslow) and C) fast deactivation kinetics (tfast) of Kv2.1 Kv9.3/, Kv2.1/Kv9.3/AMIGO1, Kv2.1/Kv9.3/AMIGO2, and Kv2.1/Kv9.3/AMIGO3. One-way ANOVA with Dunnett's test revealed that there is a statistically-significant difference between tslow of Kv2.1/Kv9.3 and Kv2.1/Kv9.3 AMIGO2 and between tfast of Kv2.1/Kv9.3 and Kv2.1/Kv9.3 /AMIGO1 with * indicating $p \leq 0.05$ and **** indicating $p < 0.001$.

Effect of H_2O_2 on the current amplitude and activation threshold of Kv2.1/AMIGO2

As demonstrated above (Figure 6.16), AMIGO2 only affects the current amplitude of Kv2.1 at 40mV onwards. In line with the results where addition of H_2O_2 did not affect the current amplitude of Kv2.1 (Figure 6.1), the presence of this ROS agent when Kv2.1 is co-expressed with AMIGO2 (Kv2.1/AMIGO2/H_2O_2) reversed the current amplitude back to the level of Kv2.1 (Figure 6.20). However, the effect of AMIGO2 in shifting the activation threshold of Kv2.1 to a more polarized potential was abolished in the presence of H_2O_2 (Figure 6.20).

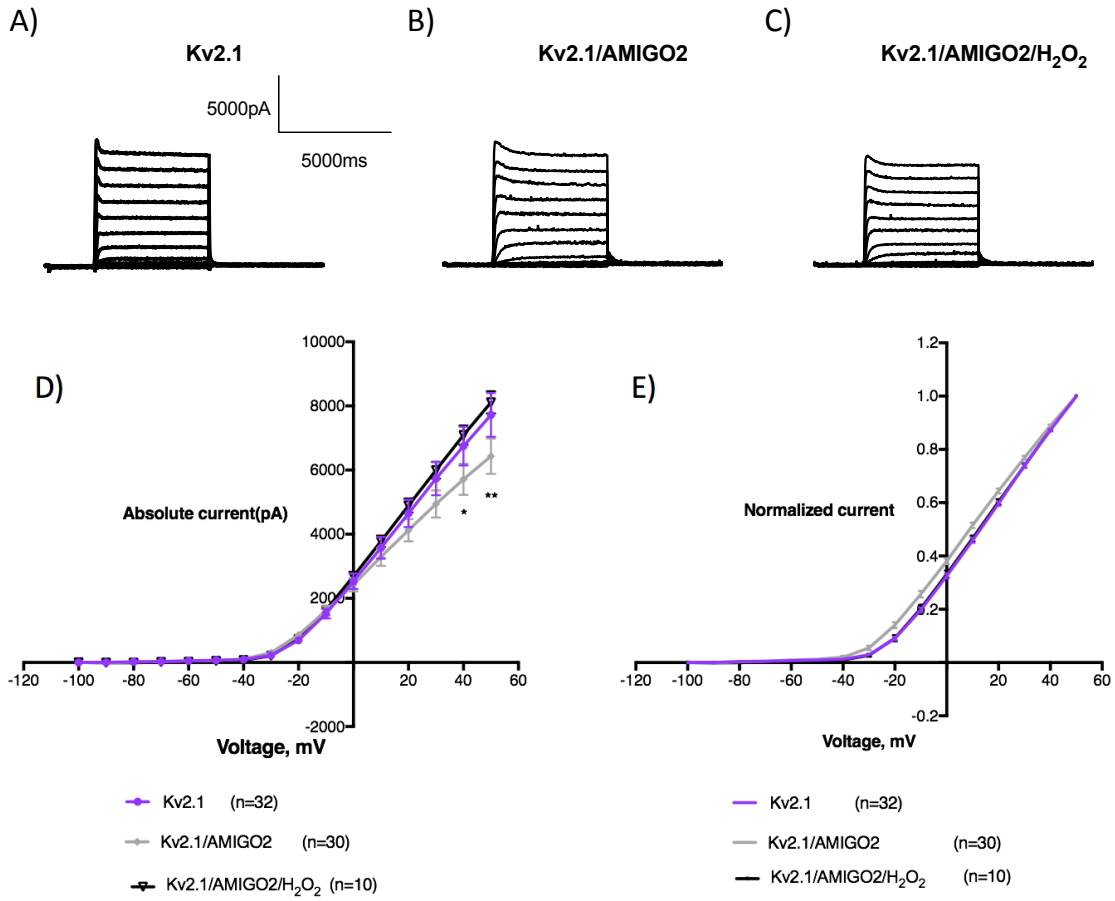

Figure 6.20: H_2O_2 does not have any effect on the current amplitude of Kv2.1/AMIGO2 but abolished the activation threshold shift effect of AMIGO2 on Kv2.1. Representative current traces for A) Kv2.1, B) Kv2.1/AMIGO2, and C) Kv2.1/AMIGO2/H_2O_2. D) IV relationship of Kv2.1, Kv2.1/AMIGO2, and Kv2.1/AMIGO2 in the presence of H_2O_2; E) Normalized current of Kv2.1, Kv2.1/AMIGO2, and Kv2.1/AMIGO2/ H_2O_2. Two-way ANOVA with Dunnett's test where Kv2.1 is set as control group showed that there is no statistical significant difference between the absolute current of Kv2.1 and Kv2.1/AMIGO2/H_2O_2 whereas current amplitudes of Kv2.1/AMIGO2 were significantly smaller at 40mV and 50mV, with * indicating $p \leq 0.05$ and ** indicating $p \leq 0.01$. One-way ANOVA with Dunnett's test revealed that there is no significant difference between normalized current of Kv2.1/AMIGO2/H_2O_2 compared with Kv2.1 at -30mV.

Effect of H_2O_2 on the current amplitude and activation threshold of Kv2.1/Kv9.3/AMIGO2

As seen in Figure 6.17, co-expression of AMIGO2 reduced the current of Kv2.1/Kv9.3 (Kv2.1/Kv9.3/AMIGO2 5437±926 pA, n=19 vs Kv2.1/Kv9.3 8246.7±488 pA, n=38) in normoxic condition. Surprisingly, the presence of H_2O_2 restored the current amplitude of Kv2.1/Kv9.3/AMIGO2 to the level of Kv2.1/Kv9.3 (9273.2±235, n=7) at 50mV (Figure 6.21). This observation could suggest that AMIGO2 is an interaction partner that needs to be present in order for Kv channels oxygen sensing to occur. H_2O_2 has yielded contradictory results, as to whether this ROS inhibits K^+ channels thus causing vasoconstriction or activating K^+ channels hence giving rise to vasodilation (Park et al., 2015b). This result particularly substantiates the latter, and perhaps also suggests that H_2O_2 mediates its effect via the oxygen-sensing capability of AMIGO2. It should be re-emphasized that Kv9.3 is needed for AMIGO2-Kv2.1 interaction, as it has been demonstrated earlier that the effect of AMIGO2 is enhanced when Kv9.3 is present (Figure 6.18). This could explain why the restoration effect is seen with Kv2.1/Kv9.3/AMIGO2, but not with Kv2.1/AMIGO2 (Figure 6.21).

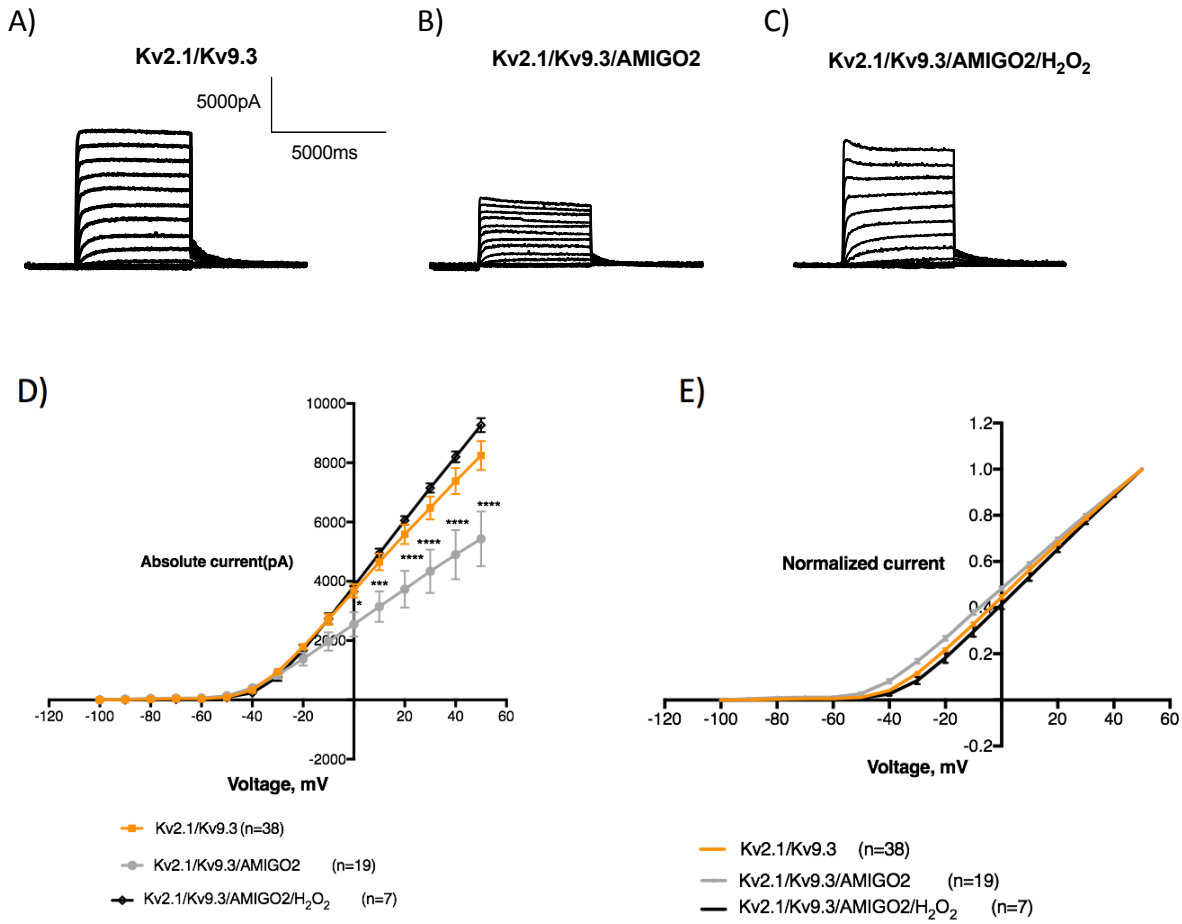

Figure 6.21: Addition of H_2O_2 restored the current amplitude of Kv2.1/Kv9.3/AMIGO2 to the control level and shifted the activation threshold to the control level. Representative current traces for A) Kv2.1/Kv9.3, B) Kv2.1/Kv9.3/AMIGO2, and C) Kv2.1/Kv9.3/AMIGO2/H_2O_2. D) IV relationship of Kv2.1/Kv9.3, Kv2.1/Kv9.3/AMIGO2, and Kv2.1/Kv9.3/AMIGO2 in the presence of H_2O_2; E) Normalized current of Kv2.1/Kv9.3, Kv2.1/Kv9.3/AMIGO2, and Kv2.1/AMIGO2/Kv9.3/H_2O_2. Two-way ANOVA with Dunnett's test where Kv2.1/Kv9.3 is set as control group showed that there is no statistical significant difference between the absolute current of Kv2.1/Kv9.3 and Kv2.1/Kv9.3/AMIGO2/H_2O_2 whereas current amplitudes of Kv2.1/Kv9.3/AMIGO2 were significantly smaller than Kv2.1/Kv9.3 from 0mV to 50mV, with * indicating $p \leq 0.05$, *** indicating $p \leq 0.001$, and **** indicating $p < 0.0001$. One-way ANOVA with Dunnett's test revealed that there is no significant difference between normalized current of Kv2.1/Kv9.3/AMIGO2/H_2O_2 compared with Kv2.1/Kv9.3 at -30mV.

Effect of H_2O_2 on deactivation kinetics of Kv2.1/AMIGO2

While the presence of H_2O_2 abolished the effect of AMIGO2 on the activation threshold of Kv2.1, it does not have any effect on the tslow of Kv2.1/AMIGO2 but significantly increases tfast of Kv2.1/AMIGO2 (Figure 6.22). The data were

analyzed with one-way ANOVA followed by Tukey's multiple comparison test as it would be interesting to know if tslow and tfast of Kv2.1/AMIGO2/H_2O_2 are significantly different than Kv2.1 and if the tslow and tfast of Kv2.1/AMIGO2/H_2O_2 are significantly different than Kv2.1/AMIGO2. The effect of H_2O_2 on tslow of Kv2.1/AMIGO2 is inconclusive as from the current results H_2O_2 did not reduce the tslow of Kv2.1/AMIGO2 to the level of Kv2.1 yet the tslow was not significantly higher than that of Kv2.1 (Figure 6.22). Meanwhile, H_2O_2 significantly increases tfast of Kv2.1/AMIGO2 (Figure 6.22).

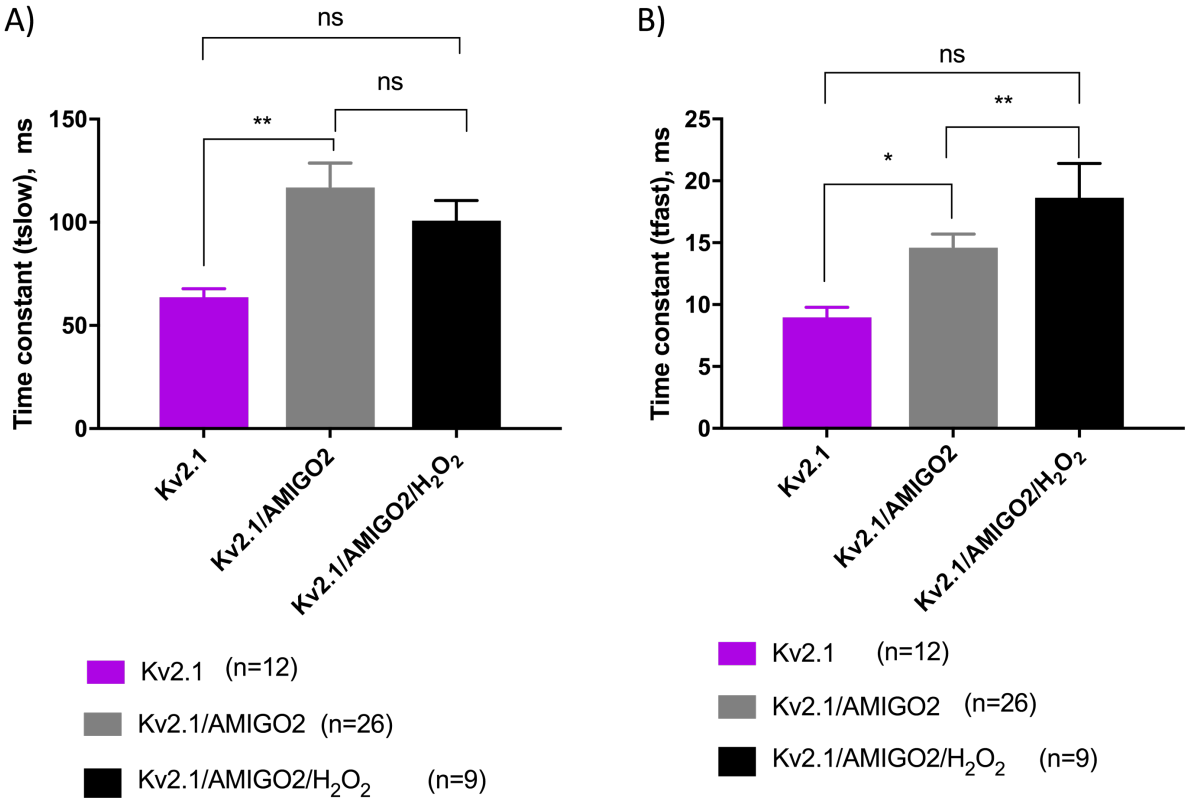

Figure 6.22: H_2O_2 does not abolish the effect of AMIGO2 elongating the tslow and tfast of Kv2.1. Bar chart showing the A) slow deactivation kinetics (tslow) and B) fast deactivation kinetics (tfast) of Kv2.1, Kv2.1/AMIGO2, and Kv2.1/ AMIGO2/H_2O_2. One-way ANOVA followed by Tukey's multiple comparison test showed that H_2O_2 has an inconclusive effect on tslow of Kv2.1/AMIGO2 yet significantly increases the tfast of Kv2.1/AMIGO2, with * indicating $p \leq 0.05$, ** indicating $p \leq 0.01$, and ns indicating that the effect is not significant.

Effect of H_2O_2 on deactivation kinetics of Kv2.1/Kv9.3/AMIGO2

It remains inconclusive as to whether the presence of H_2O_2 has any impact on the tslow and tfast of Kv2.1/Kv9.3 (Figure 6.2). In the experiment to probe the effect of H_2O_2 on the deactivation kinetics of Kv2.1/Kv9.3/AMIGO2, data were analyzed using one-way ANOVA followed by Tukey's test as we wanted to know if H_2O_2 reversed the effect of AMIGO2 in elongating the tslow of Kv2.1 to the level of Kv2.1. In the case of tslow, it seems that the presence of H_2O_2 causes the tslow of Kv2.1/Kv9.3/AMIGO2 to have an intermediate value (160.5±30 ms, n=4) between Kv2.1/Kv9.3 (120.0±5 ms, n=15) and Kv2.1/Kv9.3/AMIGO2 cells (186.3±15 ms, n=9) as the difference between tslow of Kv2.1/Kv9.3/AMIGO2/H_2O_2 compared with both Kv2.1 and Kv2.1/Kv9.3/AMIGO2 was not significant (Figure 6.23). Meanwhile there is no statistical significant difference between the populations in terms of tfast (Figure 6.23). However, the large variability in the data, especially with the reading of tfast of Kv2.1/Kv9.3/AMIGO2/H_2O_2, restricting a conclusion from being drawn.

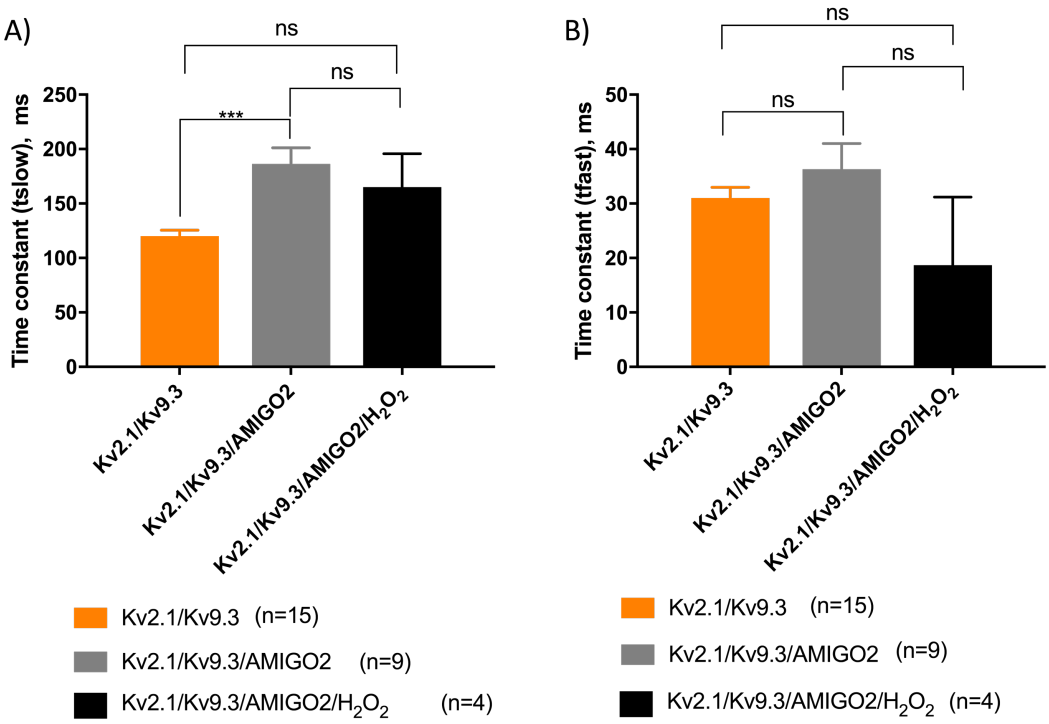

Figure 6.23: H_2O_2 does not alter the effect of AMIGO2 on the tslow and tfast of Kv2.1/Kv9.3. Bar chart showing the A) slow deactivation kinetics (tslow) and B) fast deactivation kinetics (tfast) of Kv2.1, Kv2.1/AMIGO2, and Kv2.1/ AMIGO2/H_2O_2. One-way ANOVA followed by Tukey's multiple comparison test showed that H_2O_2 has an inconclusive effect on tslow and tfast of Kv2.1/Kv9.3/AMIGO2 with ns indicating that the effect is not significant.

6.3 Discussion

The effect of H_2O_2 on Kv channels still remains elusive. A study performed in mice showed that mice expressing human catalase to breakdown H_2O_2 were reported to have a significant reduction in systolic blood pressure compared to transgene-negative littermates (Suvorava, 2005). This suggests that H_2O_2 acts as a vasoconstrictor (Suvorava, 2005). More importantly, Archer et al., 1998 have found that mitochondrial-derived H_2O_2 reduces the Kv current in ductus arteriosus smooth muscle cells (DASMC). This led to membrane depolarization and activation of the L-type Ca^{2+} channels, resulting in vasoconstriction (Archer et al., 2004). There are two major candidates in the DASMC which could be the target of H_2O_2, these are Kv1.5 and Kv2.1 (Archer et al., 2004). Hence, whether the overall effect is due to H_2O_2 acting on Kv1.5 or Kv2.1 is still unknown. This gap in the literature review has piqued interest in the effect of H_2O_2 on Kv2.1.

Studies performed to dissect the effect of H_2O_2 on coronary arteries showed that the putative target of this ROS is Kv1.5 as it is the major contributor of the Kv current there (Archer et al., 2004). H_2O_2 has been found to increase Kv1.5 current as long as the voltage is below +20mV (S. W. Park et al., 2015). In this case, activation of Kv1.5 decreases membrane excitability and thus vasodilatory effect is produced (S. W. Park et al., 2015). However, at high depolarizing voltages, H_2O_2 inhibits the channels (S. W. Park et al., 2015). Accordingly, it is still uncertain whether H_2O_2 is a vasodilator. Another example illustrating the role of H_2O_2 as a vasodilator is the observation that H_2O_2 induces the activation of KATP and KCa, which leads to the same effect as opening of Kv channels (S. W. Park et al., 2015).

Park et al., 2015b have provided strong evidence that H_2O_2 produces vasorelaxation effect in mesenteric arteries and H_2O_2 mediates its action on Kv channels, rather than on KCa channels. This is because they have found that the K^+ current was blocked by the general Kv channel blocker, 4-aminopyridine (4-AP), but was not affected by inhibitors of large-conductance Ca^{2+}-activated K^+ channel and inward rectifier K^+ channel (Kir). The Kv currents were enhanced in the presence of H_2O_2 in a concentration-dependent manner (S. W. Park et al., 2015). Furthermore, H_2O_2 also accelerates Kv channel activation and shifted steady state activation to polarizing

potentials (to the left) (S. W. Park et al., 2015). Collectively, these effects elicited a vasodilatory effect on the mesenteric arteries. Interestingly, these effects could be abolished by DTT (S. W. Park et al., 2015).

Increase in H_2O_2 leads to several cellular modifications. Since glutathione (GSH) is the most abundant reducing equivalent of H_2O_2, it has been hypothesized that S-glutathionylation, a process where H_2O_2 oxidizes the thiol groups of cysteine residues, allowing the protein to form disulfide bonds with GSH, is the most dominant process in the myocytes (S. W. Park et al., 2015). S-glutathionylation is an essential posttranslational modification process, which regulates protein structure and function. The streptavidin pull-down assays with biotinylated glutathione ethyl ester performed by Park et al., 2015b demonstrated the co-localization of glutathione (GSH) and Kv channel proteins in the presence of H_2O_2. Moreover, S-glutathionylation of Kv channels is the process responsible for causing smooth muscle relaxation in the rat mesenteric arteries (S. W. Park et al., 2015).

With these observations, it was proposed that H_2O_2 could actually be beneficial as a signalling molecule that induce S-glutathionylation which ultimately leads to vasodilation rather than acting solely as a ROS to inhibit Kv channels (S. W. Park et al., 2015). However, increased oxidative stress within mesenteric arteries, possibly due to presence of other ROS or prolonged hypoxic condition, could mask the ability of H_2O_2 to stimulate Kv channels (S. W. Park et al., 2015). Even more interesting is that such condition could reverse the initial vasodilatory effect, causing the inhibitory effect of H_2O_2 on Kv channels to be revealed (S. W. Park et al., 2015). This could mean that whether H_2O_2 exerts an activating or inhibitory effect on Kv channels is dependent on the basal redox status of the cells (S. W. Park et al., 2015).

Contrary to the observation of Park et al, 1997, who demonstrated that H_2O_2 induces vasorelaxation by enhancing Kv currents, results in this chapter showed that H_2O_2 does not have any significant impact on the absolute current and activation threshold of Kv2.1, Kv2.1/Kv9.3, Kv2.1/Nox4, and Kv2.1, Kv9.3/Nox4. Researchers from the other group have sought to determine the effects of H_2O_2 on rat mesenteric arteries (S. W. Park et al., 2015). The lack of effect of H_2O_2 on Kv2.1 and Kv2.1/Kv9.3 could suggest that these channels are not the main contributors of the delayed rectifier current in the rat mesenteric arteries.

The deactivation kinetics of Kv2.1 and Kv2.1/Kv9.3 in the absence and presence of Nox4 were also studied in this chapter. Results have shown that H_2O_2 does not affect the slow and fast components of the time constant of deactivation, tslow and tfast respectively, of Kv2.1, Kv2.1/Kv9.3, Kv2.1/Nox4, and Kv2.1/Kv9.3/Nox4. Coherent with the results obtained in Chapter 3, the tslow of Kv2.1/Kv9.3 is significantly longer than that of Kv2.1. The presence of H_2O_2 did not shorten the tslow of Kv2.1/Kv9.3.

It might be too early to draw the conclusion that Kv2.1 and Kv2.1/Kv9.3 are not the target Kv channels of H_2O_2. This is because the inability of H_2O_2 to affect Kv2.1 and Kv2.1/Kv9.3 channels could be explained by the absence of a regulatory protein that could mediate the effect of H_2O_2 on these channels. Several researchers have described the variation in the hypoxic response of Kv2.1, where Kv2.1 has been consistently reported to be sensitive to hypoxic inhibition in cDNA-transfected L cells, but only a subset of Kv2.1-transfected COS cells are shown to be sensitive to hypoxia and Kv2.1 mRNA-injected Xenopus oocytes are not sensitive to hypoxic inhibition (Conforti et al., 2000; Hulme et al., 1999; Patel et al., 1997; Patel and Honoré, 2001). These observations could indicate that the hypoxic response of Kv2.1 might be abolished due to the absence of certain regulatory factors in the heterologous expression system used.

Since the presence of Nox4 does not make a difference, it is likely that Nox4 is not the regulatory protein in question. Aforementioned in Chapter 3, future experiments could investigate into the possible interaction of other Nox proteins such as Nox1 and Nox2 with these Kv channels.

Park et al., 1997 demonstrated that DTT reduced the Kv current in rabbit PASMC. However, the result from this chapter showed that Kv2.1 current is not inhibited by DTT. This could indicate that Kv2.1 is not the main contributor to the delayed rectifier current in rabbit PASMC as there are many Kv channels expressed in PASMC (Evans et al., 1996; Moudgil et al., 2006). However, this argument should be taken with caution as Kv2.1 and Kv2.1/Kv9.3 are usually considered as good

candidates of O^2-sensitive K^+ current in the rabbit PASMC (Coppock et al., 2001). Another plausible reason which could explain the variation in result is that the variety of Kv β-subunit, that can be expressed with different Kv α-subunit, might confer different characteristics to the Kv channels. Another reason could be the different mediators or regulatory proteins that are present in the native system (rabbit PASMC) yet are absent in our heterologous expression system, tsA-201 cells. These mediators could be essential in the hypoxic response of Kv2.1 or Kv2.1/Kv9.3 to DTT. Parallel to the findings of Park et al., 1997, DTT does not affect the steady-state activation of Kv2.1 current. Although Kv9.3 is a silent channel, it has been established that co-expression of this subunit with Kv2.1 modulates the latter (Kerschensteiner et al., 2005; Kerschensteiner and Stocker, 1999). Our findings here showed that Kv9.3 does not make a difference to Kv2.1 steady-state inactivation in the presence of DTT. In addition, DTT is also not effective in reducing Kv2.1/Nox4 and Kv2.1/Kv9.3/Nox4 current amplitude or in modulating their steady-state activation.

Results from experiments with DTNB are similar to that with DTT, with the exception that DTNB slightly increases the current amplitude of Kv2.1/Kv9.3/Nox4. Other than that, DTNB also does not have any effect on the activation threshold of the cells. Our results with regards to the lack of effect of DTNB on Kv2.1 and Kv2.1/Kv9.3 agree with that published by Park et al, 1997. They have shown that 2,2'-dithiobis(5-nitropyridine) (DTNBP), which is a membrane-permeable oxidizing agent, increased the Kv current in rabbit PASMC but the membrane-impermeable DTNB has no effect on the Kv current. DTT, DTNBP, and DTNB are redox agents that target sulphydryl groups and these groups exist on both sides of the cell membrane Park et al., 1997. Our results with DTNB and those of Park et al, 1997 could indicate that the sulphydryl groups that are susceptible to modification by these redox agents might be at the intracellular side of the membrane. However, more experiments should be done with DTT, especially when the appropriate regulatory factors which mediate the effect of DTT on Kv2.1 and Kv2.1/Kv9.3 are identified, before the conclusion that intracellular sulphydryl groups of these channels are the target of these redox agents can be made.

It was of interest to test whether Ch-T is one of the ROS that contributes to the inhibition of Kv2.1 and Kv2.1/Kv9.3 current because Ch-T has been shown to suppress transient outward K^+ current (Ito) and sustained delayed rectifier K^+ current (Idr) in mouse colonic myocytes (Prasad and Goyal, 2004). Moreover, suppression of Ito has been linked to arrhythmias in the heart (Tanaka et al., 1998). The difference between the results for Ch-T in this study with those from published literature could be attributable to the different characteristics of Kv channels studied. In the research of Prasad and Goyal, 2004, the Kv channels of interest are Kv4.1, Kv4.2 and Kv4.3 which are prominent in the colonic tissues (Prasad and Goyal, 2004). The mainly colon-specific redox agents, Ch-T and NH_2Cl, have an effect on the Kv4 channels studied (Duprat et al., 2005; Koh et al., 1999; Prasad and Goyal, 2004). However, this study showed that the effect of Ch-T on Kv2.1 channel is almost negligible. Ch-T is capable of oxidizing both methionine and cysteine residues (Prasad and Goyal, 2004). The effect of various oxidizing and reducing agents which target the cysteine residues such as H_2O_2, DTNB, and DTT have been explored in other parts of the project and it has been determined that these cysteine-specific agents have negligible or modest effect on Kv2.1. When it comes to Ch-T, the negligible effect of this agent on Kv2.1 could demonstrate that the methionine residues on Kv2.1 are not susceptible to oxidation by Ch-T.

Previously, conflicting results on the effect of Ch-T on various K^+ channels have also been published, supporting the notion that different K^+ channels can be differentially modulated by Ch-T. For example, Ciorba et al., 1999 have shown that Ch-T decelerate the inactivation kinetic of KCa channels expressed in *Xenopus* oocytes, which is indicative of the enhancement of Ito and that this effect is due to oxidation of both methionine and cysteine residues . In contrast, Prasad and Goyal, 2004 showed that Ch-T inhibits Ito, through the inhibition of Kv4.

For a more complete analysis of the effect of Ch-T on Kv2.1 channel, the repolarization of the current to -50mV from various step voltages could also be analyzed in order to determine the deactivation kinetics. Such analysis have been performed by Tanaka et al., 1998, when they analyzed how the outward current from rabbit atrial cells are affected by Ch-T.

Auxiliary subunits or interacting partners of ion channels regulate the function of ion channels in several ways (Chen et al., 2012). They have an impact on the ion channel subunit assembly, transportation to the surface membrane or localization at certain compartments, protein stability, electrophysical and pharmacological properties (Chen et al., 2012). Cell adhesion molecules are commonly known for being auxiliary subunits for Na^+ channels (Chen et al., 2012) and the demonstration of AMIGO1 as an interacting partner for Kv2.1 (Kuja-Panula et al., 2003; Peltola et al., 2016, 2011; Zhao et al., 2014) is an exciting discovery that K^+ channels could also be target channels for these adhesion molecules.

Kv9.3 is an established modulatory subunit of Kv2.1, capable of regulating the ion channel's biophysical and pharmacological properties (Kerschensteiner and Stocker, 1999; Kerschensteiner et al., 2005; Patel and Honoré, 2001; Patel et al., 1997, 1999). Interestingly, separate studies indicated that downregulation of Kv9.3 and AMIGO1 are linked to altered complex behavioural traits that resemble schizophrenia and it is likely that such consequence resulted from disrupted regulation of Kv2.1 (Peltola et al., 2016). Thus, this study investigated into the effect of regulation of Kv2.1 when it is co-expressed with both Kv9.3 and AMIGO1.

Contrary to the discovery of Peltola et al, 2011, where the group showed that AMIGO1 increases the current amplitude of Kv2.1, the present study showed that AMIGO1 actually decreases the current amplitude of Kv2.1 and Kv2.1/Kv9.3. Such contradiction in results could result from the difference in the electrophysiological protocol used, where the repolarization from each voltage step differs in our protocols. AMIGO1 does not have any effect on the deactivation kinetics of Kv2.1 and Kv2.1/Kv9.3 apart from accelerating the tfast of Kv2.1/Kv9.3.

This study also investigated into the potential of the other family members of this adhesion molecule, namely AMIGO2 and AMIGO3 as auxiliary subunits of Kv2.1 and Kv2.1/Kv9.3. AMIGO2 reduces the Kv2.1 current amplitude at a more depolarized potential (from 40mV onwards) but reduces Kv2.1/Kv9.3 current starting from 0mV. While AMIGO2 shifts both Kv2.1 and Kv2.1/Kv9.3 activation threshold resulting in these channels being activated at a more hyperpolarized potential, the effect of the shift is greater when Kv9.3 is present. These observations made it

tempting to speculate that Kv9.3 is needed for the interaction of AMIGO2 with Kv2.1. However, AMIGO2 was found to increase both tslow and tfast of Kv2.1 but only prolongs tslow of Kv2.1/Kv9.3 and has no effect on tfast of Kv2.1/Kv9.3. It is unclear why AMIGO2 has a stronger effect on the current amplitude and activation threshold when Kv9.3 is present but posed a heavier influence on the deactivation kinetics when Kv9.3 is absent. Hossain et al, 2011 published that AMIGO2 is downregulated in hypoxia but overexpression of AMIGO2 could protect cells treated with 50mM of H_2O_2 for five days from cell death. In the experiments above, the presence of H_2O_2 restored (increased) the current amplitude of Kv2.1/Kv9.3/AMIGO2 to the level of Kv2.1/Kv9.3 and abolished the activation threshold shift of AMIGO2 on both Kv2.1 and Kv2.1/Kv9.3, even though H_2O_2 does not have any effect on Kv2.1 and Kv2.1/Kv9.3 when AMIGO2 is not present, as demonstrated earlier in this chapter. This could suggest that AMIGO2 is a regulatory protein modulating Kv2.1 and Kv9.3 channels and H_2O_2 manifests its effect on these channels when AMIGO2 is present. Surprisingly the presence of H_2O_2 does not affect the tslow and tfast of both Kv2.1/AMIGO2 and Kv2.1/Kv9.3/AMIGO2. This could mean AMIGO2 regulates the channels in other ways without affecting the deactivation kinetics in the presence of H_2O_2.

It is inconclusive as to whether AMIGO2 confers protective effect by reducing Kv2.1/Kv9.3 current and causing the channels to open at a more polarized potential (earlier), and without affecting the time constant of inactivation. The result supporting the argument that AMIGO does confer protective effect might be seen in how AMIGO2 increases the time constant of inactivation of Kv2.1/Kv9.3 when H_2O_2 is absent. Conversely, when H_2O_2 is present, the time constants remained increased and does not get reduced back to the level of Kv2.1 or Kv2.1/Kv9.3. When time constants of inactivation are increased, the duration of action potential is prolonged, and this prevents the next action potential to be conducted, thus reducing the excitability of the cells.

The observation that AMIGO2 significantly reduces the current amplitude of Kv2.1/Kv9.3 does not match the suggestion that AMIGO2 reduces the excitability of the cell. Another argument which highlight the negative impact of AMIGO2 expression in the PASMC is that AMIGO2 promotes cell proliferation and might be

involved in hypoxia-induced vascular remodelling (Hossain et al., 2011; H. Park et al., 2015; Rabenau et al., 2004). Pulmonary vascular remodelling occurs when the balance of cell apoptosis and proliferation is tipped towards proliferation, resulting in uncontrollable cell growth occluding the lumen. Although, Hossain et al, 2011 and H. Park et al., 2015 have provided evidence that AMIGO2 is important for endothelial cells survival (Hossain et al., 2011; H. Park et al., 2015), it must be noted that endothelial cells also produce endothelin, (Tang et al., 2009) a well-known vasoconstriction factor produced by endothelial cells which also promotes vascular remodelling (Kim et al., 2000). H. Park et al., 2015 have demonstrated that PDK1 and Akt (protein kinase B) are involved in the AMIGO2-VEGF signalling pathway to control cell proliferation (H. Park et al., 2015). For detailed explanation of how AMIGO2 forms a scaffold on which PDK1 and Akt bind, please see Appendix. Akt serves as a downstream mediator of VEGF to promote endothelial cell survival, proliferation, migration, permeability, vascular tone and angiogenesis (Dimmeler and Zeiher, 2000; Liu et al., 2000) and AMIGO2 activates Akt (H. Park et al., 2015). Akt inhibition has been correlated to reduce ovarian tumour growth, angiogenesis, endothelial cell tube formation, and morphogenesis. Endothelial cells which are cultured together with vascular smooth muscle cells have constitutively active Akt and are able to form non-functional vasculature (H. Park et al., 2015). However, partial inhibition of PI3K to suppress Akt1 will activate Erk1/2 (MAPK) pathway to promote arteriogenesis (H. Park et al., 2015). Therefore, vasculogenesis and angiogenesis can be regulated by more than one pathway (H. Park et al., 2015). Instead of relying on PI3K-Akt pathway alone, the process depends on the balance between this pathway with MAPK signalling (H. Park et al., 2015). In short, AMIGO2 silencing might only control part of the network and another compensatory pathway might be activated to contribute to cell proliferation.

Promotion of cell apoptosis is generally accepted to be beneficial in remediating pulmonary vascular remodelling with the exception of endothelial cells. Nevertheless, the effect of AMIGO2 silencing which leads to the promotion of cell apoptosis seems contradictory to the findings that AMIGO2 expression in CA2/CA3 in the hippocampus might be neuroprotective (Laeremans et al., 2013). Therefore, AMIGO2 expression might be beneficial or undesirable, depending on anatomy. Furthermore, it is not known whether the downregulation of AMIGO2 due to hypoxia

is simply a coping mechanism to reduce endothelial cells population, (thus avoiding vascular remodelling) or a detrimental consequence promoting apoptosis of the wrong cell population. In the future, AMIGO2-silenced rat model should be used to see the changes on PASMC and PAEC proliferation and inflammatory markers in hypoxic conditions.

In Rabenau et al, 2004's research, it is surprising how AMIGO2 silencing leads to chromosomal instability yet inhibits tumor growth in gastric adenocarcinoma cells. It has been documented that chromosomal instability does not necessarily drives tumorigenesis (Rabenau et al., 2004). Moreover, it has not been confirmed as to why downregulation of a cell adhesion molecule could lead to chromosomal instability. Rabenau et al, 2004 suggested that downregulation of AMIGO2 could have an effect on several currently unidentified pathways to eventually lead to chromosomal instability. This observation has been compared to the finding of human Ha-ras oncogene upregulation affecting several cellular pathways, which in turn activates the nucleolytic activity that compromises DNA repair mechanisms, to ultimately causing chromosomal aberration (Rabenau et al., 2004). Therefore, it is essential to have a thorough understanding into the pathways that are affected by AMIGO2 signal transduction before speculating the role of AMIGO2 in cell proliferation. In addition, the role of AMIGO2 in cell adhesion and/or chromosomal instability and in promoting tumourigenicity might be mutually exclusive (Rabenau et al., 2004).

In parallel, an anti-tumor drug which is under clinical trials named perifosine has been postulated to inhibit Akt by targeting the lipid-binding PH domain to prevent recruitment of Akt to the plasma membrane (H. Park et al., 2015). Interestingly, Delgado-Ramirez et al, 2016 showed that this drug also inhibits Kv2.1 by decreasing current amplitude and accelerating closed-state inactivation (Delgado-Ramírez et al., 2016). In the future, when more data supporting the hypothesis that AMIGO2 is an interacting partner of Kv2.1 are available, future work could probe into whether perifosine mediates its effect on Kv2.1 by inhibiting the transport of Akt to the plasma membrane, hence prohibiting Kv2.1 from associating with AMIGO2 (Delgado-Ramírez et al., 2016; H. Park et al., 2015)

Finally, AMIGO3 does not have any influence on Kv2.1 or Kv2.1/Kv9.3 in terms of current amplitude, activation threshold or deactivation kinetics. This could imply that AMIGO3 is not an interacting partner of Kv2.1 or Kv9.3. Although AMIGO3 has anti-oxidative effects (Ahn et al., 2015), it is possible that AMIGO3 does not confer these protective effective via Kv2.1 or Kv9.3.

Another interesting point is that there is high expression of RAGE (a receptor for AMIGOs) in the lungs, while it is usually lowly expressed in other adult tissues. It is tempting to speculate that RAGE has a functionally regulated expression in the context of pulmonary hypertension. This hypothesis could perhaps be investigated in the future.

Chapter 7: Conclusion, Discussion, and Future Direction

Although recent advances in PH research have allowed us to better categorize PH, the two primary mechanisms underlying PH in general are hypoxic pulmonary vasoconstriction (hypoxic pulmonary vasoconstriction) and pulmonary vascular remodelling (pulmonary vascular remodelling) (Kuhr et al., 2012; Olschewski et al., 2014; Ward and McMurtry, 2009). hypoxic pulmonary vasoconstriction is a physiological mechanism to divert oxygen to areas with low oxygen tension (hypoxia) (Archer et al., 1998). However, chronic hypoxia will cause PH (Morrell et al., 2009; Ward and McMurtry, 2009). Dysfunction or reduction of function of K^+ channels have been linked in PH because failure of K^+ channels to open will cause vasoconstriction and uncontrolled cell proliferation, which will worsen PH conditions (Kuhr et al., 2012). Kv1.5 and Kv2.1 are the two most studied K^+ ion channels in PH (Archer et al., 2004, 1998; Lee et al., 2006). The reason we are focused on Kv2.1 is the interesting finding that it can heteromerize and be modulated by a silent channel, Kv9.3 (Kerschensteiner, 2003; Patel et al., 1999, 1997; Patel and Honoré, 2001).

The following paragraphs summarize the key findings resulting from this thesis and how the characteristics of Kv2.1 and Kv9.3 could be implicated in PH, the limitations of the experiments performed and the future directions that can be taken to fill the literature gap in the PH.

Kv2.1 is regulated by Kv9.3

The biophysical and pharmacological regulation of Kv2.1 by Kv9.3 have been demonstrated by several authors (Patel et al, 1997, Patel et al, 1999, Kerschensteiner, 2003, Zhong et al, 2010). The results in this thesis showed that Kv9.3 modulates Kv2.1 in terms of current amplitude, activation threshold, and deactivation kinetics.

Kv9.3 increases the current amplitude of Kv2.1 at the activation voltage range (Kerschensteiner, 2003). This could mean that the K^+ efflux is bigger when the Kv2.1 channels are activated, bringing the cells back to resting membrane potential faster. This could have significant impact in the case of pulmonary hypertension. In addition, co-expression of Kv9.3 with Kv2.1 also causes Kv2.1 channels to be activated earlier (at a more negative/polarized voltage range). This could be important to prolong the action potential duration of firing so that more K^+ ions can flow out of the cells (Kerschensteiner, 2003). Kv2.1/Kv9.3 also has a longer slow component of time constant of deactivation compared with Kv2.1 (Hristov et al., 2012; Zhong et al., 2010). In order for the transduction of the next action potential (activation of Na^+ channels to allow Na^+ influx), K^+ channels have to recover from deactivation (Hristov et al., 2012; Zhong et al., 2010). Therefore, a longer duration of deactivation could prevent the next action potential to be generated, thus reducing the membrane excitability which confers beneficial effects to the cells. On the other hand, if the function of Kv2.1/Kv9.3 is compromised, there will be reduced outward delayed rectifier current, which will cause the cells to remain in the depolarized state. Membrane surface expression of Kv9.3 is only detected when it is co-expressed with Kv2.1 as Kv9.3 proteins are usually retained in the cytoplasm (Shepard and Rae, 1999). If Kv2.1 is expressed as homomers at the membrane surface without Kv9.3, the deactivation kinetics would be accelerated, allowing for faster transduction of action potential.

As mentioned in the Introduction chapter, failure of K^+ channels to open will cause the cells to remain in polarized state (more positive ions inside the cells as compared with outside), and the cell will enter cell cycle or undergo proliferation (Kuhr et al., 2012; Moudgil et al., 2006). Lee et al., 2015 have demonstrated that Kv9.3 is pro-proliferative. In this context, the presence of Kv9.3 might not be ideal in alleviating

PH. However, the study performed by Lee et al, 2015 stating that the silencing of Kv9.3 which leads to inhibition of human colon and lung cancer was performed on non-excitable cells and only investigated on the role of Kv9.3 in isolation from Kv2.1 (i.e. only studied Kv9.3 homomers without comparing with Kv2.1/Kv9.3 heteromers). Thus, there is a gap in the literature as the effects of silencing of Kv2.1 and Kv2.1/Kv9.3 on cell proliferation are unknown and were not assessed in this thesis.

Nox4 does not regulate Kv2.1 or Kv2.1/Kv9.3

It is clearly shown in Chapter 3 that Nox4 does not regulate Kv2.1. It remains unknown as to why Kv2.1/Kv9.3/Nox4 shows dual mode of steady-state activation (Figure 3.8). In one series of experiment, it was found that Nox4 abolished the effect of Kv9.3 on the activation threshold of Kv2.1. In another series of experiment, Kv2.1/Kv9.3/Nox4 cells behaved more similarly to Kv2.1/Kv9.3 cells, indicating that Nox4 does not interfere with the Kv2.1/Kv9.3 heteromer. Since there is a larger number of cells which showed the lack of effect of Nox4 on Kv2.1/Kv9.3, we drew the conclusion that Nox4 does not modulate Kv2.1/Kv9.3. This means the presence of Kv9.3 does facilitate the interaction of Nox4 with Kv2.1. One of the reasons which we could propose to explain the dual mode of steady-state of activation is that the cells expressing Kv2.1/Kv9.3/Nox4 might have a regulatory component which modulates their behaviour to resemble that of Kv2.1 (meaning this regulatory component abolished the effect of Kv9.3 on Kv2.1), while the cells used in the other series of experiment somehow do not express this regulatory component or the effect of this regulatory component is less prominent.

The argument that Nox4 does not regulate Kv2.1 or Kv2.1/Kv9.3 is in line with the results of Mittal et al, 2012, where they demonstrated that Nox4 does not colocalize with Kv2.1, but colocalizes with Kv1.5 and TASK-1 instead. However, the idea of colocalization does not automatically translate to interaction between the two proteins. This can be seen in the case of colocalization of Kv1.5 and Nox4 (Lee et al., 2006). While many authors agreed that these two proteins are colocalized, whether Nox4 modulates Kv1.5 is still under debate. Lee et al, 2006 showed that Nox4 does not modulate Kv1.5 but Mittal et al, 2012 argued otherwise. This discrepancy is

perhaps due to the experiment setup, where Mittal et al, 2012 used rats that have been subjected to chronic hypoxia for three weeks and Lee et al, 2006 performed the experiment in normoxia. This could mean that, in order for Nox4 to act as an oxygen sensor thereby modulating the function of Kv1.5, a stimulus must be present. And the stimulus in question might be hypoxia. This hypothesis fits into the speculations of other research groups, who proposed that Nox4 is hypoxia sensor (Brandes et al., 2010; Lee et al., 2013; Nisimoto et al., 2014).

While it was disappointing to draw the conclusion that Nox4 does not modulate Kv2.1, even in the presence of Kv9.3, the next question that arises from this study is whether other Nox proteins could be involved in regulating Kv2.1 and Kv2.1/Kv9.3. One of the candidates would be Nox2 (or gp91phox). Buttigieg et al, 2012 even proposed that Nox2 (or gp91phox) is the main oxygen sensor while Nox4 plays a minor role. On the other hand, Goyal et al., 2004 propounded that Nox1 plays a significant role too considering that Nox1 induces HIF-1α upregulation even in the absence of hypoxia.

Future experiments could look into the colocalization of either Nox1 or Nox2 proteins with Kv2.1 using immunostaining or immunoprecipitation techniques, before looking into the functional implications of their colocalization using patch clamp electrophysiology. It is a well-known fact that Kv2.1 behaves differently in different heterologous expression systems (L cells, Xenopus oocytes, HEK cells) (Conforti et al., 2000; Hulme et al., 1999; Patel et al., 1997; Patel and Honoré, 2001). Perhaps, it would be a good idea to analyze closely the regulatory proteins present in each expression system to shed some light on the candidate regulatory proteins that are present endogenously which could affect Kv2.1 biophysical properties.

On the other hand, there are key cysteine residues on Kv2.1 which are prone to oxidation (Cotella et al., 2012; Yu et al., 2016)c. Identification of key cysteine residues might give clues as to how Kv9.3 mediates its effect on Kv2.1. Cotella et al., 2012 reported an oxidation resistant Kv2.1 variant which has a mutation in the conserved cysteine residue, C73 to an alanine (C73A). Yu et al., 2016 reported that dasatinib, a Food and Drug Administration–approved inhibitor of Src tyrosine kinases

significantly reduced the signs of typical lesions of brain injury such as inflammation (astrocytosis), neurodegeneration, and cell death in C73A transgenic mice. In motor (rotarod) and cognitive (Morris water maze) tests, both transgenic and WT mice demonstrated improvements when treated with dasatinib. While there is reported success of dasatinib in mouse model of traumatic brain injury, the same cannot be said in the case of pulmonary hypertension. Guignabert et al, 2016 reported that dasatinib causes lung vascular toxicity and increases tendency of pulmonary hypertension in humans and rodents. Instead of counteracting the effect of oxidized Kv2.1, dasatinib is said to cause endothelial cell dysfunction and vascular damage by inducing mitochondrial ROS production, and this pathway of ROS production is independent of Src family kinases (Guignabert et al., 2016). In short, studies to identify other cysteine residues in Kv2.1 might be important in elucidating the different ROS production pathways involved in PH and thereby improving the therapeutic options for PH patients.

Animal experiments to dissect the role Kv2.1 have been well documented, but the role of Kv9.3 has not gained as much attention. Considering the hypothesis of Zhong et al, 2010 stating that the delayed rectifier current in rat middle cerebral arteries is most likely contributed by Kv2.1/Kv9.3 instead of Kv2.1 alone, perhaps it would be a good idea to repeat the experiments outlined in this thesis on animal models. The characterization of Kv2.1 and Kv2.1/Kv9.3 currents in this thesis would allow us to differentiate between the two currents in native cells.

Kv2.1 and Kv9.3 proteins are present in the rat lungs and heart

Kv2.1 and Kv9.3 proteins are expressed in rat lungs and heart. The limitation in this chapter is that controls could have been included where staining with C31 which targets endothelial cells and sm22/alpha smooth muscle actin could which target smooth muscle cells to confirm that Kv2.1 and Kv9.3 target these cell types.

Colocalization could be deciphered as co-occurring at the same place or as correlation, which means that the levels of distribution of the two proteins occurring

at the same place are also similar (Adler and Parmryd, 2012). For example, two proteins might spatially overlap but they are not distributed proportionally within the cells (Adler and Parmryd, 2012). Although the results from this experiment might suggest that Kv2.1 and Kv9.3 are present in the same location, double immunostaining using secondary antibodies conjugated with different Alexa Flour dyes to target primary Kv2.1 and Kv9.3 antibodies should be done to confirm that the two proteins overlap (Owen et al., 2009). The imaging of the cells using confocal micROS copy will allow us to determine whether there is an overlap of the two different fluorescent dyes excited at different wavelengths, which will indicate spatial colocalization (Owen et al., 2009). To analyse correlation, we could calculate the number of cells which express both of the proteins and cells which express either of the proteins to see if the relationship is proportional.

Alternatively, Förster Resonance Energy Transfer (FRET) can be done to measure the distance of two fluorophores conjugated to Kv2.1 and Kv9.3 proteins, which will give us an idea of the proximity of the proteins to each other (Sekar and Periasamy, 2003). The advantage of FRET is that it can be precise up to 10nm proximity, which is a much higher resolution compared to light microscopy (250nm proximity) (Sekar and Periasamy, 2003).

AMIGO1 and AMIGO2 regulates Kv2.1 and Kv2.1/Kv9.3 and the presence of H_2O_2 abolishes the effect of AMIGO2 on these channels

This study showed that AMIGO1 inhibits Kv2.1 and Kv2.1/Kv9.3 current amplitude. This result does not agree with the results published by Peltola et al, 2011. The reason that such discrepancy arises could be due to the difference in the electrophysiological protocol used, where the repolarization from each voltage step differs in our protocols (Peltola et al., 2011). It could also be due to the difference in the species of the AMIGO proteins. We have researched on the human AMIGO1 while the other group has used the mouse AMIGO1 and basic local alignment search tool (BLAST) result has shown that the sequences of the two variants are 84% identical.

Other new information provided by this study includes AMIGO1 does not have any effect on the deactivation kinetics of Kv2.1 and Kv2.1/Kv9.3 but accelerates the tfast of Kv2.1/Kv9.3.

While AMIGO2 does not have any effect on Kv2.1 current amplitude, it reduces Kv2.1/Kv9.3 current. AMIGO2 also shifts the activation threshold of both Kv2.1 and Kv2.1/Kv9.3 to a more negative voltage range. In terms of time constant of inactivation, AMIGO2 increases both tslow and tfast of Kv2.1 and prolongs the tslow of Kv2.1/Kv9.3.

Hossain et al, 2011 reported that the mRNA expression of AMIGO2 is reduced when the atmospheric O_2 concentration decreased to 5% and 0% and overexpression of AMIGO2 can protect cells treated with 50mM of H_2O_2 for five days from apoptosis. Following from the suggestion that AMIGO2 plays a protective role in vascular remodelling induced by hypoxia, one of the aims in the thesis was to test the effects of H_2O_2 on Kv2.1/AMIGO2 and Kv2.1/Kv9.3/AMIGO2. AMIGO2 does not affect the Kv2.1 current amplitude but reduces the Kv2.1/Kv9.3 current amplitude. Although in Chapter 6 we have demonstrated that H_2O_2 does not have any effect on the current amplitude of Kv2.1 and Kv2.1/Kv9.3, here we found that the presence of H_2O_2 restored the current amplitude of Kv2.1/Kv9.3/AMIGO2 to the level of Kv2.1/Kv9.3 and abolished the activation threshold shift of AMIGO2 on both Kv2.1 and Kv2.1/Kv9.3.

While it was postulated that AMIGO2 might have a beneficial effect in the case of PH as it protects cells from cell death, the results from this thesis argue that AMIGO2 has a role in vascular remodelling induced by hypoxia but whether the role is beneficial or not is yet to be determined. This is because it is contradictory as to why AMIGO2 reduces Kv2.1/Kv9.3 current but causes the channels to open at a more hyperpolarized potential (earlier) and prolongs the tslow of Kv2.1/Kv9.3. While the two latter actions could lead to reduced cell excitability, the action of reducing K^+ current does not elicit the same effect. Another reason is that the effect of H_2O_2 in PASMC still remains elusive, as several researchers are still divided as to whether H_2O_2 is a vasoconstrictor or vasodilator (S. W. Park et al., 2015). Results in Chapter 8 demonstrated that H_2O_2 does not affect the tslow and tfast of both Kv2.1/AMIGO2

and Kv2.1/Kv9.3/AMIGO2. This could mean AMIGO2 regulates the channels in other ways without affecting the deactivation kinetics in the presence of H_2O_2.

Similar to Kv9.3, AMIGO2 is also pro-proliferative (H. Park et al., 2015; Rabenau et al., 2004). Since Kv9.3 increases Kv2.1 current while AMIGO2 reduces the current amplitude of Kv2.1/Kv9.3, it is tempting to speculate that the pro-proliferative pathways induced by Kv9.3 and AMIGO2 are different.

AMIGO3 does not modulate Kv2.1 or Kv2.1/Kv9.3, probably because AMIGO3 is not an interacting partner of these K^+ channels in the first place. AMIGO3 has been proven to be anti-oxidative (Ahn et al., 2015), but it might confer these protective effective via pathways that do not involve Kv2.1 or Kv9.3.

The colocalization of AMIGO1 and Kv2.1 has been demonstrated, but not with Kv9.3 (Kuja-Panula et al, 2003). In addition, Kuja-Panula et al, 2003 have used mouse brain lysate, which is a positive control for a lot of proteins. Although they have demonstrated that AMIGO1 mRNA is also found in adult mouse lung and heart tissues, the differential expression of AMIGO1 in relation to Kv2.1 and Kv9.3 in these organs warrants further research. As mentioned above, results from this thesis have shown that Kv2.1 and Kv9.3 proteins are expressed in rat lungs and tissues. In the future, double or triple staining of these proteins together could be done to prove the colocalization of these proteins.

It would be interesting to assess whether AMIGO2, Kv2.1, and Kv9.3 mRNA and protein levels are differentially expressed in rat PASMC. Since results from this study showed that AMIGO2 does regulate Kv2.1, it would be a good idea to visualize the colocalization of these proteins using immunofluorescence or FRET. In order to shed light on how the levels of protein expression change during hypoxia, Western blot can be performed on cells transfected with these proteins. Although the mRNA level of AMIGO2 has been assessed in gastric adenocarcinoma patients (Rabenau et al., 2004), gastric adenocarcinoma cell line (Rabenau et al., 2004), and in human umbilical cord endothelial cells (HUVEC) (H. Park et al., 2015), the level of AMIGO2 expression in relation to Kv2.1 and Kv9.3 have never been investigated before.

Overall, the results of the thesis have elucidated not only the role of a well-studied K^+ channel, Kv2.1 in PH, but also highlighted the importance of the silent Kv9.3 channels in modulating Kv2.1 channels. Considering the speculation that Kv2.1/Kv9.3 might be the more dominant form of K^+ channels in the pulmonary vasculature, this finding would prove valuable in optimize therapeutic approaches and in diagnosis of patients. The discovery of AMIGO proteins (specifically AMIGO1 and AMIGO2) as interacting partners have also contributed to the understanding of the pathways that implicate Kv2.1. AMIGO proteins could very well have a role in PH and whether the role is beneficial or pathogenic still warrants further research.

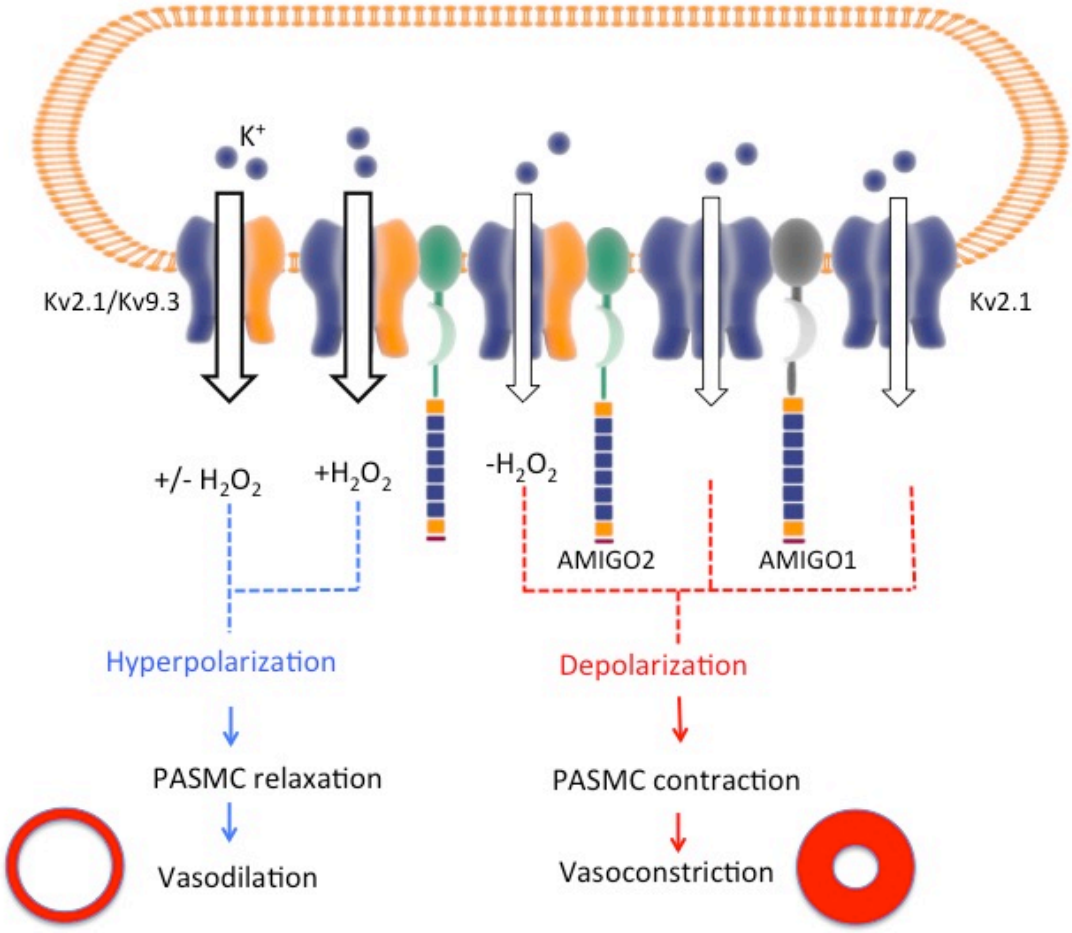

Figure 7.1: Schematic summary of the regulation of Kv2.1 and Kv2.1/Kv9.3 by H_2O_2 and AMIGO1 and AMIGO2. Starting from the left, Kv2.1/Kv9.3 has increased current amplitude compared with Kv2.1 alone regardless of absence or presence of H_2O_2. The presence of H_2O_2 restores the current amplitude of Kv2.1/Kv9.3/AMIGO2 to the Kv2.1/Kv9.3 level. Co-expression of AMIGO2 significantly reduces the current amplitude of Kv2.1/Kv9.3. Meanwhile, co-expression of AMIGO1 reduces Kv2.1 amplitude. Kv2.1 homomers have smaller current amplitude compared with Kv2.1/Kv9.3. Thickness of arrows represents the magnitude of current going through the channels. The results from this study suggested that Kv2.1/Kv9.3 and Kv2.1/Kv9.3/AMIGO2 in the presence of H_2O_2 lead to cell hyperpolarization, thus PASMC relaxation and vasodilation. On the other hand, Kv2.1, Kv2.1/AMIGO1, and Kv2.1/Kv9.3/AMIGO2 in the absence of H_2O_2 result in cell depolarization, PASMC contraction, and vasoconstriction.

Bibliography

1. Adler, J., Parmryd, I., 2012. Colocalization Analysis in Fluorescence Microscopy, in: Taatjes, D.J., Roth, J. (Eds.), Cell Imaging Techniques. Humana Press, Totowa, NJ, pp. 97–109. https://doi.org/10.1007/978-1-62703-056-4_5

2. Ahmed, Z., Douglas, M.R., John, G., Berry, M., Logan, A., 2013. AMIGO3 Is an NgR1/p75 Co-Receptor Signalling Axon Growth Inhibition in the Acute Phase of Adult Central Nervous System Injury. PLoS ONE 8, e61878. https://doi.org/10.1371/journal.pone.0061878

3. Ahn, M.Y., Hwang, J.S., Yun, E.Y., Kim, M.-J., Park, K.-K., 2015. Anti-aging Effect and Gene Expression Profiling of Aged Rats Treated with G. bimaculatus Extract. Toxicol. Res. 31, 173–180. https://doi.org/10.5487/TR.2015.31.2.173

4. Akita, T., Ohara, M., Okada, Y., 2012. Patch-Clamp Techniques: General Remarks, in: Okada, Y. (Ed.), Patch Clamp Techniques. Springer Japan, Tokyo, pp. 21–41. https://doi.org/10.1007/978-4-431-53993-3_2

5. Andres-Enguix, I., Caley, A., Yustos, R., Schumacher, M.A., Spanu, P.D., Dickinson, R., Maze, M., Franks, N.P., 2007. Determinants of the Anesthetic Sensitivity of Two-pore Domain Acid-sensitive Potassium Channels: Molecular cloning of an anestetic-activated potassium channel from *Lymnaea stagnalis*. J. Biol. Chem. 282, 20977–20990. https://doi.org/10.1074/jbc.M610692200

6. Antigny, F., Hautefort, A., Meloche, J., Belacel-Ouari, M., Manoury, B., Rucker-Martin, C., Péchoux, C., Potus, F., Nadeau, V., Tremblay, E., Ruffenach, G., Bourgeois, A., Dorfmüller, P., Breuils-Bonnet, S., Fadel, E., Ranchoux, B., Jourdon, P., Girerd, B., Montani, D., Provencher, S., Bonnet, S., Simonneau, G., Humbert, M., Perros, F., 2016. Potassium Channel Subfamily K Member 3 (KCNK3) Contributes to the Development of Pulmonary Arterial Hypertension: Clinical Perspective. Circulation 133, 1371–1385. https://doi.org/10.1161/CIRCULATIONAHA.115.020951

7. Archer, S.L., Souil, E., Dinh-Xuan, A.T., Schremmer, B., Mercier, J.C., El Yaagoubi, A., Nguyen-Huu, L., Reeve, H.L., Hampl, V., 1998. Molecular identification of the role of voltage-gated K^+ channels, Kv1.5 and Kv2.1, in hypoxic pulmonary vasoconstriction and control of resting membrane potential in rat pulmonary artery myocytes. J. Clin. Invest. 101, 2319–2330. https://doi.org/10.1172/JCI333

8. Archer, S.L., Wu, X.-C., Thébaud, B., Nsair, A., Bonnet, S., Tyrrell, B., McMurtry, M.S., Hashimoto, K., Harry, G., Michelakis, E.D., 2004.

Preferential expression and function of voltage-gated, O_2-sensitive K^+ channels in resistance pulmonary arteries explains regional heterogeneity in hypoxic pulmonary vasoconstriction: ionic diversity in smooth muscle cells. Circ. Res. 95, 308–318. https://doi.org/10.1161/01.RES.0000137173.42723.fb

9. Ashmole, I., Goodwin, P.A., Stanfield, P.R., 2001. TASK-5, a novel member of the tandem pore K^+ channel family. Pflugers Arch. 442, 828–833.

10. Ashmole, I., Vavoulis, D.V., Stansfeld, P.J., Mehta, P.R., Feng, J.F., Sutcliffe, M.J., Stanfield, P.R., 2009. The response of the tandem pore potassium channel TASK-3 (K(2P)9.1) to voltage: gating at the cytoplasmic mouth. J. Physiol. 587, 4769–4783. https://doi.org/10.1113/jphysiol.2009.175430

11. Backx, P.H., Marban, E., 1993. Background potassium current active during the plateau of the action potential in guinea pig ventricular myocytes. Circ. Res. 72, 890–900.

12. Banerjee, I., Fuseler, J.W., Price, R.L., Borg, T.K., Baudino, T.A., 2007. Determination of cell types and numbers during cardiac development in the neonatal and adult rat and mouse. AJP Heart Circ. Physiol. 293, H1883–H1891. https://doi.org/10.1152/ajpheart.00514.2007

13. Barbuti, A., Ishii, S., Shimizu, T., Robinson, R.B., Feinmark, S.J., 2002. Block of the background K^+ channel TASK-1 contributes to arrhythmogenic effects of platelet-activating factor. Am. J. Physiol. Heart Circ. Physiol. 282, H2024-2030. https://doi.org/10.1152/ajpheart.00956.2001

14. Belohlávková, S., Simák, J., Kokesová, A., Hnilicková, O., Hampl, V., 2001. Fenfluramine-induced pulmonary vasoconstriction: role of serotonin receptors and potassium channels. J. Appl. Physiol. Bethesda Md 1985 91, 755–761

15. Ben-Abu, Y., Zhou, Y., Zilberberg, N., Yifrach, O., 2009. Inverse coupling in leak and voltage-activated K^+ channel gates underlies distinct roles in electrical signaling. Nat. Struct. Mol. Biol. 16, 71–79. https://doi.org/10.1038/nsmb.1525

16. Bhattacharjee, A., Joiner, W.J., Wu, M., Yang, Y., Sigworth, F.J., Kaczmarek, L.K., 2003. Slick (Slo2.1), a rapidly-gating sodium-activated potassium channel inhibited by ATP. J. Neurosci. Off. J. Soc. Neurosci. 23, 11681–11691.

17. Binder, C., Schulz, M., Hiddemann, W., Oellerich, M., 1999. Induction of inducible nitric oxide synthase is an essential part of tumor necrosis factor-alpha-induced apoptosis in MCF-7 and other epithelial tumor cells. Lab. Investig. J. Tech. Methods Pathol. 79, 1703–1712.

18. Bocksteins, E., 2016. Kv5, Kv6, Kv8, and Kv9 subunits: No simple silent bystanders. J. Gen. Physiol. 147, 105–125. https://doi.org/10.1085/jgp.201511507

19. Bonnet, S., Archer, S.L., 2007. Potassium channel diversity in the pulmonary arteries and pulmonary veins: implications for regulation of the pulmonary vasculature in health and during pulmonary hypertension. Pharmacol. Ther. 115, 56–69. https://doi.org/10.1016/j.pharmthera.2007.03.014

20. Brandes, R.P., Weissmann, N., Schröder, K., 2010. NADPH oxidases in cardiovascular disease. Free Radic. Biol. Med. 49, 687–706. https://doi.org/10.1016/j.freeradbiomed.2010.04.030

21. Brickley, S.G., Aller, M.I., Sandu, C., Veale, E.L., Alder, F.G., Sambi, H., Mathie, A., Wisden, W., 2007. TASK-3 Two-Pore Domain Potassium Channels Enable Sustained High-Frequency Firing in Cerebellar Granule Neurons. J. Neurosci. 27, 9329–9340. https://doi.org/10.1523/JNEUROSCI.1427-07.2007

22. Buttigieg, J., Pan, J., Yeger, H., Cutz, E., 2012. NOX2 (gp91phox) is a predominant O2 sensor in a human airway chemoreceptor cell line: biochemical, molecular, and electrophysiological evidence. Am. J. Physiol. Lung Cell. Mol. Physiol. 303, L598-607. https://doi.org/10.1152/ajplung.00170.2012

23. Charpentier, F., 2007. Understanding the cardiac role of K2P channels: A new TASK for electrophysiologists. Cardiovasc. Res. 75, 5–6. https://doi.org/10.1016/j.cardiores.2007.05.011

24. Chen, C., Okayama, H., 1987. High-efficiency transformation of mammalian cells by plasmid DNA. Mol Cell Bio 7.

25. Chen, M., Kellett, W.F., Petkov, G.V., 2010. Voltage-gated K^+ channels sensitive to stromatoxin-1 regulate myogenic and neurogenic contractions of rat urinary bladder smooth muscle. AJP Regul. Integr. Comp. Physiol. 299, R177–R184. https://doi.org/10.1152/ajpregu.00036.2010

26. Chen, Y., Aulia, S., Li, L., Tang, B.L., 2006. AMIGO and friends: an emerging family of brain-enriched, neuronal growth modulating, type I transmembrane proteins with leucine-rich repeats (LRR) and cell adhesion molecule motifs. Brain Res. Rev. 51, 265–274. https://doi.org/10.1016/j.brainresrev.2005.11.005

27. Chen, Y., Hor, H.H., Tang, B.L., 2012. AMIGO is expressed in multiple brain cell types and may regulate dendritic growth and neuronal survival. J. Cell. Physiol. 227, 2217–2229. https://doi.org/10.1002/jcp.22958

28. Chiara, M.D., Monje, F., Castellano, A., López-Barneo, J., 1999. A small domain in the N terminus of the regulatory alpha-subunit Kv2. 3 modulates Kv2.1 potassium channel gating. J. Neurosci. Off. J. Soc. Neurosci. 19, 6865–6873.

29. Choi, K.L., Aldrich, R.W., Yellen, G., 1991. Tetraethylammonium blockade distinguishes two inactivation mechanisms in voltage-activated K^+ channels. Proc. Natl. Acad. Sci. U. S. A. 88, 5092–5095.

30. Choisy, S.C.M., Hancox, J.C., Arberry, L.A., Reynolds, A.M., Shattock, M.J., James, A.F., 2004. Evidence for a novel K(+) channel modulated by alpha(1A)-adrenoceptors in cardiac myocytes. Mol. Pharmacol. 66, 735–748. https://doi.org/10.1124/mol.104.000760

31. Ciorba, M.A., Heinemann, S.H., Weissbach, H., Brot, N., Hoshi, T., 1999. Regulation of voltage-dependent K^+ channels by methionine oxidation: effect of nitric oxide and vitamin C. FEBS Lett. 442, 48–52.

32. Clarke, C.E., Veale, E.L., Green, P.J., Meadows, H.J., Mathie, A., 2004. Selective block of the human 2-P domain potassium channel, TASK-3, and the native leak potassium current, IKSO, by zinc. J. Physiol. 560, 51–62. https://doi.org/10.1113/jphysiol.2004.070292

33. Cogolludo, A., Frazziano, G., Cobeño, L., Moreno, L., Lodi, F., Villamor, E., Tamargo, J., Perez-Vizcaino, F., 2006. Role of reactive oxygen species in Kv channel inhibition and vasoconstriction induced by TP receptor activation in rat pulmonary arteries. Ann. N. Y. Acad. Sci. 1091, 41–51. https://doi.org/10.1196/annals.1378.053

34. Conforti, L., Bodi, I., Nisbet, J.W., Millhorn, D.E., 2000. O2-sensitive K^+ channels: role of the Kv1.2 -subunit in mediating the hypoxic response. J. Physiol. 524 Pt 3, 783–793.

35. Coppock, E.A., Martens, J.R., Tamkun, M.M., 2001. Molecular basis of hypoxia-induced pulmonary vasoconstriction: role of voltage-gated K^+ channels. Am. J. Physiol. Lung Cell. Mol. Physiol. 281, L1-12.

36. Costigan, M., Belfer, I., Griffin, R.S., Dai, F., Barrett, L.B., Coppola, G., Wu, T., Kiselycznyk, C., Poddar, M., Lu, Y., Diatchenko, L., Smith, S., Cobos, E.J., Zaykin, D., Allchorne, A., Shen, P.-H., Nikolajsen, L., Karppinen, J., Mannikko, M., Kelempisioti, A., Goldman, D., Maixner, W., Geschwind, D.H., Max, M.B., Seltzer, Z., Woolf, C.J., 2010. Multiple chronic pain states are associated with a common amino acid-changing allele in KCNS1. Brain 133, 2519–2527. https://doi.org/10.1093/brain/awq195

37. Cotella, D., Hernandez-Enriquez, B., Wu, X., Li, R., Pan, Z., Leveille, J., Link, C.D., Oddo, S., Sesti, F., 2012. Toxic Role of K^+ Channel Oxidation in Mammalian Brain. J. Neurosci. 32, 4133–4144. https://doi.org/10.1523/jneurosci.6153-11.2012

38. Cox, R.H., Fromme, S., 2016. Comparison of Voltage Gated K^+ Currents in Arterial Myocytes with Heterologously Expressed K v Subunits. Cell Biochem. Biophys. 74, 499–511. https://doi.org/10.1007/s12013-016-0763-4

39. Cutz, E., Pan, J., Yeger, H., 2009. The Role of NOX2 and "Novel Oxidases" in Airway Chemoreceptor O_2 Sensing, in: Gonzalez, C., Nurse, C.A., Peers, C. (Eds.), Arterial Chemoreceptors. Springer Netherlands, Dordrecht, pp. 427–438. https://doi.org/10.1007/978-90-481-2259-2_49

40. Delgado-Ramírez, M., Morán-Zendejas, R., Aréchiga-Figueroa, I.A., Toro-Castillo, C., Ramírez-Martínez, J.F., Rodríguez-Menchaca, A.A., 2016. Modulation of the voltage-gated potassium channel Kv2.1 by the anti-tumor alkylphospholipid perifosine. Pharmacol. Rep. 68, 457–461. https://doi.org/10.1016/j.pharep.2015.11.006

41. del Pino, I., García-Frigola, C., Dehorter, N., Brotons-Mas, J.R., Alvarez-Salvado, E., Martínez de Lagrán, M., Ciceri, G., Gabaldón, M.V., Moratal, D., Dierssen, M., Canals, S., Marín, O., Rico, B., 2013. Erbb4 Deletion from Fast-Spiking Interneurons Causes Schizophrenia-like Phenotypes. Neuron 79, 1152–1168. https://doi.org/10.1016/j.neuron.2013.07.010

42. Dimmeler, S., Zeiher, A.M., 2000. Endothelial cell apoptosis in angiogenesis and vessel regression. Circ. Res. 87, 434–439.

43. Dong, Q., Zhao, N., Xia, C., Du, L., Fu, X., Du, Y., 2012. Hypoxia induces voltage-gated K^+ (Kv) channel expression in pulmonary arterial smooth muscle cells through hypoxia-inducible factor-1 (HIF-1). Bosn J Basic Med Sci 12, 158–163.

44. Druzin, M., Malinina, E., Grimsholm, O., Johansson, S., 2011. Mechanism of Estradiol-Induced Block of Voltage-Gated K^+ Currents in Rat Medial Preoptic Neurons. PLoS ONE 6, e20213. https://doi.org/10.1371/journal.pone.0020213

45. Duprat, F., Girard, C., Jarretou, G., Lazdunski, M., 2005. Pancreatic two P-domain K^+ channels TALK-1 and TALK-2 are activated by nitric oxide and reactive oxygen species. J. Physiol. 562, 235–244. https://doi.org/10.1113/jphysiol.2004.071266

46. Duprat, F., Lesage, F., Fink, M., Reyes, R., Heurteaux, C., Lazdunski, M., 1997. TASK, a human background K^+ channel to sense external pH variations near physiological pH. EMBO J. 16, 5464–5471. https://doi.org/10.1093/emboj/16.17.5464

47. Enyedi, P., Czirjak, G., 2010. Molecular Background of Leak K^+ Currents: Two-Pore Domain Potassium Channels. Physiol. Rev. 90, 559–605. https://doi.org/10.1152/physrev.00029.2009

48. Escoubas, P., Diochot, S., Célérier, M.-L., Nakajima, T., Lazdunski, M., 2002. Novel tarantula toxins for subtypes of voltage-dependent potassium channels in the Kv2 and Kv4 subfamilies. Mol. Pharmacol. 62, 48–57.

49. Evans, A.M., Clapp, L.H., Gurney, A.M., 1994. Augmentation by intracellular ATP of the delayed rectifier current independently of the glibenclamide-sensitive K-current in rabbit arterial myocytes. Br. J. Pharmacol. 111, 972–974.

50. Evans, A.M., Osipenko, O.N., Gurney, A.M., 1996. Properties of a novel K^+ current that is active at resting potential in rabbit pulmonary artery smooth muscle cells. J. Physiol. 496 (Pt 2), 407–420.

51. Fournier, A.E., GrandPre, T., Strittmatter, S.M., 2001. Identification of a receptor mediating Nogo-66 inhibition of axonal regeneration. Nature 409, 341–346. https://doi.org/10.1038/35053072

52. Gainetdinov, R.R., Mohn, A.R., Caron, M.G., 2001. Genetic animal models: focus on schizophrenia. Trends Neurosci. 24, 527–533.

53. Gao, X., Harris, T.K., 2006. Role of the PH domain in regulating in vitro autophosphorylation events required for reconstitution of PDK1 catalytic activity. Bioorganic Chem. 34, 200–223. https://doi.org/10.1016/j.bioorg.2006.05.002

54. Gardener, M.J., Johnson, I.T., Burnham, M.P., Edwards, G., Heagerty, A.M., Weston, A.H., 2004. Functional evidence of a role for two-pore domain potassium channels in rat mesenteric and pulmonary arteries. Br. J. Pharmacol. 142, 192–202. https://doi.org/10.1038/sj.bjp.0705691

55. Georgiev, D., Arion, D., Enwright, J.F., Kikuchi, M., Minabe, Y., Corradi, J.P., Lewis, D.A., Hashimoto, T., 2014. Lower gene expression for KCNS3 potassium channel subunit in parvalbumin-containing neurons in the prefrontal cortex in schizophrenia. Am. J. Psychiatry 171, 62–71. https://doi.org/10.1176/appi.ajp.2013.13040468

56. Goldberg, A.B., Mazur, W., Kalra, D.K., 2017. Pulmonary hypertension: diagnosis, imaging techniques, and novel therapies. Cardiovasc. Diagn. Ther. 7, 405–417. https://doi.org/10.21037/cdt.2017.04.11

57. Goldstein, S.A., Bockenhauer, D., O'Kelly, I., Zilberberg, N., 2001. Potassium leak channels and the KCNK family of two-P-domain subunits. Nat. Rev. Neurosci. 2, 175–184. https://doi.org/10.1038/35058574

58. Gönczi, M., Szentandrássy, N., Johnson, I.T., Heagerty, A.M., Weston, A.H., 2006. Investigation of the role of TASK-2 channels in rat pulmonary arteries; pharmacological and functional studies following RNA interference procedures. Br. J. Pharmacol. 147, 496–505. https://doi.org/10.1038/sj.bjp.0706649

59. Goyal, P., Weissmann, N., Grimminger, F., Hegel, C., Bader, L., Rose, F., Fink, L., Ghofrani, H.A., Schermuly, R.T., Schmidt, H.H.H.W., Seeger, W., Hänze, J., 2004. Upregulation of NAD(P)H oxidase 1 in hypoxia activates hypoxia-inducible factor 1 via increase in reactive oxygen species. Free Radic. Biol. Med. 36, 1279–1288. https://doi.org/10.1016/j.freeradbiomed.2004.02.071

60. Graham, F.L., van der Eb, A.J., 1973. A new technique for the assay of infectivity of human adenovirus 5 DNA. Virology 52, 456–467. https://doi.org/10.1016/0042-6822(73)90341-3

61. Graham, V., Zhang, H., Willis, S., Creazzo, T.L., 2006. Expression of a two-pore domain K^+ channel (TASK-1) in developing avian and mouse ventricular conduction systems. Dev. Dyn. Off. Publ. Am. Assoc. Anat. 235, 143–151. https://doi.org/10.1002/dvdy.20558

62. Guignabert, C., Phan, C., Seferian, A., Huertas, A., Tu, L., Thuillet, R., Sattler, C., Le Hiress, M., Tamura, Y., Jutant, E.-M., Chaumais, M.-C., Bouchet, S., Manéglier, B., Molimard, M., Rousselot, P., Sitbon, O., Simonneau, G., Montani, D., Humbert, M., 2016. Dasatinib induces lung vascular toxicity and predisposes to pulmonary hypertension. J. Clin. Invest. 126, 3207–3218. https://doi.org/10.1172/JCI86249

63. Guignabert, C., Tu, L., Girerd, B., Ricard, N., Huertas, A., Montani, D., Humbert, M., 2015. New Molecular Targets of Pulmonary Vascular Remodeling in Pulmonary Arterial Hypertension. Chest 147, 529–537. https://doi.org/10.1378/chest.14-0862

64. Gurney, A.M., Joshi, S., 2006. The role of twin pore domain and other K^+ channels in hypoxic pulmonary vasoconstriction. Novartis Found. Symp. 272, 218-228-233, 274–279.

65. Gurney, A.M., Joshi, S., Manoury, B., 2010. KCNQ potassium channels: new targets for pulmonary vasodilator drugs? Adv. Exp. Med. Biol. 661, 405–417. https://doi.org/10.1007/978-1-60761-500-2_26

66. Gurney, A.M., Osipenko, O.N., MacMillan, D., McFarlane, K.M., Tate, R.J., Kempsill, F.E.J., 2003. Two-pore domain K channel, TASK-1, in pulmonary artery smooth muscle cells. Circ. Res. 93, 957–964. https://doi.org/10.1161/01.RES.0000099883.68414.61

67. Harrison, D.G., Gongora, M.C., Guzik, T.J., Widder, J., 2007. Oxidative stress and hypertension. J. Am. Soc. Hypertens. 1, 30–44. https://doi.org/10.1016/j.jash.2006.11.006

68. Herrington, J., Zhou, Y.-P., Bugianesi, R.M., Dulski, P.M., Feng, Y., Warren, V.A., Smith, M.M., Kohler, M.G., Garsky, V.M., Sanchez, M., Wagner, M., Raphaelli, K., Banerjee, P., Ahaghotu, C., Wunderler, D., Priest, B.T., Mehl, J.T., Garcia, M.L., McManus, O.B., Kaczorowski, G.J., Slaughter, R.S., 2006. Blockers of the delayed-rectifier potassium current in pancreatic beta-cells enhance glucose-dependent insulin secretion. Diabetes 55, 1034–1042.

69. Hoshi, T., Zagotta, W.N., Aldrich, R.W., 1991. Two types of inactivation in Shaker K^+ channels: effects of alterations in the carboxy-terminal region. Neuron 7, 547–556.

70. Hossain, S., Ahmed, M.U., Alam, S., Watanabe, A., Harashima, A., Yonekura, H., Yamamoto, H., 2011. Expression and Roles of AMIGO Gene Family in Vascular Endothelial Cells. Int. J. Mol. Med. Adv. Sci. 7, 5–11. https://doi.org/10.3923/ijmmas.2011.5.11

71. Hristov, K.L., Chen, M., Soder, R.P., Parajuli, S.P., Cheng, Q., Kellett, W.F., Petkov, G.V., 2012. KV2.1 and electrically silent KV channel subunits control excitability and contractility of guinea pig detrusor smooth muscle. AJP Cell Physiol. 302, C360–C372. https://doi.org/10.1152/ajpcell.00303.2010

72. Huang, C.-H., Pei, J.-C., Luo, D.-Z., Chen, C., Chen, Y.-W., Lai, W.-S., 2014. Investigation of gene effects and epistatic interactions between Akt1 and neuregulin 1 in the regulation of behavioral phenotypes and social functions in genetic mouse models of schizophrenia. Front. Behav. Neurosci. 8, 455. https://doi.org/10.3389/fnbeh.2014.00455

73. Huang, J., Liu, Y., Sun, P., Lv, X., Bo, K., Fan, X., 2010. Novel Strategy for Treatment of Pulmonary Arterial Hypertension: Enhancement of Apoptosis. Lung 188, 179–189. https://doi.org/10.1007/s00408-010-9233-8

74. Huffaker, S.J., Chen, J., Nicodemus, K.K., Sambataro, F., Yang, F., Mattay, V., Lipska, B.K., Hyde, T.M., Song, J., Rujescu, D., Giegling, I., Mayilyan, K., Proust, M.J., Soghoyan, A., Caforio, G., Callicott, J.H., Bertolino, A., Meyer-Lindenberg, A., Chang, J., Ji, Y., Egan, M.F., Goldberg, T.E., Kleinman, J.E., Lu, B., Weinberger, D.R., 2009. A primate-specific, brain isoform of KCNH2 affects cortical physiology, cognition, neuronal repolarization and risk of schizophrenia. Nat. Med. 15, 509–518. https://doi.org/10.1038/nm.1962

75. Hulme, J.T., Coppock, E.A., Felipe, A., Martens, J.R., Tamkun, M.M., 1999. Oxygen Sensitivity of Cloned Voltage-Gated K^+ Channels Expressed in the Pulmonary Vasculature. Circ. Res. 85, 489–497. https://doi.org/10.1161/01.RES.85.6.489

76. Humbert, M., Sitbon, O., Simonneau, G., 2004. Treatment of Pulmonary Arterial Hypertension. N. Engl. J. Med. 351, 1425–1436. https://doi.org/10.1056/NEJMra040291

77. Jiang, Y., Lee, A., Chen, J., Cadene, M., Chait, B.T., MacKinnon, R., 2002. The open pore conformation of potassium channels. Nature 417, 523–526. https://doi.org/10.1038/417523a

78. Jones, S.A., Morton, M.J., Hunter, M., Boyett, M.R., 2002. Expression of TASK-1, a pH-sensitive twin-pore domain K^+ channel, in rat myocytes. Am. J. Physiol. - Heart Circ. Physiol. 283, H181–H185. https://doi.org/10.1152/ajpheart.00963.2001

79. Kajander, T., Kuja-Panula, J., Rauvala, H., Goldman, A., 2011. Crystal structure and role of glycans and dimerization in folding of neuronal leucine-rich repeat protein AMIGO-1. J. Mol. Biol. 413, 1001–1015. https://doi.org/10.1016/j.jmb.2011.09.032

80. Kerschensteiner, D., 2003. Structural Determinants of the Regulation of the Voltage-gated Potassium Channel Kv2.1 by the Modulatory alpha -Subunit Kv9.3. J. Biol. Chem. 278, 18154–18161. https://doi.org/10.1074/jbc.M213117200

81. Kerschensteiner, D., Soto, F., Stocker, M., 2005. Fluorescence measurements reveal stoichiometry of K^+ channels formed by modulatory and delayed rectifier alpha-subunits. Proc. Natl. Acad. Sci. U. S. A. 102, 6160–6165. https://doi.org/10.1073/pnas.0500468102

82. Kerschensteiner, D., Stocker, M., 1999. Heteromeric assembly of Kv2.1 with Kv9.3: effect on the state dependence of inactivation. Biophys. J. 77, 248–257. https://doi.org/10.1016/S0006-3495(99)76886-4

83. Ketchum, K.A., Joiner, W.J., Sellers, A.J., Kaczmarek, L.K., Goldstein, S.A.N., 1995. A new family of outwardly rectifying potassium channel proteins with two pore domains in tandem. Nature 376, 690–695. https://doi.org/10.1038/376690a0

84. Kim, H., Yung, G.L., Marsh, J.J., Konopka, R.G., Pedersen, C.A., Chiles, P.G., Morris, T.A., Channick, R.N., 2000. Endothelin mediates pulmonary vascular remodelling in a canine model of chronic embolic pulmonary hypertension. Eur. Respir. J. 15, 640–648.

85. Kim, H.-Y., 2015. Statistical notes for clinical researchers: *post-hoc* multiple comparisons. Restor. Dent. Endod. 40, 172. https://doi.org/10.5395/rde.2015.40.2.172

86. Kim, Y., Bang, H., Kim, D., 2000. TASK-3, a new member of the tandem pore K^+ channel family. J. Biol. Chem. 275, 9340–9347.

87. Kim, Y., Bang, H., Kim, D., 1999. TBAK-1 and TASK-1, two-pore K^+ channel subunits: kinetic properties and expression in rat heart. Am. J. Physiol. 277, H1669-1678.

88. Ko, E.A., Park, W.S., Firth, A.L., Kim, N., Yuan, J.X.-J., Han, J., 2010. Pathophysiology of voltage-gated K^+ channels in vascular smooth muscle cells: Modulation by protein kinases. Prog. Biophys. Mol. Biol. 103, 95–101. https://doi.org/10.1016/j.pbiomolbio.2009.10.001

89. Koh, S.D., Ward, S.M., Dick, G.M., Epperson, A., Bonner, H.P., Sanders, K.M., Horowitz, B., Kenyon, J.L., 1999. Contribution of delayed rectifier potassium currents to the electrical activity of murine colonic smooth muscle. J. Physiol. 515 (Pt 2), 475–487.

90. Kuhr, F.K., Smith, K.A., Song, M.Y., Levitan, I., Yuan, J.X.-J., 2012. New mechanisms of pulmonary arterial hypertension: role of Ca^{2+} signaling. Am. J. Physiol. Heart Circ. Physiol. 302, H1546-1562. https://doi.org/10.1152/ajpheart.00944.2011

91. Kuja-Panula, J., Kiiltomäki, M., Yamashiro, T., Rouhiainen, A., Rauvala, H., 2003. AMIGO, a transmembrane protein implicated in axon tract development, defines a novel protein family with leucine-rich repeats. J. Cell Biol. 160, 963–973. https://doi.org/10.1083/jcb.200209074

92. Kumari, V., Sharma, T., 2002. Effects of typical and atypical antipsychotics on prepulse inhibition in schizophrenia: a critical evaluation of current evidence and directions for future research. Psychopharmacology (Berl.) 162, 97–101. https://doi.org/10.1007/s00213-002-1099-x

93. Laeremans, A., Nys, J., Luyten, W., D'Hooge, R., Paulussen, M., Arckens, L., 2013. AMIGO2 mRNA expression in hippocampal CA2 and CA3a. Brain Struct. Funct. 218, 123–130. https://doi.org/10.1007/s00429-012-0387-4

94. Lee, D.-Y., Wauquier, F., Eid, A.A., Roman, L.J., Ghosh-Choudhury, G., Khazim, K., Block, K., Gorin, Y., 2013. Nox4 NADPH Oxidase Mediates Peroxynitrite-dependent Uncoupling of Endothelial Nitric-oxide Synthase and Fibronectin Expression in Response to Angiotensin II: Role of Mitochondrial Reactive Oxygen Species. J. Biol. Chem. 288, 28668–28686. https://doi.org/10.1074/jbc.M113.470971

95. Lee, Y.-M., Kim, B.-J., Chun, Y.-S., So, I., Choi, H., Kim, M.-S., Park, J.-W., 2006. NOX4 as an oxygen sensor to regulate TASK-1 activity. Cell. Signal. 18, 499–507. https://doi.org/10.1016/j.cellsig.2005.05.025

96. Leithner, K., Hirschmugl, B., Li, Y., Tang, B., Papp, R., Nagaraj, C., Stacher, E., Stiegler, P., Lindenmann, J., Olschewski, A., Olschewski, H., Hrzenjak, A., 2016. TASK-1 Regulates Apoptosis and Proliferation in a Subset of Non-Small Cell Lung Cancers. PLOS ONE 11, e0157453. https://doi.org/10.1371/journal.pone.0157453

97. Leonoudakis, D., Gray, A.T., Winegar, B.D., Kindler, C.H., Harada, M., Taylor, D.M., Chavez, R.A., Forsayeth, J.R., Yost, C.S., 1998. An open rectifier potassium channel with two pore domains in tandem cloned from rat cerebellum. J. Neurosci. Off. J. Soc. Neurosci. 18, 868–877.

98. Levitan, I.B., 2002. The neuron: cell and molecular biology, 3rd ed. ed. Oxford University Press, Oxford; New York.

99. Levitan, I.B., Kaczmarek, L.K., 2002. The Neuron: cell and molecular biology. Oxford University Press, New York.

100. Li, X.T., Dyachenko, V., Zuzarte, M., Putzke, C., Preisig-Müller, R., Isenberg, G., Daut, J., 2006. The stretch-activated potassium channel TREK-1 in rat cardiac ventricular muscle. Cardiovasc. Res. 69, 86–97. https://doi.org/10.1016/j.cardiores.2005.08.018

101. Liu, W., Ahmad, S.A., Reinmuth, N., Shaheen, R.M., Jung, Y.D., Fan, F., Ellis, L.M., 2000. Endothelial cell survival and apoptosis in the tumor vasculature. Apoptosis Int. J. Program. Cell Death 5, 323–328.

102. Liu, W., Saint, D.A., 2004. Heterogeneous expression of tandem-pore K^+ channel genes in adult and embryonic rat heart quantified by real-time polymerase chain reaction. Clin. Exp. Pharmacol. Physiol. 31, 174–178.

103. Lopes, C.M.B., Rohács, T., Czirják, G., Balla, T., Enyedi, P., Logothetis, D.E., 2005. PIP $_2$ hydrolysis underlies agonist-induced inhibition and regulates voltage gating of two-pore domain K^+ channels: PIP $_2$ regulation of two-pore domain K^+ channels. J. Physiol. 564, 117–129. https://doi.org/10.1113/jphysiol.2004.081935

104. Lotshaw, D.P., 2007. Biophysical, pharmacological, and functional characteristics of cloned and native mammalian two-pore domain K^+ channels. Cell Biochem. Biophys. 47, 209–256. https://doi.org/10.1007/s12013-007-0007-8

105. Ma, L., Chung, W.K., 2017. The role of genetics in pulmonary arterial hypertension: Genetics of pulmonary arterial hypertension. J. Pathol. 241, 273–280. https://doi.org/10.1002/path.4833

106. Ma, L., Roman-Campos, D., Austin, E.D., Eyries, M., Sampson, K.S., Soubrier, F., Germain, M., Trégouët, D.-A., Borczuk, A., Rosenzweig, E.B., Girerd, B., Montani, D., Humbert, M., Loyd, J.E., Kass, R.S., Chung, W.K., 2013. A Novel Channelopathy in Pulmonary Arterial Hypertension. N. Engl. J. Med. 369, 351–361. https://doi.org/10.1056/NEJMoa1211097

107. Mafune, K., Ravikumar, T.S., 1992. Anti-sense RNA of 32-kDa laminin-binding protein inhibits attachment and invasion of a human colon carcinoma cell line. J. Surg. Res. 52, 340–346.

108. Maingret, F., 2001. The endocannabinoid anandamide is a direct and selective blocker of the background K^+ channel TASK-1. EMBO J. 20, 47–54. https://doi.org/10.1093/emboj/20.1.47

109. Mathie, A., Al-Moubarak, E., Veale, E.L., 2010a. Gating of two pore domain potassium channels: Gating of K2P channels. J. Physiol. 588, 3149–3156. https://doi.org/10.1113/jphysiol.2010.192344

110. Mathie, A., Rees, K.A., El Hachmane, M.F., Veale, E.L., 2010b. Trafficking of neuronal two pore domain potassium channels. Curr. Neuropharmacol. 8, 276–286. https://doi.org/10.2174/157015910792246146

111. Meloche, J., Le Guen, M., Potus, F., Vinck, J., Ranchoux, B., Johnson, I., Antigny, F., Tremblay, E., Breuils-Bonnet, S., Perros, F., Provencher, S., Bonnet, S., 2015. miR-223 reverses experimental pulmonary arterial hypertension. Am. J. Physiol. - Cell Physiol. 309, C363–C372. https://doi.org/10.1152/ajpcell.00149.2015

112. Mittal, M., Gu, X.Q., Pak, O., Pamenter, M.E., Haag, D., Fuchs, D.B., Schermuly, R.T., Ghofrani, H.A., Brandes, R.P., Seeger, W., Grimminger, F., Haddad, G.G., Weissmann, N., 2012. Hypoxia induces Kv channel current inhibition by increased NADPH oxidase-derived reactive oxygen species. Free Radic. Biol. Med. 52, 1033–1042. https://doi.org/10.1016/j.freeradbiomed.2011.12.004

113. Mittal, M., Roth, M., Konig, P., Hofmann, S., Dony, E., Goyal, P., Selbitz, A.-C., Schermuly, R.T., Ghofrani, H.A., Kwapiszewska, G., Kummer, W., Klepetko, W., Hoda, M.A.R., Fink, L., Hanze, J., Seeger, W., Grimminger, F., Schmidt, H.H.H.W., Weissmann, N., 2007. Hypoxia-Dependent Regulation of Nonphagocytic NADPH Oxidase Subunit NOX4 in the Pulmonary Vasculature. Circ. Res. 101, 258–267. https://doi.org/10.1161/CIRCRESAHA.107.148015

114. Modun, D., Giustarini, D., Tsikas, D., 2014. Nitric Oxide-related Oxidative Stress and Redox Status in Health and Disease. Oxidative Med and Cellular Longevity. 2014, 1-3. http://dx.doi.org/10.1155/2014/129651

115. Morales, M.J., Wee, J.O., Wang, S., Strauss, H.C., Rasmusson, R.L., 1996. The N-terminal domain of a K^+ channel beta subunit increases the rate of C-type inactivation from the cytoplasmic side of the channel. Proc. Natl. Acad. Sci. U. S. A. 93, 15119–15123.

116. Morrell, N.W., Adnot, S., Archer, S.L., Dupuis, J., Lloyd Jones, P., MacLean, M.R., McMurtry, I.F., Stenmark, K.R., Thistlethwaite, P.A., Weissmann, N., Yuan, J.X.-J., Weir, E.K., 2009. Cellular and Molecular Basis of Pulmonary Arterial Hypertension. J. Am. Coll. Cardiol. 54, S20–S31. https://doi.org/10.1016/j.jacc.2009.04.018

117. Moudgil, R., Michelakis, E.D., Archer, S.L., 2006. The role of K^+ channels in determining pulmonary vascular tone, oxygen sensing, cell proliferation, and apoptosis: implications in hypoxic pulmonary vasoconstriction and pulmonary arterial hypertension. Microcirc. N. Y. N 1994 13, 615–632. https://doi.org/10.1080/10739680600930222

118. Musacchio, M., Perrimon, N., 1996. The Drosophila kekkon genes: novel members of both the leucine-rich repeat and immunoglobulin superfamilies expressed in the CNS. Dev. Biol. 178, 63–76. https://doi.org/10.1006/dbio.1996.0198

119. Nagaraj, C., Tang, B., Balint, Z., Wygrecka, M., Hrzenjak, A., Kwapiszewska, G., Stacher, E., Lindenmann, J., Weir, E.K., Olschewski, H., Olschewski, A., 2013. Src tyrosine kinase is crucial for potassium channel function in human pulmonary arteries. Eur. Respir. J. 41, 85–95. https://doi.org/10.1183/09031936.00211811

120. Navas Tejedor, P., Tenorio Castaño, J., Palomino Doza, J., Arias Lajara, P., Gordo Trujillo, G., López Meseguer, M., Román Broto, A., Lapunzina Abadía, P., Escribano Subía, P., 2017. An homozygous mutation in *KCNK3* is associated with an aggressive form of hereditary pulmonary arterial hypertension: Homozygous mutation in *KCNK3*. Clin. Genet. 91, 453–457. https://doi.org/10.1111/cge.12869

121. Neher, E., Marty, A., 1982. Discrete changes of cell membrane capacitance observed under conditions of enhanced secretion in bovine adrenal chromaffin cells. Proc. Natl. Acad. Sci. U. S. A. 79, 6712–6716.

122. Nielsen, G., Wandall-Frostholm, C., Sadda, V., Oliván-Viguera, A., Lloyd, E.E., Bryan, R.M., Jr, Simonsen, U., Köhler, R., 2013. Alterations of N-3 polyunsaturated fatty acid-activated K2P channels in hypoxia-induced pulmonary hypertension. Basic Clin. Pharmacol. Toxicol. 113, 250–258. https://doi.org/10.1111/bcpt.12092

123. Nieves-Cintrón, M., Nystoriak, M.A., Prada, M.P., Johnson, K., Fayer, W., Dell'Acqua, M.L., Scott, J.D., Navedo, M.F., 2015. Selective Down-regulation of K $_{V}$ 2.1 Function Contributes to Enhanced Arterial Tone during Diabetes. J. Biol. Chem. 290, 7918–7929. https://doi.org/10.1074/jbc.M114.622811

124. Nisimoto, Y., Diebold, B.A., Cosentino-Gomes, D., Lambeth, J.D., 2014. Nox4: A Hydrogen Peroxide-Generating Oxygen Sensor. Biochemistry (Mosc.) 53, 5111–5120. https://doi.org/10.1021/bi500331y

125. O'Kelly, I., Goldstein, S.A.N., 2008. Forward Transport of K2p3.1: mediation by 14-3-3 and COPI, modulation by p11. Traffic Cph. Den. 9, 72–78. https://doi.org/10.1111/j.1600-0854.2007.00663.x

126. Olschewski, A., Li, Y., Tang, B., Hanze, J., Eul, B., Bohle, R.M., Wilhelm, J., Morty, R.E., Brau, M.E., Weir, E.K., Kwapiszewska, G., Klepetko, W., Seeger, W., Olschewski, H., 2006. Impact of TASK-1 in human pulmonary artery smooth muscle cells. Circ. Res. 98, 1072–1080. https://doi.org/10.1161/01.RES.0000219677.12988.e9

127. Olschewski, A., Papp, R., Nagaraj, C., Olschewski, H., 2014. Ion channels and transporters as therapeutic targets in the pulmonary circulation. Pharmacol. Ther. 144, 349–368. https://doi.org/10.1016/j.pharmthera.2014.08.001

128. Ono, T., Sekino-Suzuki, N., Kikkawa, Y., Yonekawa, H., Kawashima, S., 2003. Alivin 1, a novel neuronal activity-dependent gene, inhibits apoptosis and promotes survival of cerebellar granule neurons. J. Neurosci. Off. J. Soc. Neurosci. 23, 5887–5896.

129. Owen, G.R., Hakkinen, L., Wu, C., Larjava, H., 2009. A reproducible technique for specific labeling of antigens using preformed fluorescent molecular IgG-F(ab′) 2 complexes from primary antibodies of the same species. Microsc. Res. Tech. NA-NA. https://doi.org/10.1002/jemt.20803

130. Palencia-Desai, S., Rost, M.S., Schumacher, J.A., Ton, Q.V., Craig, M.P., Baltrunaite, K., Koenig, A.L., Wang, J., Poss, K.D., Chi, N.C., Stainier, D.Y.R., Sumanas, S., 2015. Myocardium and BMP signaling are required for endocardial differentiation. Development 142, 2304–2315. https://doi.org/10.1242/dev.118687

131. Papaleo, F., Lipska, B.K., Weinberger, D.R., 2012. Mouse models of genetic effects on cognition: relevance to schizophrenia. Neuropharmacology 62, 1204–1220. https://doi.org/10.1016/j.neuropharm.2011.04.025

132. Park, H., Lee, S., Shrestha, P., Kim, J., Park, J.A., Ko, Y., Ban, Y.H., Park, D.-Y., Ha, S.-J., Koh, G.Y., Hong, V.S., Mochizuki, N., Kim, Y.-M., Lee, W., Kwon, Y.-G., 2015. AMIGO2, a novel membrane anchor of PDK1, controls cell survival and angiogenesis via Akt activation. J. Cell Biol. 211, 619–637. https://doi.org/10.1083/jcb.201503113

133. Park, M.K., Bae, Y.M., Lee, S.H., Ho, W.-K., Earm, Y.E., 1997a. Modulation of voltage-dependent K^+ channel by redox potential in pulmonary and ear arterial smooth muscle cells of the rabbit. Pflugers Arch. 434, 764–771. https://doi.org/10.1007/s004240050463

134. Park, S.W., Noh, H.J., Sung, D.J., Kim, J.G., Kim, J.M., Ryu, S.Y., Kang, K.J., Kim, B., Bae, Y.M., Cho, H., 2015. Hydrogen peroxide induces vasorelaxation by enhancing 4-aminopyridine-sensitive Kv currents through S-glutathionylation. Pflüg. Arch. - Eur. J. Physiol. 467, 285–297. https://doi.org/10.1007/s00424-014-1513-3

135. Park, W.S., Firth, A.L., Han, J., Ko, E.A., 2010. Patho-, physiological roles of voltage-dependent K^+ channels in pulmonary arterial smooth muscle cells. J. Smooth Muscle Res. Nihon Heikatsukin Gakkai Kikanshi 46, 89–105.

136. Patel, A.J., Honoré, E., 2001. Molecular physiology of oxygen-sensitive potassium channels. Eur. Respir. J. 18, 221–227.

137. Patel, A.J., Lazdunski, M., Honoré, E., 1999. Kv2.1/Kv9.3, an ATP-dependent delayed-rectifier K^+ channel in pulmonary artery myocytes. Ann. N. Y. Acad. Sci. 868, 438–441.

138. Patel, A.J., Lazdunski, M., Honoré, E., 1997. Kv2.1/Kv9.3, a novel ATP-dependent delayed-rectifier K^+ channel in oxygen-sensitive pulmonary artery myocytes. EMBO J. 16, 6615–6625. https://doi.org/10.1093/emboj/16.22.6615

139. Peers, C., Boyle, J.P., 2015. Oxidative Modulation of K^+ Channels in the Central Nervous System in Neurodegenerative Diseases and Aging. Antioxid. Redox Signal. 22, 505–521. https://doi.org/10.1089/ars.2014.6007

140. Peltola, M.A., Kuja-Panula, J., Lauri, S.E., Taira, T., Rauvala, H., 2011. AMIGO is an auxiliary subunit of the Kv2.1 potassium channel. EMBO Rep. 12, 1293–1299. https://doi.org/10.1038/embor.2011.204

141. Peltola, M.A., Kuja-Panula, J., Liuhanen, J., Võikar, V., Piepponen, P., Hiekkalinna, T., Taira, T., Lauri, S.E., Suvisaari, J., Kulesskaya, N., Paunio, T., Rauvala, H., 2016. AMIGO-Kv2.1 Potassium Channel Complex Is Associated with Schizophrenia-Related Phenotypes. Schizophr. Bull. 42, 191–201. https://doi.org/10.1093/schbul/sbv105

142. Pérez-García, M.T., López-López, J.R., 2000. Are Kv channels the essence of O_2 sensing? Circ. Res. 86, 490–491.

143. Perez-Vizcaino, F., Cogolludo, A., Moreno, L., 2010. Reactive oxygen species signaling in pulmonary vascular smooth muscle. Respir. Physiol. Neurobiol. 174, 212–220. https://doi.org/10.1016/j.resp.2010.08.009

144. Platoshyn, O., Remillard, C.V., Fantozzi, I., Mandegar, M., Sison, T.T., Zhang, S., Burg, E., Yuan, J.X.-J., 2004. Diversity of voltage-dependent K^+ channels in human pulmonary artery smooth muscle cells. Am. J. Physiol. Lung Cell. Mol. Physiol. 287, L226-238. https://doi.org/10.1152/ajplung.00438.2003

145. Powell, S.B., Weber, M., Geyer, M.A., 2012. Genetic models of sensorimotor gating: relevance to neuropsychiatric disorders. Curr. Top. Behav. Neurosci. 12, 251–318. https://doi.org/10.1007/7854_2011_195

146. Prasad, M., Goyal, R.K., 2004. Differential modulation of voltage-dependent K^+ currents in colonic smooth muscle by oxidants. AJP Cell Physiol. 286, 671C–682. https://doi.org/10.1152/ajpcell.00137.2003

147. Putzke, C., Hanley, P.J., Schlichthörl, G., Preisig-Müller, R., Rinné, S., Anetseder, M., Eckenhoff, R., Berkowitz, C., Vassiliou, T., Wulf, H., Eberhart, L., 2007. Differential effects of volatile and intravenous anesthetics on the activity of human TASK-1. Am. J. Physiol. Cell Physiol. 293, C1319-1326. https://doi.org/10.1152/ajpcell.00100.2007

148. Rabenau, K.E., O'Toole, J.M., Bassi, R., Kotanides, H., Witte, L., Ludwig, D.L., Pereira, D.S., 2004. DEGA/AMIGO-2, a leucine-rich repeat family member, differentially expressed in human gastric adenocarcinoma: effects on ploidy, chromosomal stability, cell adhesion/migration and tumorigenicity. Oncogene 23, 5056–5067. https://doi.org/10.1038/sj.onc.1207681

149. Rabinovitch, M., 2008. Molecular pathogenesis of pulmonary arterial hypertension. J. Clin. Invest. 118, 2372–2379. https://doi.org/10.1172/JCI33452

150. Rajan, S., Wischmeyer, E., Xin Liu, G., Preisig-Müller, R., Daut, J., Karschin, A., Derst, C., 2000. TASK-3, a novel tandem pore domain acid-sensitive K^+ channel. An extracellular histiding as pH sensor. J. Biol. Chem. 275, 16650–16657. https://doi.org/10.1074/jbc.M000030200

151. Ravens, U., Wang, X.L., Wettwer, E., 1989. Alpha adrenoceptor stimulation reduces outward currents in rat ventricular myocytes. J. Pharmacol. Exp. Ther. 250, 364–370.

152. Reid, J.D., Lukas, W., Shafaatian, R., Bertl, A., Scheurmann-Kettner, C., Guy, H.R., North, R.A., 1996. The *S. cerevisiae* outwardly-rectifying potassium channel (DUK1) identifies a new family of channels with duplicated pore domains. Receptors Channels 4, 51–62.

153. Richardson, F.C., Kaczmarek, L.K., 2000. Modification of delayed rectifier potassium currents by the Kv9.1 potassium channel subunit. Hear. Res. 147, 21–30.

154. Sekar, R.B., Periasamy, A., 2003. Fluorescence resonance energy transfer (FRET) microscopy imaging of live cell protein localizations. J. Cell Biol. 160, 629–633. https://doi.org/10.1083/jcb.200210140

155. Shepard, A.R., Rae, J.L., 1999. Electrically silent potassium channel subunits from human lens epithelium. Am. J. Physiol. 277, C412-424.

156. Shiau, Y.-S., Huang, P.-T., Liou, H.-H., Liaw, Y.-C., Shiau, Y.-Y., Lou, K.-L., 2003. Structural Basis of Binding and Inhibition of Novel Tarantula Toxins in Mammalian Voltage-Dependent Potassium Channels. Chem. Res. Toxicol. 16, 1217–1225. https://doi.org/10.1021/tx0341097

157. Speca, D.J., Ogata, G., Mandikian, D., Bishop, H.I., Wiler, S.W., Eum, K., Wenzel, H.J., Doisy, E.T., Matt, L., Campi, K.L., Golub, M.S., Nerbonne, J.M., Hell, J.W., Trainor, B.C., Sack, J.T., Schwartzkroin, P.A., Trimmer, J.S., 2014. Deletion of the Kv2.1 delayed rectifier potassium channel leads to neuronal and behavioral hyperexcitability: Kv2.1 deletion and hyperexcitability. Genes Brain Behav. 13, 394–408. https://doi.org/10.1111/gbb.12120

158. Standen, Quayle, 1998. K^+ channel modulation in arterial smooth muscle: K^+ channel modulation in arteries. Acta Physiol. Scand. 164, 549–557. https://doi.org/10.1046/j.1365-201X.1998.00433.x

159. Suh, J., Foster, D.J., Davoudi, H., Wilson, M.A., Tonegawa, S., 2013. Impaired hippocampal ripple-associated replay in a mouse model of schizophrenia. Neuron 80, 484–493. https://doi.org/10.1016/j.neuron.2013.09.014

160. Suvorava, T., 2005. Endogenous Vascular Hydrogen Peroxide Regulates Arteriolar Tension In Vivo. Circulation 112, 2487–2495. https://doi.org/10.1161/CIRCULATIONAHA.105.543157

161. Talley, E.M., Bayliss, D.A., 2002. Modulation of TASK-1 (Kcnk3) and TASK-3 (Kcnk9) potassium channels: volatile anesthetics and neurotransmitters share a molecular site of action. J. Biol. Chem. 277, 17733–17742. https://doi.org/10.1074/jbc.M200502200

162. Tanaka, H., Habuchi, Y., Nishio, M., Suto, F., Yoshimura, M., 1998. Modulation by chloramine-T of 4-aminopyridine-sensitive transient outward current in rabbit atrial cells. Eur. J. Pharmacol. 358, 85–92.

163. Tang, B., Li, Y., Nagaraj, C., Morty, R.E., Gabor, S., Stacher, E., Voswinckel, R., Weissmann, N., Leithner, K., Olschewski, H., Olschewski, A., 2009. Endothelin-1 Inhibits Background Two-Pore Domain Channel TASK-1 in Primary Human Pulmonary Artery Smooth Muscle Cells. Am. J. Respir. Cell Mol. Biol. 41, 476–483. https://doi.org/10.1165/rcmb.2008-0412OC

164. Tannoury, C.A., An, H.S., 2014. Complications with the use of bone morphogenetic protein 2 (BMP-2) in spine surgery. Spine J. 14, 552–559. https://doi.org/10.1016/j.spinee.2013.08.060

165. Thomas, P., Smart, T.G., 2005. HEK293 cell line: A vehicle for the expression of recombinant proteins. J. Pharmacol. Toxicol. Methods 51, 187–200. https://doi.org/10.1016/j.vascn.2004.08.014

166. Too, L.K., Ball, H.J., McGregor, I.S., Hunt, N.H., 2014. A novel automated test battery reveals enduring behavioural alterations and cognitive impairments in survivors of murine pneumococcal meningitis. Brain. Behav. Immun. 35, 107–124. https://doi.org/10.1016/j.bbi.2013.09.007

167. Touyz, R.M., 2004. Reactive Oxygen Species, Vascular Oxidative Stress, and Redox Signaling in Hypertension: What Is the Clinical Significance? Hypertension 44, 248–252. https://doi.org/10.1161/01.HYP.0000138070.47616.9d

168. Tsantoulas, C., Zhu, L., Yip, P., Grist, J., Michael, G.J., McMahon, S.B., 2014. Kv2 dysfunction after peripheral axotomy enhances sensory neuron responsiveness to sustained input. Exp. Neurol. 251, 115–126. https://doi.org/10.1016/j.expneurol.2013.11.011

169. Veale, E.L., Buswell, R., Clarke, C.E., Mathie, A., 2007. Identification of a region in the TASK3 two pore domain potassium channel that is critical for its blockade by methanandamide. Br. J. Pharmacol. 152, 778–786. https://doi.org/10.1038/sj.bjp.0707436

170. Ward, J.P., McMurtry, I.F., 2009. Mechanisms of hypoxic pulmonary vasoconstriction and their roles in pulmonary hypertension: new findings for an old problem. Curr. Opin. Pharmacol. 9, 287–296. https://doi.org/10.1016/j.coph.2009.02.006

171. Whitford, K.L., Marillat, V., Stein, E., Goodman, C.S., Tessier-Lavigne, M., Chédotal, A., Ghosh, A., 2002. Regulation of cortical dendrite development by Slit-Robo interactions. Neuron 33, 47–61.

172. Yellen, G., 2002. The voltage-gated potassium channels and their relatives. Nature 419, 35–42. https://doi.org/10.1038/nature00978

173. Yu, W., Parakramaweera, R., Teng, S., Gowda, M., Sharad, Y., Thakker-Varia, S., Alder, J., Sesti, F., 2016. Oxidation of KCNB1 Potassium Channels Causes Neurotoxicity and Cognitive Impairment in a Mouse Model of Traumatic Brain Injury. J. Neurosci. 36, 11084–11096. https://doi.org/10.1523/JNEUROSCI.2273-16.2016

174. Yuill, K.H., Stansfeld, P.J., Ashmole, I., Sutcliffe, M.J., Stanfield, P.R., 2007. The selectivity, voltage-dependence and acid sensitivity of the tandem pore potassium channel TASK-1: contributions of the pore domains. Pflugers Arch. 455, 333–348. https://doi.org/10.1007/s00424-007-0282-7

175. Zhao, X., Kuja-Panula, J., Sundvik, M., Chen, Y.-C., Aho, V., Peltola, M.A., Porkka-Heiskanen, T., Panula, P., Rauvala, H., 2014. Amigo adhesion protein regulates development of neural circuits in zebrafish brain. J. Biol. Chem. 289, 19958–19975. https://doi.org/10.1074/jbc.M113.545582

176. Zhong, X.Z., Abd-Elrahman, K.S., Liao, C.-H., El-Yazbi, A.F., Walsh, E.J., Walsh, M.P., Cole, W.C., 2010. Stromatoxin-sensitive, heteromultimeric Kv2.1/Kv9.3 channels contribute to myogenic control of cerebral arterial diameter: Heteromultimeric Kv2.1/Kv9.3 channels and cerebral myogenic response. J. Physiol. 588, 4519–4537. https://doi.org/10.1113/jphysiol.2010.196618

177. Zhu, H.-L., Brain, K.L., Aishima, M., Shibata, A., Young, J.S., Sueishi, K., Teramoto, N., 2008. Actions of two main metabolites of propiverine (M-1 and M-2) on voltage-dependent L-type Ca^{2+} currents and Ca^{2+} transients in murine urinary bladder myocytes. J. Pharmacol. Exp. Ther. 324, 118–127. https://doi.org/10.1124/jpet.107.130021

178. Zuzarte, M., Heusser, K., Renigunta, V., Schlichthörl, G., Rinné, S., Wischmeyer, E., Daut, J., Schwappach, B., Preisig-Müller, R., 2009. Intracellular traffic of the K^+ channels TASK-1 and TASK-3: role of N- and C-terminal sorting signals and interaction with 14-3-3 proteins: Intracellular traffic of TASK-1 and TASK-3. J. Physiol. 587, 929–952. https://doi.org/10.1113/jphysiol.2008.164756

Appendix

1) Subset of data supporting the notion that Kv2.1/Nox4 behaves similarly to Kv2.1 and Kv2.1/Kv9.3/Nox4 to Kv2.1/Kv9.3

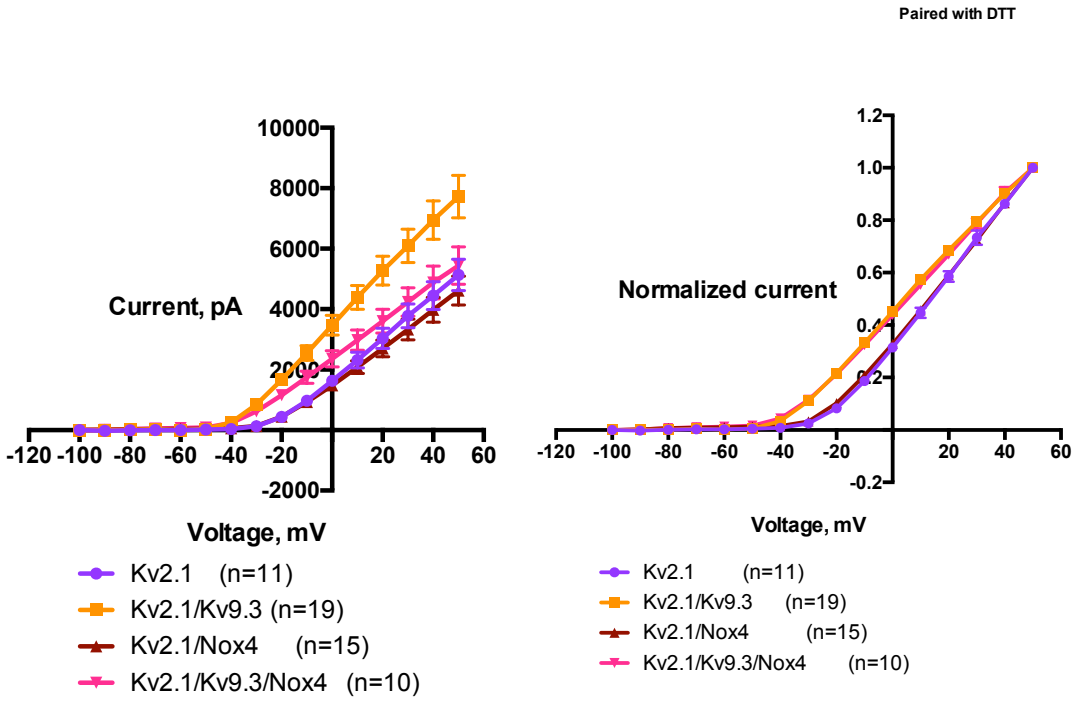

Figure 8.1: Absolute current of the cells without DTT (Left) and the normalized current for assessing the activation thresholds of cells without DTT (Right). The results are from cells that are perfused with external solution before being perfused with DTT.

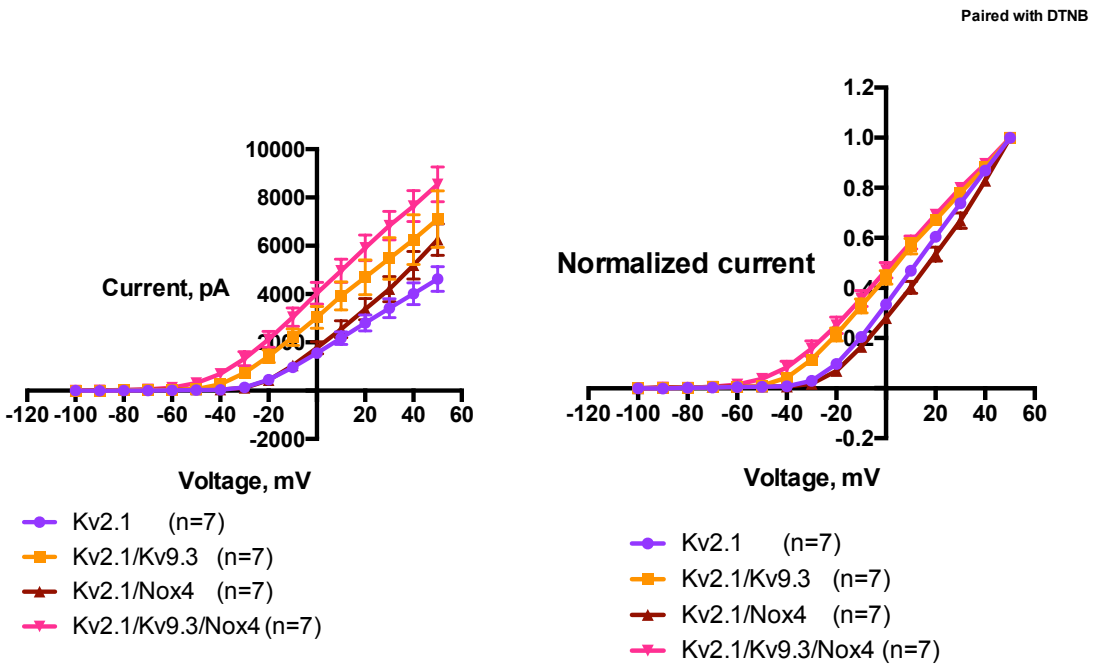

Figure 8.2: Absolute current for the cells without DTNB (Left) and Activation thresholds of the cells without DTNB (Right). The results are from cells that are perfused with external solution before being perfused with DTNB.

2) Relationship of AMIGO2 with PDK1 and Akt to control cell proliferation

AMIGO2 is important in forming an extracellular matrix on the cell membrane, which then causes PDK1 to be recruited to the surface and docked on the matrix (H. Park et al., 2015). PDK1 then binds to the secondary messenger, PIP_3, at its pleckstrin homology domain (H. Park et al., 2015). According to Gao and Harris, 2006, the autophosphorylation of PDK1 at serine 241 within the catalytic domain can be inhibited easily by the pleckstrin homology domain that is not bound to PIP3 (Gao and Harris, 2006). The PDK1-PIP_3 interaction allows trans-phosphorylation of PDK1 at threonine 513 within the PH domain which destabilizes the 'autoinhibition' conformation and thus permitting the protein to activate Akt. In endothelial cells where AMIGO2 is silenced, there has been reduced transportation of PDK1 to the cell membrane and hence reduced PDK1 and Akt phosphorylation (H. Park et al., 2015). By forming a scaffold, it is likely AMIGO2 brings PIP_3-activated PDK1 nearer to PIP3-activated Akt (refer Figure 10.3) (H. Park et al., 2015).

The group also established that it is the protein transduction domain A-2 (PTD-A2), which contains the amino acid residues 465–474 (conserved residues in AMIGO1-3) located at the cytoplasmic domain of AMIGO2 that is responsible for interaction with PH domain of PDK1. Astonishingly, addition of soluble PTD-A2 inhibited PDK1 and Akt phosphorylation and was even effective in suppressing pathological angiogenesis in murine tumour and oxygen-induced retinopathy models (H. Park et al., 2015). This might be because soluble PTD-A2 compromises the formation of AMIGO2 scaffold, causing PDK1 to be retained in cytosol and so prevents PDK1 and Akt from being phosphorylated (H. Park et al., 2015). This could partially explain as to why addition of AMIGO1 extracellular domain in the culture medium inhibited the fasciculation of neuritis as compared to immobilizing AMIGO1 extracellular matrix on a well plate that has been reported by Kuja-Panula et al, 2003 (Kuja-Panula et al., 2003; H. Park et al., 2015). The finding that soluble PTD-A2 has anti-tumour property is also testimony that disruption of AMIGO2 scaffold-forming process could be beneficial in preventing pathological angiogenesis in pulmonary vascular remodelling.

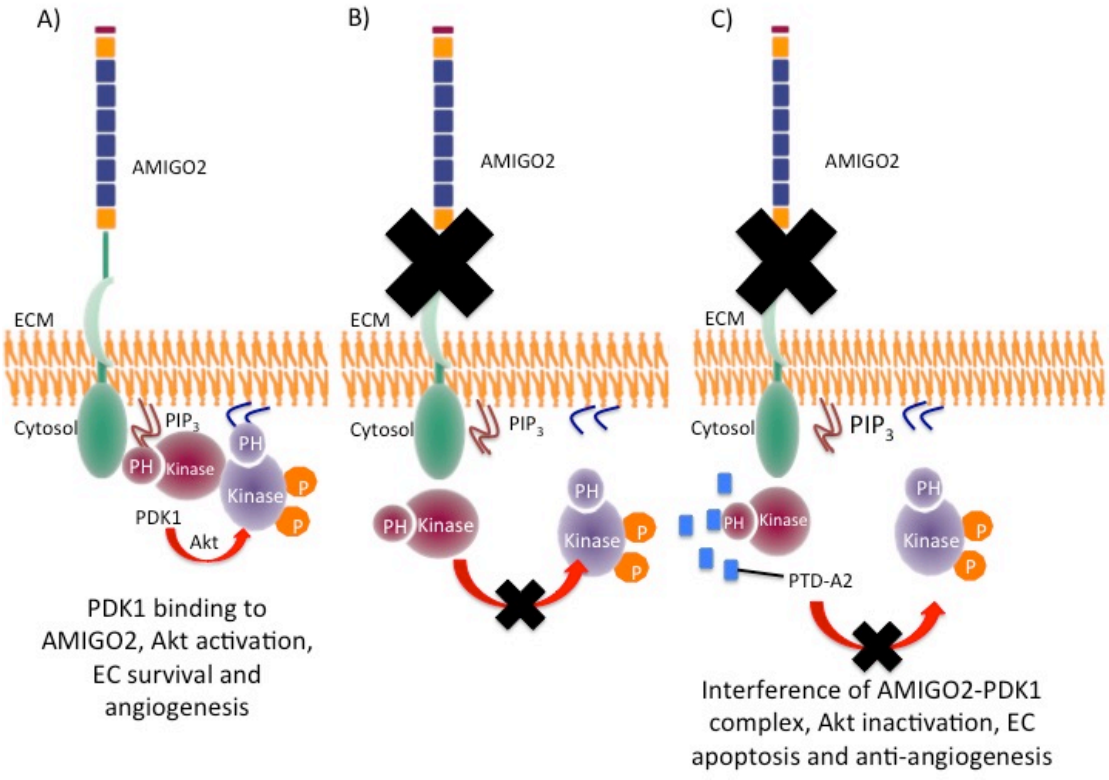

Figure 8.3: Schematics of the relationship between AMIGO2, PDK1, and Akt. Adapted from H. Park et al, 2015.

The group has examined the AMIGO2-VEGF relationship more closely by assessing whether Akt activation is affected when AMIGO2 is absent *in vitro* and *in vivo.* In endothelial cells where AMIGO2 is silenced and cultured in normal growth media (without VEGF), Akt phosphorylation (threonine 308 and serine 473) was reduced (H. Park et al., 2015). In contrast, Akt phosphorylation was increased when AMIGO2 was overexpressed (H. Park et al., 2015). AMIGO2-silenced mice also displayed decreased Akt phosphorylation in hyaloid vessels and retinas (H. Park et al., 2015). AMIGO2 knockdown endothelial cells treated with VEGF revealed that while VEGF receptor 2 (VEGF2) phosphorylation at tyrosine 1175 was not affected, Akt phosphorylation was inhibited (H. Park et al., 2015). This might indicate that AMIGO2 has a higher importance in controlling Akt activation (H. Park et al., 2015).

Although Akt inhibition has been correlated to reduce ovarian tumour growth, angiogenesis, endothelial cell tube formation, and morphogenesis, capillary-like network formation was unaffected (H. Park et al., 2015). Endothelial cells which are cultured together with vascular smooth muscle cells have constitutively active Akt and are able to form non-functional vasculature (H. Park et al., 2015). Partial inhibition of PI3K suppresses Akt1, in turn activates Erk1/2 (MAPK) pathway to promote arteriogenesis (H. Park et al., 2015). Therefore, vasculogenesis and angiogenesis can be regulated by more than one pathway (H. Park et al., 2015). Instead of relying on PI3K-Akt pathway alone, the process depends on the balance between this pathway with MAPK signalling (H. Park et al., 2015).